THE ARCHITECTURE OF PNEUMATIC REGENERATIVE SYSTEMS FOR THE DIESEL ENGINE

by

Ran Bao

A Doctoral Thesis

Submitted in partial fulfilment of the requirements

for the award of

Doctor of Philosophy of Loughborough University

August 2015

CERTIFICATE OF ORIGINALITY

This is to certify that I am responsible for the work submitted in this thesis, that the original work is my own except as specified in acknowledgments or in footnotes, and that neither the thesis nor the original work contained therein has been submitted to this or any other institution for a degree.

…… (Signed)

…… (Date)

ABSTRACT

For vehicles whose duty cycle is dominated by start-stop operation, fuel consumption may be significantly improved by better management of the start-stop process. Pneumatic hybrid technology represents one technology pathway to realise this goal. Vehicle kinetic energy is converted to pneumatic energy by compressing air into air tank(s) during the braking. The recovered air is reused to supply an air starter, or supply energy to the air path in order to reduce turbo-lag.

This research aims to explore the concept and control of a novel pneumatic hybrid powertrain for a city bus application to identify the potential for improvements in fuel economy and drivability.

In order to support the investigation of energy management, system architecture and control methodologies, two kinds of simulation models are created. Backward-facing simulation models have been built using Simulink. Forward-facing models have been developed in the GT-POWER and Simulink co-simulation.

After comparison, the fully controllable hybrid braking system is chosen to realize the regenerative braking function. A number of architectures for managing a rapid energy transfer into the powertrain to reduce turbo-lag have been investigated.

A city bus energy control strategy has been proposed to realize the Stop-Start Function, Boost Function, and Regenerative Braking Function as well as the normal operations. An optimisation study is conducted to identify the relationships between operating parameters and respectively fuel consumption, performance and energy usage.

In conclusion, pneumatic hybrid technology can improve the city bus fuel economy by at least 6% in a typical bus driving cycle, and reduce the engine brake torque response and vehicle acceleration. Based on the findings, it can be learned that the pneumatic hybrid technology offers a clear and low-cost alternative to the electric hybrid technology in improving fuel economy and vehicle drivability.

PUBLICATIONS

[1] **Bao, R.** and Stobart, R., "Design and Optimisation of the Propulsion Control Strategy for a Pneumatic Hybrid City Bus," SAE Int. J. Alt. Power. 5(1):2016, doi:10.4271/2016-01-1175.

[2] **Bao, R.** and Stobart, R., "Evaluating the Performance Improvement of Different Pneumatic Hybrid Boost Systems and Their Ability to Reduce Turbo-Lag", SAE Technical Paper 2015-01-1159, 2015, doi:10.4271/2015-01-1159.

[3] **Bao, R.** and Stobart, R., "Study on Optimisation of Regenerative Braking Control Strategy in Heavy-Duty Diesel Engine City Bus using Pneumatic Hybrid Technology", SAE Technical Paper 2014-01-1807, 2014, doi:10.4271/2014-01-1807.

[4] **Bao, R.** and Stobart, R., "Using Pneumatic Hybrid Technology to Reduce Fuel Consumption and Eliminate Turbo-Lag", SAE Technical Paper 2013-01-1452, 2013, doi:10.4271/2013-01-1452.

ACKNOWLEDGEMENTS

This project was supported by the UK Engineering and Physical Sciences Research Council (EPSRC) under grant reference EP/I00601X/1.

First of all, I would like to express my most gratitude to my supervisor, Professor Richard Stobart for his guidance, encouragement and support throughout my PhD study at Loughborough University.

I also would like to thank Professor Hua Zhao and members of the Centre for Advanced Powertrain and Fuels Research (CAPF) at Brunel University London for sharing their simulation models and Valuable feedbacks.

I am very grateful to the Loughborough colleagues for their thought-provoking discussions, helpful comments and assistance of modelling work on my research, the technicians at the Department of Aeronautical and Automotive Engineering for their great professional help and support, and the engineers at Support Group in the Gamma Technologies Inc. for their technical support of using GT-SUITE:

- Farraen Mohd-Azmin, Rifqi Irzuan Abdul Jalal, Dr Thomas Steffen, Dr Dezong Zhao, Gill Youngs, Bonnie Erdelyi-Betts, Rawinder Nottra, Robert Flint, David Travis, Adrian Broster, Graham Smith, Drew Mason and Martin Coleman – Loughborough University
- Dr Guangyu Dong (former Loughborough colleague) - University of Brighton
- Dr Bo Wang (former Loughborough colleague) - Romax Technology Limited
- Joseph Wimmer, Christopher A. Contag and Mike Arnett - Gamma Technologies Inc.

Finally, the greatest thank to my family for the support, understanding and encouragement.

CONTENTS

LIST OF FIGURES

LIST OF TABLES

NOMENCLATURE

Latin Letters

A	[m^2, J]	Open area of the valve, Frontal area of the vehicle, Availability
a	[m]	Distance from gravity centre to front wheel centre
b	[m]	Distance from the gravity centre to front wheel centre
C	[-]	Constant, Discharge coefficient, Drag coefficient, Specific heat
c	[-]	Constant
D	[s]	Duration of the intake valve second opening in crank angle
E	[J]	Energy
F	[N]	Braking force, Friction
f	[-]	Rolling resistance coefficient
G	[-, m/s^2]	Rotating inertia, Gravity of the vehicle
g	[m/s^2]	Gravitational acceleration
h	[m]	Height
i	[-]	Number of the cylinders
j	[m/s^2]	Deceleration rate of the vehicle
k	[-]	Ratio of specific heats
L	[m]	Wheel base
M	[kg]	Vehicle mass
m	[g]	Air mass
N	[rpm, -]	Engine speed, Number
n	[-]	Polytropic index
P	[kW]	Power
p	[bar]	Pressure

R	[-]	Ideal gas constant, Geometric compression ratio
r	[-]	Compression ratio
T	[k, Nm]	Temperature, Torque
t	[s]	Time
v	[m/s]	Speed
V	[l]	Volume
W	[J]	Work, Load

Greek Symbols

α	[-]	Constant
δ	[-]	Rotational inertia factor
η	[-]	Efficiency
ρ	[kg/m^3]	Density
τ	[Nm]	Torque
μ	[-]	Friction coefficient, Adhesion coefficient, Control variables
ω	[rad/s]	Angular velocity

Subscripts and Superscripts

0	Intake manifold, Initial
a	Air
aux	Auxiliary Chamber
c	Cylinder clearance, Compressor
D	Aerodynamic
d	Driving
dis	Discharge cases
e	Measured

f	Front, Final
final	Final point
g	Gravity centre
in	Upstream
m	Motor
max	Maximum
min	Minimum
out	Downstream
R	Crank revolutions for each power stroke per cylinder
r	Rear, Tire, Rolling
rech	Recharge cases
s	Cylinder swept
T	Turbine
t	Air tank, Traction
TC	Turbocharger
w	Aerodynamic friction

Abbreviations

AC	Air Compression
AM	Air Motor
ATV	Air Tank Valve
BDC	Bottom Dead Centre
BREES	BRaking Exhaust Energy Storage
CA	Crank Angle
CB	Compression Braking
CM	Compressor Mode
CPS	Cam Profile Switching

CREB	Compression Release Engine Braking
CV	Check Valve
DP	Dynamic Programming
EAT	Electric Assist Technology
ECE	Economic Commission of Europe
ECMS	Equivalent Consumption Minimization Strategy
ECV	Energy Control Valve
EGR	Exhaust Gas Recirculation
EHV	Electro-Hydraulic Valvetrain
EM	Expander Mode
EPSRC	Engineering and Physical Sciences Research Council
ESB	Exhaust Side Boost
EV	Electric Vehicle
GA	Genetic Algorithm
GPS	Generalized Pattern Search
HEV	Hybrid Electric Vehicles
HHV	Hydraulic Hybrid Vehicle
HIL	Hardware-In-the-Loop
ICE	Internal Combustion Engine
IEA	International Energy Agency
IM	Improvement Method
IMEP	Indicated Mean Effective Pressure
IMV	Intake Manifold Valve
IPV	Intake Port Valves
ISB	Intake Side Boost
IVSC	Intake Valve Second Close
MDI	Motor Development International

MLTB	Millbrook London Transport Bus
MOGA	Multi-Objectives Genetic Algorithm
MOO	Multi-objective optimisation
MVEG	Motor Vehicle Emissions Group
NA	Naturally Aspirated
NEDC	New European Drive Cycle
NSGA	Nondominated Sorting Genetic Algorithm
NSGA-II	Nondominated Sorting Genetic Algorithm II
PBS	Pneumatic Boost System
PS	Pattern Search
p-V	Pressure-Volume
QSS-TB	Quasi Steady State Toolbox
RegenEBD	Regenerative Engine Braking Device
RMSE	Root Mean Square Error
SAE	Society of Automotive Engineers
SFC	Specific Fuel Consumption
SIL	Software-In-the-Loop
SOC	State of Charge
SOGA	Single Objective Genetic Algorithm
SPEA	Strength Pareto Evolutionary Algorithm
SUV	Sport Utility Vehicles
TDC	Top Dead Centre
TV	Throttle Valve
VGT	Variable Geometry Turbine
YUCHAI	Guangxi Yuchai Machinery Company Limited

CHAPTER 1

INTRODUCTION

1.1 Introduction and Outline of the Thesis

This research is based on the project, *A Cost-Effective Regenerative Air Hybrid Powertrain for Low Carbon Buses and Delivery Vehicles*, which is supported by the UK Engineering and Physical Sciences Research Council (EPSRC) under grant reference EP/I00601X/1. It is carried out as part of a joint project between Loughborough University and Brunel University London. The pneumatic hybrid system hardware design and engine experimental research have been conducted at Brunel University London, while the pneumatic hybrid system and vehicle modelling, simulation research and control methodology development have been studied at Loughborough University. Guangxi Yuchai Machinery Company Limited (YUCHAI) provides a six-cylinder diesel engine to Brunel University London, and modifies it to realize the proposed pneumatic hybrid system operations.

Chapter 1 gives an overview of the structure of the thesis. Then the research background and motivation are analysed. Research aims and objectives are also summarized. Finally, the methodology and software using in the research are introduced.

Chapter 2 is a review of relevant literatures to identify specific research gaps and narrow down the focus. It firstly summaries the compressed air vehicle and air engine history. Then the state-of-the-art of pneumatic hybrid technology research is presented. The literature review supports and defines the scope of the chosen research topics and summarizes those topics that lie outside the scope.

Chapter 3 presents the principle of operation and confirms the potential of the pneumatic hybrid system to both generate a supply of compressed air and to manage the contribution of the engine to vehicle braking. The pneumatic hybrid engine Compressor Mode (CM) is considered from a theoretical perspective based on an air cycle analysis

and validated. Finally an understanding of the sensitivity of work done (braking torque created during the CM) to design parameters is given.

Chapter 4 presents an evaluation of the fuel economy improvement ability of pneumatic hybrid technology for the city bus application by realizing the Stop-Start Function through different bus driving cycles. Also, an investigation is made into how multiple air tanks give an additional degree of freedom for management of recovered air. A backward-facing simulation model of the city bus with the pneumatic hybrid powertrain has been applied to investigate the improvement of fuel economy by using one and two air tanks in different driving cycle.

Chapter 5 presents an analysis of vehicle braking behaviour through different bus driving cycles and compares two configurations of the hybrid braking system, the parallel hybrid brake system and the fully controllable hybrid brake system. The comparison shows the fully controllable hybrid braking system has a distinct advantage and is chosen to realize the regenerative braking function. A braking simulation model has been built in to support an investigation of an optimum air tank pressure and configuration for energy recovery.

Chapter 6 presents an analysis of the reasons for engine turbo-lag and the methods developed for reducing the turbo-lag and improving transient response first. Then, a number of architectures for managing a rapid energy transfer into the powertrain to assist acceleration of the turbocharger have been proposed and investigated from two aspects, engine brake torque response and vehicle acceleration, by using the 1-D engine simulation.

Chapter 7 presents the design of an energy control strategy based on the use of thresholds in the degree of energy storage and regeneration (a "logic threshold" methodology) for the pneumatic hybrid city bus. A forward facing pneumatic hybrid city bus simulation model has been developed in GT-POWER with MATLAB/Simulink co-simulation. To obtain the maximum overall fuel economy, the amount of air and energy recovered during the braking and minimum loss of availability during acceleration, a number of variables in the control strategy must be optimized. Three global optimisation algorithms, Pattern Search (PS), Genetic Algorithm (GA) and multi-objective Non-

dominated Sorting Genetic Algorithm II (NSGA-II), are compared and employed for the optimisation of the control strategy considered at three levels respectively.

Chapter 8 presents the conclusions and the extent of this research and, suggestions for future works.

The outline of the thesis is also shown in Figure 1-1.

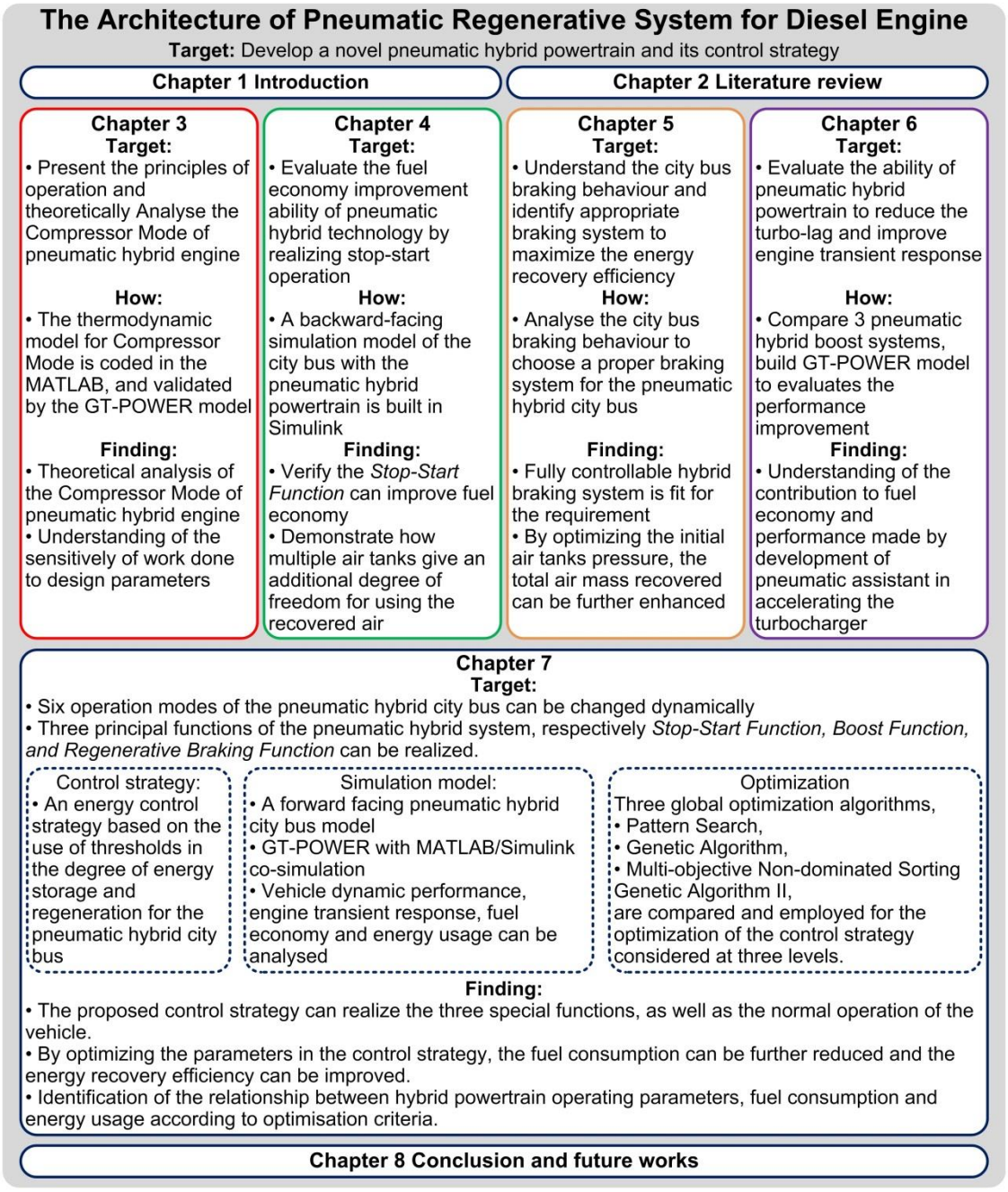

Figure 1-1 Outline of the thesis

1.2 Background

From the recent International Energy Agency (IEA) report [1], transport is the second largest sector for CO_2 emissions in 2012, and produces more than one-fifth of global CO_2 emissions. As illustrated in Figure 1-2, the transport sector contributed 23% of CO_2 emissions all over the world in 2012. The component of transport sector includes light duty vehicles (such as automobiles, Sport Utility Vehicles (SUV), minivans, pick-ups and motorcycles) and heavy duty vehicles (for example large trucks and buses).

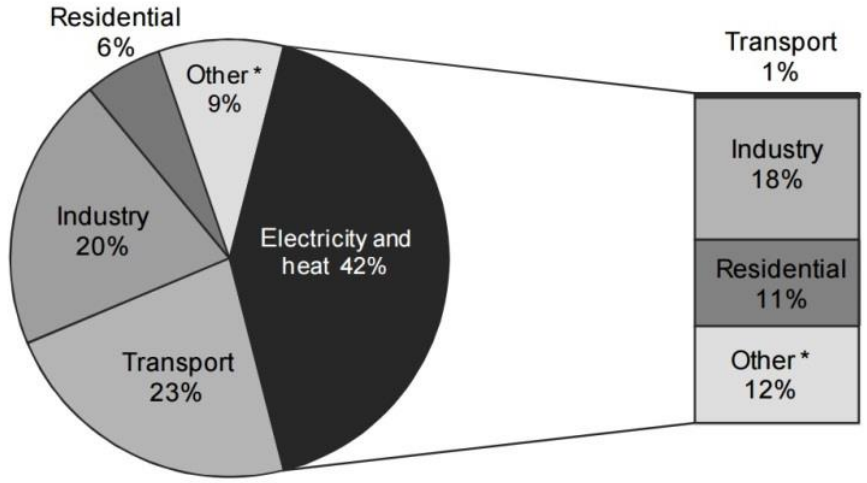

Note: Also shows allocation of electricity and heat to end-use sectors.

* Other includes commercial/public services, agriculture/forestry, fishing, energy industries other than electricity and heat generation, and other emissions not specified elsewhere.

Figure 1-2 World CO_2 emissions by sector in 2012 [1]

Due to this reason, more and more pressure is coming from the government and the public to reduce the vehicle exhaust emissions. The ever-stringent vehicle emission legislations are developed. Figure 1-3 shows how the finalized and proposed fuel economy or CO_2 regulations around the world will develop, normalized to CO_2 emissions on the New European Drive Cycle (NEDC). The European 2020 regulation of 95 g/km CO_2 is most demanding. The US (103 g/km by 2025 for passenger cars), Japan (105 g/km by 2020), and Canada (103 g/km by 2025) have set similar targets. China and India are also tightening to the similar level, 117 g/km and 113 g/km, respectively [2].

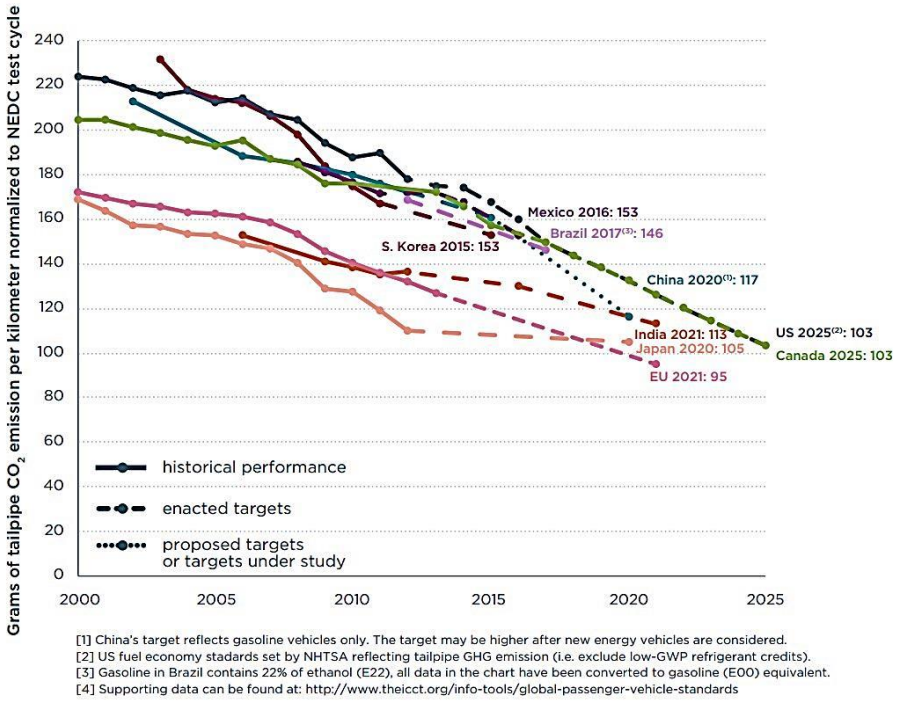

Figure 1-3 Comparison of finalized and proposed fuel economy or CO_2 regulations around the world, normalized to CO_2 emissions on the NEDC [2]

Now, the automotive industry is facing the biggest revolution in its history. Historically, engine technologies were largely influenced by and developed for meeting criteria emissions regulations [3]. Due to hybrid powertrain and pure battery electric powertrain technologies development, the traditional engines start to be replaced by the hybrid powertrain or even entirely by the pure battery electric powertrain. But for the short to medium term, hybrid powertrain with regenerative recovery is recognised as one of the most effective means to reduce CO_2 emissions for the automotive industry [4].

1.3 Hybrid Vehicle

A hybrid vehicle is defined by Society of Automotive Engineers (SAE) as: A vehicle with two or more energy storage systems both of which must provide propulsion power – either together or independently [5]. It aim to have the advantages of both IC engine and other kind powertrain systems [6]. The "energy storage systems" in hybrid vehicle could be a gasoline or diesel engine, electric motor/battery pack, or other source of motive power. The goal of the hybrid vehicle is to provide the equivalent performance range and safety as a conventional vehicle while reducing fuel consumption and harmful emissions by better managing the two or more energy source. The reason for using more

than one power sources is because of the disadvantages of conventional vehicles with Internal Combustion (IC) engines like the low fuel economy and high environmental pollution. These disadvantages cause by the mismatch of engine fuel efficiency characteristic with the real operation requirement, dissipation of vehicle kinetic energy during braking and low efficiency of hydraulic transmission in the current vehicle in stop-start function [6]. Compare with petroleum fuels, other power resources like electric powertrain, hydraulic powertrain and pneumatic powertrain have some advantages such as high-energy efficiency and lower environmental pollution. But these powertrains also have some disadvantages such as low energy density and high cost.

Figure 1-4 shows the Ragone chart which can be used to compare performance of the different energy storage system. In Ragone chart, the vertical axis describes how much energy is available, while the horizontal axis shows how quickly that energy can be delivered, otherwise known as power. A point in a Ragone chart thus represents the amount of time during which the energy (per mass) on the Y-axis can be delivered at the power (per mass) on the X-axis, and that time (in hours) is given as the ratio between the energy and the power densities. A prominent example is the comparison of conventional batteries and conventional capacitors. While batteries have high energy densities but only low power densities, capacitors have rather high power densities but low energy densities [7].

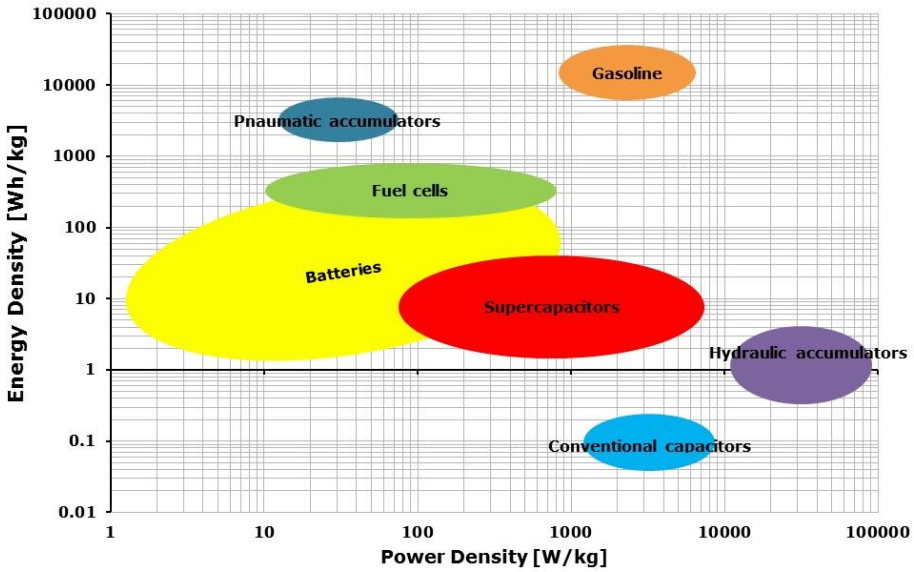

Figure 1-4 Ragone chart - Energy vs. Power for various energy storage systems

From Figure 1-4, it can be seen that the supercapacitors have an unusually high energy density. They have advantages such as high energy storage compared to conventional capacitor technologies and fast charge and discharge ability. As can be seen in Figure 1-4, the supercapacitors reside in between batteries and conventional capacitors. They are typically used in applications where batteries have a short fall when it comes to high power and life, and conventional capacitors cannot be used because of a lack of energy, and offer a high power density along with adequate energy density for most short term high power applications.

From Figure 1-4, it also can be seen that hydraulic accumulators are one kind of short-term storage systems which have the ability to accept high rates and high frequencies of charging/discharging. The devices are characterized by a lower energy density and higher power density than electrochemical batteries. It can supply very high density of power. The hydraulic hybrid system can easily capture the vehicle braking energy. Because of the high efficiency of the system components such as the accumulator and the pump/motor, the operational efficiencies can exceed 70% which is far better than any other form of hybridization such as batteries system [8, 9]. However, hydraulic hybrid technology has several limitations such as its relatively low energy density and limited storage of energy which restricts the time of continuous operation.

The pneumatic accumulators pressurises air as the energy storage medium. Compressed air has relatively low energy density. Air at 300 bar (30 MPa) contains about 50 Wh of energy per liter [9]. For comparison, a lead–acid battery contains 60-75 Wh/l energy density; and a lithium-ion battery contains about 250-620 Wh/l energy density. Although the pneumatic accumulators cannot be used as an energy source to drive the vehicle alone, it can be a supplementary to the IC engine in the HEV.

The braking energy is the only energy the vehicle can earn without any energy cost. But the conventional IC engine cannot get this energy and reuse it. Normally, a hybrid vehicle has a powertrain can recover this energy. For the purpose of getting the maximum braking energy, a hybrid powertrain usually has a powertrain that allow energy to flow backward from the wheel to the energy source and another one can flow either forward or backward. Figure 1-5 shows the concept of the hybrid powertrain and the possible different power flow routes.

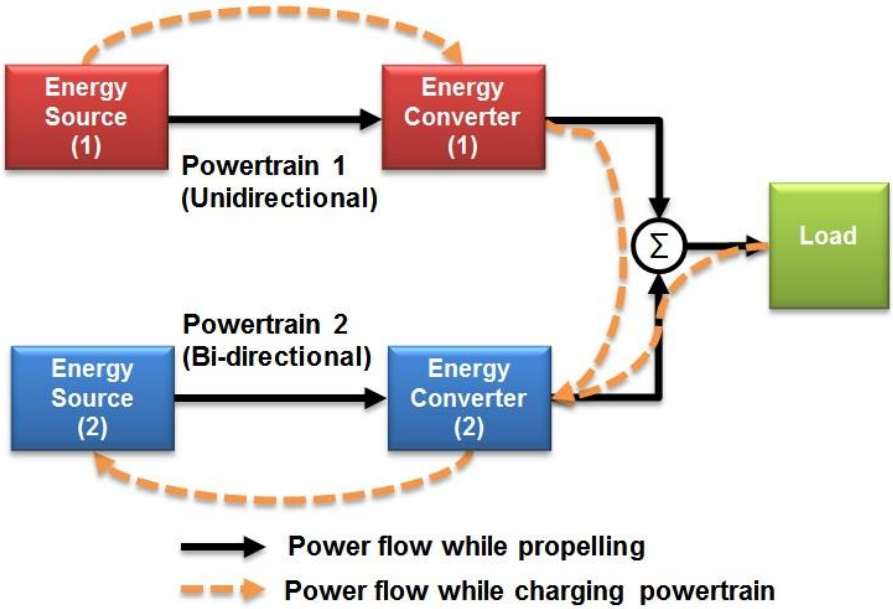

Figure 1-5 Conceptual illustration of the hybrid powertrain

From Table 1-1, there are 9 operation conditions of the hybrid powertrain to meet the load requirement:

Table 1-1 The operation conditions of hybrid powertrain

Condition	Powertrain 1	Powertrain 2
1	Deliver power to load	-
2	-	Deliver power to load
3	Deliver power to load	Deliver power to load
4	-	Obtain power from load
5	Deliver power to Powertrain 2	Obtain power from Powertrain 1
6	Deliver power to Powertrain 2	Obtain power from Powertrain 1 and load
7	Deliver power to load and Powertrain 2	Obtain power from Powertrain 1
8	Deliver power to Powertrain 2	Deliver power to load
9	Deliver its power to load	Obtain power from load

Usually, more than two power sources in a hybrid vehicle will make the propulsion system very complicated. This kind of hybrid vehicle will not be discussed in this research.

1.3.1 Hybrid Electric Vehicle

Normally, the term hybrid vehicle most often refers to the Hybrid Electric Vehicle (HEV), which consists of an IC engine and one or more electric motors. The reason for using more than one electric motor is that the second one works as an electricity generator to charge the battery. The energy storage for HEV is usually a battery or in some cases, a supercapacitor.

Before 2000, the HEVs usually classified two basic types: series and parallel. In 2000, some newly introduced HEVs cannot be classified into these two types. Hence, the combined series-parallel HEV and complex HEV added into the hybrid vehicle family [6].

The HEV is classified into four types:

(i) Series HEV: the electric motor propels the vehicle alone, the electricity can be obtained from either battery or an electricity generator driven by IC engine.
(ii) Parallel HEV: the IC engine and the electric motor can propel the vehicle individually or simultaneously.
(iii) Combined (series-parallel) HEV: this kind of hybrid vehicle has a power-split device allowing for power flow routes from the engine to the wheels that can be either mechanical or electrical.
(iv) Complex HEV: similar with the combined hybrid, but the electric coupling function is moved from the power converter to the battery and one more power converter is added between the motor/generator and the battery [6].

The configurations of four kinds of HEVs are shown in Figure 1-6 to Figure 1-9. The key features of four types HEV are compared in the Table 1-2.

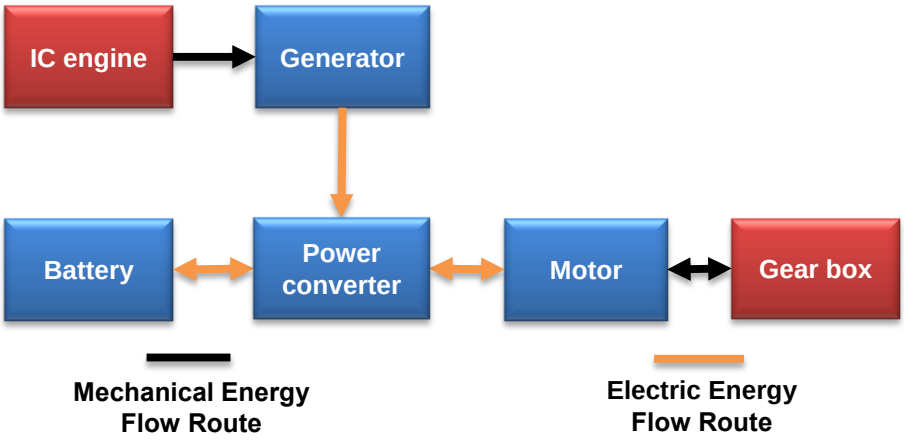

Figure 1-6 Series HEV configuration

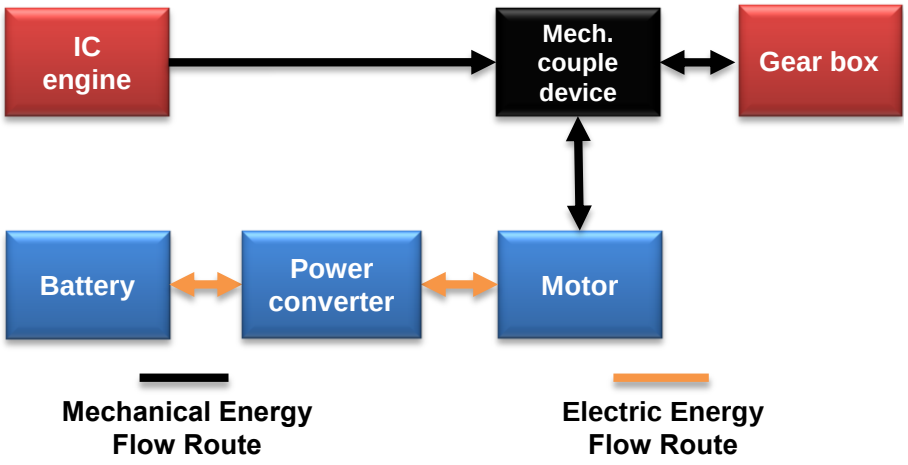

Figure 1-7 Parallel HEV configuration

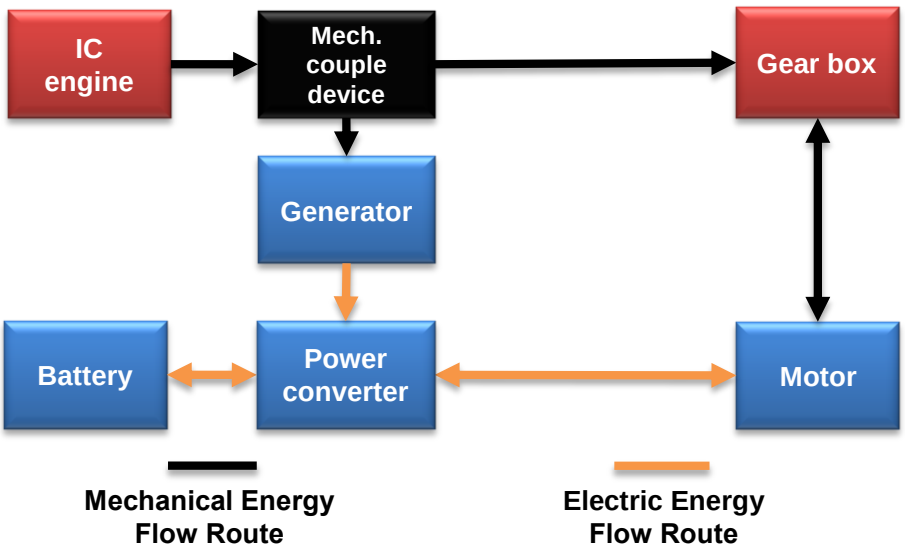

Figure 1-8 Combined (series-parallel) HEV configuration

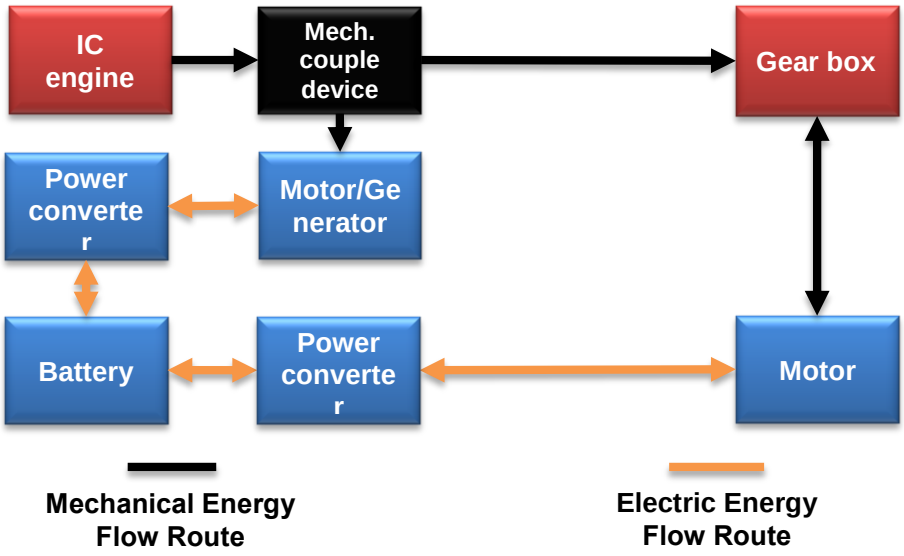

Figure 1-9 Complex HEV configuration

Table 1-2 Key features of HEV

	Series HEV	Parallel HEV	Combined (series-parallel) HEV	Complex HEV
Key feature	Two electric powers are added together in the power converter, an electrical power couple device	Two mechanical powers are added together in a mechanical power couple device	Using both mechanical and electrical power couple device together	Similar with combined HEV, but using battery to be an electrical power couple device

The most researched and developed hybrid vehicles are electric based. But the applications of the electric hybrid powertrain to buses, trucks and delivery vehicles are limited by the huge additional cost of numbers of batteries and the cost to combined electric and mechanical powertrain and transmission systems together. From Ranganathan's report, the average price of a 12 m hybrid bus typically ranges from $450,000 - $550,000 when compared to $280,000 - $300,000 for a conventional diesel bus [10]. The price variation in hybrids is due to the order volumes and individual specifications. In UK, there are currently a few of electric hybrid buses operating in some cities. Such electric hybrid buses can cost additional £100,000 to rebuild or manufacture, they need heavily finical support and will not be fit for commercially viable large volume production in this stage [11].

1.3.2 Hydraulic Hybrid Vehicle

The Hydraulic Hybrid Vehicle (HHV) is based on the hydraulic hybrid powertrain which includes an IC engine and a hydraulic pump/motor [12]. The energy stores in the hydraulic accumulator. The HHVs also can divide into series and parallel two types. Figure 1-10 is a typical series HHV configuration.

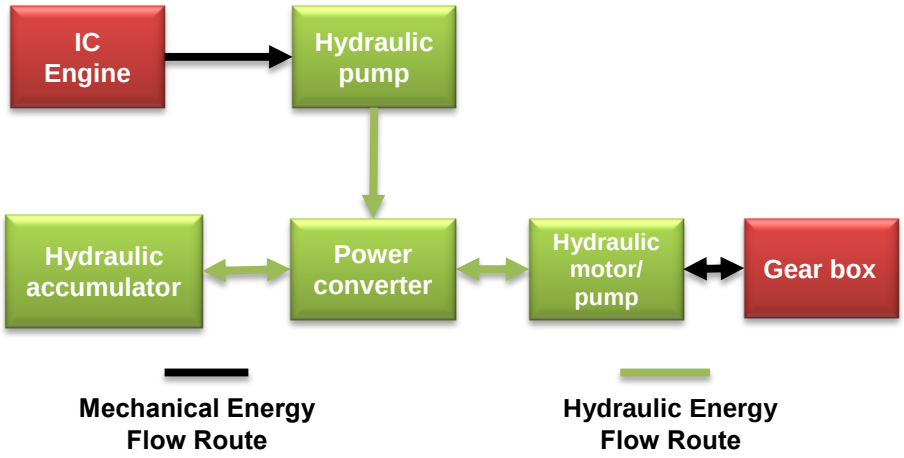

Figure 1-10 Typical series HHV configuration

All types of hydraulic hybrid powertrain include a high-pressure accumulator and a low-pressure reservoir. The accumulator contains the hydraulic fluid and a gas such as nitrogen (N_2) or methane (CH_4), separated by a membrane. When the hydraulic fluid flows in, the gas is compressed. During the discharge phase, the fluid flows out through the motor and then into reservoir [6].

Due to the characteristic of the hydraulic fluid and hydraulic accumulator, the hydraulic hybrid powertrain has the ability to accept both high frequencies and high rate of charging/discharging operations, such as the NYC COMP cycle, which has an average of 4.96 stops per km and an average kinetic intensity of 2.67 per km [13]. This feature is fit for recovering the vehicle's kinetic energy during braking. That means the hydraulic hybrid powertrain is the ideal choice for the buses and delivery vehicles in cities and urban areas where the traffic conditions involve a lot of stop-start operations. Compare with the electric hybrid powertrain, the hydraulic hybrid powertrain for trucks and buses can be less expensive by using the hydraulic accumulator as an energy storage device instead of the high price amount of batteries.

Similarly with the HEVs, the hydraulic hybrid vehicles will be added a completely separate and additional unit, the cost and weight would be expected as high as the equivalent HEVs.

1.3.3 Pneumatic Hybrid Vehicle

The pneumatic hybrid vehicle is based on pneumatic hybrid powertrain which typically using the fully variable actuation valve to change the conventional IC engine to a pneumatic pump and a pneumatic motor [14-24]. A typical pneumatic hybrid powertrain structure is shown in Figure 1-11.

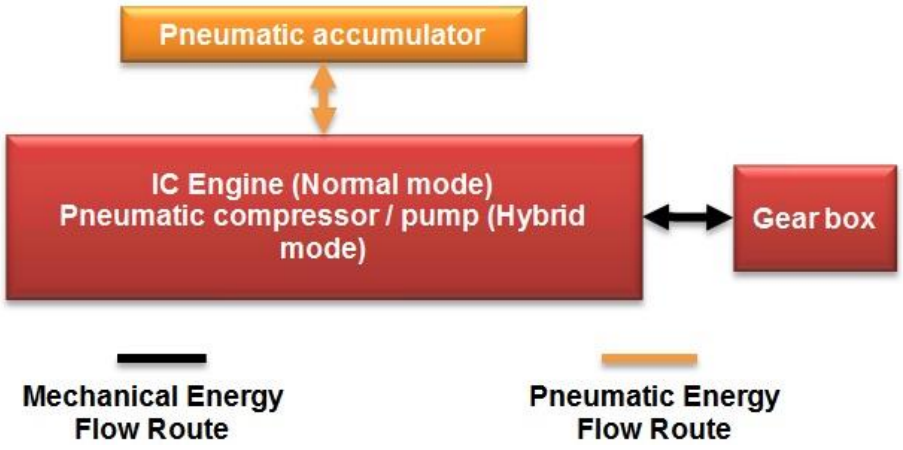

Figure 1-11 Typical pneumatic hybrid powertrain structure

Because of the existing of the fully variable actuation valve, during the compression stroke, the IC engine can compress the air into high pressure air tank, and at the intake stroke, the high pressure air stored in the air tank can come into the cylinder and propel the piston. In the pneumatic hybrid powertrain, the energy storage device is the air tank. Because of the energy density of air, the pneumatic hybrid powertrain similar with the hydraulic hybrid powertrain is fit for accepting both high frequencies and high rate of charging/discharging operations. This feature can significantly improve the fuel economy by implementing regenerative energy recovery operation, particularly for buses and delivery vehicles in cities and urban areas where the working conditions include a lot of stop-start operations [11]. Because of in such conditions, a large amount of fuel is needed to accelerate the vehicle, and much of this is converted to heat in brake friction during deceleration. Capturing, storing and reusing this braking energy can therefore improve fuel efficiency, and this can be achieved by using the momentum of the vehicle

during coasting and deceleration to charge the energy storage device and later reuse the energy to save the fuel consumption.

Moreover, a pneumatic hybrid powertrain ideally complements a down-size and supercharged engine [16, 25]. In fact, turbocharged engines usually have a turbo-lag because the relatively slow acceleration of the compressor-turbine during load steps. Although by choosing small turbines, which minimize the delays but will cause a rather lower efficiency [16]. In the pneumatic hybrid powertrains, the air available in the air tank is provided to the cylinder by a fully variable charge valve during in the heavy transients, the torque can be raised from idling to full-load from one engine cycle to the next or in the shortest time possible. Also, this will give more freedom to design the turbines for an optimal economy. Moreover, the combustion with the large amount of fresh air and fuel accelerates the turbocharger much faster, resulting in a fast pressure rise in the intake manifold. Therefore, the additional air from the pressure tank is needed only for a very short time such that relatively small air tanks can be used [16].

Unlike the electric and hydraulic hybrid vehicles, pneumatic hybrid vehicles can be implemented without adding an additional propulsion system to the vehicle when it has already applied an IC engine. In this case, the engine transmitting power through the pistons and the crankshaft of the engine by working as a compressor during braking/deceleration or an air motor at starting/acceleration. The vehicles can use the existing braking or propelling drivetrain. For buses and delivery vehicles, air energy will be stored in a moderate pressure compressed air storage tank already available on such vehicles. Compare with HEVs and HHVs, the pneumatic hybrid vehicles do not need add the large weight and complexity modifications to the vehicle. In addition, the stored high pressure air is available readily in demand for other uses to improve drivability and reduce emissions, such as briefly boosting the engine to eliminate turbo-lag in a turbo-charged engine resulting in better response and removal of the black smoke typically seen from accelerating diesel vehicles. For buses and commercial vehicles, compressed air is required for air assisted braking system and the operation of pneumatic equipment (e.g. door opening and closing) and is currently produced by an engine driven compressor. Pneumatic hybrid powertrain technology will enable further and readily achievable fuel savings to be realized by providing the service compressed air from the regenerative engine braking in place of the engine driven compressor. Finally, the

compressed air produced can also be used briefly in combination with the Exhaust Gas Recirculation (EGR) in a diesel engine to improve the dynamic trade-off between NO_x and smoke emissions. These are exciting synergies enhancing many attributes of the engine at minimum cost and are immediately available, not possible with the other hybrid energy types and unique only with the pneumatic hybrid because of the readily available air supply. Therefore, the exploitation of such synergies will result in a pneumatic hybrid powertrain system with significant and concurrent improvements in fuel consumption, emission, and performance.

1.4 Research Aims and Objectives

For vehicles whose duty cycle is dominated by start-stop operations, fuel consumption may be significantly improved by better management of the start-stop process. Pneumatic hybrid technology represents one technology pathway to realise this goal. Vehicle kinetic energy is converted to pneumatic energy by compressing air into the air tanks installed in the vehicle. The compressed air is reused (i) to power an air starter to realize the stop-start operation, (ii) to supply energy to the air path in order to reduce turbo-lag. However, there has been no in-depth study yet that how to implement the pneumatic hybrid technology on the city bus and realize these two functions.

To close this gap, this research therefore aims to develop a novel pneumatic hybrid powertrain for city bus applications and its control strategy with significant and concurrent improvements in fuel economy and performance over the current IC engines. The proposed pneumatic hybrid powertrain offers a clear and low-cost alternative to the electric hybrid technology in improving fuel economy, and vehicle drivability.

The specific objectives are:

(i) To fully understand the principle of the operation of the pneumatic hybrid engine and the quantification of the sensitivity of the work done to design parameters during the Compressor Mode.
(ii) To evaluate the fuel economy improvement ability of pneumatic hybrid technology for the city bus through different bus driving cycles.
(iii) To analyse engine braking characteristics during the vehicle's deceleration and braking process during different bus driving cycles and hence identify

appropriate braking system structure and its control strategy for maximum energy recovery.

(iv) To study the benefits of extra boost on reducing turbo-lag, improved engine performance, and reduce fuel consumption.

(v) To formulate a pneumatic hybrid city bus control strategy and the vehicle driving cycle simulation programme and identify the relationship between respectively the operating parameters, fuel consumption and energy usage according to optimisation criteria.

1.5 Methodology and Software

Methodology

Approaches of both theoretical analysis and computer simulation are chosen for this research. During the whole research period, computer simulation research will conduct with the aim to investigate the feasibility of the pneumatic hybrid engine concept and develop the control strategy for the pneumatic hybrid city bus. Then, the simulation result is compared and verified with the experimental result from the engine experiment had already been carried out in Brunel University London before.

Two main approaches, backward facing simulation and forward facing simulation, are used in the research. Backward facing simulation takes the assumption that the vehicle meets the target requirement, and calculates the component states. On the contrast, forward facing simulation simulates the physical behaviours of each component with control instruction, handles state changes, and generates vehicle performance as output. Backward facing approach is beneficial in simplicity and computation cost, while the forward-facing approach is advantageous in exploiting performance details.

Software

There are several modelling tools can be utilised in the process of modelling hybrid configurations and its control strategies. They can be divided into two types from the simulation direction. The first one is based on the backward facing simulation method which normally developed in the MATLAB/Simulink environment. Another is based on the

forward facing simulation method which normally includes the detailed engine model to realize the 1-D simulation.

MATLAB®, developed by The MathWorks, Inc., can be used for creating and developing mathematical models for engineering applications and solutions, the Simulink toolbox components include specific items for developing controls, signal processing and real-time programming [26]. Simulink provides a graphical editor, customizable block libraries, and solvers for modelling and simulating dynamic systems [27]. It is integrated with MATLAB, enabling the user to incorporate MATLAB algorithms into models and export simulation results to MATLAB for further analysis [27].

GT-SUITE®, a product of Gamma Technologies Inc., is a single software tool for modelling and simulation of systems in automotive and transportation industry as well as in other industries [28, 29]. GT-SUITE can be used to develop different applications such as [28]:

- Engine performance modelling - including combustion and turbocharging
- Exhaust after treatment
- Hybrid and electric vehicles - electric machines, fuel cells
- Vehicle dynamics - drive cycles, drivelines

GT-POWER®, part of the GT-SUITE, is a code for engine simulations. At its core, the GT-POWER solver is based on the 1-D solution of the fully unsteady, nonlinear Navier-Stokes equations. It is applicable to different sizes and types of engines, contains models for engine performance analysis, and allow the engineer to analyse a number of engine configurations and performance characteristics, including [30]:

- Torque and power curves, airflow, vol. efficiency, fuel consumption, emissions
- Steady state or full transient analysis, under different driving scenarios
- Turbocharged, supercharged, turbocompound, e-boost, pneumatic assist

GT-SUITE also offers a toolbox for modelling vehicles and drivelines and simulation of vehicle dynamics. Vehicle models can address a range of vehicle engineering issues: vehicle performance, fuel economy, emissions, and etc. It furthermore offers a set of tools for the simulation of vehicles with HEV or Electric Vehicle (EV) drivelines.

The versions of the software using in the research are listed in Table 1-3.

Table 1-3 The versions of the software used in the research

	Chapter 3	Chapter 4	Chapter 5	Chapter 6	Chapter 7
MATLAB/Simulink	R2012a	R2012a	R2012a	-	R2014a
GT-SUITE	V7.3.0	-	-	V7.3.0	V7.4.0

1.6 Contributions to Knowledge

The work reported in this thesis establishes a new understanding of the principles of application of pneumatic hybrid methods to the braking and drivability of heavy duty vehicles. In particular:

(i) The representation of the thermodynamic process during the Compressor Mode and the quantification of the sensitivity of the work done to the design parameters.

(ii) The evaluation of the fuel economy improvement ability of pneumatic hybrid technology for the city bus through different bus driving cycles.

(iii) Demonstrate how the proposed pneumatic hybrid powertrain contributes to vehicle braking and identify the design guideline to integrate the pneumatic braking system to the vehicle friction braking system.

(iv) The understanding of the contribution to fuel economy and performance made by the pneumatic assistance in accelerating the turbocharger.

(v) The identification and quantification of the relationship between respectively the pneumatic hybrid powertrain operating parameters, fuel consumption and energy usage according to optimisation criteria.

CHAPTER 2
LITERATURE REVIEW

2.1 Introduction

In this chapter, the history of the use of compressed air in vehicles is briefly introduced, considering that the concept of both pneumatic hybrid engine and air engine has evolved alongside the development of compressed air vehicles. Then the air engine and pneumatic hybrid engine development are summarized. After that, five most active pneumatic hybrid technology research groups' achievements are introduced in detail. The five research groups at different universities are: Brunel University London [31-37], ETH University [16, 38-42], Lund Institute of Technology [21, 43-46], University of Orléans [14, 19, 47-52], and UCLA Research Group [17, 24].

2.2 Compressed Air Vehicle History

A compressed air vehicle is defined as a vehicle powered by an air engine, using compressed air, which is stored in a tank [53]. Instead of mixing fuel with air and burning it in the engine to drive pistons with hot expanding gases, compressed-air vehicles use the expansion of compressed air to drive the pistons [53].

The compressed air had been used to power locomotives and trams since the 19th century [53-56]. The first compressed air vehicle was devised by Bompas, who developed a patent for a locomotive being taken out in England in 1828. The patent had two storage tanks between the frames, with conventional cylinders and cranks [54]. In 1872 and 1873, Louis Mekarski took out patents for the Mekarski system which was the fundamental design for the most successful tramcars later [56]. The Mekarski system had a single stage engine and a special design. The air was warmed before entering the engine from air tank to overcome the common problem that the air cools as it expands, which lead to the formation of ice in the power cylinders [57]. For the following half a century, the air-powered locomotive was a serious contender for the top spot in transportation because of its obvious advantages: simplicity, safety, economy, and

cleanliness [55]. Until the 1930s and 1940s the air locomotive had no serious competition from electric or internal combustion engines in the mining industry because the heat and spark made these competitors unsafe in closed-in and gassy places [55].

In 1898, the Pneumatic Carriage Company of New York City developed a car that ran on compressed air [54]. The air was believed to store in a steel cylinder running the length of the lower body. In 1903, the Liquid Air Company, located in London, England, manufactured a number of compressed-air and liquefied-air cars [58]. The major problem with these cars and all compressed-air cars was the lack of torque produced by the "engines" and the cost of compressing the air [53].

The term "air engine" disappeared from engineering textbooks between 1931 to the end of the Second World War because the gas engines had been perfected, the power of the oil industry was established, and gas became cheaper [55]. Serious interest in air cars was rekindled by the petroleum shortages of the 1970s.

Motor Development International (MDI), established by Guy Nègre, is a French company designing compressed air car prototypes marketed under the title "the Air car" for twenty years [59]. The AIRPod is an alternative fuel vehicle in development by MDI which was first shown at Geneva Motor Show 2009. The AIRPod planned to be produced in three different configurations that will vary the number of seats and amount of cargo storage while keeping the same basic chassis. It has a reversible compressed air engine which has 2 cylinders inline each having an included active chamber, variable valve timing, crankcase and head in aluminium. The engine displacement is 430 cm^3, max power is 7 kW @ 1500 rpm, and max torque is 45 Nm @ 1500 rpm. The vehicle has an automatic gearbox with three gears and a reverse gear, and can realize the kinetic energy recovery during the deceleration phases with an electronic management. The air stores in two 125 litre air tanks which are made of the thermoplastic liner and carbon fibre wiring. MDI claimed that the AIRPod will be able to travel 130 km (80 miles) in urban driving, and the top speed is 80 km/h (50 mph). MDI has been promising production of the AIRPod since 2000 but as of March 2015 none have gone on sale [60].

In 2013, the PSA Peugeot Citroën introduced the Hybrid Air concept which is a new type of full-hybrid powertrain that combines a petrol engine and compressed air for energy storage instead of a battery, offering an alternative to electric hybrid solutions [61]. A

1.2 liter petrol engine (rated power 82 bhp) provides most of the power, driving through an automatic transmission. During deceleration, the wheels' energy drives a hydraulic pump that pushes hydraulic fluid into an accumulator and compresses the nitrogen gas within [62]. When the car accelerates, the powertrain works in the opposite way: The pressurized nitrogen gas pushes the hydraulic fluid, which drives a hydraulic motor connected to the transmission. The Hybrid Air car can operate in zero emissions air mode, petrol-engine-only mode, or petrol and air in combination. PSA claimed its system can improve fuel economy up to 45% in urban driving compared with conventional engines with the same power rating, and fuel consumption stood at 2.9 l/100km in combined-cycle driving, for CO_2 emissions of around 69 g/km for standard body style models such as the Citroën C3 or Peugeot 208 [61]. PSA planned to initially fit the technology on B-segment models from 2016 and will make it available in vehicles both inside and outside Europe.

2.3 The Review of Previous Research

2.3.1 Model Pneumatic Hybrid Engine Concept

The recently popular pneumatic hybrid engine concept was proposed by Schechter first time in 1999 [15]. He introduced a new idea that the normal IC engine can become a compressor and an air motor by equipping a new cylinder head. As shown in the Figure 2-1, a new valve, charge valve, connecting the cylinder and air tank is added into the cylinder head. When the engine works as a compressor or an air motor, the charge valve is active to inject the high pressure air into the cylinder or compress the air to the air tank. In [15], Schechter indicated during a 45 second driving cycle, the fuel consumption reduces 50% by using the pneumatic hybrid technology.

In 2000, Schechter used the same cylinder head configuration to achieve different engine loads by changing the valve timings [63]. He also defined the regenerative braking efficiency as a fraction of the energy, absorbed during deceleration, which can be used in the subsequent acceleration. Based on this definition, Schechter calculated that a regenerative braking efficiency of 74% for the regenerative braking system during the braking of a typical vehicle from an initial speed of 48 km/h can be achieved.

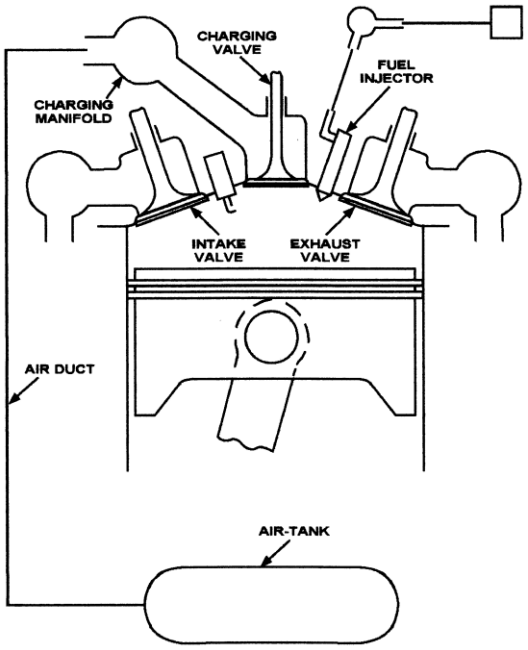

Figure 2-1 Schematic diagram of Schechter's proposed system [15]

In 2007, Schechter patented a new two-stage pneumatic hybrid engine configuration [64]. In this new structure of the engine, a system of valves that permits various engine cylinders to operate in different modes of operation was added into the engine. During braking, some of the engine cylinders receive atmospheric air, compress it, and transfer it to an intermediate air-container. Other cylinders receive compressed air from the intermediate air-container, further compress it, and transfer it to a high-pressure air-reservoir for storage. During acceleration, some of the engine cylinders receive compressed air from the high-pressure air reservoir, expand it to a lower level of pressure, and transfer it to the intermediate air-container. Other cylinders receive air from the intermediate air-container, further expand it, and use it for combustion. During short stops, the engine is shut down, and then, it is restarted with compressed air. During cruise, the engine operates as a conventional IC engine. This is quite similar to the stop-start function in the micro hybrid system.

After Schechter's initial investigation, five research groups mentioned before start the pneumatic hybrid technology research. In the next sections, the progress of each research group is reviewed separately.

2.3.2 Brunel University London

Cho-Yu et al. proposed a new pneumatic hybrid concept without using a fully variable valve actuation systems in 2009 [37]. In this new configuration, a Cam Profile Switching (CPS) system was utilized to control the active intake valve 6 as shown in Figure 2-2. The engine with the CPS system can operate as an air compressor or an air expander, in conjunction with a one-way valve in the intake port and an external air tank valve. The schematic diagram is showed in the Figure 2-2.

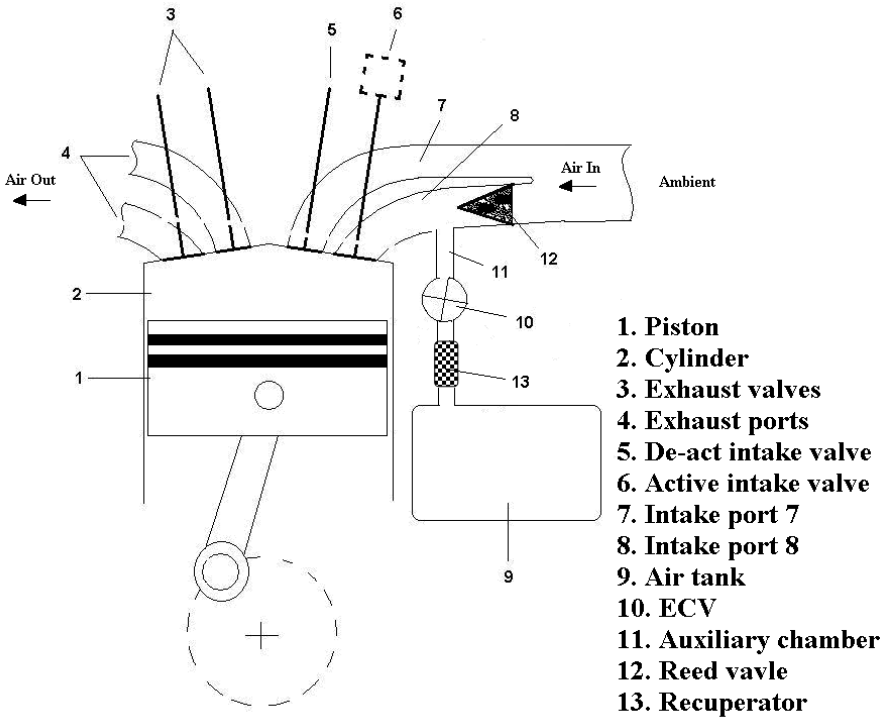

Figure 2-2 Schematic diagram of 1st Brunel pneumatic hybrid engine [37]

Analytical studies had been done to show that valves timings had significant effects on the performance of Compressor Mode (CM) and Expander Mode (EM) operations in this configuration. The closing timing of the active intake valve can be optimized for maximum braking work, while the closing timing of the Energy Control Valve (ECV) determines the expansion work during the EM operation. The ECV adopted a solenoid valve which was easy to control opening and closing timing. Positions of reed valve and the ECV also decided auxiliary chamber volume which also affected either CM or EM performance. Cho-Yu et al. reported the regenerative braking efficiency could be 14.38% to 15.18% while tank pressure works between 10 to 15 bar in such specific engine [37].

In 2010, Cho-Yu et al. proposed Brunel 2nd pneumatic hybrid system [36]. Figure 2-3 shows the Brunel 2nd pneumatic hybrid schematic system. From the figure, it can be learned that this system can be applied to an engine with either joint intake ports or separate intake ports.

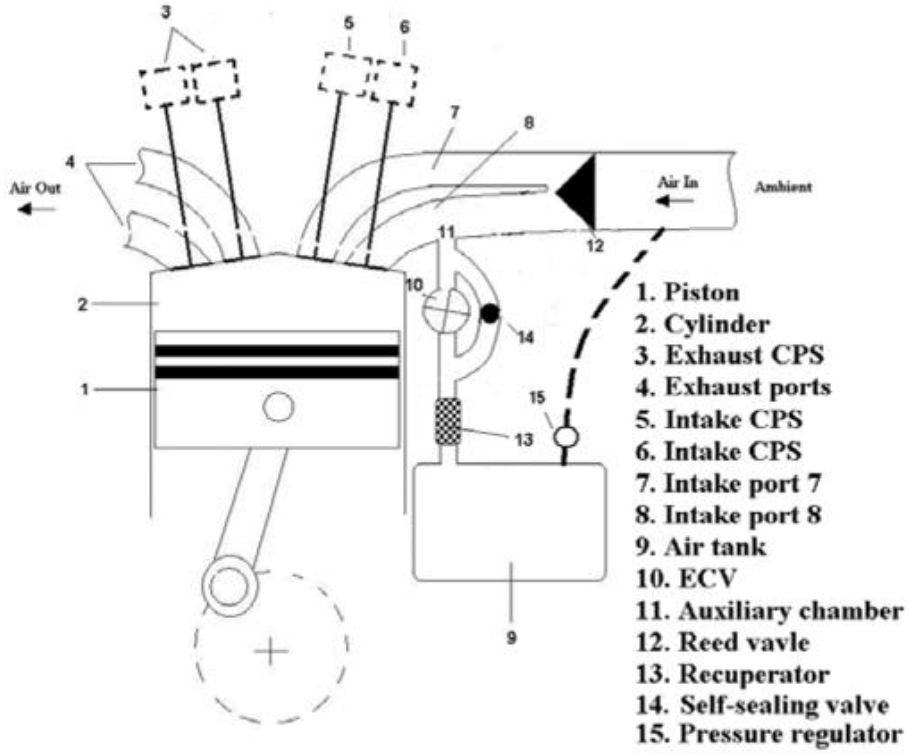

Figure 2-3 Schematic diagram of Brunel 2nd pneumatic hybrid engine [36]

Comparing to the first pneumatic hybrid system, the second pneumatic hybrid system had some changes. A one-way valve, the reed valve shown in Figure 2-3, connecting to each cylinder was in place of the port throttle valve. This one-way valve can be incorporated in a sandwich plate between the cylinder head and the intake manifold so that no modification to the cylinder head is required. The 2nd pneumatic hybrid system can charge a 40 litre air tank from 6.8 bar tank pressure to 8 bar tank pressure in 4.8 seconds in CM operation.

In 2011, Cho-Yu et al. proposed a novel cost-effective pneumatic hybrid powertrain concept for buses and commercial vehicles, Regenerative Engine Braking Device (RegenEBD) technology [35]. RegenEBD was designed to convert kinetic energy into pneumatic energy in the compressed air saved in an air tank. The compressed air can then be used to drive an air starter to achieve regenerative stop-start operations. As

shown in Figure 2-4, a standard production air starter can be readily employed to crank start the engine using the compressed air produced during the CM operation.

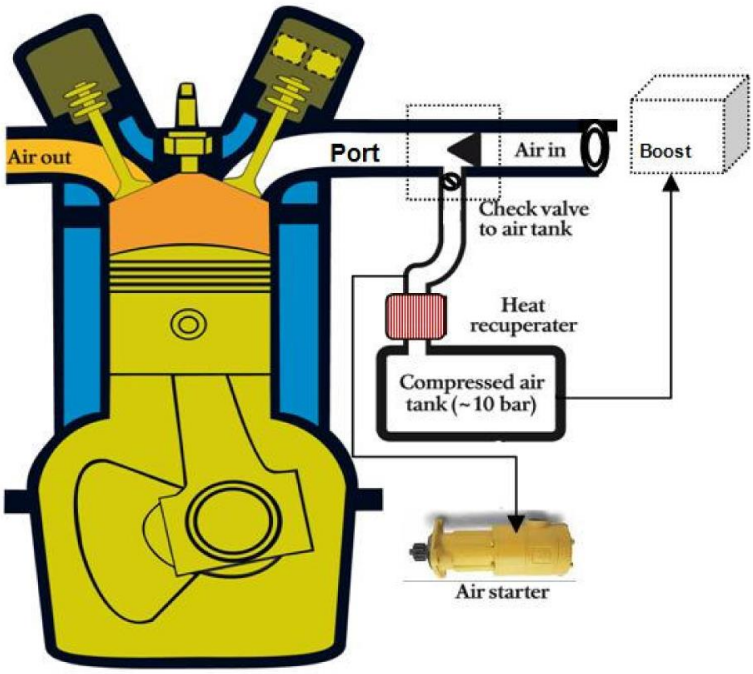

Figure 2-4 Schematic diagram of the air hybrid engine with an air starter [35]

The result showed that for a 151 litre air tank, it took 120 engine revolutions to charge the air tank pressure from 4 bar to 6 bar (4.8 seconds at 1500 rpm engine speed). A comparison of fuel consumption over the Millbrook London Transport Bus (MLTB) driving cycle between the standard vehicle and air hybrid vehicle was given out. Standard vehicle operation during the MLTB driving cycle consumed 3888.4 g of fuel. The pneumatic hybrid vehicle used 3645.4 g of fuel, which represents a 6.2% reduction in fuel consumption as a result of the regenerative stop-start operations [35].

2.3.3 ETH Zurich

Guzzella et al. proposed a pneumatic hybrid engine concept using an extra camless valve connecting the cylinder and the air tank to eliminate the need for a complete set of fully camless valves [40, 41]. As shown in the Figure 2-5, the intake and exhaust valves remained camshaft-driven.

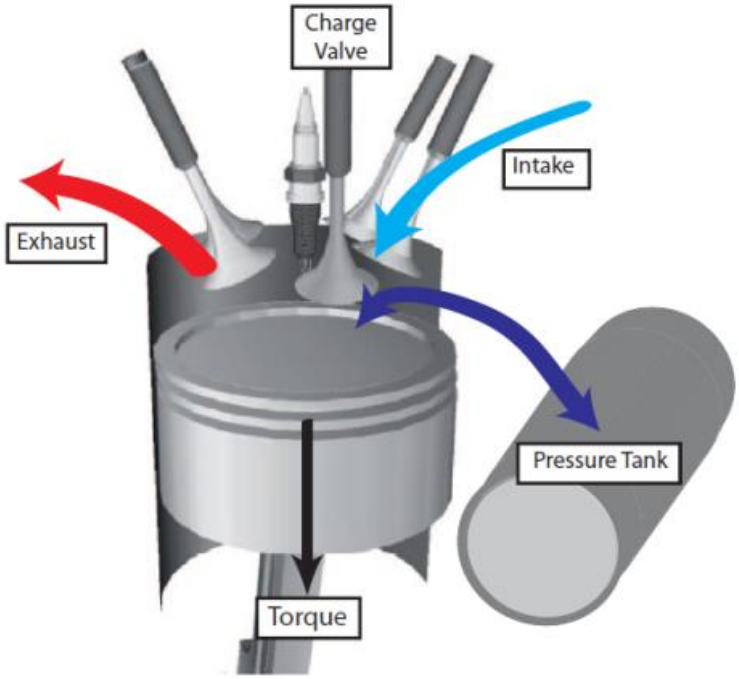

Figure 2-5 Schematic diagram of Guzzella's hybrid pneumatic engine [40]

Guzzella et al. indicated that the more efficiency method to use the compressed air in the air tank was to supercharge the engine, because they classified the air tank as an ultra-short term storage device due to the low energy density of pressurized air [40]. Their experiment showed that when the supercharged mode was activated, the torque reached 80 Nm, which is 1.8 times higher than the Naturally Aspirated (NA) engine at full load. The simulations showed compared to a NA engine with the same rated power, the downsized and supercharged pneumatic hybrid engine can save fuel as much as 32%. Their experiments had verified the engine instantaneous torque response resulting from applying this "supercharged" mode. Based on the result, Guzzella et al. concluded the best way to use the tank-pressurizes air was to supercharger the engine. In their opinion, since the engine can be supercharged even at low torque and speed, a lager engine can be downsized in an air hybrid powertrain and there is no need to design the engine turbocharger for an optimal dynamic performance [41]. Their other contributions included manufacturing the pneumatic hybrid engine and successfully operating it in all operation modes, including conventional mode.

Another paper, published by Guzzella et al. in 2009, focused on how to minimize fuel consumption by optimal using the energy stored in the air tank [42]. A deterministic

dynamic programming algorithm was implemented in this study to choose the mode of engine operation at every time instant of the driving cycle while guaranteeing charge sustenance. They concluded that the hybrid pneumatic engine concept based on fixed camshafts combined with a downsized engine has the potential to be more cost-efficient than fully variable hybrid pneumatic engines and hybrid electric propulsion systems. Obtained result showed that the combination of engine downsizing and pneumatic hybridization yields a fuel consumption reduction of up to 34% for the Motor Vehicle Emissions Group (MVEG) driving cycle [42].

2.3.4 Lund Institute of Technology

In 2005, Andersson et al. proposed a new pneumatic hybrid concept which had two air tanks [21]. The main difference between this novel pneumatic hybrid system and other pneumatic hybrid concepts was using a pressure tank a the supplier of low air pressure to instead of the atmosphere. By this modification, a very high torque can be achieved in Compression Braking (CB) mode as well as in Air Motor (AM) mode. The proposed configuration is shown in Figure 2-6.

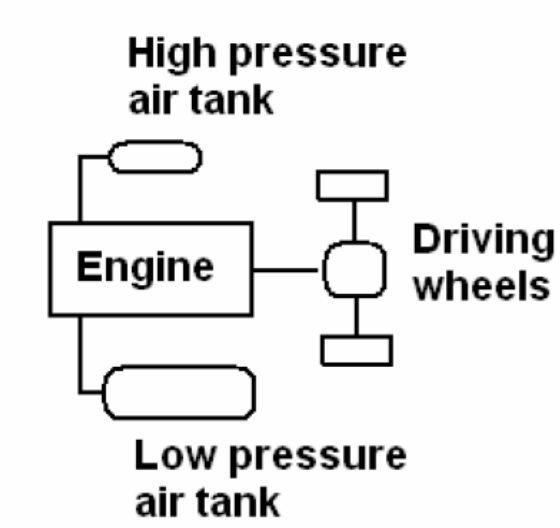

Figure 2-6 Pneumatic hybrid concept using two tanks [21]

The authors reported for a city bus driven according to the Braunschweig driving cycle, the reduction in fuel consumption is approximately 23%. Also, the simulations have shown that a fairly high proportion (approximately 55%) of the shaft work absorbed by

the engine during CB mode can be returned to the vehicle during acceleration in AM mode.

In 2007, Trajkovic et al. in the same research group converted a Scania D12 single-cylinder diesel engine to a pneumatic hybrid engine [46]. Pneumatic valve actuators mounted on top of the cylinder head of the engine had been used to make the pneumatic hybrid system possible. A pressure tank had been connected to one of the inlet ports and one of the inlet valves had been modified to work as a tank valve. They tested and studied two working mode, CB and AM and investigated the relationship between the Engine's Indicated Mean Effective Pressure (IMEP) and tank pressure with different valve timings and engine speeds at the AM and CB. They reported the maximum regenerative braking efficiency obtained in this study is 33% [46].

Trajkovic et al. published their second paper about the investigation on the same pneumatic hybrid engine in 2008 [45]. This paper described the introduction of new tank valve geometry to the system with the intent to increase the pneumatic hybrid regenerative efficiency. The new tank valve has a larger valve head diameter than the previously used setup described in [46], in order to decrease the pressure drop over the tank valve. The total regenerative braking efficiency had been increased from 33% with the small tank valve setup to 48% with the large tank valve setup, primarily due to a larger valve head diameter and optimal valve timing.

Later in 2010, Trajkovic et al. conducted a vehicle driving cycle simulation of the pneumatic hybrid [43]. The pneumatic hybrid powertrain had been modelled in GT-POWER and validated against the experimental data to generate the pneumatic hybrid powertrain performance maps. Based on the performance map, a driving cycle simulation model had been developed in MATLAB/Simulink to evaluate the fuel consumption. They reported that driving cycle simulations showed that fuel consumption can be reduced by up to 30% over the Braunschweig driving cycle. However, only regenerative braking accounts for about 10% of fuel consumption reduction, which corresponds to a regenerative braking efficiency of about 20%. The remaining 20% of fuel consumption reduction is due to stop-start functionality.

2.3.5 University of Orléans

In 2002, Higelin et al. published a paper to present a new hybrid pneumatic-combustion engine and the associated thermodynamic cycles [14]. The Pneumatic-hybrid configuration is shown in Figure 2-7. From the figure, it can be seen that their concept also had one additional valve, called the charging valve, connecting the combustion chamber of each cylinder to an air tank. This valve's opening and closing was driven by an additional camshaft. The energy, stored in the form of compressed air, can be issued from a braking phase or from a combustion phase at low power. The potential energy from the air tank can then be restored to start the engine, or charge the engine at full load. Higelin reported that regenerative breaking and the suppression of the idling phases could provide an improvement in terms of fuel economy as high as 15% or more if combined with engine downsizing.

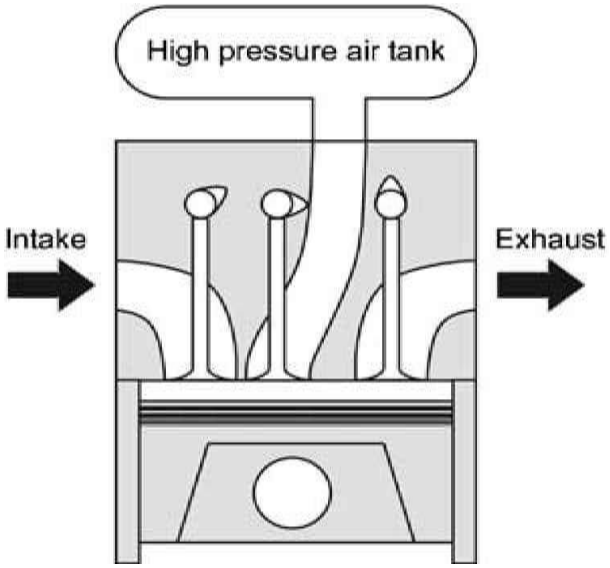

Figure 2-7 Schematic diagram of Higelin's hybrid pneumatic engine [14]

In 2004, Higelin et al. [19] published a paper to investigate the relationship between the operation parameters and fuel consumption by using the same engine model developed in [14]. They reported the global fuel consumption could be reduced by around 12% without any specific optimisation. By optimizing the tank maximum allowed pressure, the tank volume and the engine displacement, the global fuel economy during the driving cycle could be further improved to 31% compared to conventional operation.

In the paper Higelin et al. published at 2009, different energy management strategies for hybrid pneumatic engine concept were proposed and compared [52]. They provided a scale of the energy management strategies for the pneumatic hybrid engine working on the real-time environment and leading to the close to optimal fuel saving. They reported all strategies had provided significant fuel saving, and compared to the dynamic programming, which required the perfect knowledge of the future pattern, also close to optimal result [52]. It was also concluded that the strategy based on pattern recognition with an associated variable pattern coefficient was the one with the lowest fuel consumption, which was also the nearest of dynamic programming.

2.3.6 UCLA Research Group

In 2003, Tai et al. published a paper to describe the engine modifications, thermodynamics of various operating modes and vehicle driving cycle simulation and proposed a new pneumatic hybrid concept [17]. The engine design concept is illustrated in Figure 2-8. This paper explored the fuel economy potential of an air hybrid engine in a passenger car. It described the engine modifications, thermodynamic of various operating modes and vehicle driving cycle simulation. Unlike other pneumatic hybrid concept, in order to enable the air hybrid operation, two new systems had been incorporated, a camless electrohydraulic valvetrain and intake air switching. The modelling of the 1531 kg vehicle with the air hybrid engine resulted in fuel economy improvement of 64% and 12% in city and highway driving respectively, compared to the conventional baseline vehicle.

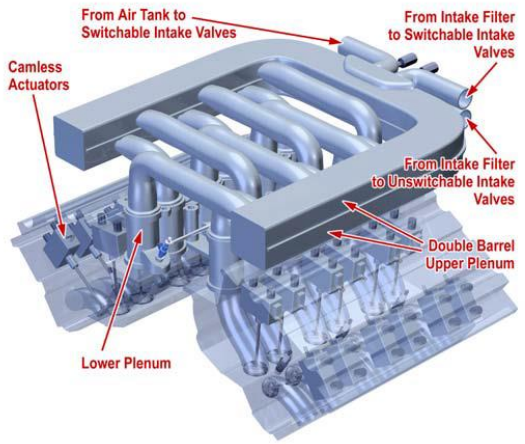

Figure 2-8 Schematic diagram of Tai's hybrid pneumatic engine [17]

In 2008, Kang et al. published a paper to describe a new air-power-assist engine technology in heavy duty application [24]. The air-power-assist engine concept is showed in Figure 2-9. The air-power-assist engine absorbed the vehicle's kinetic energy during braking, put it into storage in the form of compressed air, and reused it to assist in subsequent vehicle acceleration. They demonstrated that (i) the air-power-assist engine can compress air into high pressure air tank by controlling the valve timing and using the air handling system, (ii) the air compression mode efficiency had relationship with the valve timing optimisation, and (iii) the air-power-assist engine can generate positive power by using the compressed air from the air tank without injecting fuel.

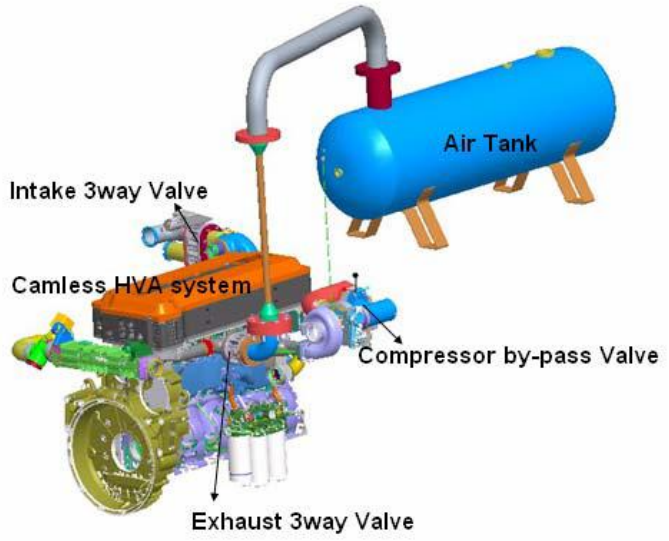

Figure 2-9 Schematic diagram of Kang's air-power-assist engine [24]

In 2009, Wang et al. published a paper to analyse the air cycles in a systematic way to understand the physics of the air hybrid operations and propose the optimal system operating strategies [65]. Their engine design, called MD11, is shown in Figure 2-10. The air handing system of the engine was modified to accommodate air flow in different directions under different running modes. The air handing system included three air switching valves: compressor bypass valve, intake three-way valve, and exhaust three-way valve. The proposed system was modelled using GT-POWER. Then, the GT-POWER model was used to generate optimal operating map for vehicle simulation. The vehicle simulation model was a backward-facing vehicle model and based on ADVISOR® Simulink package. Various driving cycles are used to evaluate the fuel economy improvement of

the garbage refuse truck equipped with the air hybrid engine. The fuel economy improvement ranged from 4% to 18% and it strongly dependent on the driving cycles.

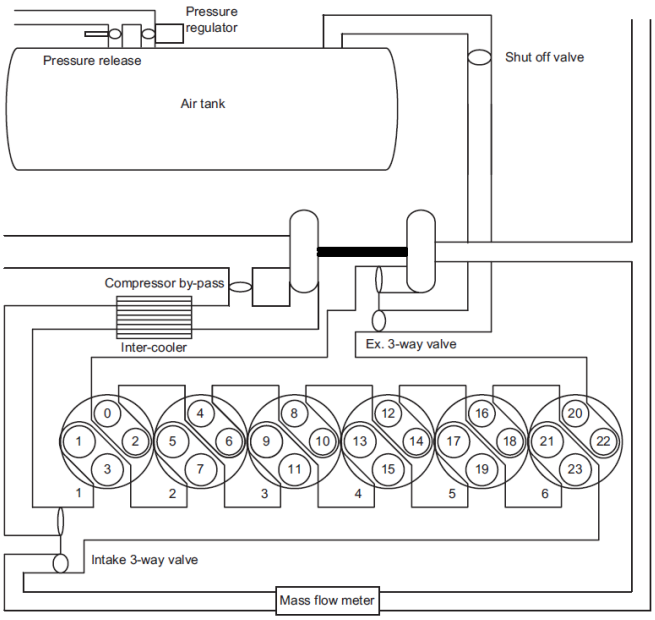

Figure 2-10 MD11 air hybrid configuration [65]

2.3.7 Fuel Consumption Result Comparison and Analysis

Table 2-1 shows a comparison of result of the fuel consumption from different research group. In this table, the different research results are not directly compared because of different assumptions and constraints. But it still gives a rough overview of the magnitude of the expected fuel savings. From the table, it can be seen that the total fuel gains in the range of 4% to 50% can be expected depending on the vehicles and drive cycles used. Also it demonstrates that most of the benefit may come from the engine downsizing. This is because some research groups focus on using the pneumatic hybrid technology to run the engine at air motor mode or air power assist mode. In these two modes, the recover air in the air tank power the engine to start the engine alone or assist the engine during the acceleration. As a result, the engine displacement can be decreased to save fuel consumption. If only considering using the pneumatic hybrid technology as a micro hybrid to realize the Stop-Start function, the fuel consumption improvement is in the range of 6% to 20% depending on the vehicles and test cycles used. In addition, some research group indicated that a part of fuel consumption

reduction is due to the increased transmission efficiency caused by the possibility to operate the engine at very low rotational speed in CB and AM mode.

Table 2-1 Summary table of fuel consumption result

Research Group	Year	Engine	Vehicle	Tank Size	Maximum Tank Pressure	Fuel Consumption Reduction		Test cycle
Michael M. Schechter	1999	2 l Gasoline	1360 kg Car	36.2 l	-	Total Stop-Start Engine Downsizing	50% - -	45 s city driving cycle
Brunel University London	2011	7.25 l Diesel	16500 kg Bus	151 l	10 bar	Total Stop-Start Engine Downsizing	6.2% 6.2% 0	MLTB
ETH Zurich	2009	2 l Gasoline	1450 kg Car	30 l	24.2 bar	Total Stop-Start Engine Downsizing	34% 6% 28%	MVEG-95
Lund University	2005	11.7 l Diesel	15000 kg Bus	143 l 600 l	- -	Total Stop-Start Engine Downsizing	23% - -	Braunschweig
Lund University	2010	12 l Diesel	15000 kg Bus	40 l	27 bar	Total Stop-Start Engine Downsizing	28% 20% -	Braunschweig
University of Orléans	2003	2 l Gasoline	800 kg Car	50 l	20 bar	Total Stop-Start Engine Downsizing	31% - -	NEDC
UCLA	2003	2.5 l	1531 kg Car	65 l	24 bar	Total City Highway	- 64% 12%	FTP
UCLA	2008	10.8 l	Garbage refuse truck	280 l	15 bar	Total Stop-Start Engine Downsizing	4-18% - -	Different test cycles

2.4 Summary

In this chapter, a literature view about the pneumatic hybrid engine concepts was presented. By summarizing the research before, it can be learned that there are several research topics are not investigated or deeply studied before:

(i) Thermodynamic analysis of the operation of the pneumatic hybrid engine to supply an understanding of the sensitivity of the work done to design parameters.

(ii) How to implement the pneumatic hybrid powertrain to an appropriate braking system to maximize the energy recovery efficiency during braking.

(iii) Understanding of the contribution of the pneumatic hybrid powertrain to vehicle braking and how the braking effect in alongside friction braking.

(iv) Understanding of the contribution to fuel economy and performance made by the development of pneumatic assistant in accelerating the turbocharger.

(v) Detailed investigating how to reduce turbo-lag and improve engine transient response by pneumatic hybrid technology.

(vi) Using forward-facing simulation to evaluate the fuel economy improvement by pneumatic hybrid technology.

(vii) Develop a pneumatic hybrid vehicle control algorithm to realize the energy storage and regeneration as well as the normal operation of the vehicle.

(viii) Identify the relationship between hybrid powertrain operating parameters, fuel consumption and energy usage according to optimisation criteria.

The research topics above have been detailed investigated in this research. Topic (i) has been investigated in Chapter3. Topic (ii-iii) has been studied in Chapter 5. Topic (iv-v) has been analysed in Chapter 6. And Topic (vi-viii) has been researched in Chapter 7.

CHAPTER 3

PRINCIPLES OF PENUMATIC HYBRID ENGINE

3.1 Introduction

This investigation into the pneumatic hybrid concept is based on the YUCHAI YC6A diesel engine. The intention of this chapter is to present the principles of operation and to confirm the potential of the new systems to both generate a supply of compressed air and to manage the contribution of the engine to vehicle braking.

The Chapter is arranged as follows:

(i) The engine and a series of proposed modifications are described in detail to explain the pneumatic hybrid engine operating process.
(ii) The pneumatic hybrid engine CM is considered from a theoretical perspective based on an air cycle analysis.
(iii) Based on this analysis, the implementation of a single cylinder model in CM operation is described and demonstrated. The model is validated by means of an independently developed model using the GT-POWER engine simulation code.
(iv) Results from the model show the effect of respectively the air tank pressure, engine speed, intake valve second opening time and actual compression ratio are studied using the model. (Note that the actual compression ratio R_c decrease from the geometric compression ratio as the volume of the auxiliary chamber is included in the cylinder's total clearance volume when the engine is in CM.)

3.2 Pneumatic Hybrid Engine Concept

3.2.1 Configuration of the Pneumatic Hybrid Engine

The YUCHAI YC6A six cylinders 7.25 l diesel engine commonly used in passenger bus and freight vehicle applications provides the engine technology context for the work that is the basis of this thesis. The YC6A engine is a typical engine in this class and it has no

doubt that the results derived from this engine can be extended to other medium and heavy duty engines. Figure 3-1 shows a schematic diagram of this engine. A split intake port provides a flow path to the air tank. In normal operating mode, a Throttle Valve (TV) located in the intake port will be fully opened. Air flows through the intake valves via separate intake ports during the intake stroke and leaves exhaust ports during the exhaust stroke. One of the intake valves is equipped with a Compression Release Engine Braking (CREB) device normally used on the exhaust valve for the purpose of engine braking [34], named CREB intake valve here. When the vehicle brakes and the CM is selected, fuel supply is cut. With the clutch engaged, the engine has now become a compressor to provide regenerative braking to recover the energy by converting a proportion of the vehicle kinetic energy to the internal energy of pressurised air in the air tank.

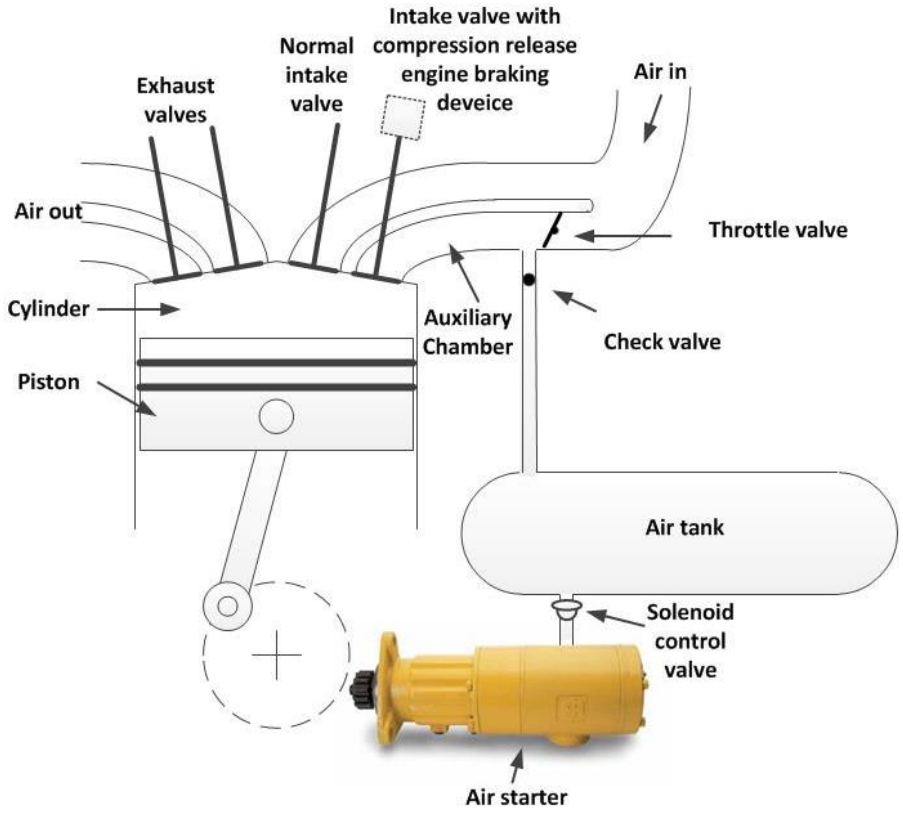

Figure 3-1 Schematic diagram of the pneumatic hybrid engine

In CM operation, during the compression stroke, the CREB intake valve is opened and the air is compressed into the intake port. At the same time, the throttle valve is fully closed to prevent compressed air escaping into the intake manifold. The Check Valve (CV) which seals the air tank will open when the intake manifold pressure is higher than the tank

pressure. The air will be compressed into the air tank. The air tank has the same construction as the standard one on commercial vehicles or buses with a peak pressure of 10 bar which is limited to this value for safety reasons. The auxiliary chamber is a small chamber which accommodates the CREB intake valve, CV and TV. All engine cylinders are equipped with the same valves and porting as shown in Figure 3-1. The engine and the pneumatic hybrid system main technical parameters are summarized in Table 3-1.

Table 3-1 Main technical parameters of the engine and pneumatic hybrid system

Displacement (l)	7.25
Electronic control system	High pressure & common rail
No. of Cylinders (-)	6
Bore (mm)	108
Stroke (mm)	132
Compression ratio (-)	17.5:1
Intake way	Turbo-charging & inter-cooling
Rated power/speed (kW/rpm)	177/2300
Max torque/speed (Nm/rpm)	900/1400~1600
Intake valve (-)	2
Diameter (mm)	32.5
Opening point (normal)	61°BTDC
Closing point (normal)	91°ABDC
Exhaust valve (-)	2
Diameter (mm)	29.5
Opening point (normal)	105°BBDC
Closing point (normal)	67°ATDC
Air tank volume (l)	151

In this research, the air tanks are uninsulated. A simulation is conducted by Lee et.al to compare the air tank temperature change between an insulated air tank and an uninsulated air tank using the same engine used here [34]. The result is shown in Figure

3-2. It shows the compressed air temperature in an insulated air tank and an uninsulated air tank against engine revolutions. In the case of an insulated air tank, the zero value of the wall heat transfer is applied to assume it is in adiabatic condition. From Figure 3-2, it can be seen that the compressed air reaches 795 K after a charging process of 800 engine revolutions at 1500 rpm in the insulation air tank. In the normal tank without insulation, the compressed air temperature reaches the ambient temperature after 1200 engine revolutions at same engine speed.

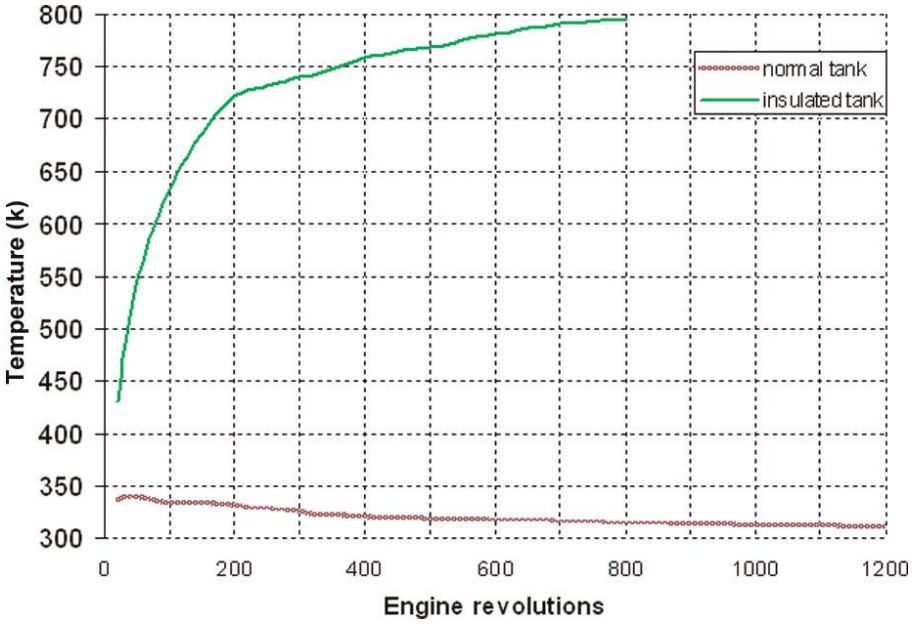

Figure 3-2 Tank temperatures for 1500 r/min engine speed [34]

Lee et.al also evaluated the air tank temperature for the pneumatic hybrid engine by comparing the experimental and predicted results [4]. The 13 l air tank was charged at 1500 rpm for 700 engine revolutions. The result is shown in Figure 3-3. It indicates that the difference between the experimental and predicted temperature is less than 5 K.

In fact, it would be ideal to store both the pneumatic and thermal energy in the form of hot compressed air in an adiabatic air tank or through a heat recuperator. The hot compressed air can then be used to restart the engine [34]. However, the maximum operating temperature of the current air starter is limited to 100°C [34]. Therefore, in the subsequent research, the pneumatic hybrid powertrain will be modelled with an uninsulated air tank in order to produce more realistic results.

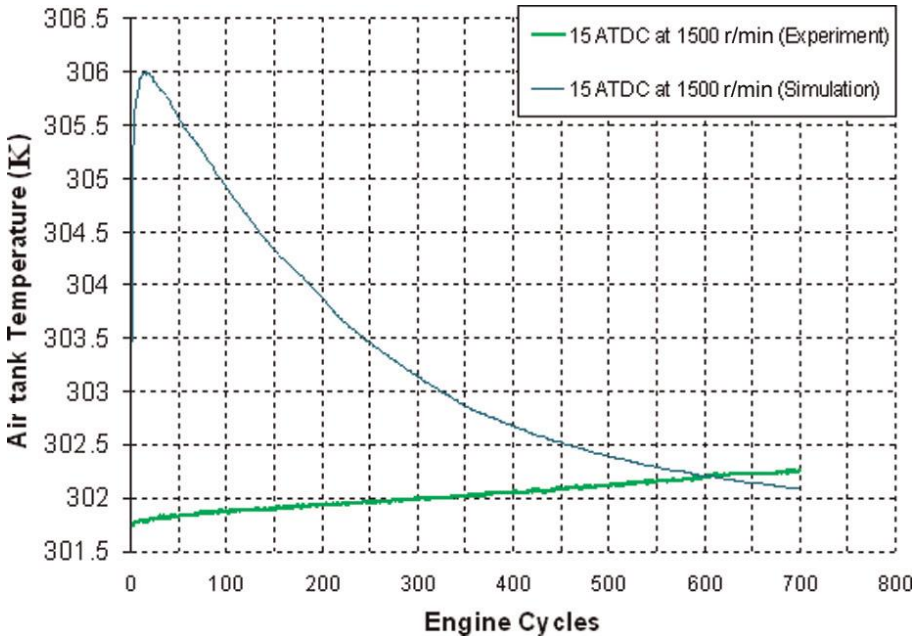

Figure 3-3 Experimental and predicted air tank temperature at 1500 r/min engine speed for 700 engine cycles [4]

3.2.2 Principle of Operation

Figure 3-4 shows the valve timing diagram for the normal mode and CM. During the normal mode, the CREB intake valve operates as an intake valve whose lift profile is exactly the same as another intake valve of the same cylinder. In order to keep the air flow rate in the intake manifold as high as possible, the throttle valve is always opened to its maximum value during normal operation.

During vehicle deceleration and braking, the engine becomes a compressor and no fuel is injected into the cylinders. In all cylinders, intake valves are opened to let the air into the cylinder during the intake stroke. Then the normal intake valve is closed and as the piston passes Bottom Dead Centre (BDC) and would normally begin the compression stroke, the CREB intake valve opens to allow air to enter the auxiliary chamber. At the same time, the throttle valve is closed and the check valve opened. Air is compressed into the air tank.

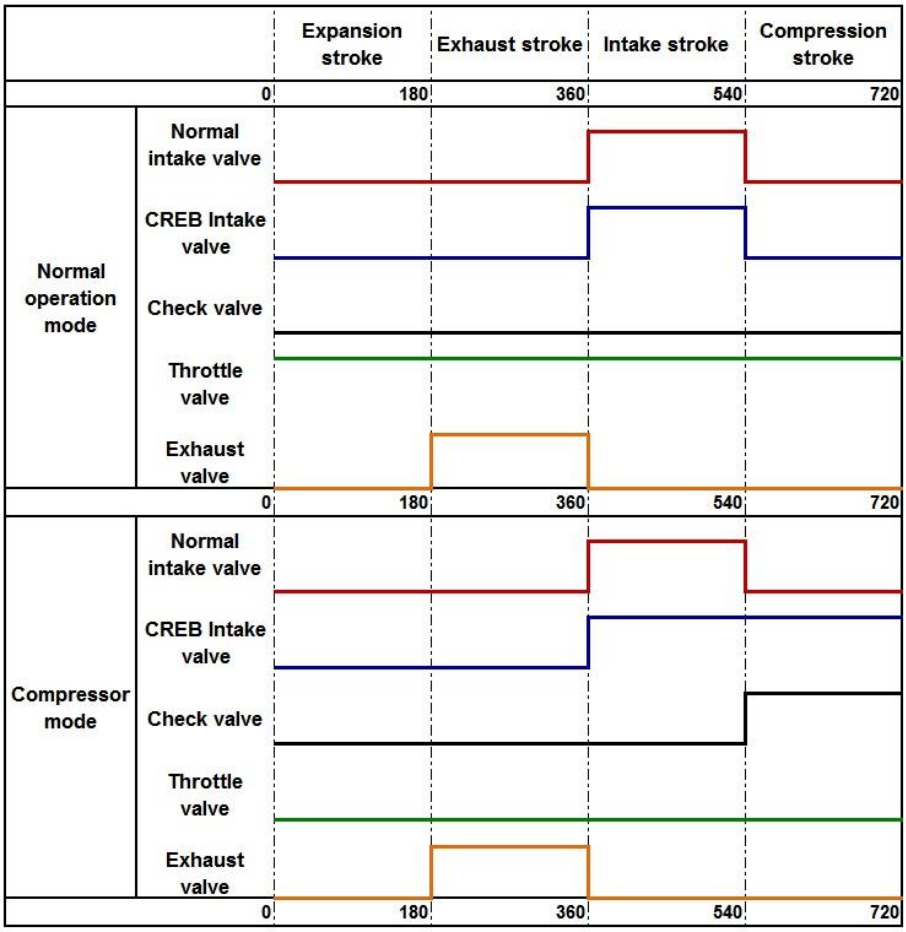

Figure 3-4 Theoretical valve timing diagram of the normal operation mode and CM

The compressed air can be used to start the engine by controlling the engine to work as an air motor, which requires using six bi-directional solenoid valves instead of the check valves. When air motor mode is activated, the solenoid valves open to let the air go from the air tank to the cylinders during the intake stroke. The high pressure air will produce a positive torque that will propel the pistons to cranking the engine. At the same time, by synchronizing the firing order of six cylinders, the engine can be started. But to realize this function, the engine will require six bi-directional solenoid valves leading to a complex control system and strategy. In order to simplify the structure, an air starter is chosen controlled by a solenoid valve. When the regenerative stop-start operation is activated, this valve opens to let the air starter start the engine. Compared to the direct use of compressed air to crank start the engine, the employment of an air starter is a much simpler system and easier to implement, by dispensing with the need of fast acting solenoid valves and sophisticated controls [4].

The size of the auxiliary chamber of this engine, is an important design parameter that affects the efficiency of the CM. The size of this chamber depends on the positions of the CV and TV [10]. The compression ratio of this engine changes when working in CM because of the additional volume of the auxiliary chamber is added in. The actual compression ratio R_c of CM for the engine using in this research is calculated by Lee et al. which is 5.3:1 [10]. In the later section, how the actual compression ratio affecting the CM performance will be discussed in detail.

3.3 Pneumatic Hybrid Engine Compressor Mode

During vehicle braking, when the CM is activated, the engine operates as a compressor driven from the wheels by vehicle motion and pumping compressed air into the air tank. Work done by the pistons causes the vehicle to decelerate, converting a proportion of its kinetic energy into the energy of compressed air. To fully understand the physics of the CM operation, the thermodynamic cycle of a one cylinder engine will be described and analysed. Based on the analysis, engine performance, brake torque, air tank pressure and valves timing can be calculated as a function of engine speed.

3.3.1 Theoretical Analysis of the Pneumatic Hybrid Engine Compressor Mode

Unlike most pneumatic hybrid engines that operate two strokes to recover the energy during the air compress mode [63, 65], the pneumatic hybrid engine used in this research continues to follow four-stroke operation during CM. The four strokes in CM are Intake Stroke, Compression Stroke, Expansion Stroke and Exhaust Stroke. Figure 3-5 illustrates the ideal *p*-*V* (pressure-volume) diagram of this cycle, which shows the pressure variation in the cylinder as a function of the piston position. In this diagram, V_s is the cylinder swept volume, V_c is the cylinder clearance volume, V_{aux} is the volume of the auxiliary chamber, p_0 is the pressure of the intake manifold, and p_t is the air tank pressure.

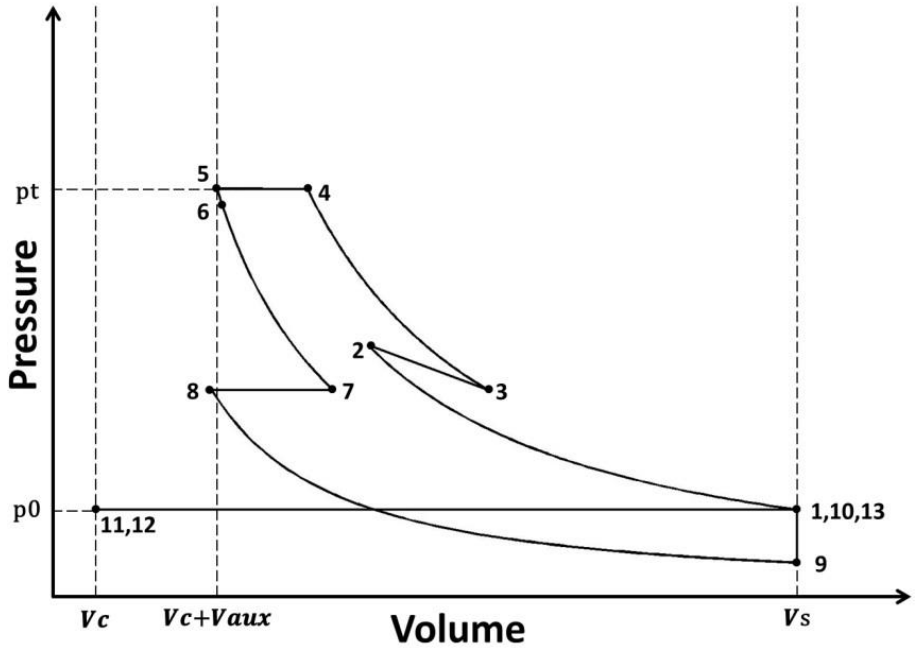

Figure 3-5 Ideal *p-V* diagram during the CM

The following assumptions simplify the analysis process without undermining the accuracy.

(i) Valves open and close instantaneously. (Valves moving speed is fast compared with piston motion.)

(ii) Filling and emptying proceeds rapidly to equilibrium without losses. (At normal operation speed, gas flow is rapid compared with position motion.)

(iii) Intake and exhaust pressure constant during valve events. (Both pressures vary slightly compared with variation of cylinder pressure.)

Compression Stroke

The Compression Stroke (1-5) comprises four distinct stages during piston movement from BDC to Top Dead Centre (TDC).

Stage 1-2: Starting with the piston at BDC (point 1), finishing with the inlet valves open (point 2). From point 1 to point 2, the intake valves and exhaust valves are all fully closed as shown in the Figure 3-6. The piston on its rising stroke will compress the air and the pressure in the cylinder increases. (Note that the CREB intake valve opens at point 2.)

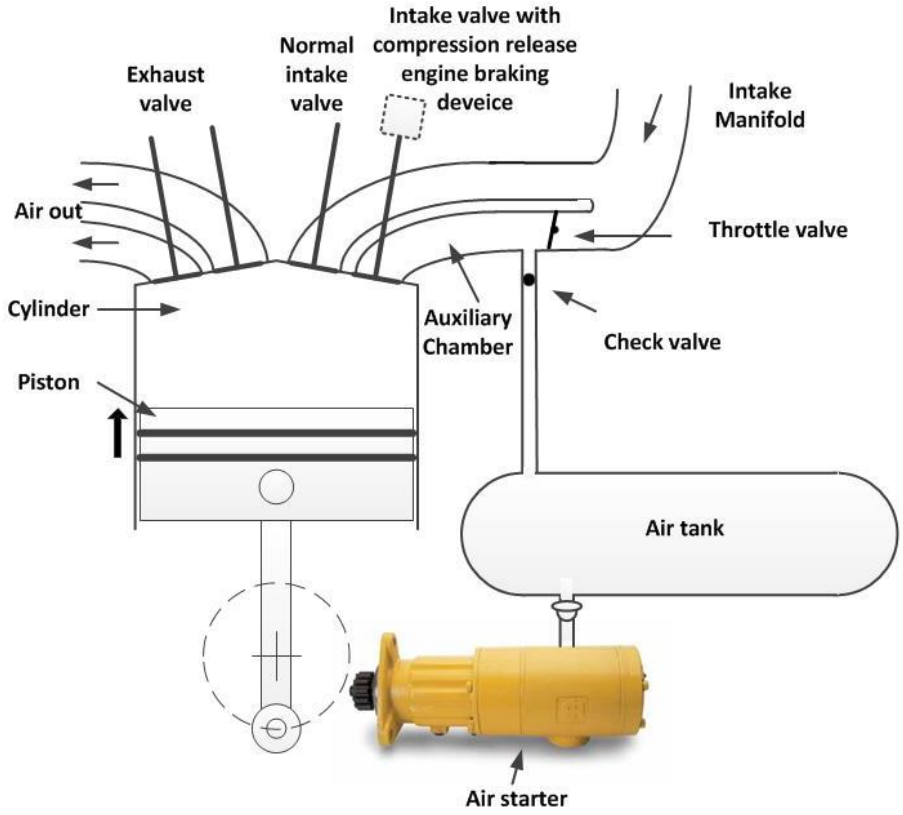

Figure 3-6 Schematic diagram of the start of the Compression Stroke in CM

Stage 2-3: The CREB intake valve opens again at point 2, while the CV and the TV are closed, as shown in Figure 3-7. At this point, the working volume is increased by the additional volume of the auxiliary chamber. Because before the CREB intake valve second open, the pressure in the auxiliary chamber is constant. Furthermore, it is assumed that the valve open instantaneously. As a result, at the CREB intake valve opening point, the pressure of the cylinder is higher than the pressure of the auxiliary chamber. Once the CREB intake valve open, the high pressure air in the cylinder flow to the auxiliary chamber which cause a pressure drop from point 2 to point 3. It is shown on the *p*-*V* diagram as an increase in volume and a decrease in pressure. In fact, it should always keep the air pressurized during the work stroke. But the CREB intake valve cannot be always open. Furthermore, although the pressure is drop, the CREB intake valve open again increase the air mass being compressed. This is because the air in the auxiliary chamber is added to be compressed by the piston.

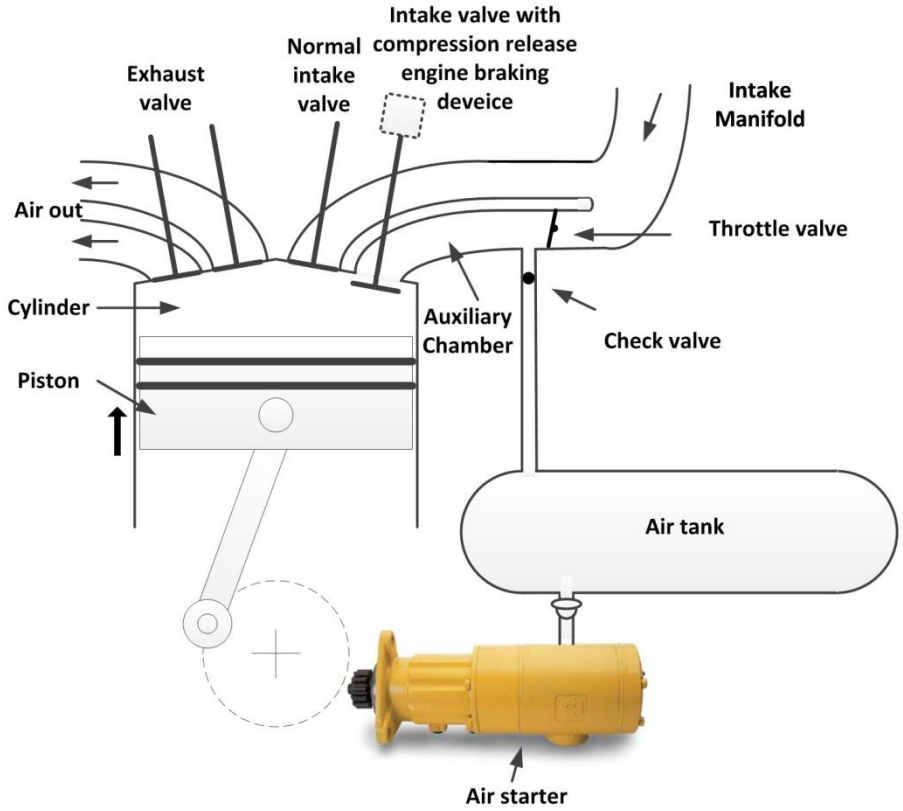

Figure 3-7 Schematic diagram of the CREB intake valve opens during the Compression Stroke in CM

Stage 3-4: From point 3, the piston continues its upward motion to compress the air. The effective compression ratio of the cylinder decreases as according to the volume of the auxiliary chamber that is added to the cylinder's clearance volume.

Stage 4-5: At point 4, when the pressure in the cylinder and the auxiliary chamber is equal to the pressure in the air tank, the CV opens as shown in Figure 3-8. The air starts to be compressed into the air tank. During this stage, the piston continues to move upwards until the pressure reaches its peak. At point 5, the piston reaches TDC at which point the compression stroke is complete.

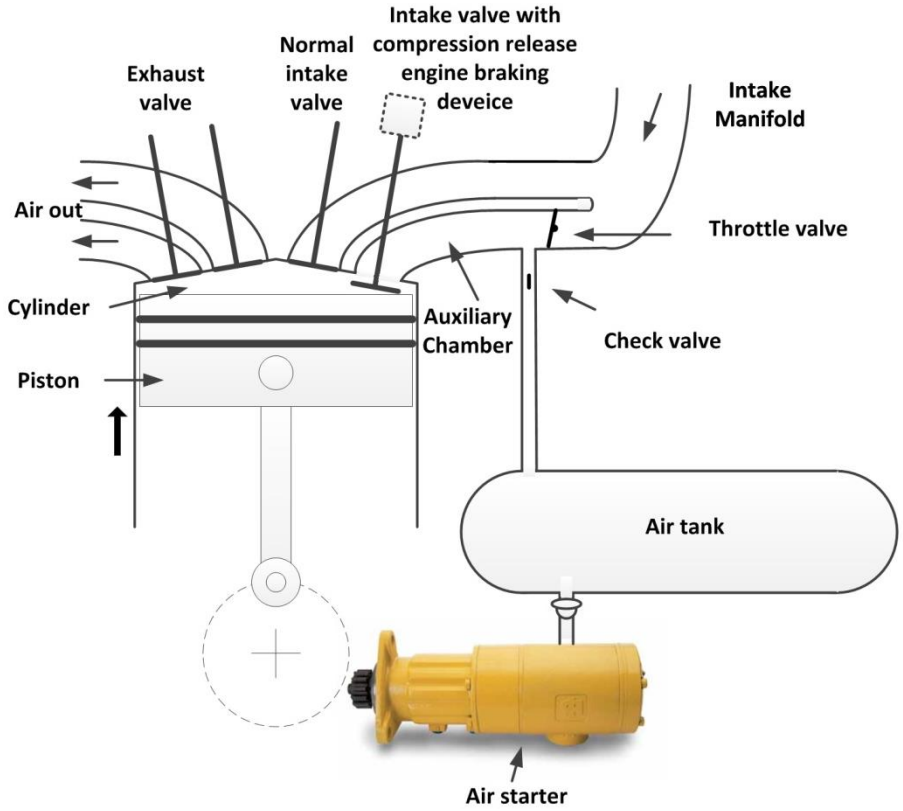

Figure 3-8 Schematic diagram of the end of the Compression Stroke in CM

Expansion Stroke

The Expansion Stroke (5-9) includes four stages between piston's down-stroke from TDC to BDC.

Stage 5-6: From point 5, the piston continues the downward motion. At point 6, the pressure in the cylinder and the auxiliary chamber drop below the pressure in the air tank. The CV automatically closes.

Stage 6-7: From point 6, the piston continues to move down and the pressure decreases. At point 7, the CREB intake valve closes.

Stage 7-8: At point 7, with the inlet valve closed, the working volume decreases to the cylinder clearance volume. Because of the assumption that the valve closes instantaneously, the cylinder pressure does not change after the intake valve closure either in the cylinder or in the auxiliary chamber. The line from point 7 to 8 reflects the decreased volume on the *p*-*V* diagram.

Stage 8-9: The piston continues its down-stroke until reaching the BDC at point 9. The Expansion Stroke ends at point 9.

Exhaust Stroke

The Exhaust Stroke starts at point 9, and ends at point 11. At point 9, both exhaust valves fully open, the pressure in the cylinder increase to the exhaust manifold pressure suddenly at point 10, then the exhaust valve is fully closed at point 11.

Intake Stroke

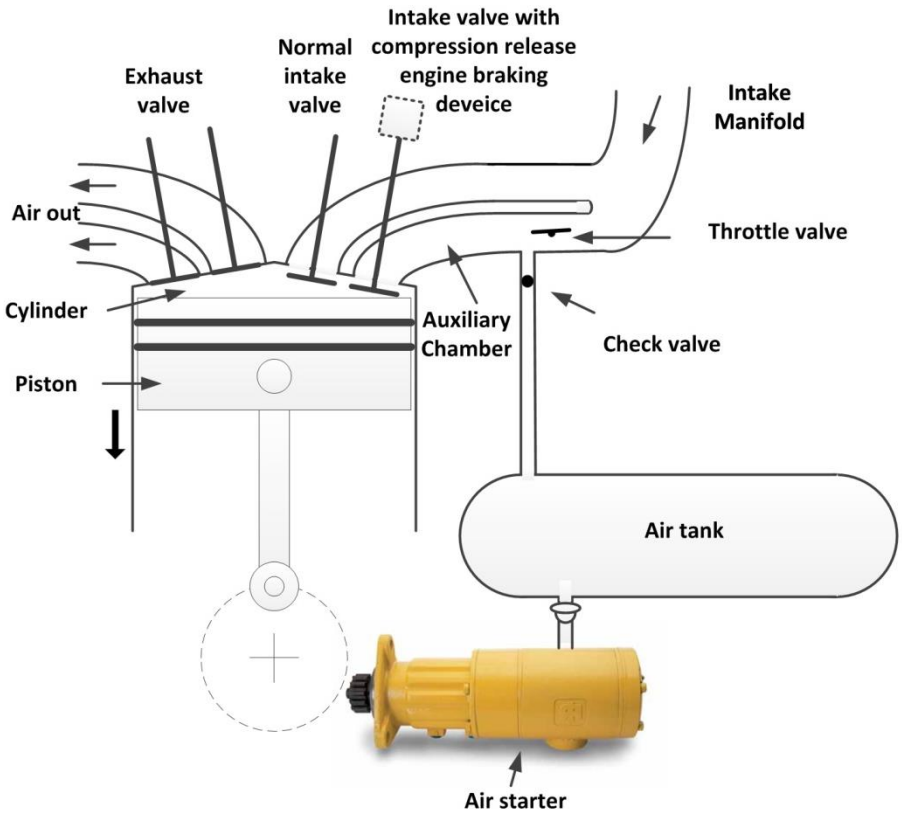

Figure 3-9 Schematic diagram of the start of the Intake Stroke in CM

At point 11, both two intake valves and TV are fully open as shown in Figure 3-9. The pressure in the cylinder remains constant and is equal to the pressure in the intake manifold. Then at point 13, these three valves are fully closed.

The above account is about an ideal thermodynamic analysis with gas exchanges from the intake manifold into the cylinder, from the cylinder into the auxiliary chamber, from the auxiliary chamber to the air tank and from the cylinder to the exhaust manifold

taking place in a reversible manner. In practice, this can never be realised, but sets an ideal against which actual performance can be judged.

If only the pressure in the cylinder is considered, the *p*-*V* diagram will transform to the diagram shown in Figure 3-10. In Figure 3-10, the solid line indicates the pressure change in the cylinder, while the dashed line shows the pressure variation in the volume that additionally includes the auxiliary chamber. From Figure 3-10, at point 4 when the check valve opens, because of the pressure drop of the CV, the pressure in the cylinder cannot be equal to the pressure in the air tank. As a result, the pressure in the cylinder continues to rise up as the piston goes up until TDC. Point 5 shows the upper bound of the pressure variation at the end of the position rising up stroke which is the maximum pressure can be achieved.

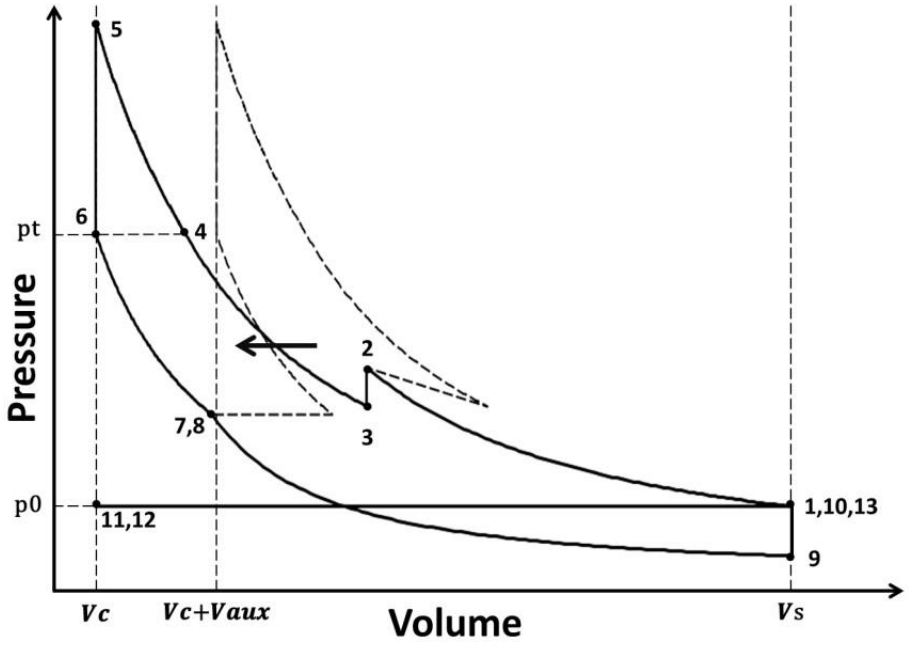

Figure 3-10 Modified *p*-*V* diagram during the CM

Based on cycle shown in Figure 3-10, the thermodynamic analysis of the CM, where the control volume is bounded by the piston, cylinder walls and the auxiliary chamber is shown in Figure 3-11, is presented in the next section of this Chapter.

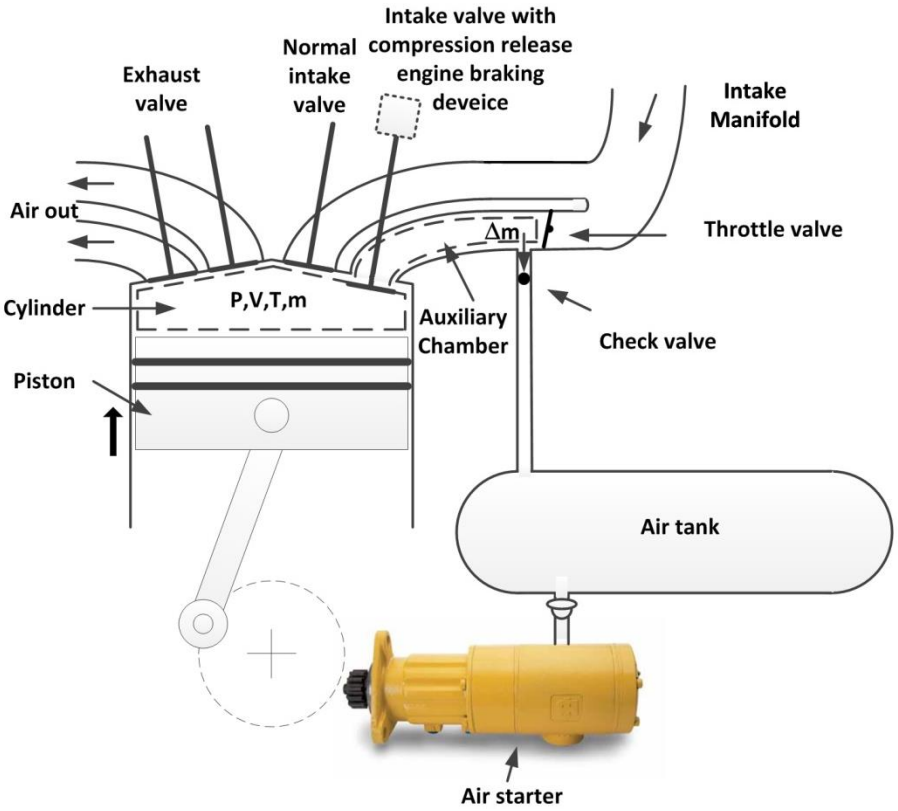

Figure 3-11 Schematic diagram of the control volume

Firstly, the relations between the gas mass *m* and the state variable pressure *p*, temperature *T* and volume *V*, are determined by the ideal gas equation of state as

$$pV = mRT \tag{3-1}$$

where *R* - ideal gas constant.

Secondly, for the polytropic compression or expansion that takes place during the cycle, the work, final pressure, volume and temperature can be obtained by

$$p_{final} = p\left(\frac{V}{V_{final}}\right)^{n} \tag{3-2}$$

$$V_{final} = V\left(\frac{P}{P_{final}}\right)^{1/n} \tag{3-3}$$

$$T_{final} = T\left(\frac{V}{V_{final}}\right)^{n-1} \tag{3-4}$$

$$W = \frac{pV^{n}\left(V^{1-n} - V_{final}^{1-n}\right)}{(n-1)} \tag{3-5}$$

where p_{final} – final pressure,

p – initial pressure,

V – initial volume,

V_{final} – final volume,

W – work done during the compression or expansion,

n – polytropic index.

Thirdly, for the final volume of polytropic compression like stage 1-2, can be obtained by

$$V_{final} = \frac{(D-IVSC)V}{180} + \frac{(180+IVSC-D)V_c}{180} \tag{3-6}$$

where D – duration of the CREB intake valve second opening in crank angle,

$IVSC$ – CREB Intake Valve Second Close (IVSC) time after TDC,

V – initial volume,

V_c – cylinder clearance volume.

This is because, at point 2, the CREB intake valve opens again to let the air start to be compressed into the auxiliary chamber which is governed by the intake valve second opening timing.

For the compression stage 4-5, because of the check valve open, the air is compressed into the air tank through the check valve. The air flow through the check valve can be obtained by

$$\dot{m} = c_d A\sqrt{2\rho}\sqrt{p_{in} - p_{out}} \tag{3-7}$$

where $\dot{m}$ – mass flow through the valve,

A – open area of the valve,

C_d – discharge coefficient,

ρ – density of the air,

p_{in} – pressure upstream of the valve

p_{out} – pressure downstream of the valve.

The mass remained in the control volume can be expressed as

$$m_5 = m_4 - \dot{m}t \tag{3-8}$$

where m_5 – air mass at point 5,

m_4 – air mass at point 4,

$\dot{m}$ – mass flow through the valve,

t – time that check valve open.

Then, for the stage 2-3 and 9-10, because the valve is assumed to be ideal which opens instantaneously, these two expansions can be considered as a constant-volume process. The work done by these two stages is equal 0.

For the stage 10-11 and 12-13, because it assumed that the air filling into and discharging from the cylinder to the exhaust and intake system reaches equilibrium rapidly and without loss, these two stages can be considered as an isobaric process. The work done on the system by the piston during these two stages can be obtained by

$$W = p\left(V_{final} - V\right) \tag{3-9}$$

Finally, the indicated work $W_{c,i}$ done by the piston on the gas during one engine cycle in one cylinder is

$$W_{c,i} = \oint p\, dV \tag{3-10}$$

If it is assumed that the pressure recorded by the indicator diagram is the same as the pressure which acts on the piston face [66]. Here, the indicated work $W_{c,i}$ is equal to the total of the work done in the each stage:

$$\begin{aligned} W_{c,i} = {} & W_{1-2} + W_{2-3} + W_{3-4} + W_{4-5} + W_{5-6} + W_{6-7} + W_{7-8} \\ & + W_{8-9} + W_{9-10} + W_{10-11} + W_{11-12} + W_{12-13} \end{aligned} \tag{3-11}$$

Based on Equations (3-1) to (3-11), the indicated work for the cycle $W_{c,i}$ can be calculated.

IMEP (p_{mi}) is a measure of the indicated work output per unit swept volume of one cylinder ($V_{c,h}$), in a form independent of engine size and engine speed.

$$p_{mi} = \frac{W_{c,i}}{V_{c,h}} \tag{3-12}$$

The indicated power P_i of the engine is

$$P_i = \frac{p_{mi} V_{c,h} iN}{n_R} \tag{3-13}$$

where n_R – number of the crank revolutions for each power stroke per cylinder which 1 for two-stroke and 2 for four-stroke engines,
i – number of the cylinders,
N – engine speed.

The effective power differs from the indicated power essentially in the frictional losses (piston, bearings), the power-transmission losses from the control elements (camshaft, valves), and the power of the accessories (oil, water and fuel injection pumps, alternator).

For the mechanical efficiency:

$$\eta_m = \frac{P_e}{P_i} \tag{3-14}$$

where P_e – measured power output.

Normal mechanical efficiencies are load-dependent and at full load are typically about 90%, while at low part load (10% load) about 70% [67]. Therefore, the measured power of the engine is

$$P_e = P_i \eta_m \tag{3-15}$$

Hence, the brake torque T is:

$$T = \frac{60 \cdot 1000}{2\pi} \frac{P_e}{N} = \frac{9549 P_e}{N} \tag{3-16}$$

Here, the brake torque of the engine during the vehicle braking can be calculated out.

3.3.2 Pneumatic Hybrid Engine Compressed Mode Model Validation and Performance Analysis

3.3.2.1 Model Validation

Based on the theoretical analysis above, a program in Matlab, called *Theoretical model* here, which can simulate the performance of the engine CM under different conditions, is coded and introduce in Appendix-I. To validate the theoretical model, the result of a one

cylinder prototype pneumatic hybrid engine model is built in the engine simulation code, GT-POWER, and the results compared with the theoretical model result. The parameters setting of the simulation is shown in the Table 3-2 for both GT-POWER and theoretical models.

Table 3-2 Parameters setting of the simulation

Bore (mm)	108
Stroke (mm)	132
Diameter of the intake valves (mm)	32.5
Diameter of the exhaust valves (mm)	29.5
Duration of the CREB intake valve second opening (°CA)	100
IVSC time after TDC (°CA)	30
Ambient temperature (k)	298
Ambient pressure (bar)	1
Engine speed (rpm)	1500

The *p-V* diagrams of different simulation models are shown in Figure 3-12. From the figure, it can be seen that the GT-POWER model *p-V* diagram almost has the same appearance with the theoretical model. But for the reason of leakage and friction in the GT-POWER model, there is a small difference between their values.

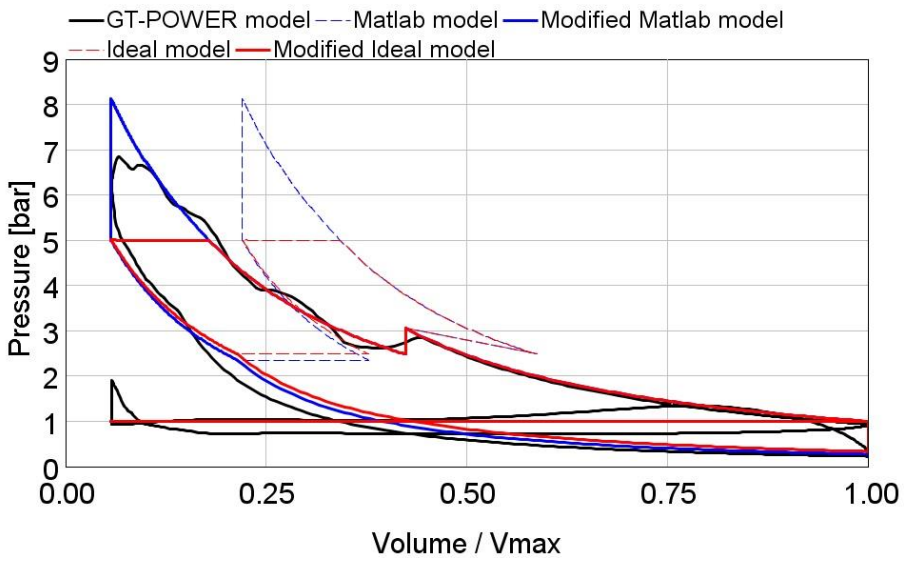

Figure 3-12 *p-V* diagram comparison

To generate the engine response map, the GT-POWER model and the theoretical model are running the steady-state simulation respectively. The results are shown in Table 3-3 and Table 3-4.

Table 3-3 Theoretical model engine brake torque (Nm) map

		Engine speed (rpm)			
		500	**1000**	**1500**	**2000**
Air tank pressure (bar)	**4**	-21.0692	-23.1357	-24.9664	-26.8605
	5	-19.8087	-21.5004	-23.1762	-24.9868
	6	-18.1194	-19.6078	-21.2043	-22.973
	7	-16.1869	-17.5763	-19.1357	-20.8852
	8	-14.1173	-15.4694	-17.0154	-18.758

Table 3-4 GT-POWER model engine brake torque (Nm) map

		Engine speed (rpm)			
		500	**1000**	**1500**	**2000**
Air tank pressure (bar)	**4**	-18.1272	-20.7343	-23.153	-25.5917
	5	-17.009	-19.497	-21.9799	-24.5333
	6	-15.5407	-18.0149	-20.5717	-23.31
	7	-13.9945	-16.3552	-19.0587	-21.9298
	8	-13.9564	-16.3042	-18.8979	-21.6776

From the two tables above and Figure 3-15, it can be seen that when the engine speed increases, the brake torque increases. Conversely, at constant engine speed as air tank pressure increases, the brake torque decreases. It can be seen that the difference between the GT-POWER model and the theoretical model falls as the engine speed increases. The result also indicates that the thermodynamic model can be used to calculate the engine brake torque in CM and is sufficiently reliable to be used for the analysis of the engine performance of CM.

Figure 3-13 shows that the in-cylinder pressure, auxiliary chamber pressure and the air tank pressure during one engine cycle of the GT-POWER model. It can be seen that in-cylinder pressure rises after both intake valves close after BDC and the pressure in the auxiliary chamber increases immediately after the CREB intake valve second opening. Both pressures remain the same during the opening period of the CV near TDC when the auxiliary chamber pressure becomes higher than the air tank pressure. After TDC, the air flow stops when the auxiliary chamber pressure is lower than the air tank pressure. After that, the auxiliary chamber pressure remains constant until the intake valves open again in the next cycles.

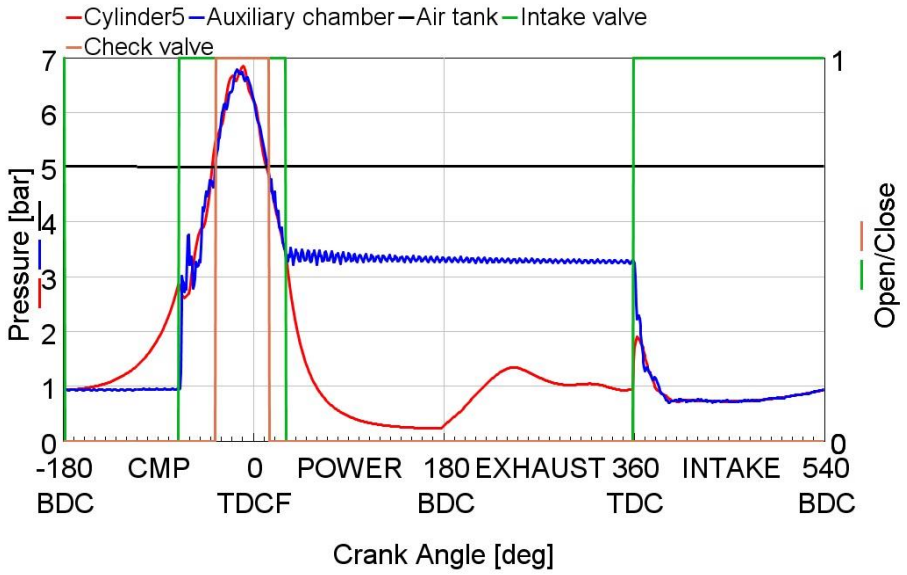

Figure 3-13 Pressure diagram in the CM

3.3.2.2 Performance Analysis

Figure 3-14 shows the *p-V* diagrams for various air tank pressures at 1500 rpm simulated by the theoretical model. The figure indicates that different air tank pressure can cause different engine brake torque performance during the CM. It can be seen that the lower air tank pressure can create more brake torque which is shown in Figure 3-14 as the biggest area surrounded by the red line. The 7 bar air tank pressure lead the lowest brake torque which has the smallest area *p-V* diagram. This is because the lower air tank pressure causes an earlier check valve open time which resulting in long piston working time. Thus, the engine brake torque is a function of tank pressure.

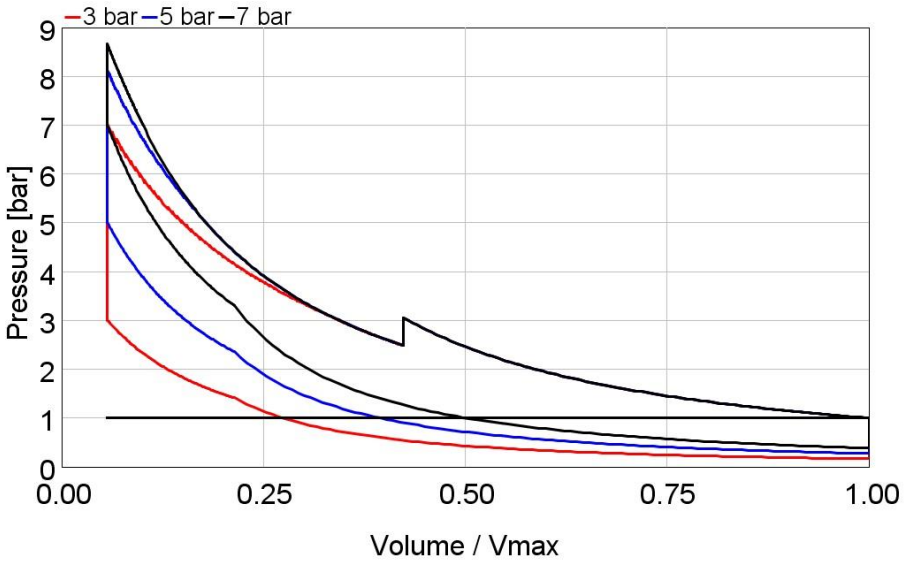

Figure 3-14 *p-V* diagram at 1500 rpm engine speed

Figure 3-15 not only validates the above conclusion that lower air tank pressure creates a high brake torque, but also indicates that not only at 1500 rpm, but from the engine speed from 500 to 2000 rpm, at intervals of 500 rpm, large engine speed and small air tank pressure are both beneficial to improve the engine braking performance.

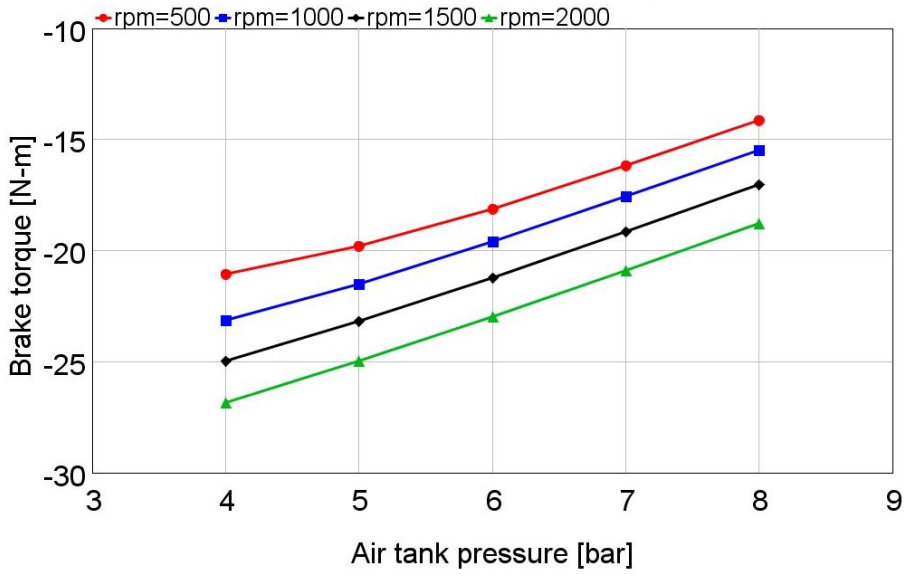

Figure 3-15 Brake torque for various air tank pressure and engine speed

Figure 3-16 shows when the engine speed at 1500 rpm and 5 bar air tank pressure, the engine brake torque for the different CREB intake valve second opening duration and closing time. The IVSC gives out when the CREB intake valve will second close, for

example, 'IVSC=0' means the CREB intake valve second closing happens at piston exactly reaches the TDC; 'IVSC=10' means it will close at 10° CA after the piston reaches TDC. The duration means the time that the CREB intake valve second opening will last. A larger number of duration means a long second opening time of the CREB intake valve. From the figure, it can be learned that, if the CREB intake valve closing time after TDC is fixed, the longer second open duration decreases the brake torque performance of the engine. In other words, it means earlier second open the CREB intake valve during the piston upstroke, resulting in lower brake torque. The reason is when the CREB intake valve second opens, the cylinder connects the auxiliary chamber resulting in an increased volume and decrease the compression ratio which leads the cylinder pressure cannot be compressed to high pressure, as a result, the low braking performance.

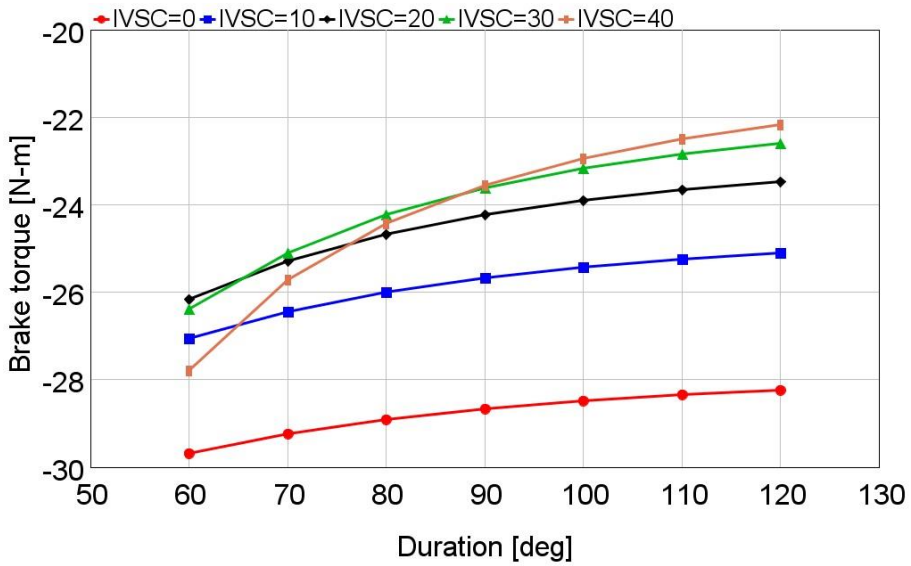

Figure 3-16 Brake torque for different intake timings

The figure also shows that the CREB intake valve closure after TDC can affect the engine brake performance. If the CREB intake valve closure is exactly at TDC, it always has the maximum engine brake torque output no matter how long it opens. This is due to if the CREB intake valve close after the piston reaches TDC, which means the piston start its downstroke, the cylinder pressure starts to decrease, the air from the auxiliary chamber may flow back to cylinder and do positive work to propel the piston resulting in low brake torque. Basically, the CREB intake valve closing more early after TDC can get more engine brake torque output when the open duration is bigger than 90°CA. When the second open duration is less the 90°CA, later close the CREB intake valve sometimes can

create bigger brake torque output if the CREB intake vale second opening duration is too short. This is because, for this situation, the short CREB second opening cannot supply enough time for the air in the cylinder be compressed into the auxiliary chamber before the piston reaches the TDC. Which means the cylinder pressure can be compressed higher resulting in the high brake torque.

Figure 3-17 shows how the different actual compression ratios affect the engine brake torque performance at different engine speed. From the figure, it can be seen that the higher actual compression ratio creates more engine brake torque output. This is because, the higher actual compression ratio, the higher peak cylinder pressure can be achieved before the piston arrives TDC, resulting in high engine brake torque. By the observation of brake torque sensitivity to the actual compression ratio, it can be concluded that brake torque is a strong function of the actual compression ratio.

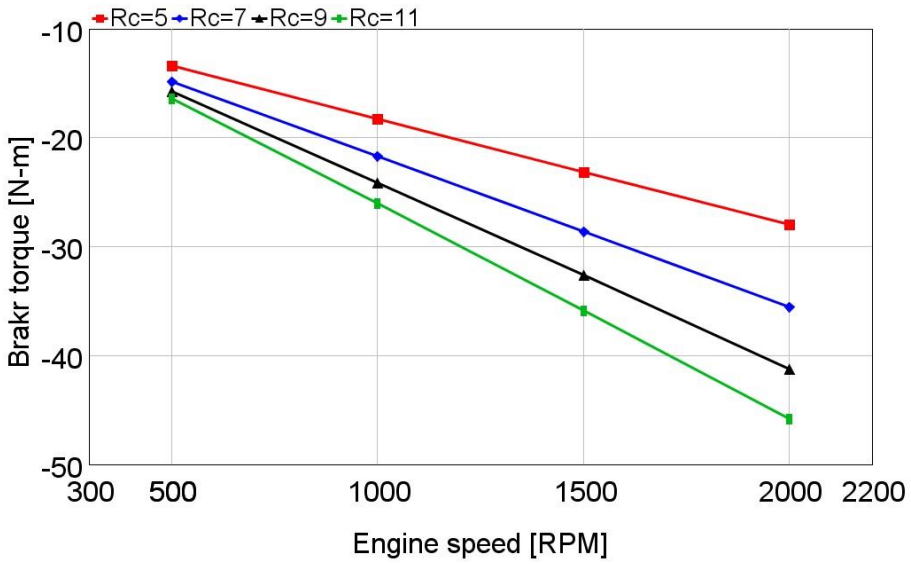

Figure 3-17 Brake torque for various engine speeds and the actual compression ratio

3.4 Conclusion

In this chapter, the principle of operation has been introduced. The potential of the pneumatic hybrid system to both generate a supply of compressed air and to manage the contribution of the engine to vehicle braking had been confirmed. The pneumatic hybrid engine CM is considered from a theoretical perspective based on an air cycle analysis and validated. The effects of the air tank pressure, engine speed, intake valve second

opening time and actual compression ratio are evaluated. The simulation results demonstrate

(i) The lower air tank pressure can create more brake torque at the same engine speed which means small air tank pressure is beneficial to improve the engine braking performance. This is because the lower air tank pressure causes an earlier check valve open time which resulting in long piston working time.
(ii) The longer CREB intake valve second opening duration decreases the brake torque performance of the engine. The reason is that the cylinder pressure cannot be compressed to high pressure, as a result, the low braking performance.
(iii) It always has the maximum engine brake torque output when the CREB intake valve second closing time is right at TDC which means IVSC is 0°CA. This is due to if the CREB intake valve close after the piston reaches TDC, which means the piston start its downstroke, the cylinder pressure starts to decrease which may cause low brake torque.

The method and the result obtained in this chapter are of great help to fully understand the pneumatic hybrid engine compressor mode and supply the following fundamental knowledge for the future research.

(i) The valve timing, engine structure parameters such as the actual compression ratios can significantly affect engine braking performance during CM.
(ii) The simulation results prove that the pneumatic hybrid engine can realize regenerative braking during the CM which means it can be a supplement to the vehicle friction braking system.
(iii) The finding that the engine brake torque is a function of tank pressure supplies the basic understanding of how to control the pneumatic hybrid powertrain.

CHAPTER 4
DRIVING CYCLE SIMULATION OF PNEUMATIC REGENERATIVE STOP-START SYSTEM

4.1 Introduction

For vehicles that follow a duty cycle characterised by frequent start-stop cycles, fuel consumption can be reduced significantly by implementing an engine stop-start function. The engine is stopped when the vehicle comes to a halt and is restarted as soon as the operator commands a speed. A vehicle equipped with pneumatic hybrid technology achieves this goal by converting kinetic energy to pneumatic energy, compressing air into tanks installed on the vehicle. The compressed air is then reused to power an air starter motor to realize a regenerative stop-start function.

The aim of this chapter is an evaluation of the fuel economy improvement ability for a city bus application. The Stop-Start Function is considered for different bus driving cycles and an investigation is made into how multiple air tanks give an additional degree of freedom for management of recovered air. A backward-facing simulation model of the city bus with the pneumatic hybrid powertrain has been applied to investigate the improvement of fuel economy by using one and two air tanks in different driving cycles in Simulink.

4.2 Vehicle Driving Cycle Simulation Setup

A YUCHAI YC6A six cylinders heavy-duty diesel engine with a pneumatic regenerative device is used as the research object in this chapter. Figure 4-1 shows a schematic diagram of the engine with one air tank pneumatic hybrid system which has the same structure with the engine using in Chapter 3. The air tank connects to one of the split intake ports. In order to recover the air during vehicle braking, a TV is added to the manifold to prevent the flow of compressed back to the compressor and effectively lost to the recovery process. The CV between the manifold and the air tank represents an

automatic switch. One of the intake valves is equipped with a CREB device of a type normally used on the exhaust valve for the purpose of engine braking [34]. During vehicle braking, the CREB device will open the intake valve. With the piston going up, air is compressed into the intake port. At the same time, the TV is fully closed to stop the compressed air escaping into the intake manifold. The CV will open when the pressure of the delivered air is higher than the tank pressure. The air is then compressed into the air tank. The air tank follows normal commercial vehicle practice with a peak working pressure of 10 bar for safety reasons. The engine model also includes five more cylinders, which are not shown in Figure 4-1. They all have the same structure.

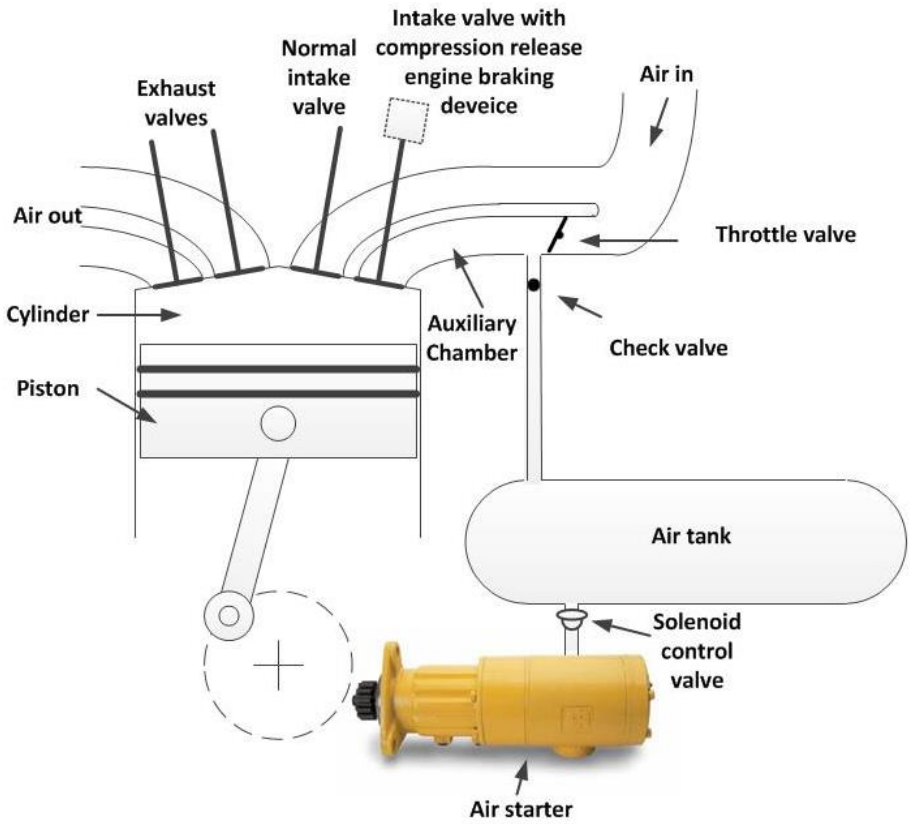

Figure 4-1 Schematic diagram of the pneumatic hybrid engine with one air tank

As shown in Figure 4-1, a standard production air starter SS175 supplied by Ingersoll Rand, is chosen to start the engine. Some performance characteristics are given by Ingersoll Rand in their specification [68]. Based on the practical experience of the engine manufacturer, YUCHAI, the engine can be started in 1 s during normal conditions. The air mass used during each cranking operation is calculated from the air flow at maximum power as shown by Ingersoll Rand for a cranking period of 1 s at each tank pressure.

From the specification, the air flow rates at different tank pressures are given [68]. Table 4-1 is the performance information about the SS175 air starter. From this table, the air flow rates in different tank pressure are supplied. For example, when the tank pressure is 6.2 bar, the air flow would be 142 l/s to give a 1s cranking time, which means it consumes 166.3 g air for 1 s operation in standard conditions for temperature and pressure, 298 k and 1 bar. As a result, tank pressure will drop down to 5.2 bar after one start-up operation.

Table 4-1 Air starter performance information [68]

Pressure (Bar (PSI))	Breakaway Torque (Nm)	Speed @ Max HP (RPM)	Max Power (kW (HP))	Flow @ Max HP (l/s)
6.2 (90)	42	2500	7 (10)	142
8.3 (120)	54	2700	10 (14)	189
10.3 (150)	70	2800	13 (18)	236

Also the specification gives the potential number of starts at various tank pressures and for different tank sizes which shown in Table 4-2. In order to store sufficient compressed air for the usage of the air starter, the size of the air tank is decided following the recommendation of the air starter manufacturer [34]. The 151 l air tank is chosen to be the energy storage device. It has a maximum working pressure of 10 bar and can support 7 cranking attempts. The air starter also needs a minimum pressure of 5.2 bar below which it will not operate reliably. The requirement placed on the control strategy is therefore to keep the air tank pressure between 5.2 and 10 bar.

Table 4-2 SS175 number of starts per tank [68]

		Max tank pressure (bar)							
		6	**8**	**10**	**12**	**14**	**16**	**18**	**20**
Tank size (l)	**151**	2	4	7	9	11	13	15	17
	227	3	7	10	13	16	20	23	26
	302	4	9	13	17	22	26	31	35
	378	5	11	16	22	27	33	38	44
	454	7	13	20	26	33	39	46	52
	529	8	15	23	31	38	46	53	61
	605	9	17	26	35	44	52	61	70
	680	10	20	29	39	49	59	69	79

In most previous pneumatic hybrid powertrain research work, the number of air tanks is just one [32, 40, 46]. The advantage of one air tank is that the control strategy will be straightforward and the system simple. But the use of a single air tank is a severe limit on the control degrees of freedom and the system efficiency cannot be enhanced. In order to avoid this problem, a second air tank is added. The two air tanks pneumatic hybrid system structure is shown in Figure 4-2. In this configuration, two air tanks have the same size, 151 l, and can separately receive the air from the cylinder during CM and will power the air starter when cranking. There is no connection between these two air tanks in order to simplify the model. There are several choices for the size and number of the multiple air tanks pneumatic hybrid powertrain. It could be two different air tanks, one for energy recovery, and another for driving the air starter. Or use more than two same size air tanks to realize the same functions. Furthermore, a single tank has big volume is also a choice. The reason for choosing two same size air tanks is explain below. Firstly, depending on the air starter manual, 151 l is the smallest size to supply the cranking operation of the air starter [68]. This means at least one air tank should be 151 l to support the air starter operations. Second, in the backward facing simulation, the air consumption of the air starter during the cranking and the air mass recovery during the braking comes from two look up tables. The data in these two tables is from the engine test bench experiment and should be validated. As this project is working together with

Brunel University London, they chose 151 l air tank as the research objective and doing the experimental test. In this stage, only the 151 l air tank has the confirmed data for the two look up tables in the backward facing simulation. As a result, choosing two 151 l air tank can guarantee the accuracy of the simulation. Also this research is meant to investigate the potential ability of pneumatic hybrid powertrain in saving fuel for the bus applications; it is not to optimize the pneumatic hybrid powertrain structure and parameters. The result of this research supplies the fundamental understanding of the pneumatic hybrid powertrain for the future research. The systems with more than two air tanks are beyond the scope of this research. Therefore, two same size air tanks are chosen for the two air tanks pneumatic hybrid powertrain. The remainder of the engine is the same with one air tank pneumatic hybrid engine as shown in Figure 4-1.

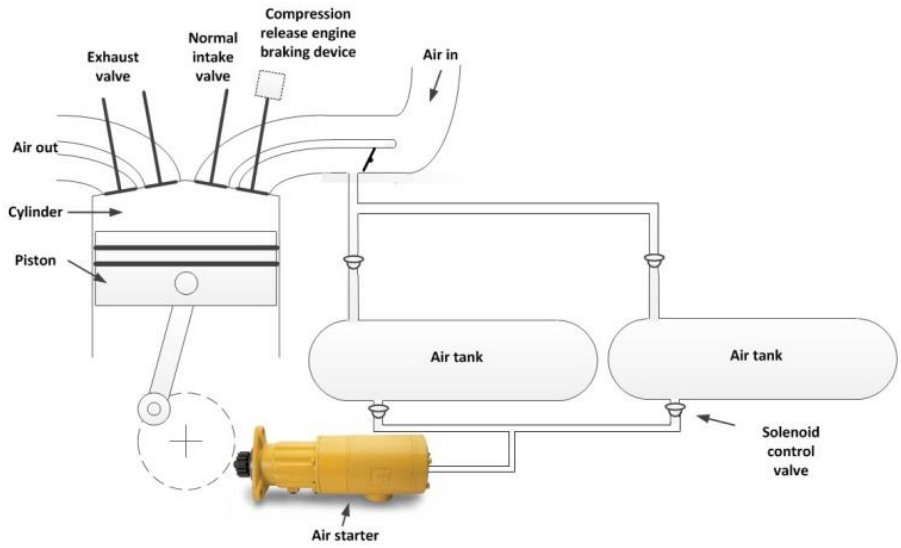

Figure 4-2 Two air tanks pneumatic hybrid system structure

A pneumatic hybrid vehicle simulation model has been built using MATLAB/Simulink as shown in Figure 4-3. This model is built with Quasi Steady State Toolbox (QSS-TB) with some new blocks added. QSS-TB is a collection of MATLAB/Simulink blocks and the appropriate parameter files that can be run in any MATLAB/Simulink environment [69]. QSS-TB permits a fast and simple estimation of the fuel consumption for many powertrain systems. It can be used to calculate the vehicle fuel consumption, engine speed and load required to achieve a given vehicle speed, rate of acceleration and resistive loads such as rolling resistance, drag and frictional losses in the powertrain [70]. Vehicle and powertrain parameters, such as the mass of the vehicle, vehicle cross section

area, wheel diameter, engine combustion maps, gear ratios, and driving cycle data, can be defined in the different blocks of the model [69]. The QSS-TB is used in on-going research projects and in the exercises to the lecture "Vehicle Propulsion Systems" by ETH Zurich [71].

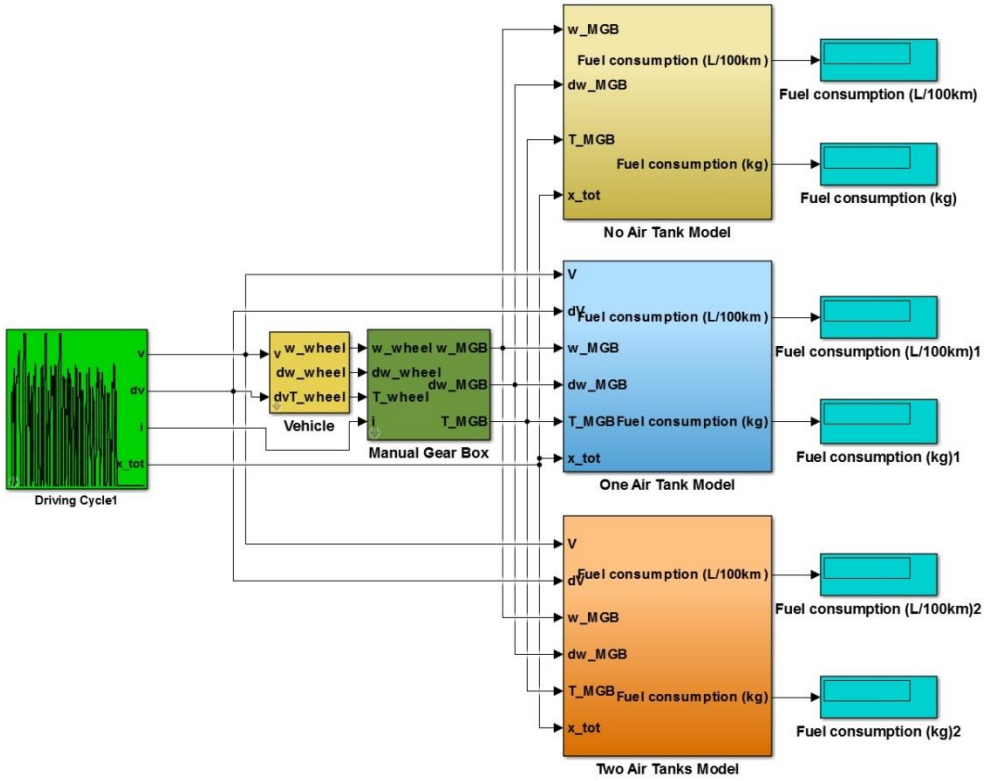

Figure 4-3 Pneumatic hybrid vehicle simulation model

Concerning this model, three different vehicle models are deployed. The models are respectively "No Air Tank Model", "One Air Tank Model" and "Two Air Tanks Model". The purpose of building the models with a common base specification is to compare results directly. From Figure 4-3, it is evident that this is a backward vehicle driving cycle simulation model. The driving cycle can be chosen (for example, Braunschweig cycle in Figure 4-3) in the "Driving Cycle" block. The outputs of this block are the demand speed *v*, demand acceleration *dv*, gear number and total distance of the driving cycle. Then, the *v* and *dv* are the inputs of block "Vehicle". In this block, the torque at the wheel (i.e. resistances plus acceleration) is calculated and input to block "Manual Gear Box". The block "Manual Gear box" converts the wheel torque to a demanded net engine torque, then input to three different blocks. In these three different blocks, based on different pneumatic hybrid type, the torque combined with the speed of the engine will be

calculated to obtain the fuel consumption. Within the block "Tank" those consumption data are summarized and converted to a figure in l/100km. The equations for the models mentioned before can be found in [69, 71].

Among the three models, the block structures are different, reflecting the different vehicle architectures. The "No Air Tank Model" is based on the basic vehicle simulation model in the QSS-TB. It gives the fuel consumption of a conventional diesel engine city bus. The control strategy of this model is simple and is not developed further in the report. The control strategies of "One Air Tank Model" and "Two Air Tanks Model" are discussed in detail in the next section.

In order to achieve modularization of control system development and reduce the possible cost of control system development, such as hardware design in the future, Stateflow® in the MATLAB is used to complete the modelling and simulation. Stateflow is an environment for modelling and simulating combinatorial and sequential decision logic based on state machines and flow charts [72]. With Stateflow the logic for supervisory control, task scheduling, and fault management applications can be designed. Stateflow includes state machine animation and static and run-time checks for testing design consistency and completeness before implementation making it easy to debug and update the model [72]. The principal reason however for using Stateflow is that the function of the pneumatic hybrid systems naturally consists of a number of states. Based on state transition conditions, the model will transfer from one state to another. In complex circumstances, secondary models manage a state transition within high level states.

The relevant bus parameters are given in Table 4-3.

Table 4-3 City bus data [34]

Kerb weight (kg)	16500
Aerodynamic drag coefficient (-)	0.5
Frontal area (m^2)	5.69
Air density (kg/m^3)	1.225
Wheel radius (m)	0.508
Rolling resistance coefficient (-)	0.013
Air tank volume (l)	151
1st gear ratio (-)	6.9
2nd gear ratio (-)	4.13
3rd gear ratio (-)	2.45
4th gear ratio (-)	1.49
5th gear ratio (-)	1
Final drive ratio (-)	5.125
Additional mass of air starter (kg)	15
Additional mass of air tank (kg)	100

For simulation work, two driving cycles are considered separately: the Braunschweig driving cycle and the Millbrook London Transport Bus (MLTB) driving cycle.

The Braunschweig driving cycle was developed by the Technical University of Braunschweig for an urban bus in Braunschweig (Brunswick) city in Germany [73]. Figure 4-4 shows the Braunschweig driving cycle time–speed diagram over a period of 1740 s. The total distance is 10.87 km.

MLTB is a real-world driving cycle based on the data collected from buses in service in central London [74]. It include two phases, the medium speed 'Outer London' phase simulating the journey from Brixton Station to Trafalgar Square and the low speed 'Inner London' phase simulating the journey from Trafalgar Square to the end of Oxford Street. The Outer London phase includes a nominal distance of 6.45 km for the duration of 1380 s. The Inner London phase includes a nominal distance of 2.47 km for the duration of

901 s. It covers in total 8.92 km for the duration of 2281 s. The time–speed diagram of MLTB is shown in Figure 4-5.

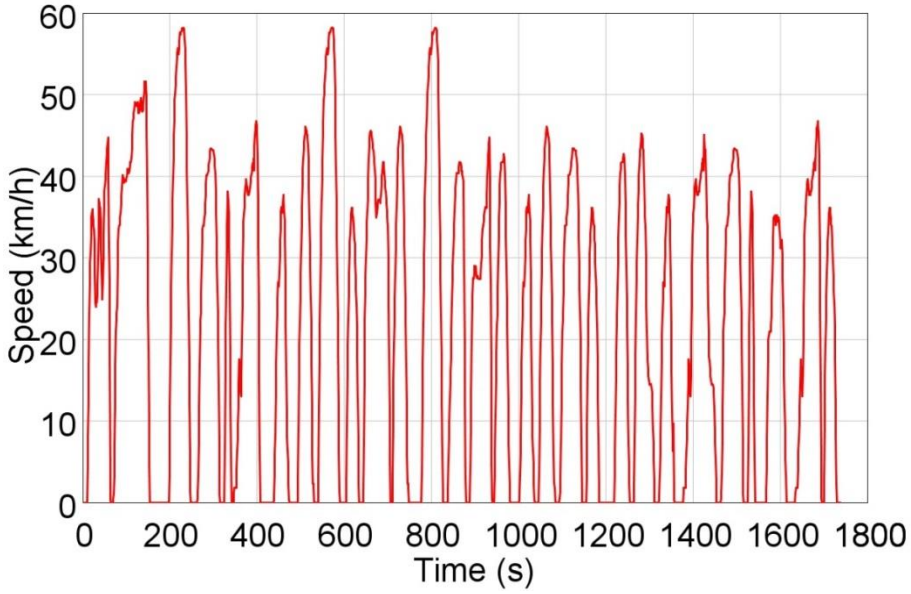

Figure 4-4 Braunschweig driving cycle time–speed diagram

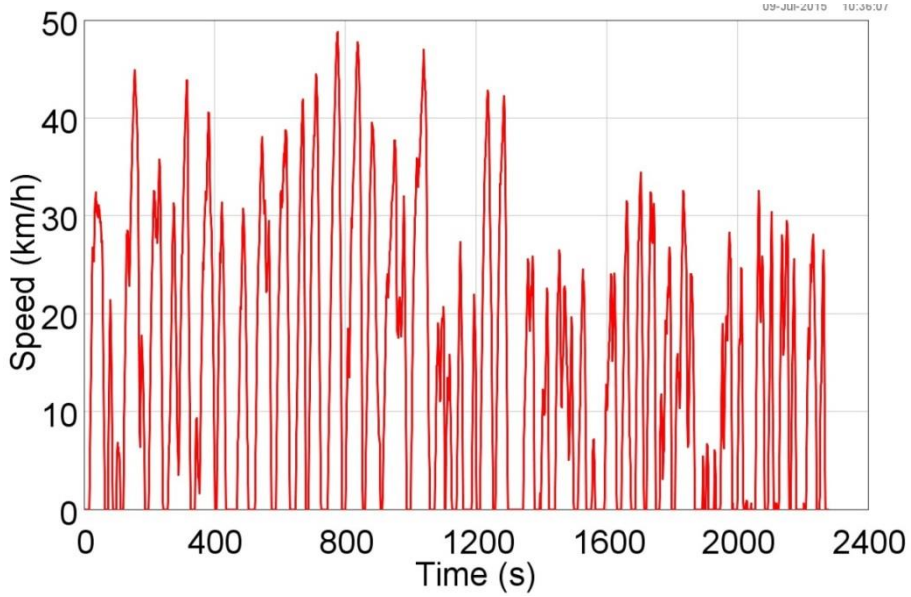

Figure 4-5 MLTB driving cycle time–speed diagram

Compared with the MLTB driving cycle, the Braunschweig driving cycle is characterized with higher vehicle speeds and less stop–start operations over a slightly longer distance. Table 4-4 shows the basic parameters of the Braunschweig driving cycle and the MLTB driving cycle respectively.

Table 4-4 Basic parameters of the MLTB driving cycle and Braunschweig driving cycle

	Braunschweig driving cycle	MLTB driving cycle
Time (s)	1740	2281
Distance (km)	10.87	8.92
Acceleration (%)	39.7	40.7
Deceleration (%)	30.8	30
Idle (%)	29.5	29.3
Number of stops (-)	30	52

4.3 Pneumatic Hybrid Powertrain Control Strategy

In the above pneumatic hybrid vehicle simulation models, the fuel consumption can be reduced by (i) turning the engine off when the vehicle is stopped when the engine would otherwise idle, or (ii) cut-off the fuel injection when implementing CM during vehicle deceleration. Today, most diesel engines use fuel cut-off technology during the deceleration to save the fuel. As a result, the only fuel that can be directly saved is that used for idle. This means that when the vehicle is stopped and the engine would otherwise be at idle speed, the engine is turned off. To realize this function, during the deceleration, the pneumatic hybrid powertrain works in CM to compress air into the air tank. When the vehicle implements the stop-start function, the compressed air is supplied to the air starter to start the vehicle. The control strategy for the pneumatic hybrid powertrain reflects the various functions of the system.

In the majority of prior work on pneumatic hybrid systems, the implementation employs a single air tank, making the design and control solution relatively straightforward. However, a second air tank provides an important degree of freedom to the control system that leads to an enhancement of efficiency. The work reported in the following sections includes the formulation and evaluation of a two tank model.

Much of the control strategy for respectively the one and two air tank models is common. Firstly, once the engine braking torque which can be generated by the CM is less than the braking torque, the CM is switched on. The air is compressed into the air tank. The amount of air stored is then computed via the engine's CM response map produced by

the air hybrid engine simulation program from [34]. Both the engine speed and the tank pressure are used as the input to two two-dimensional lookup tables to generate two outputs: (a) the engine braking torque demand and (b) the amount of compressed air storage, by using the interpolation and extrapolation method in every fixed-step simulation time during the deceleration phase [34].

Because the air starter needs a minimum pressure in the air tank to start the engine, the minimum pressure in the air tank must be 5.2 bar, no matter how many tanks. Activation the stop–start mode is decided on the basis of the tank pressure.

The response map for the cranking mode takes into account the engine cranking speed and compressed air mass consumption data from the air starter manual [75]. The final air tank pressure is determined by the sum of compressed air production during CM and consumption during the cranking.

This control strategy is suitable for the one air tank model. Figure 4-6 shows the control block of one air tank model in the form of a Simulink model. The state diagram of control strategy is shown in Figure 4-7 and its implementation in Stateflow is shown in Figure 4-8.

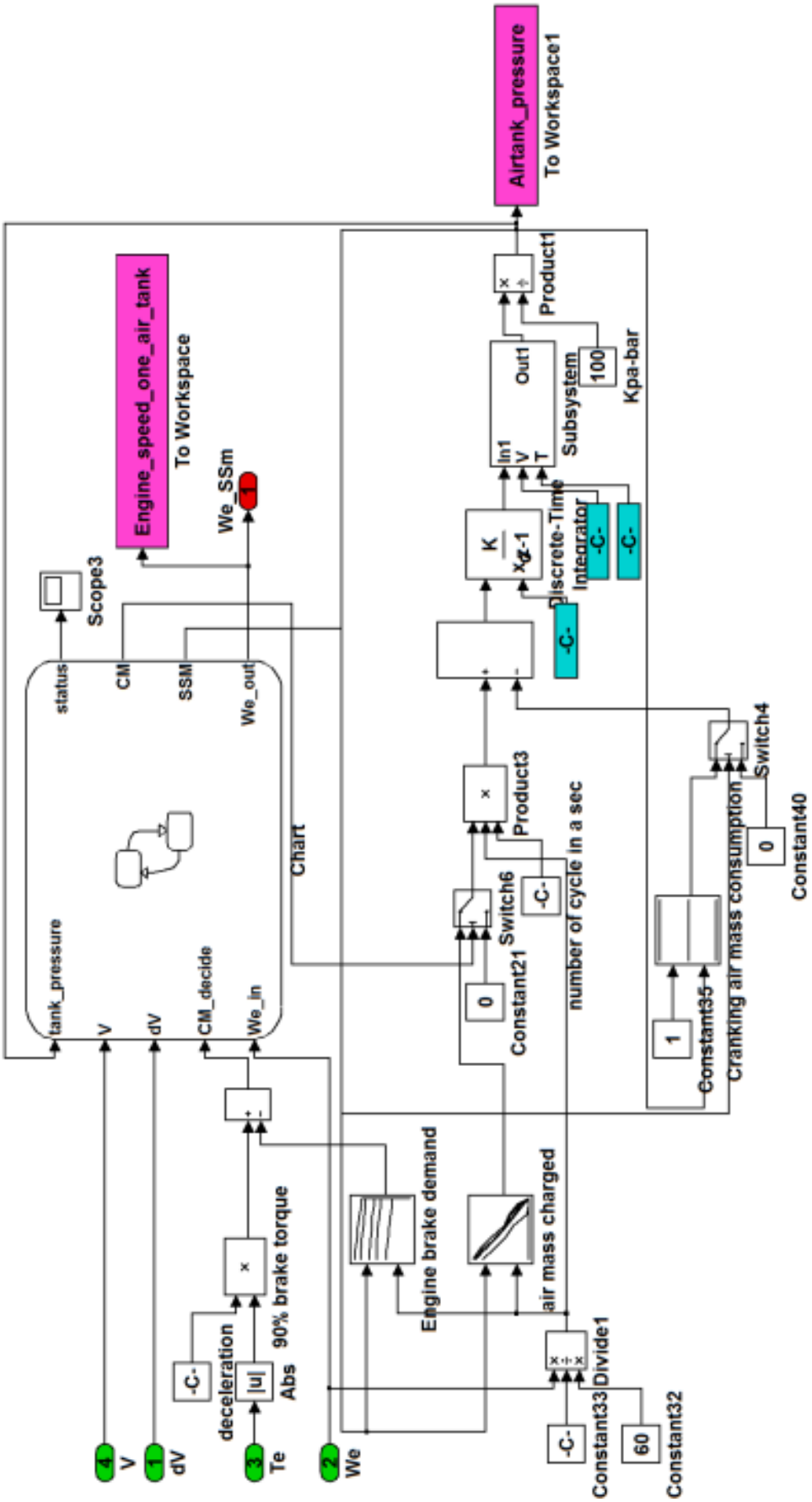

Figure 4-6 One air tank simulation model control block

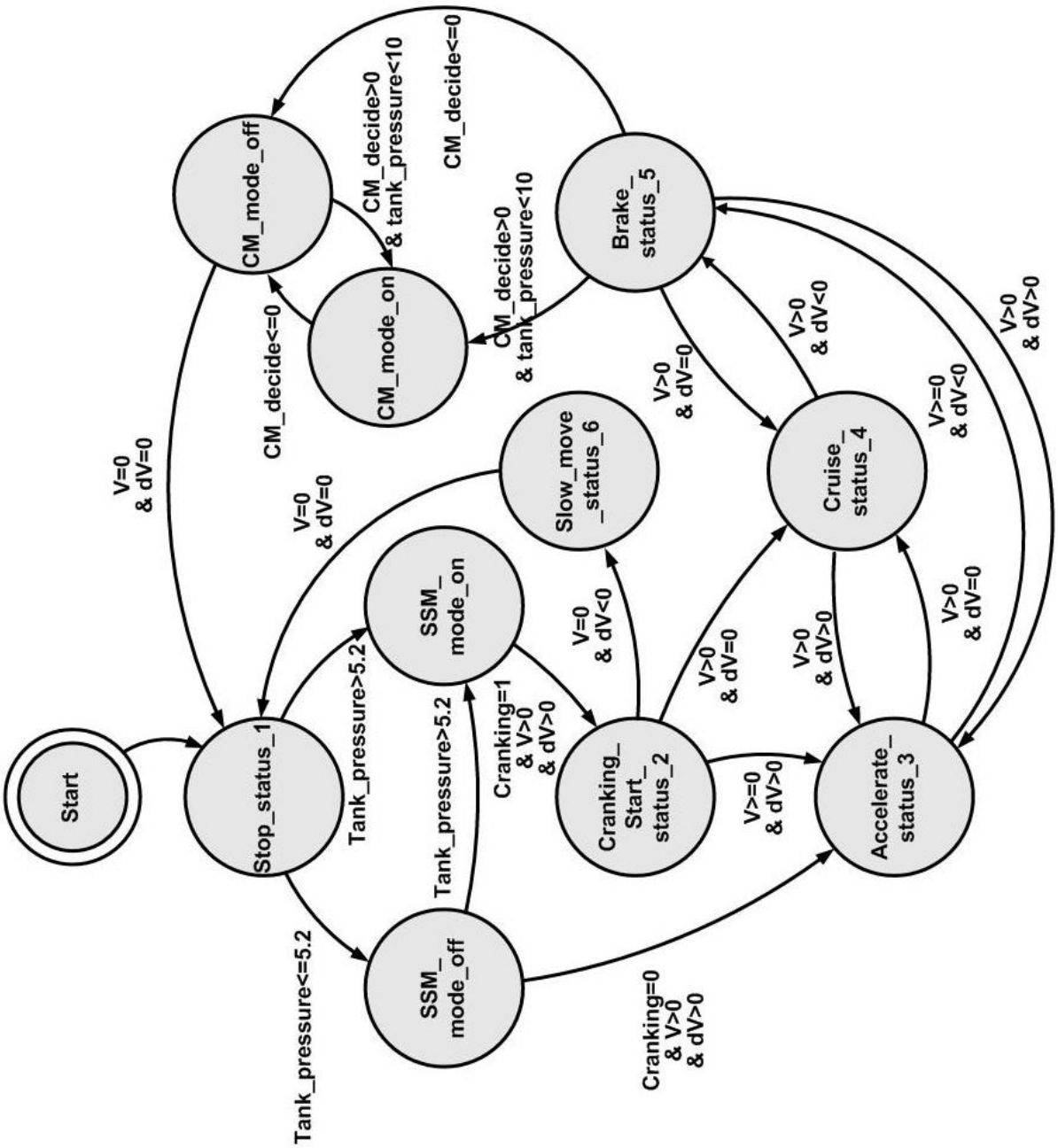

Figure 4-7 The state diagram of control strategy for one air tank model

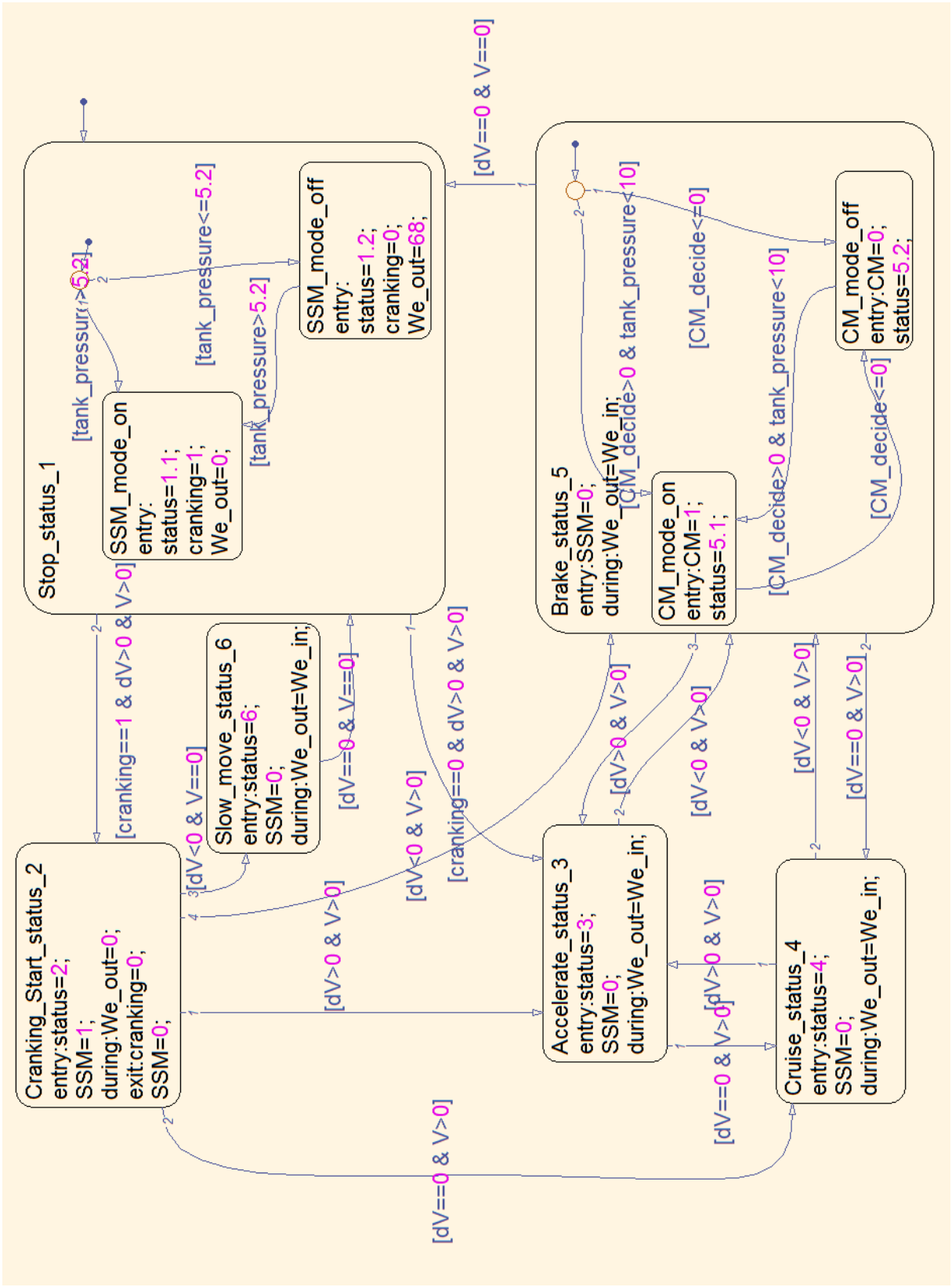

Figure 4-8 One air tank model Stateflow diagram in Simulink

Compared with the single air tank model, the two air tanks model is more complex. Unlike the one air tank model, the air tank part of two air tanks model does not build base on any existing engine structure. The model built here is to demonstrate the benefit of using two air tanks in the pneumatic hybrid engine. In this model, two air tanks can separately receive the air from the cylinder in the CM and drive the air starter when cranking. There is no connection between these two air tanks. The reason to choose the separate air tanks is because of the advantage that this structure can maintain at least one air tank pressure as low as possible, and at same time to keep another air tank pressure above the minimum air starter operation pressure 5.2 bar.

The key principle of the control strategy is to maximise the efficiency in CM. From the previous research [34, 37], the air mass flow from cylinder to air tank in CM is determined by the air tank pressure and engine speed. The lower air tank pressure can recovery more air mass during the baking and supply more brake torque. Therefore, in the two air tanks model, the control strategy is kept simple. When the vehicle enters CM, a comparison is made of the pressure in the respective tanks and air tank with the lower pressure will receive the air from the cylinder. When the vehicle starts, the lower pressure air tank is allocated to supply the air starter, as long as it is above the minimum pressure of 5.2 bar. So in the two air tanks model, the pressures need to be monitored and compared. The control strategy compares the two pressures and decides which tank is to receive the air during CM and which one supplies air to start the engine. The control block, state diagram and Stateflow diagram are shown in Figure 4-9, Figure 4-10 and Figure 4-11. Since this research is to investigate how to manage the pneumatic energy, it only considers the aspects related to the energy. Other aspects such as how to actual implement the system, how to engage the clutch will not be discussed here.

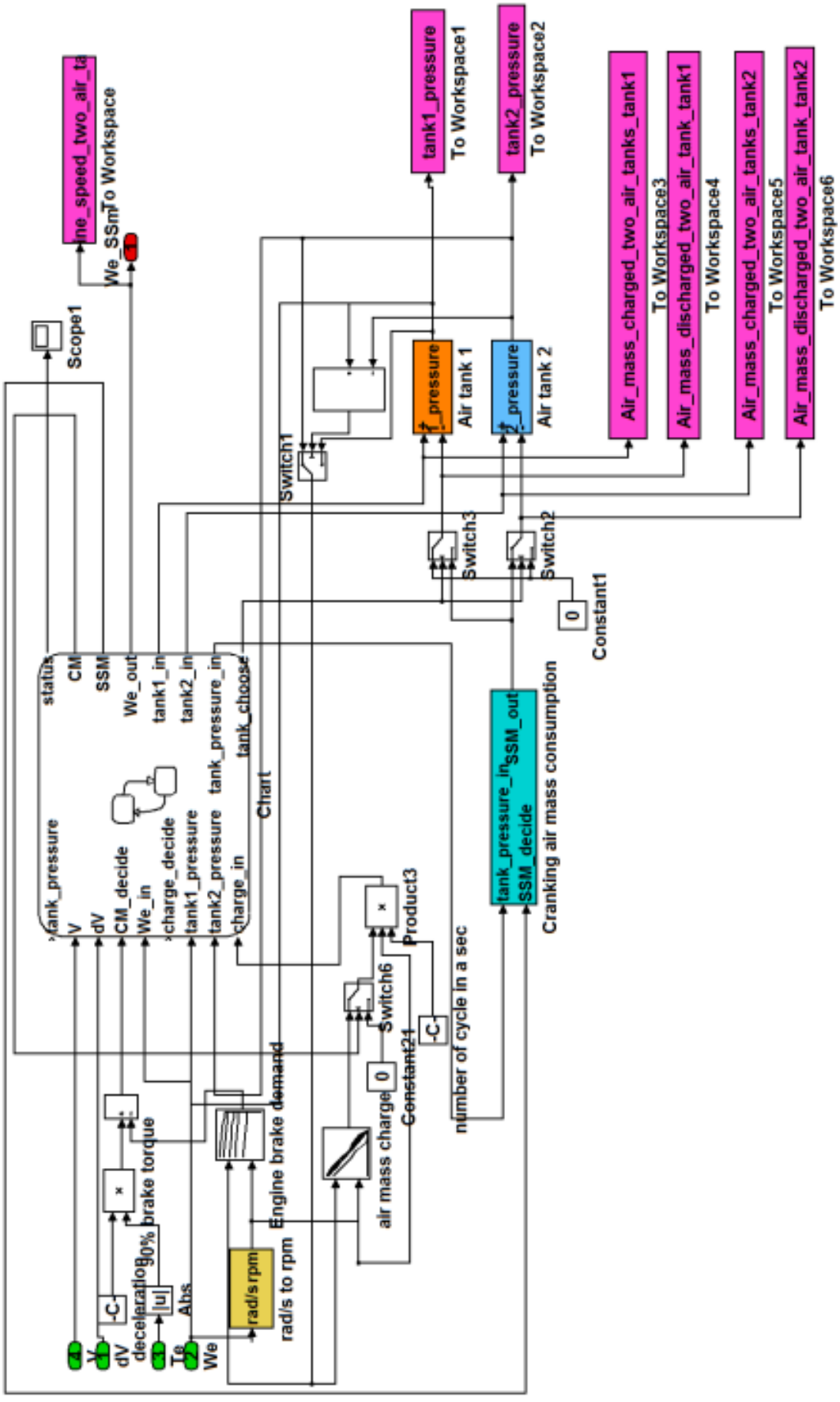

Figure 4-9 Two air tanks model control block

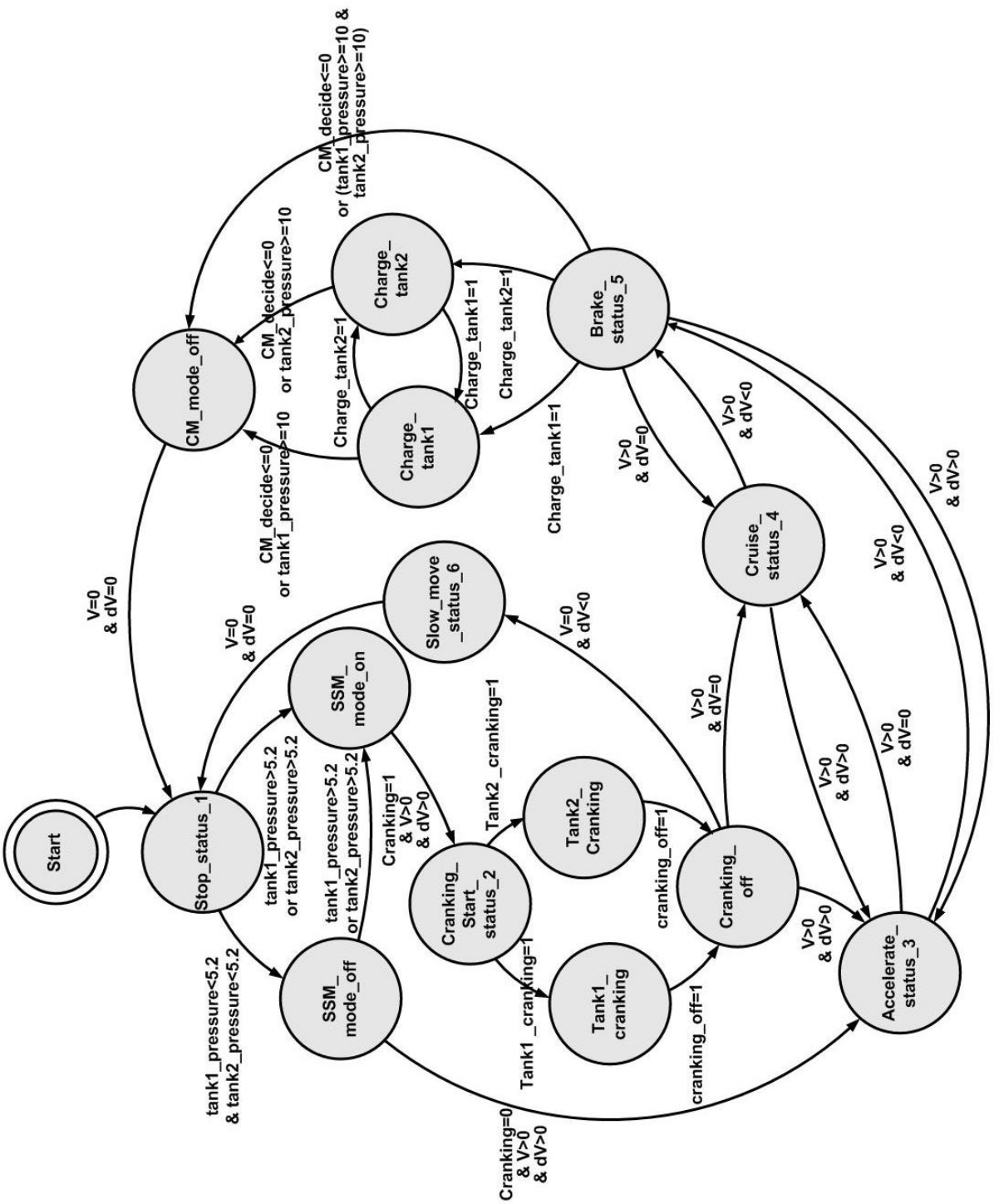

Figure 4-10 The state diagram of control strategy for two air tanks model

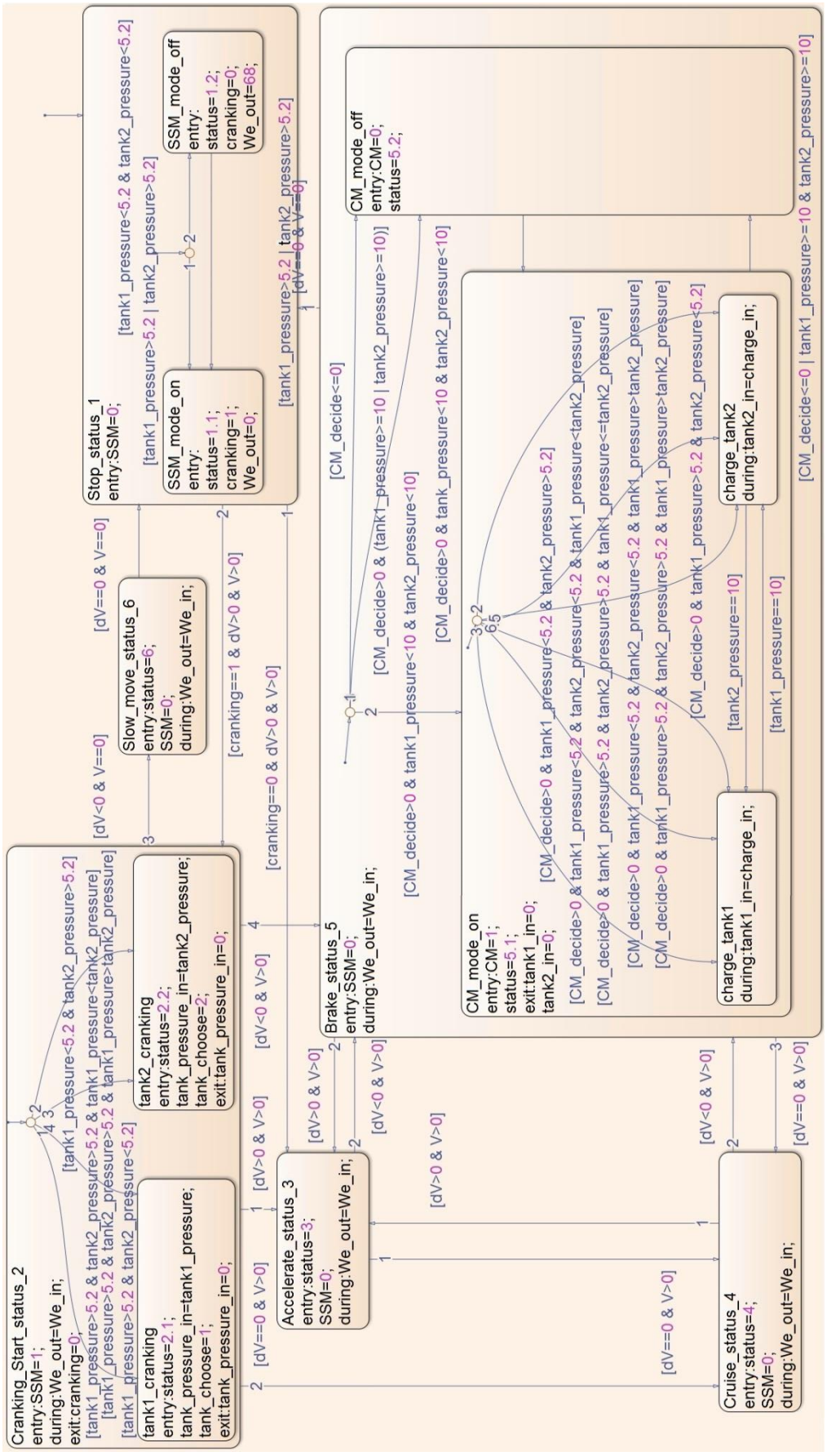

Figure 4-11 Two air tanks model Stateflow diagram in Simulink

4.4 Vehicle Driving Cycle Simulation Result

4.4.1 Braunschweig Driving Cycle

Figure 4-12 shows the engine speed profiles of three models during the whole Braunschweig driving cycle. From the figure, it can be seen that the normal vehicle's engine speed is 650 rpm (solid red line) when the vehicle is stationary, which means the engine is turn on when the vehicle stops. On the contrast, both one and two air tank model turn off the engine to save the idle fuel consumption.

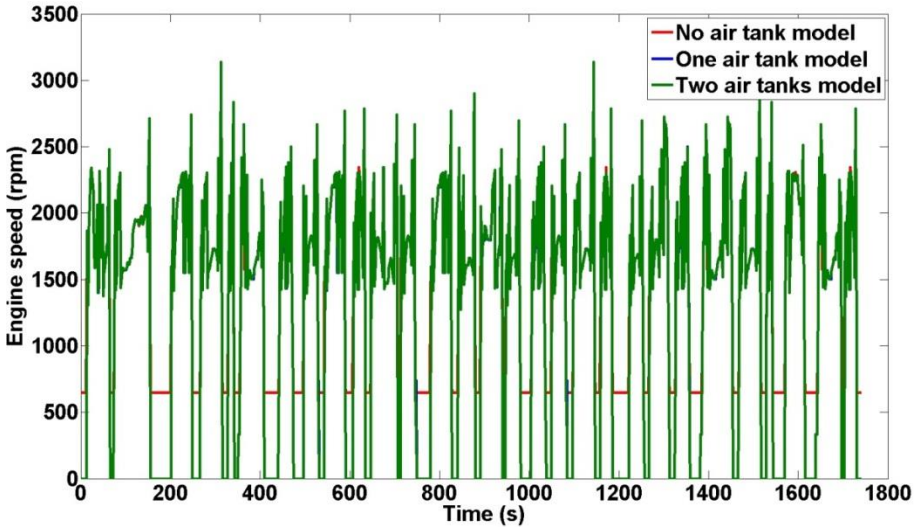

Figure 4-12 Engine speeds during Braunschweig driving cycle

Figure 4-13 shows the air tank pressure when using one air tank in the Braunschweig driving cycle. The simulation start in the extreme situation, where the initial air tank pressure is 5.2 bar which it is only enough to support one cranking event. If the vehicle cannot recover enough energy, after the next engine stop it will not start again. From this figure, the tank pressure is seen to be always above 6 bar which is higher than the stop-start mode operation limit 5.2 bar. This means in the whole cycle, the bus can operate in the stop-start mode.

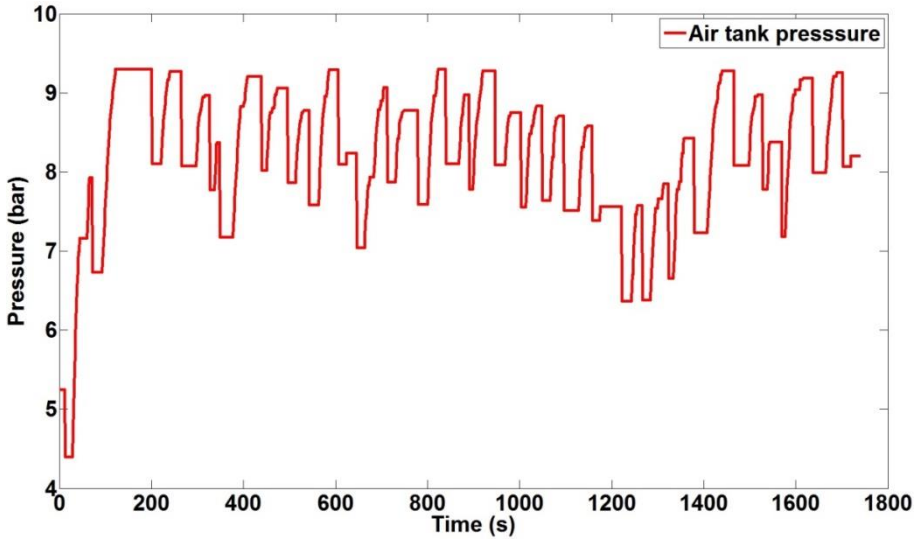

Figure 4-13 Air tank pressure of one air tank model during Braunschweig driving cycle

Figure 4-14 shows the air tank pressure for the two air tanks model for the whole Braunschweig driving cycle. It also considers the extreme situation, where the initial air tanks pressure are 5.2 bar and 4.5 band respectively. This means if the vehicle cannot recover enough energy during the driving cycle, it will not start again after next engine stop. As with the one air tank model, from this figure, we can know that the two air tanks pressure are always above 5.5 bar which is also higher than the stop-start mode operation limit 5.2 bar. At the end of the simulation, the two air tanks pressure are 7 bar and 6.7 bar respectively, which are both higher than their initial pressure. This result proves that the two air tank model can recover enough energy to support all the stop-start operations during the Braunschweig driving cycle.

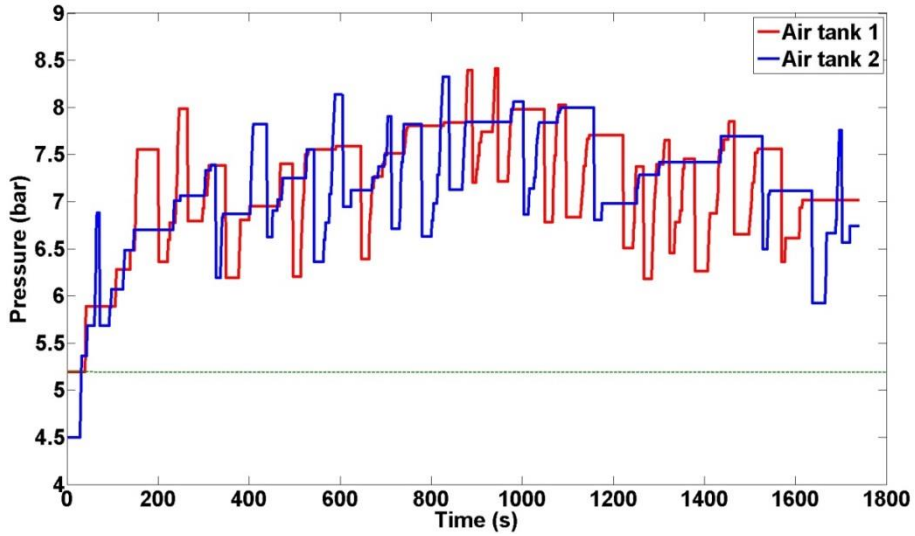

Figure 4-14 Air tanks pressure of two air tanks model during Braunschweig driving cycle

Figure 4-15 shows the air mass charged and discharged in the one air tank model. The air is compressed into air tank when the vehicle is decelerating and the required braking torque is higher than the engine braking torque produced by compressing the air into the air tank.

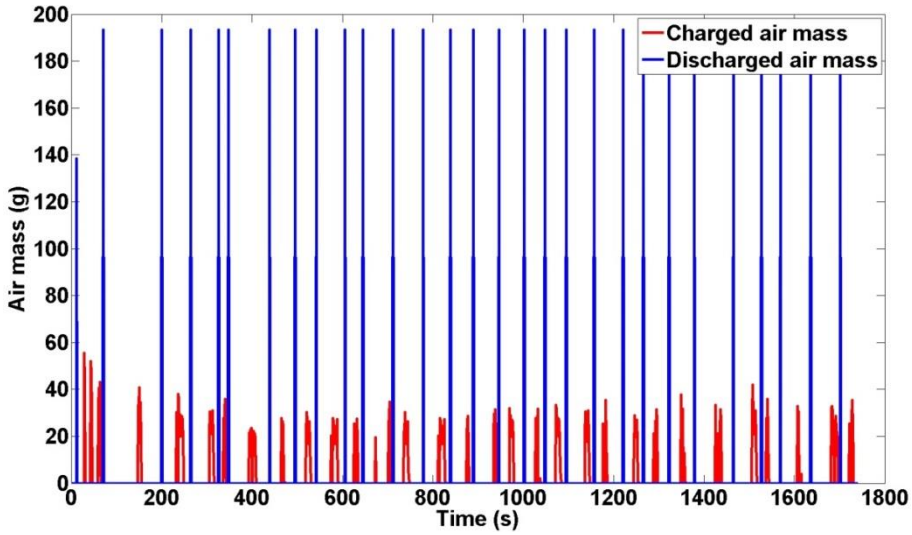

Figure 4-15 Air mass charged and discharged of one air tank model

From the Figure 4-16, it can be learned that two air tanks model can recover 6377.5 g air compared with 5926.9 g of one air tank model. This means the two air tanks model can recover 7.6% more air.

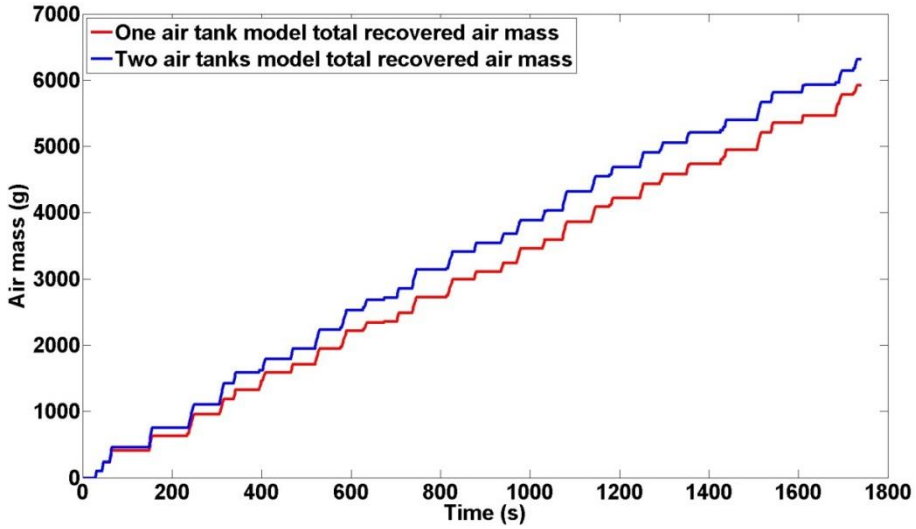

Figure 4-16 Total air mass recovered of one and two air tanks model

Figure 4-17 shows a comparison of fuel consumption over the Braunschweig driving cycle between the no air tank model, one air tank model and two air tanks model. The no air tank model consumes 3384.8 g of fuel which is equivalent 42.61 l/100km during the Braunschweig driving cycle. The one air tank model uses 3171.8 g of fuel which is equivalent 39.93 l/100km, which represents a 6.29% reduction in fuel consumption. The two air tanks model has the same fuel consumption with the one air tank model which is 3171.8 g fuel. Therefore, in Figure 4-17, the one air tank fuel consumption (blue line) is covered by the two air tanks model fuel consumption (green line) as they have the same fuel consumption. This is because over the one air tank model can recover enough air to support all the stop-start operations during the Braunschweig driving cycle. This means the one and two air tank models can turn off the engine when the vehicle is stationary and save the idle fuel consumption during the whole Braunschweig driving cycle. From the previous analysis, it can be learned that the Braunschweig has less stops compared with other bus driving cycles such as MLTB. But if the driving cycle is different, more stops events happen, and the one air tank model may not recover enough energy to support all the Stop-Start function to save the idle fuel consumption.

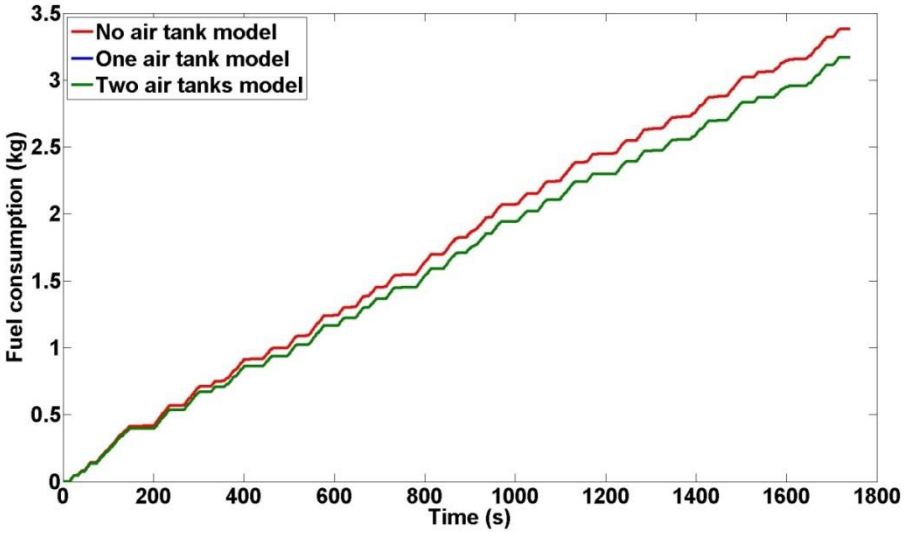

Figure 4-17 Fuel consumption throughout the Braunschweig driving cycle

4.4.2 MLTB Driving Cycle

Figure 4-18 shows the engine speed profiles of the one and two air tanks model during the MLTB driving cycle. From the figure, it can be seen that for all the time that vehicle is stationary, the two air tank model engine speed is 0 rpm (solid blue line), which means

the engine is turned off when the vehicle stops. On the contrast, the one air tank model turn on the engine for 4 times, which shows in the Figure 4-18 is engine speed at 650 rpm (solid red line). It means the one air tank model eliminate more than 90% (48 of 52) of the idling time. The reason that cannot eliminate 100% is because during the MLTB driving cycle, one air tank model cannot recover enough air to support all the stop-start operations which means the air tank pressure will drop below 5.2 bar before the vehicle stops sometimes. As a result, the engine cannot be switched off to avoid the situation that there is no enough air to support one cranking event.

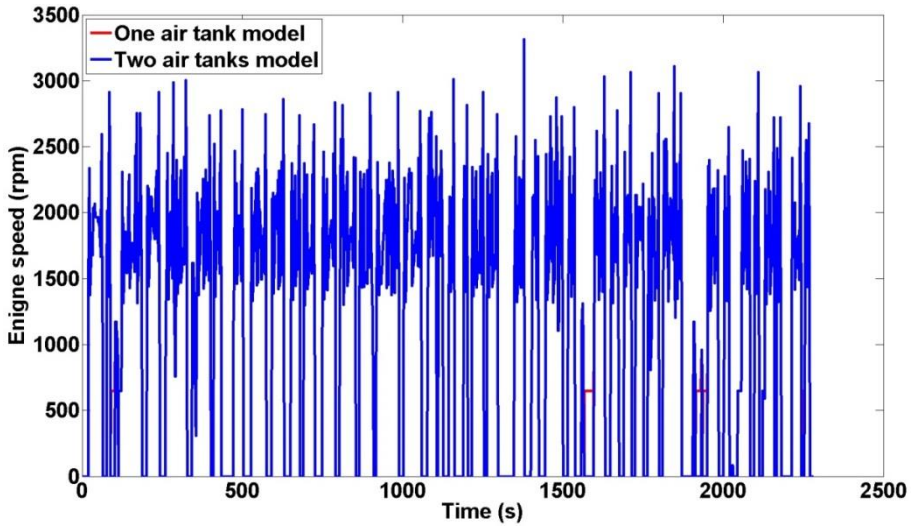

Figure 4-18 Engine speeds during MLTB driving cycle

Figure 4-19 shows the air tank pressure of one air tank model. Similar to the Braunschweig driving cycle simulation, this simulation start in the extreme situation, where the initial air tank pressure is 5.2 bar. At the end of the simulation, the air tank pressure is 5.5 bar which is still higher than its initial pressure. In this figure, the pressure of air tank will drop below the working limit, 5.2 bar. This is because, in the MLTB driving cycle, the interval between two stops is too short which cause the vehicle cannot recover enough energy. For example, after 1500 s in the MLTB, there are four continuous stops which are shown in Figure 4-19 is four pressure drops of the air tank. It means the engine is turned off four times and implemented four cranking events. The result is that the tank pressure drops from 8.2 bar to 4.5 bar. In other words, it means the vehicle needs more air to drive the air starter compared with the opportunity to recover air. But comparing with the air tanks pressure of two air tanks model in Figure

4-20, it can be seen that in two air tanks mode, at least one air tank pressure is always higher than 5.2 bar during the cycle.

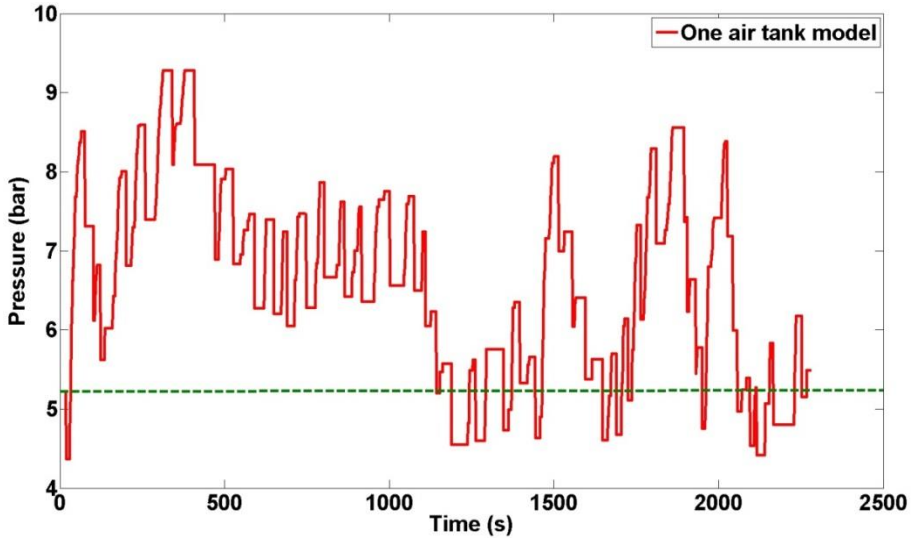

Figure 4-19 Air tank pressure of one air tank model during MTLB driving cycle

Figure 4-20 shows the pressure history for two air tanks. The simulation start with the initial air tanks pressure is both 5.2 bar. At the end of the simulation, the two air tanks pressure are 5.4 bar and 5.7 bar which means that the two air tank model can recover enough energy to support all the stop-start operations during the MLTB driving cycle. This is the advantage of the two air tanks pneumatic hybrid powertrain that it offers the possibility of at least one air tank pressure being higher than the lower limit. In addition, the lower air tank pressure results in higher energy capture during the CM. As a result, the fuel saving potential of the two air tanks system will be higher. From Figure 4-20, it also can be seen that the control strategy for two air tanks model can well manage the energy throughout the MLTB driving cycle. It uses the lower air tank to recovery the air during the braking and also uses the lower air tank to drive the air starter. This is based on the Chapter 3 result, the lower air tank pressure can recovery more air mass during the braking. The result is the two air tanks pressure change from both 5.2 bar at the beginning to both above 5.2 bar at the end of driving cycle. It means that the two air tanks is enough for energy recovery and can eliminate all the idle fuel consumption during the MLTB driving cycle. It also proves that no need any more air tanks to realize the Stop-Start function through the whole MLTB driving cycle.

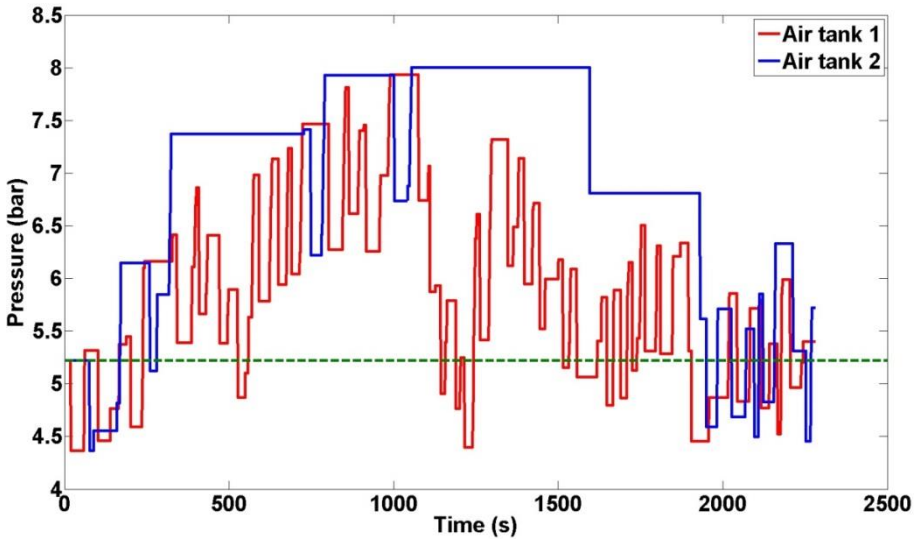

Figure 4-20 Air tanks pressure of two air tanks model throughout MLTB driving cycle

Figure 4-21 shows a comparison of fuel consumption over the MLTB driving cycle between the no air tank model, one air tank model and two air tanks model. The no air tank model consumes 3743.2 g of fuel which is equivalent 57.14 l/100km during the MLTB driving cycle. The one air tank model uses 3501.7 g of fuel which is equivalent 53.45 l/100km, which represents a 6.45% reduction in fuel consumption. The two air tanks model uses 3477.6 g of fuel which is equivalent 53.09 l/100km, which represents a 7.1% reduction in fuel consumption compared with no air tank model. The two air tanks model also reduces the fuel consumption 0.7% compared to the one air tank model. This is because the two air tanks model can recover enough air to support all the stop-start operations during the MLTB driving cycle, while the one air tank model only can support most of the stop-start operations. The result proves that by turning off the engine when the vehicle is stationary to save the idle fuel consumption, a 7.1% reduction in fuel consumption can be achieved in the MLTB driving cycle. In Chapter 2, a fuel consumption result comparison is given out. From the result, it can be seen that if only considering the stop-start operations, the fuel consumption improvement is in the range of 6% to 20% depending on the vehicles and test cycles used. This means the fuel consumption saving of 7.1% here is similar to the result reported within the literatures.

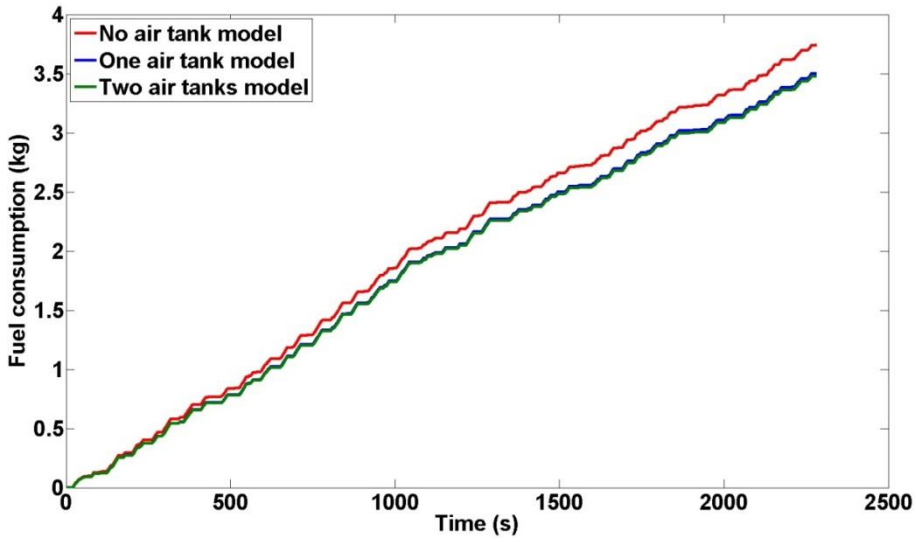

Figure 4-21 Fuel consumption throughout the MLTB driving cycle

4.5 Conclusion

This chapter takes the pneumatic hybrid engine as the research object, focusing on the evaluation the fuel economy improvement ability of pneumatic hybrid technology for the city bus by realizing the Stop-Start Function and further improvement of fuel economy by using multiple air tanks in different test cycles including Braunschweig driving cycle and MLTB driving cycle.

A six-cylinder diesel engine with respectively one or two air tanks has been built in the MATLAB/Simulink environment. Based on these models, the pneumatic hybrid vehicle driving cycle simulation program has been applied to analyse the charging and discharging processes during various bus duty cycles. In order to achieve modularization of control system development and reduce cost in the future, Stateflow in the MATLAB software platform is used to complete the above modelling and simulation.

The result shows

(i) The pneumatic hybrid engine with two air tanks can reduce fuel consumption at least 6% by realizing stop-start operation, and eliminate 90% of the idling time.

(ii) In the case of the modelled bus cycles, significant fuel savings of 7.1% can be achieved during MLTB driving cycles because of the large braking energy and

frequent stop–start operations required during the type of bus operation exemplified by this cycle.

(iii) The two air tanks pneumatic hybrid system has the higher fuel saving potential which is because it can offer the possibility of at least one air tank's pressure being higher than the lower limit and other lower pressure air tank results in higher energy capture during the CM.

The fuel consumption improvements of different kind of models have been summaries in Table 4-5.

Table 4-5 Summary table of fuel consumption improvements

	Braunschweig driving cycle			**MLTB driving cycle**		
	Normal vehicle model	**One air tank model**	**Two air tanks model**	**Normal vehicle model**	**One air tank model**	**Two air tanks model**
Fuel consumption (g)	3384.8	3171.8	3171.8	3743.2	3501.7	3477.6
Fuel consumption (l/100km)	42.61	39.93	39.93	57.14	53.45	53.09
Improvement (-)	-	6.29%	6.29%	-	6.45%	7.1%

CHAPTER 5
ANALYSIS OF THE PNEUMATIC REGENERATIVE BRAKING SYSTEM

5.1 Introduction

Recovering braking energy and reusing it can significantly improve the fuel economy of a vehicle which is subject to frequent braking events such as a city bus. As one way to achieve this goal, the pneumatic hybrid technology converts kinetic energy to pneumatic energy by compressing air into the tanks during braking, and then reuses the compressed air to power an air starter to realize a regenerative Stop-Start function. This has already been investigated in Chapter 4. The pneumatic hybrid city bus uses the driven rear axle to achieve the regenerative braking function. Because the majority of hybrid and electric and battery electric vehicle employ front wheel drive, this aspect of the architecture represents a significant difference with light duty vehicles which has consequences for the choice of braking strategy. This chapter discusses the research into the blending of pneumatic regenerative braking and mechanical frictional braking at the rear axle. The aim of the braking function is to recover as much energy as possible and at the same time distribute the total braking effort between the front and rear axles to achieve stable braking performance.

This chapter firstly presents an analysis of vehicle behaviour through different bus driving cycles and during braking events, and then compares two configurations of the hybrid braking system. The respective configurations, a parallel hybrid brake system and a fully controllable hybrid brake system, are compared and the control strategy presented and discussed. The comparison shows the fully controllable hybrid braking system has a distinct advantage and is chosen to realize the regenerative braking function.

A pneumatic hybrid braking optimisation simulation model has been built in the MATLAB/Simulink environment to facilitate an investigation of an optimum air tank pressure for energy recovery. Similar to the models in Chapter 4, this model is also built

with QSS-TB with some new blocks added. Based on the optimisation result, a new control strategy is implemented along with a baseline simulation model to explore the benefits of the new control strategy.

5.2 Braking Energy Consumed and Braking Intensity Distribution in Driving Cycles

5.2.1 Braking Energy Consumed in Driving Cycle

To recover as much of braking energy as possible, the braking behaviour and its characteristics with respect to vehicle speed, braking power and deceleration rate during different driving cycles need first to be well understood. One widely-used city bus driving cycles which have already introduced in Chapter 4, the Braunschweig driving cycle is used as the basis for the reported work. The characteristic of the Braunschweig driving cycles is summarized here.

Compared with the other bus driving cycle, such as MLTB driving cycle, the Braunschweig driving cycle is characterized with higher vehicle speeds and less stop–start operations over a slightly longer distance. Table 5-1 shows the basic parameters of the Braunschweig driving cycle.

Table 5-1 Basic parameters of the Braunschweig driving cycle

	Braunschweig driving cycle
Time (s)	1740
Distance (km)	10.87
Acceleration (%)	39.7
Deceleration (%)	30.8
Idle (%)	29.5
Number of stops (-)	30

When the vehicle is driving on the flat road, the driving power can be calculated using Equation (5-1).

$$P_d = \frac{v}{1000}\left(Mgf_r + \frac{1}{2}\rho_a C_D A v^2 + M\delta\frac{dv}{dt}\right) \quad (5\text{-}1)\ [6]$$

where P_d - driving power,

M - vehicle mass,

g - gravitational acceleration,

f_r - tire rolling resistance coefficient,

ρ_a - air mass density,

C_D - aerodynamic drag coefficient,

A - frontal area of the vehicle,

v - vehicle speed,

δ - rotational inertia factor,

dv/dt - vehicle acceleration or deceleration (m/s^2).

If P_d>0, the powertrain of the vehicle exports power to the wheels to drive the vehicle forward. Otherwise, P_d<0, the braking and kinetic energy of the vehicle is dissipated by the braking system. This is the energy that should be recovered and reused to reduce the fuel consumption.

The parameters of the city bus used in the reported work are listed in Table 5-2.

Table 5-2 City bus data

Vehicle Total weight (kg)	16500
Aerodynamic drag coefficient (-)	0.5
Frontal area (m^2)	5.69
Wheel radius (m)	0.508
Rolling resistance coefficient (-)	0.013
Wheel base (m)	6.1
Distance from gravity centre to front wheel centre (m)	4
Gravity centre height (m)	1

The traction and braking energy dissipated during the Braunschweig driving cycle are calculated and shown in Figure 5-1 which indicates that in the urban area the bus's braking power can reach to 80% of the total traction power.

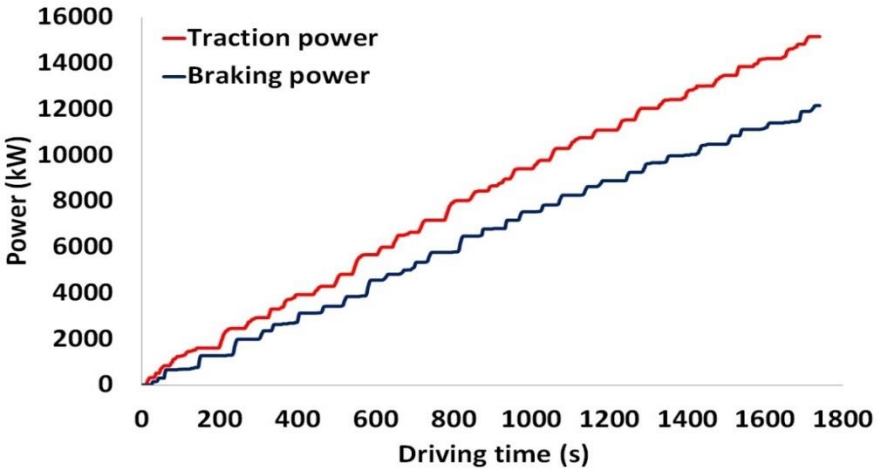

Figure 5-1 Traction and braking power dissipation in Braunschweig driving cycle

5.2.2 Braking Intensity Distribution in Driving Cycles

Another important consideration is the braking intensity in different city bus driving cycles. Understanding this is very helpful to the proper design of an optimal control strategy and the system sizing. Figure 5-2 and Figure 5-3 show the deceleration distribution during the Braunschweig driving cycle and the MLTB driving cycle. It can be seen in these figures that, during the Braunschweig driving cycle and the MLTB driving cycle respectively, the braking of the city bus is very gentle with most of the deceleration rate below 0.2 g, compared with the passenger car whose mean fully developed deceleration is 0.51 g (equal to 5.0 m/s^2) [67]. Therefore, this work only considers braking behaviour corresponding to decelerations up to 0.4 g.

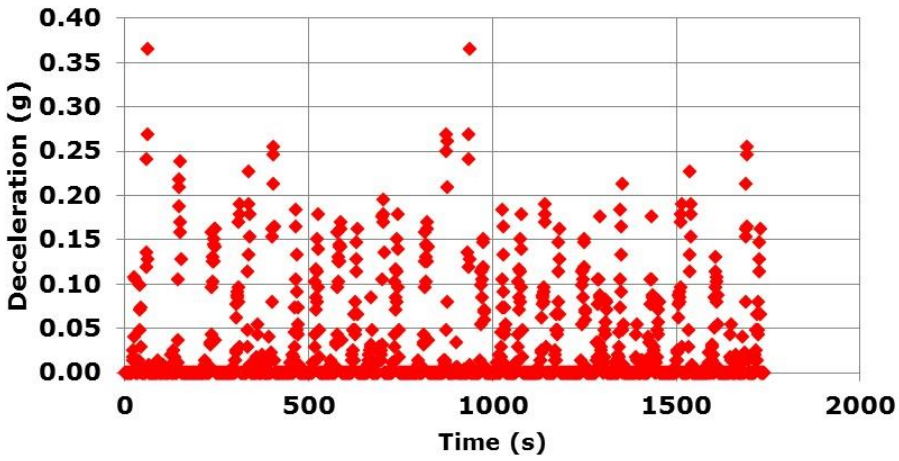

Figure 5-2 Deceleration distribution during Braunschweig driving cycle

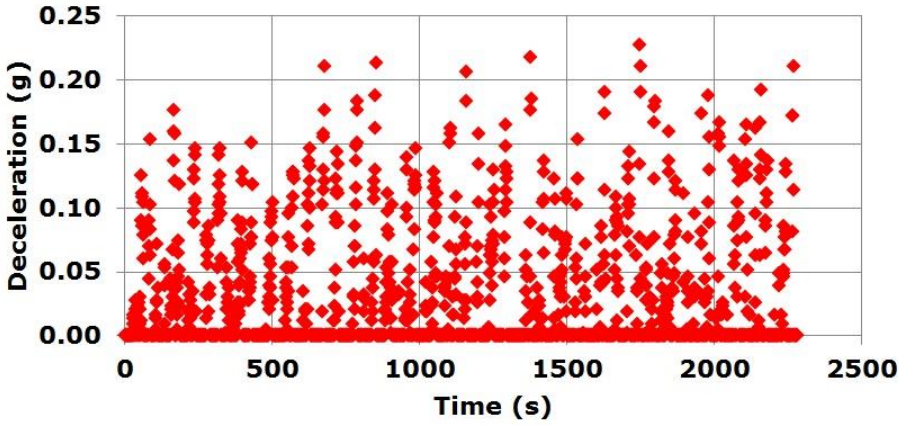

Figure 5-3 Deceleration distribution during MLTB driving cycle

5.3 Pneumatic Regenerative Braking System Configuration

As mentioned before, to implement the pneumatic regenerative braking, the structure of normal city bus powertrain needs slight modifications. One high pressure air tank connected to the engine manifold is added to the vehicle to store the regenerated energy. A CREB device is added to the normal engine to let the engine work as a compressor during braking [11]. During vehicle braking, no fuel is injected into the cylinders, and the engine operates as a compressor driven from the wheels by vehicle motion, pumping compressed air into the air tank [63, 76]. Work done by the pistons causes the vehicle to decelerate, converting its kinetic energy into the energy of compressed air.

Figure 5-4 shows a schematic diagram of the engine with the pneumatic regenerative system. As explained in Chapter 4, during the CM, by opening the CREB intake valve and check valve, closing the throttle valve during the Compress Stroke, the air can be compressed into the air tank. When the vehicle starts, a standard production air starter, SS175 supplied by Ingersoll Rand, is chosen to start the engine.

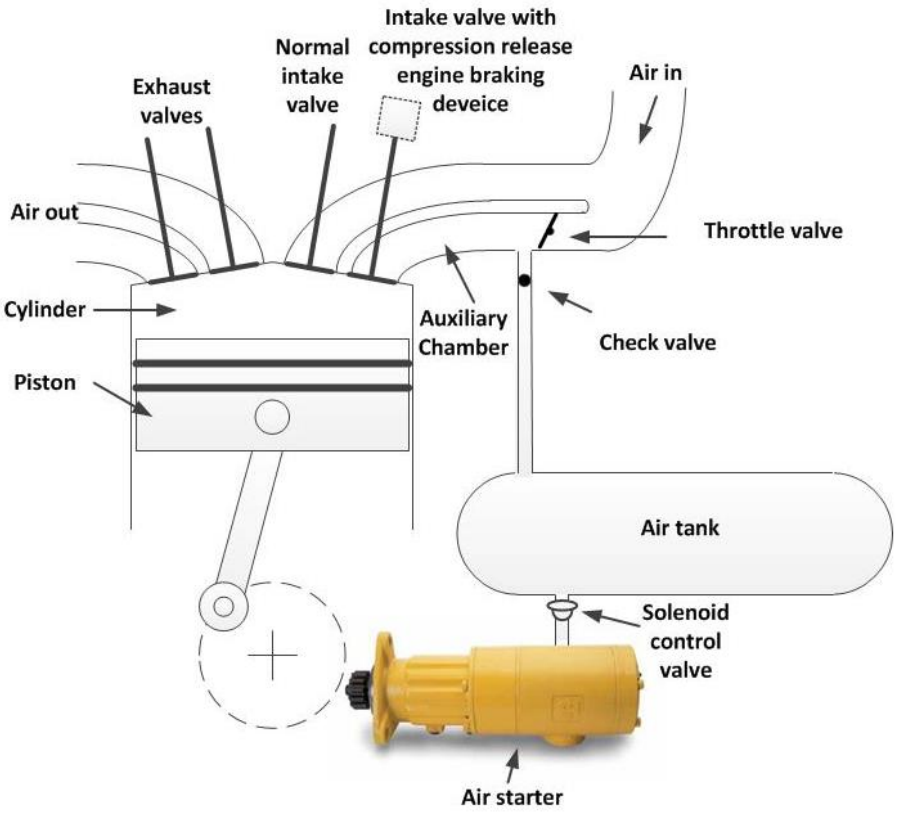

Figure 5-4 Schematic diagram of the engine with pneumatic regenerative system

5.4 Pneumatic Regenerative Braking Control Strategy

Like the regenerative braking system in vehicles with electric propulsion, there are also two configurations of hybrid braking system in the pneumatic hybrid city bus, respectively

(i) the parallel hybrid brake system,
(ii) the fully controllable hybrid brake system.

(i) has a simple structure and control and retains all the major components of the conventional braking system; (ii) can fully control the braking force for each individual wheel, thus greatly enhancing the vehicle's braking performance on all types of roads [6]. In the pneumatic hybrid city bus, during braking, the engine becomes a compressor and directly applies its braking torque to the rear axle. The research question is then - how to distribute and blend this torque with the vehicle mechanical braking torque on the rear axle and front axle? This question will be answered in the following sections.

5.4.1 Parallel Hybrid Pneumatic City Bus Braking System Control Strategy

The parallel hybrid braking system retains all the major components of the conventional mechanical brakes and adds the pneumatic braking torque on the rear axle. The pneumatic braking torque will be created by the engine and managed by the controller. The controller will calculate the ratio of mechanical braking force and pneumatic braking force based on vehicle speed, deceleration and the pressure of the air tank.

Figure 5-5 shows the braking force distribution strategy which is the key point of the control strategy of this kind of system. In the parallel hybrid braking system, the mechanical braking system still has a fixed ratio of braking force distribution on the front and rear axles represented by the β-line [77].

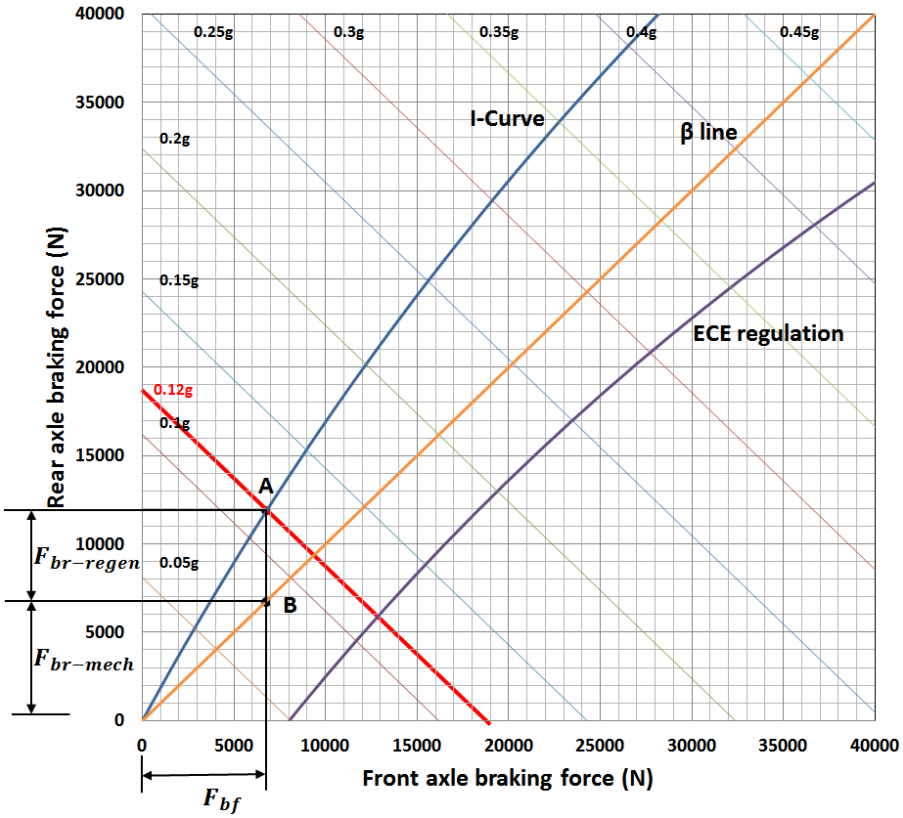

Figure 5-5 Control strategy for the parallel hybrid braking system

When the vehicle is braking, the loads of the front and rear wheels vary with the deceleration of the vehicle. In order to keep the vehicle stable while braking, the braking

force acting on the front and rear wheels should be limited in a reasonable range [78]. The normal load on the front axle W_f can be determined as

$$W_f = \frac{mg}{L}(b + h_g \frac{j}{g}) \quad \text{(5-2) [78]}$$

Similarly, the normal load acting on the rear axle W_r can be expressed as

$$W_r = \frac{mg}{L}(a - h_g \frac{j}{g}) \quad \text{(5-3) [78]}$$

where j – deceleration rate of the vehicle,

h_g – gravity centre height of the vehicle,

a – distance from gravity centre to front wheel centre,

b – distance from the gravity centre to front wheel centre,

g – gravitational acceleration,

L – wheel base.

Braking force acting on the front and rear wheels are required to be proportional to their corresponding normal load. Such a distribution of the braking forces on front and rear wheels can be obtain the maximum braking stability of the vehicle [79]. Therefore, the relationship of the braking force on front and rear wheels, associating with the deceleration of the vehicle, can be expressed as:

$$\frac{F_f}{F_r} = \frac{a + h_g \frac{j}{g}}{b - h_g \frac{j}{g}} \quad \text{(5-4) [78]}$$

The summation of the braking forces of the front and rear wheels (the total barking force of the vehicle) is related to the vehicle deceleration by

$$F_f + F_r = mgj \quad \text{(5-5) [78]}$$

Substituting Equation (5-5) into (5-4) gives out the ideal distribution of the braking forces on the front and rear wheels as:

$$F_r = \frac{1}{2}\left[\frac{G}{h_g}\sqrt{b^2 + \frac{4h_g L}{G}F_f} - \left(\frac{Gb}{h_g} + 2F_f\right)\right] \quad \text{(5-6) [6]}$$

where F_r – total braking force on the rear wheels,

G – gravity of the vehicle,

h_g – gravity centre height,

b – distance from gravity centre to rear wheel centre,

L – wheel base,

F_f – total braking force on the front wheels.

The I-Curve shown in Figure 5-5 and Figure 5-7 can be calculated by this equation. The I-Curve shows the ideal braking force distribution of the vehicle [80]. This ideal distribution curve gives the maximum braking force that makes the front and rear wheels lock simultaneously for each friction coefficient. When the braking force is distributed to the front and rear wheels on the I-Curve, safe braking is assured.

If most of the braking force is applied to the rear wheel and a very small force to the front wheels, there will be a reduced utilization of road adhesion. To avoid this situation, brake design regulations have been developed. Typical is The Economic Commission of Europe (ECE) brake regulation [81]. The ECE regulation indicates the minimum braking force on the rear wheels, which can be calculated by Equation (5-7), and also shown in Figure 5-5 and Figure 5-7 The physical meaning of this equation is that when the front wheels are locked, the rear braking force must be large enough to make the vehicle yield a deceleration rate not smaller than the value dictated by Equation (5-7) [80].

$$\frac{j}{g} \geq 0.1 + 0.85(\mu - 0.2) \qquad \text{(5-7) [80]}$$

where j – deceleration rate of the vehicle,

μ – adhesion coefficient,

g – gravitational acceleration.

The total braking force on the rear axle consists of mechanical braking, $F_{br\text{-}mech}$, and pneumatic braking, $F_{br\text{-}regen}$, as shown in the Figure 5-5. In order to recover maximum braking energy, the pneumatic hybrid braking system should employ the pneumatic braking force on the rear axle as much as possible during the whole vehicle operation range. Based on the investigation mentioned before, during the MLTB driving cycle and Braunschweig driving cycle, the braking is very gentle with most of the deceleration rate below 0.2 g, while the maximum deceleration rate of these two driving cycle is 0.4 g. For this reason when the deceleration is less than 0.4 g, both mechanical and pneumatic braking systems share the total rear axle braking force. When the required deceleration

is greater than 0.4 g, the pneumatic braking force is reduced to zero and only mechanical braking works on the rear axle to get stable and sufficient braking force. Although the system can maintain the pneumatic braking force as high as possible, and simply supplement with the friction braking system when the deceleration is greater than 0.4 g. It may cause an unsafe situation when the driver brakes urgently. The driver would release to clutch to stop the vehicle during the braking period. The releasing the clutch would stop the braking force from pneumatic braking system and this may cause the braking force dropping sharply which made the vehicle braking behaviour unstable. As a result, the ideal control strategy for a parallel braking system is when the deceleration is less than 0.4 g and the braking force distribution follows the I-curve, otherwise, it follows the β-line. However, this strategy cannot be realised in a practical implementation of the parallel hybrid braking system, the reason will be explained in the following paragraphs.

For example, in Figure 5-5, if the vehicle's deceleration rate is 0.12 g, the red line, the maximum braking force ratio that makes the front and rear wheels lock simultaneously is point A which is on the I-Curve. The mechanical braking system can supply a fixed ratio braking force on the front and rear axles that follow the β line, point B in Figure 5-5. From A to B is the range of force that the pneumatic braking system needs to supply. If it is an electric regenerative braking system, the controller can control the electric motor to create the requested braking force if it does not exceed the motor's working range. But in the pneumatic braking system, during braking, the pneumatic braking system may not be able to supply the exact braking force $F_{br\text{-}regen}$, which is shown in Figure 5-5 as A to B at every moment. This is because the pneumatic hybrid braking system's characteristic that the braking torque created by the pneumatic braking system is related to the air tank pressure. During braking, the engine operates as a compressor driven from the wheels by vehicle motion and pumping compressed air into the air tank. At the same time, there is no fuel injected into the cylinders. Work performed by the pistons slows down the vehicle and converts its kinetic energy into energy of compressed air [4]. The result from Chapter 3, as shown in Figure 3-15, has already supplied the relationship between the brake torque and air tank pressure, which is the lower air tank pressure can create more brake torque at the same engine speed. It means the small air tank pressure is beneficial to improve the engine braking performance based on the engine using in this research.

Also in Schechter's research [63], Figure 5-6 clearly indicated that the engine IMEP is related to the air tank pressure which the lower air tank pressure may not create higher IMEP. It can be seen when the air tank pressure higher than 0.8 MPa (equal to 8 bar), the IMEP decreases when the air tank pressure increases, which accord with the Chapter 3 result, the lower air tank pressure can create more brake torque. But when the air tank pressure is lower than 0.8 MPa, the result is different with the result from Chapter 3. This is because Schechter used a different engine structure in his research. Also in the same paper, an Equation (5-8) was derived to compute the peak value of IMEP as a function of air-tank pressure during the braking process [63].

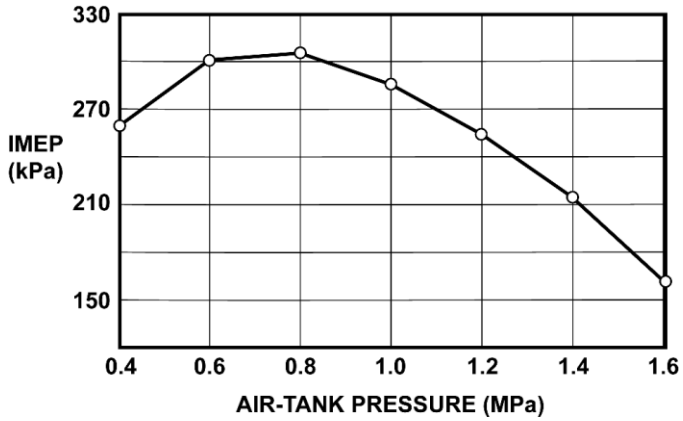

Figure 5-6 IMEP in a Type 1 compression-braking cycle [63]

$$IMEP = 2(\rho c_v T_2 + p_2)(r^{k-1} - 1)(R - r)/(R - 1) \quad \text{(5-8) [63]}$$

where ρ – air density,

c_v – specific heat at constant volume,

T_2 – air temperature,

p_2 – air pressure,

r – compression ratio from point 2 to point 3,

k – ratio of specific heats,

R – geometric compression ratio.

Based on the Equation (5-8), the braking force $F_{br\text{-}regen}$ created by the engine during the braking can be calculated from engine's IMEP. Unlike the electric regenerative braking technology, this braking force, $F_{br\text{-}regen}$ is based on the air tank pressure at each instant. That means the pneumatic braking system may not be able to supply the exact braking

force that the controller requires. As a result, the vehicle may not be able to follow the I-curve. This represents a fundamental difficulty in the application of this method. Instead, a fully controllable system that is able to follow the I-Curve is reviewed in the following sections of the paper.

5.4.2 Fully Controllable Pneumatic Hybrid City Bus Braking System Control Strategy

In recent years, more advanced braking systems have emerged that allow the control of the braking force on each wheel independently [6]. The fully controllable hybrid braking system is based on these new technologies and consists of both a mechanical braking system and a pneumatic braking system [6]. In the fully controllable hybrid braking system, the braking torque applied at each wheel is independently produced by a corresponding brake actuator, which is commanded by its controller. The torque command to each wheel is generated based the signals from different sensors such as the pressure sensor, brake pedal position sensor and wheel speed sensor. As a result, unlike the parallel braking system, the mechanical braking system does not have a fixed ratio of braking force distribution on the front and rear axles so there is not a fixed β line in the braking force distribution diagram shown in Figure 5-7. Similar to the parallel braking system, the strategy of the fully controllable system is to follow the I-curve to ensure the vehicle's best braking performance and to recover as much as much energy as possible.

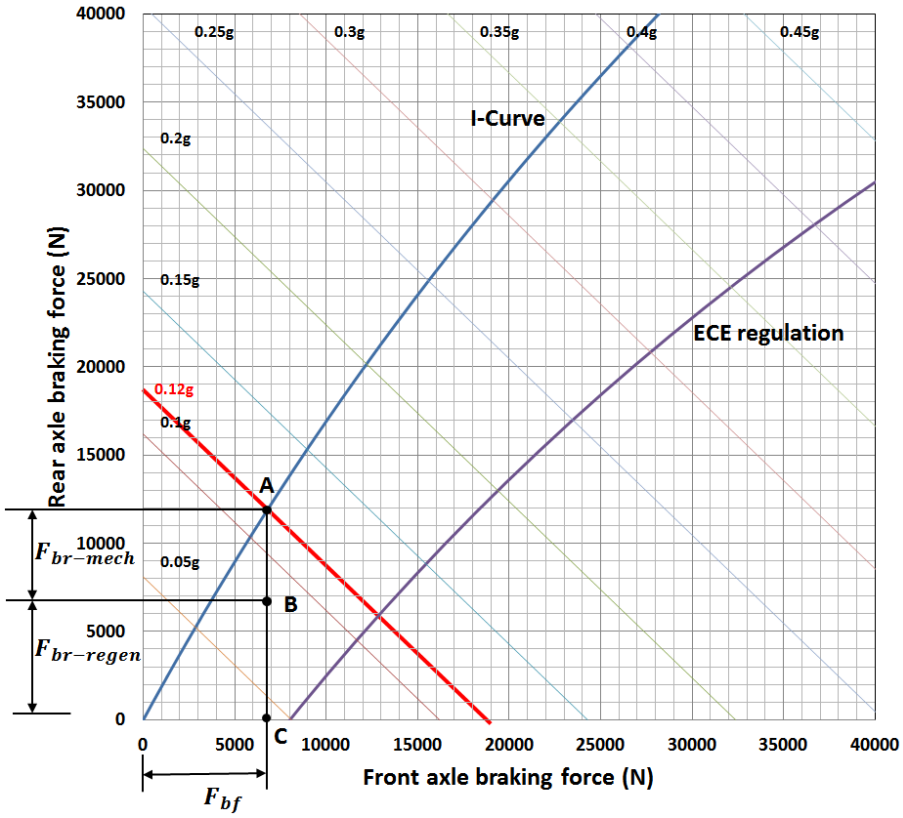

Figure 5-7 Control strategy for the fully controllable hybrid braking system

Figure 5-7 illustrates the principle of the control strategy of a city bus with pneumatic hybrid powertrain, on which the pneumatic hybrid braking is available only on the rear axle. Similar to parallel hybrid braking system when the deceleration is less than 0.4 g, both mechanical and pneumatic braking systems share the total rear axle braking force. When the deceleration is higher than 0.4 g, the pneumatic braking force falls to zero with only mechanical braking working on the rear axle. During the hybrid braking mode, when the required total braking force on the rear axle is smaller than that produced by the engine braking, the pneumatic hybrid braking system produces the total braking force and no mechanical braking force is applied. At the same time, the mechanical braking system produces the total braking force for the front axle to let the vehicle follow the I-curve. Because of the characteristics of the pneumatic hybrid braking system, the density of air is too low to produce a large braking force, this working condition is rare. From our research result, during the whole Braunschweig driving cycle, the braking force on the rear axle supplied by the pneumatic braking system never exceeded the braking force required to keep the vehicle on the I-Curve for the rear axle. When the required total

braking force on the rear axle is greater than that produced by the engine braking, both pneumatic braking and mechanical braking have to be applied.

To recover as much braking energy as possible, the pneumatic hybrid braking system is controlled to work at high efficiency and to supply the corresponding braking force. For example, in Figure 5-7, if the vehicle's deceleration rate is 0.12 g, shown by the red line, the maximum braking force ratio that makes the front and rear wheels lock simultaneously is point A which is on the I-Curve. Because the braking force, $F_{br\text{-}regen}$, is based on the air tank pressure at each instant, the $F_{br\text{-}regen}$ can change from 0 to point A in Figure 8 which means point B can be anywhere on the line AC. Unlike the parallel hybrid braking system, the mechanical braking system in the fully controllable hybrid braking system does not have to supply fixed ratio braking force on the front and rear axles. This means the remaining braking force on the rear axle can be supplied by the mechanical braking system which is from A to B in the Figure 5-7. Meanwhile, the mechanical braking system controls both the front axle braking force and the rear axle braking force to ensure that the braking follows the I-curve.

5.5 Design Optimisation

5.5.1 Optimisation Problem Statement

To recover as much braking energy as possible, the pneumatic hybrid braking system should be controlled to work under the most efficient conditions. An optimisation requirement is formulated to identify the best initial air tank pressure to maximize the air mass recovered during the braking in a typical bus driving cycle, Braunschweig driving cycle. As mentioned before, the air tank sizes and number are fixed for this research. So the only variable can be optimised and related to the energy efficiency is the intimal air tank pressure. As a result, the objective of this optimisation is to identify the initial air tank pressure to increase the total air tank pressure increment for the Braunschweig driving cycle. The cost function is defined as Equation (5-9):

$$J = maxf(X) = min\left[-\left(J_{pressure}(X)\right)\right] = min[-(\int \dot{m}_p dt)] \tag{5-9}$$

where, $J_{pressure}$ is the instantaneous pressure increment of the air tank per unit time, X is the variable vector which includes the parameters of the control strategy and is shown in Table 5-3.

Table 5-3 Design variable for initial air tank pressure optimisation

Design variable	Description	Lower bound (bar)	Upper bound (bar)
p	The initial pressure of air tank	5.2	10

In order to drive the air starter motor to crank the engine, the lowest air tank need to above 5.2 bar. As a result, the air tank lower bound set to be 5.2 bar. The air tank is designed to have a maximum operation pressure of 10 bar, as a result, the maximum air tank pressure should not be above 10 bar [23]. Therefore, the upper bound for the air tank is 10 bar.

The vehicle powertrain system may have a large number of local optimums which mean that the gradient-based optimisation algorithm may not converge to a global solution [82]. Compared with other approaches to optimisation, global optimisation can be used to solve optimisation problems where the objective or constraint functions are continuous, discontinuous, stochastic, may not possess derivatives, or include simulations or black-box functions with undefined values for some parameter settings [83]. As a result, the global optimisation algorithm is employed for the design optimisation. For the optimisation problems for which the objective function is not differentiable, or is not even continuous, the direct search may be used [83]. The direct search algorithm chosen here is called the Generalized Pattern Search (GPS) algorithm. GPS algorithm has a robust theoretical background and they have been successfully applied in several real-world applications [84].

A pneumatic hybrid braking optimisation simulation model has been built in the MATLAB/Simulink as shown in Figure 5-8. This model is built with the QSS-TB with some new modules added. In the optimisation implemented here, the fitness function and options are first input by using the Optimisation Toolbox in MATLAB. Then the Optimisation Toolbox completes the GPS steps such as polling, expanding and

contracting to implement the optimisation. The GPS optimisation is introduced in Appendix-V in detail.

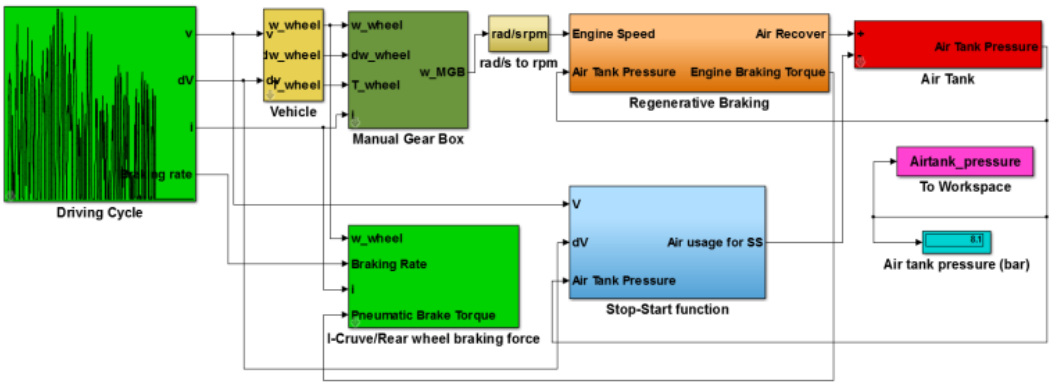

Figure 5-8 Pneumatic hybrid braking optimisation simulation model

5.5.2 Optimisation Result

Table 5-4 shows the optimisation result. The increment of air tank pressure during the Braunschweig driving cycle increases from 0.37 bar to 2.91 bar with the initial air pressure are 7.5 bar and 5.2 bar respectively.

Table 5-4 Pattern Search optimisation result

	Variables - Initial air tank pressure (bar)	Final air tank pressure (bar)	Objective - The increment of Pressure (bar)
Before optimisation	7.5	7.87	0.37
After optimisation	5.2	8.11	2.91

Figure 5-9 shows the result of the optimisation for the initial air tanks pressure for the Braunschweig driving cycle. It can be seen that after 18 iterations, the objective function value remained unchanged for 18 iterations and the optimisation process stopped. So the global optimum has been found. Therefore, in light of the optimisation, the initial air tank pressure should be set at 5.2 bar based on the simulation result.

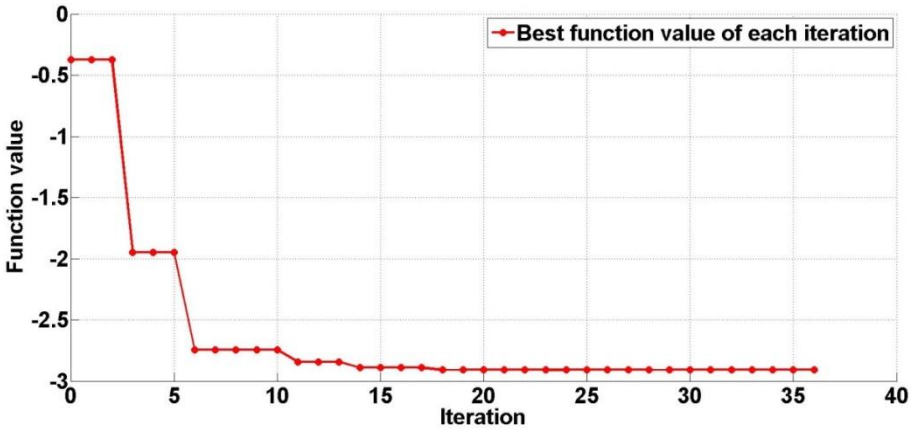

Figure 5-9 Trace of objective function value over iterations of the optimisation

Another simulation is also conducted here to prove the optimisation result. The increment of pressure during the driving cycle based on the different initial air tank pressure is shown in Figure 5-10. The result indicated that the lower initial air tank pressure gives the more air mass recovered for the driving cycle. This is consistent with the result in Chapter 3 and reported by Lee [9], that a lower tank pressure is needed to provide a higher braking torque from the engine.

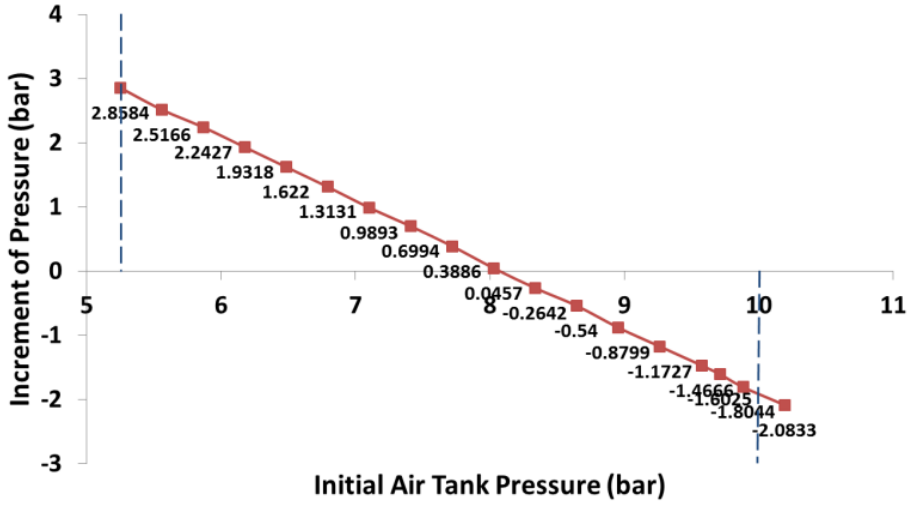

Figure 5-10 The increment of pressure during the driving based on different initial air tank pressure

5.6 Simulation Result

To evaluate the optimisation result, a simulation is conducted here to compare the recovered air mass between two control strategies. This aspect of the research uses the

simulation model built in Chapter 4. The main difference of two control strategies is the initial air tanks pressure. The new control strategy is based on the optimized result. The relevant bus powertrain parameters are summarized in Table 5-5.

Table 5-5 Two air tanks pneumatic hybrid city bus parameter data

No. of cylinders (-)	6
Cylinder bore (mm)	105
Piston stroke (mm)	132
Displacement volume (l)	7.25
Compression ratio (-)	17.5:1
1st gear ratio (-)	6.9
2nd gear ratio (-)	4.13
3rd gear ratio (-)	2.45
4th gear ratio (-)	1.49
5th gear ratio (-)	1
Final drive ratio (-)	5.125
Air tanks volume (l)	151
Additional mass of air starter (kg)	15
Additional mass of air tanks (kg)	200

In Chapter 4, the research had developed two kinds of pneumatic hybrid powertrain differentiated by the number of the air tanks. The previous simulation result showed that compared with one air tank model, the fuel consumption of two air tanks model can be further reduced. As a result, the two air tank pneumatic hybrid engine is chosen to be the research object here to evaluate the control strategy and optimisation procedure. The two air tanks pneumatic hybrid engine structure is summarized and shown in Figure 5-11. In this configuration, two air tanks can separately receive the air from the cylinder in the CM and drive the air starter motor when cranking. There is no connection between these two air tanks in order to simplify the model.

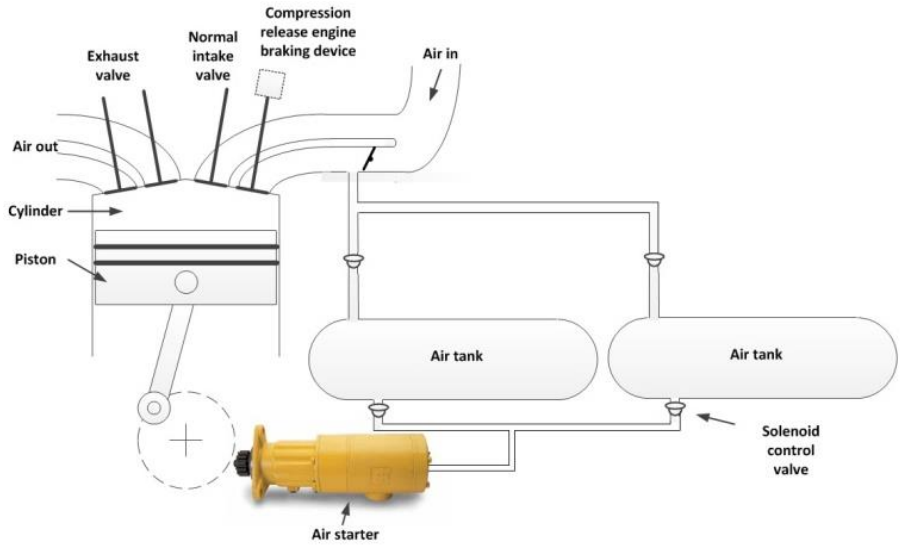

Figure 5-11 Two air tanks pneumatic hybrid engine structure

The previous optimisation result shows that 5.2 bar air tank pressure is the best pressure for the braking energy recovery. The amount of air mass supplied to the air tank decrease as the air tank's pressure increases during the braking. So the control strategy should keep the pressure of the air tank as low as possible to enhance the efficiency of energy recovery. But in order to start the vehicle without using an additional electric starter, the controller should always keep at least one air tank's pressure is above 5.2 bar to support one engine cranking. The control strategy will compare the pressure of two air tanks at regular intervals. When the city bus starts to decelerate, the controller chooses the lower pressure air tank to recover the air. When the engine must be restarted, the lower pressure air tank is chosen for the air starter to reduce the pressure in the air tank in order to enhance the energy recovery efficiency in the future deceleration. Meanwhile, the controller monitors the pressure of two air tanks to keep at least one air tank at a sufficient pressure for the next cranking. The simulation considers the extreme case, with only enough air to support one cranking event, where the initial pressures of two air tanks are 5.2 and 3 bar respectively. If the vehicle cannot recover enough energy, after the next engine stop it will not start again.

Figure 5-12 shows the air tank pressure of the two air tanks model for the whole Braunschweig driving cycle. From this figure, it can be seen that the pressure of the air tanks increase respectively from 3 to 7 bar and 5.2 to 8.2 bar after one driving cycle. That means the air tanks become almost "Full" from almost "Empty" at the beginning.

This also proves that the braking energy is sufficient to implement stop-start operation during the driving cycle.

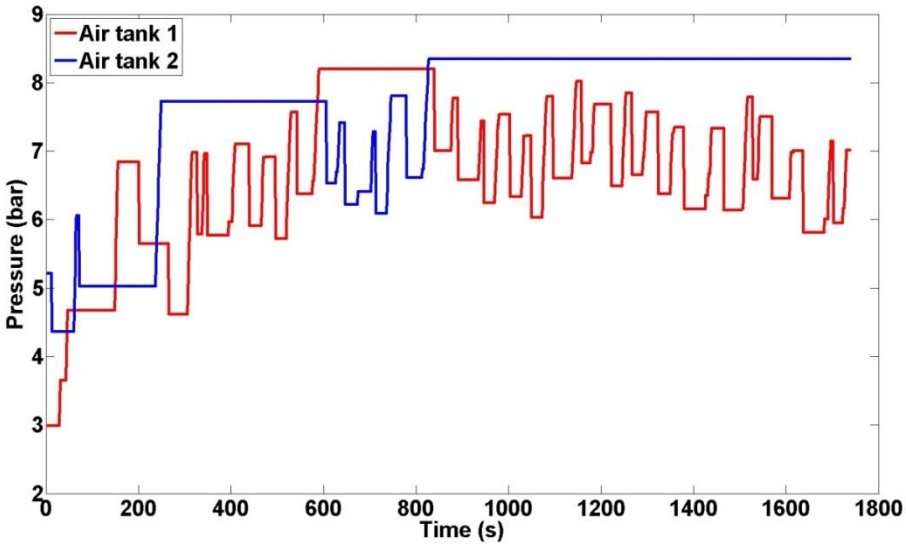

Figure 5-12 Air tanks pressure of two air tanks model during Braunschweig driving cycle

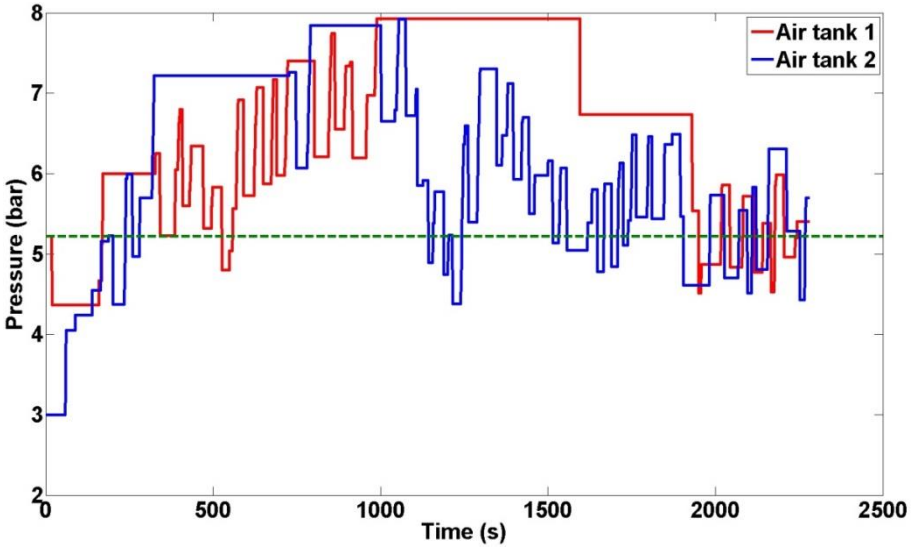

Figure 5-13 Air tanks pressure of two air tanks model during MLTB driving cycle

Figure 5-13 shows the pressures in the two respective as they vary during the MLTB driving cycle. The green line indicates the limitation of the lowest pressure of air tank to implement the stop-start operation and the best energy recovery pressure. The simulation starts with the initial air tanks pressure are 5.2 and 3 bar respectively. At the end of the simulation, the two air tanks pressure are 5.5 bar and 5.8 bar which means that the two air tank model can recover enough energy to support all the stop-start

operations during the MLTB driving cycle. In addition, the lower air tank pressure results in higher energy capture during the CM. As a result, the energy recovery potential of the two air tanks system will be higher.

The simulation results with both the Braunschweig and MLTB driving cycles in Figure 5-12 and Figure 5-13 also demonstrates that the braking energy recovery rate relates to the speed and number of stops of the vehicle. The Braunschweig driving cycle has less Stop–Start operations which can produce a higher mass of recovered air per vehicle stop, so can keep the pressure of air tank at a higher level compared with the MLTB driving cycle.

Figure 5-14 shows a comparison of air mass recovery of two air tanks over the Braunschweig driving cycle. Tank 1 recover 2841.4 g and tank 2 recover 3536.1 g respectively. Compared with the pressure at the start of the cycle, it can be found with a lower initial pressure more air can be recovered in a single driving cycle because the lower air tank pressure can enhance the net recovery of energy.

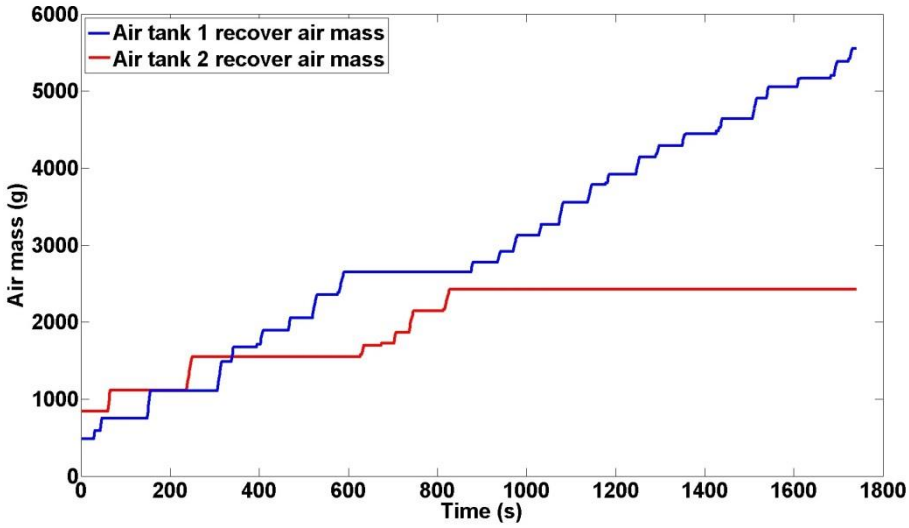

Figure 5-14 Air mass recovery during the Braunschweig driving cycle

Table 5-6 shows the comparison of air mass recovered during the Braunschweig driving cycle between the new control strategy and the previous one in Chapter 4. The previous initial air tanks pressure, 5.2 bar and 4.5 bar, is shown to recover 6377.5 g air, 171.4 g less than the newly optimized initial air tanks pressure, 5.2 bar and 3 bar. This is because the lower air tank pressure can recover more air mass during the braking which is not only proved by the optimisation result, but also confirmed in Chapter 3. As a result,

the simulation starts with lower air tanks pressure can recover more air mass during the braking. Although the increment is only 2.7%, it still proves that optimising the initial air tanks pressure is worth doing for the research. This is because during the Braunschweig driving cycle, the optimised control strategy still can support all the Stop-Start operations which mean the air amount used to drive the air starter is not change. The 2.7% increment all come from the energy recovery efficiency increased during the braking. This means the optimisation of the initial air tanks pressure can increase the energy recovery efficiency.

Table 5-6 Comparison of air mass recovered during Braunschweig driving cycle between the new control strategy and the previous one

	Air mass in the previous control strategy (g)			**Air mass in the new control Strategy with optimisation result (g)**		
	Start	**End**	**Increment**	**Start**	**End**	**Increment**
Air mass in tank 1 (g)	840	3681.4	2841.4	840	2926.1	2086.1
Air mass in tank 2 (g)	500	4036.1	3536.1	500	4962.8	4462.8
Total air mass recovered (g)	-	-	6377.5	-	-	6548.9
Improvement (-)	-	-	-	-	-	171.4 (2.7%)

5.7 Conclusion

This analysis of vehicle behaviour through different bus drive cycles and during braking events, including a comparison of two configurations of the hybrid braking system points to the fully controllable hybrid braking system is the focus of the investigation.

The funding includes

(i) It indicates that in the urban area the bus's braking power can reach to 80% of the total traction power, and the braking of the city bus is very gentle with most of the deceleration rate below 0.2 g, compared with the passenger car.

(ii) The fully controllable hybrid braking system is fit for the requirement of the pneumatic hybrid regenerative system which can either work at high efficiency

to recover as much braking energy as possible and supply the corresponding braking force.

(iii) The optimisation result shows that the 5.2 bar air tank pressure is the best pressure for braking energy recovery.

(iv) The model with the newly optimized initial air tanks pressure can enhance 2.7% the total air mass recovered during the braking compared with the previous control strategy which means the air tanks pressure is the function of the energy recovery rate.

These findings give the fundamental fact for the future research to develop the pneumatic hybrid city bus control strategy which not only can realize the Stop-Start function, but also other functions such as Boost function which will be discussed in Chapter 6.

CHAPTER 6
EVALUATING THE PERFORMANCE IMPROVEMENT OF PNEUMATIC REGENERATIVE SYSTEM

6.1 Introduction

Pneumatic hybrid technology refers to the use of storage of compressed air as a means of energy recovery in a vehicle system. A pneumatic hybrid system stores compressed air during the braking process. The compressed air can be re-used either to realize a regenerative Stop-Start function or to improve the engine performance by injecting compressed air into the inlet manifold to build-up engine torque more rapidly compared with the unassisted engine [11].

This chapter theoretically analyses the reasons for engine turbo-lag and the methods developed for reducing the turbo-lag and improving transient response first. Then, a number of architectures for managing a rapid energy transfer into the powertrain to assist acceleration of the turbocharger have been proposed and investigated from two aspects, engine brake torque response and vehicle acceleration, by using the 1-D engine simulation.

6.2 Theoretical Analysis of the Methods to Reduce Turbo-lag

As described in [11], the pneumatic hybrid technology has benefits that accrue from using the stored compressed air to reduce turbo-lag. Turbo-lag is observed when the engine load is increased. Increasing air flow to the cylinders is the result of a series of energy transfers in the air system which requires time to stabilize. Consequently, the air-fuel ratio falls since the air-supply cannot immediately match the increased fuelling that corresponds to the load demand on the engine. To limit particulate emissions, the quantity of fuel injected is controlled by a smoke limiting function implemented in the engine management system and is adjusted to match the supply of fresh air [85]. As a result, the engine spends longer at part load conditions so that both fuel consumption

and exhaust emissions may be adversely affected. The response time of the air system may be reduced either by directly increasing the air-supply to the cylinders or by directly accelerating the turbocharger using an external torque source such as an electric motor [86]. The direct supply of air, made possible in the pneumatic hybrid system, can rapidly help develop the cylinder torque corresponding to a normal level of boost.

For the turbocharged diesel engine on the vehicular application, there are three approaches to cope the turbo-lag problematic behaviour[86]:

(i) Controlling of the fuel flow.
(ii) Speeding up of the system (engine, manifolds and turbocharger) response.
(iii) Increasing of the number of transmission gears for vehicular applications.

The first method, controlling of the fuel flow, had been analysed in detail [86], as one way to manage turbo-lag. It is recognized as a 'passive' method because the low air supply and low injected fuel mass cause a slower engine response and poor vehicle drivability. The third method, increasing of the number of transmission gears, has also been considered as a 'passive' method for the reason that more gear ratios to make use of the available torque worsen drivability owing to the much more frequent gear changes required. Both first and third methods are intended to cure the symptom of black smoke emission rather than the underlying cause of the turbocharger delay [86]. The second method, speed-up of the system (engine, manifolds and turbochargers) response, is considered an 'active' method in [86], because it improves the transient response of the engine, manifolds and turbocharger. The focus of this chapter is on the realization of the second method by use of stored compressed air during braking events.

An analysis of three system concepts is given. The systems are:

(i) Intake Boost System (System I),
(ii) Intake Port Boost System (System IP), and
(iii) Exhaust Boost System (System E).

Three proposed systems are considered first by integrating into a six cylinders 7.25 l heavy-duty diesel engine (YUCHAI YC6A engine) respectively. The three concepts have been respectively modelled in a 1-D engine code, and the performance changes,

analysed in detail. First, when the engine accelerates from no load to full load at 1600 rpm, the development of brake torque has been compared and analysed. Then the performances of respectively two different pneumatic hybrid city bus configurations (Systems I and IP), have been considered. The acceleration capability of the two types of vehicle has been simulated and the results compared.

6.3 Investigation of the Response Time Improvement

In general, when an additional load is applied to an engine, the current torque output of the engine cannot instantly match the increased load requirement and as a result, the engine speed drops. Note that a sophisticated feed-forward control could seek to match fuelling and a predicted load, but there is always likely to be some mismatch. A speed change is monitored by the engine controller which will increase the fuel injection mass to increase engine speed. However, the turbocharger cannot instantly supply the corresponding required air flow to the cylinders which tends to cause a reduction in the air-fuel ratio. Therefore, the higher fuel mass and lower air supply tend to cause inefficient combustion and insufficient exhaust gas energy to speed-up the turbocharger. The two most prominent examples are respectively the vehicle climbing a hill or engaging the clutch after a gear change.

The speed transient event normally happens when the driver requires a significant acceleration. After the driver fully depresses the accelerator pedal, the engine controller sends out the maximum fuel mass injection signal. Since the resistance torque remains unchanged and the compressor air-supply cannot yet match the higher injected fuel mass, the air-fuel ratio decreases as the air supply slowly increases. The low air-fuel ratio in both load and speed increase transient events lead to poor combustion and consequently increased particulate emissions and poor fuel economy.

6.3.1 Analysis of the Approaches to Improve Turbocharger Response Time

In a turbocharged engine, there is no mechanical connection between the turbocharger and the engine crankshaft. Therefore, turbocharger and engine speeds are coupled through the gas dynamics of inlet and exhaust. The boost pressure and mass flow rate of the compressor are related compressor map such as the one shown in Figure 6-1. The

map is developed at steady state conditions and can be considered as a reasonable approximation for transient conditions where changes propagate at the local speed of sound. However, for significant transient changes, this information is supplemented by both turbine maps and the dynamic behaviour of the turbocharger.

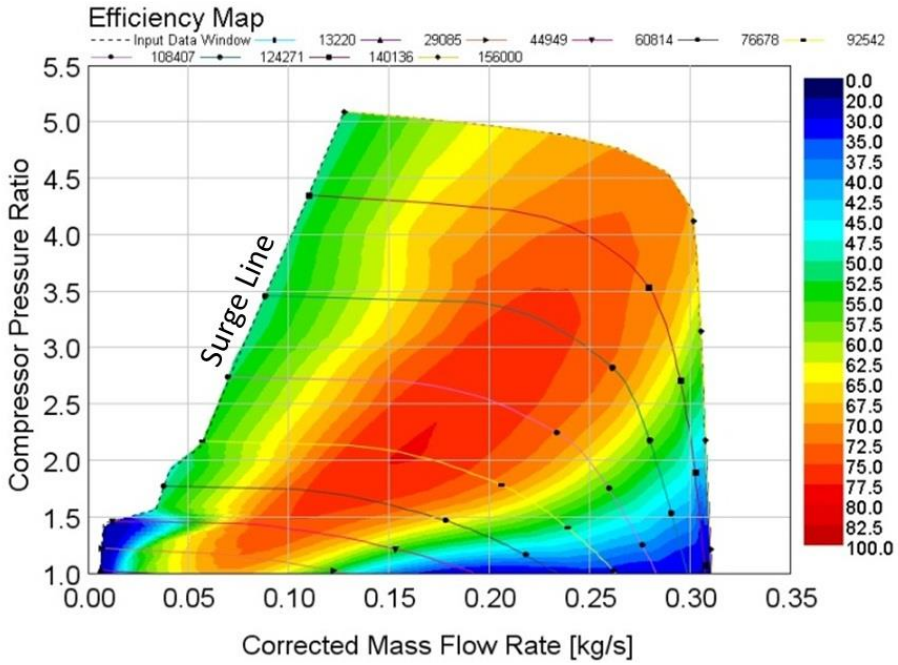

Figure 6-1 Typical map of aerodynamic type turbocharger compressor

From the compressor map, it can be seen that it is unrealistic for the turbocharger to achieve both high boost pressure and air-mass flow rate at its low working speed. An acceleration process is required to take the device from its low boost pressure and air-mass flow rate operation point to its high load condition. To achieve the new operating point, the turbine power must exceed the compressor power to speed-up the turbocharger. The following differential equation describes the angular rotation of the turbocharger shaft as a result of applied torques. All the mechanical losses are encapsulated in the mechanical efficiency.

$$\eta_{mTC}\tau_T - |\tau_C| = G_{TC}\frac{d\omega_{TC}}{dt} \qquad \text{(6-1) [86]}$$

where, t_C – instantaneous value for the compressor indicated torque,

t_T – instantaneous value for the turbine indicated torque,

η_{mTC} – turbocharger mechanical efficiency,

G_{TC} – turbocharger rotating inertia,

ω_{TC} – turbocharger angular velocity.

From the Equation (6-1), it can be seen that to improve the transient response during a demand for greater air flow, the approaches can be:

Approach 1: Increasing the turbine torque, means increasing or supplementing the t_T,

Approach 2: Reducing the moment of inertia of turbocharger, means reducing the G_{TC},

Approach 3: Reducing the turbocharger shaft mechanical losses, means increasing the η_{mTC}.

The overall target for these methods is to increase the turbocharger angular acceleration, $\frac{d\omega_{TC}}{dt}$. Approach 2 and Approach 3 both relate to the turbocharger configuration and have been analysed in detail in [86], and will not be covered in this research. Furthermore, Approach 3 seems like an effective means to improve the turbocharger transient response from theoretical analysis, but it can only offer small scope for improvement. Some suggestions based on the Approach 2 and Approach 3 are given in [86] and summarized as follows:

(i) Adopting lighter materials to reduce the turbocharger moment of inertia appears straightforward since the machine aerodynamics is unchanged although manufacturing costs may be increased.
(ii) Use of more than one small turbocharger instead of a single (larger) unit reduces inertia, but represents a major increase in the system complexity.
(iii) Reduction of turbine (and compressor) rotor diameters respectively will strongly influence turbocharger and, consequently, engine speed response.

Approach 1, increasing the turbine torque, is the key topic of this research and will be discussed in detail. In order to increase the turbocharger transient response, two possible solutions are:

Solution 1: Supplement the turbine torque using an additional torque input device on the turbocharger shaft.

Solution 2: Increasing the amount of the available energy in the exhaust gas.

Approach 1 will be analysed in detail in the following sections. Figure 6-2 shows a classification of various methods of reducing turbo-lag. In this chapter, the methods in the orange background are investigated, and the method in the blue background will be briefly introduced as a reference here.

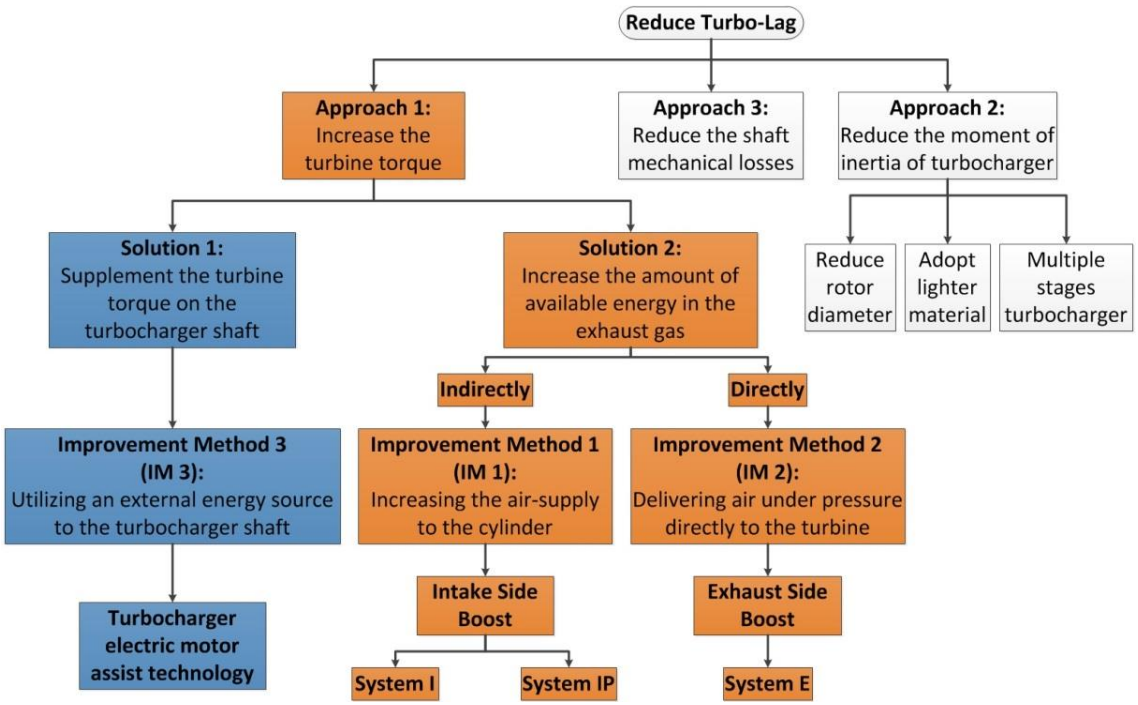

Figure 6-2 Classification of various method of reducing turbo-lag

Electric assistance for turbocharging is gaining in popularity, but is included here for comparison purposes. This thesis would not present any further analysis, but recognise that a detailed comparison on the basis of fuel economy and cost effectiveness is warranted and may form an aspect of our continuing work.

6.3.2 Methods of Improving the Turbocharger Transient Response by Increasing the Turbine Torque

The methods to improve the turbocharger transient response by increasing the turbine torque can be implemented at the intake, exhaust or the turbocharger shaft itself.

The main mechanism of these methods to improve the turbocharger transient response is shown in Figure 6-3.

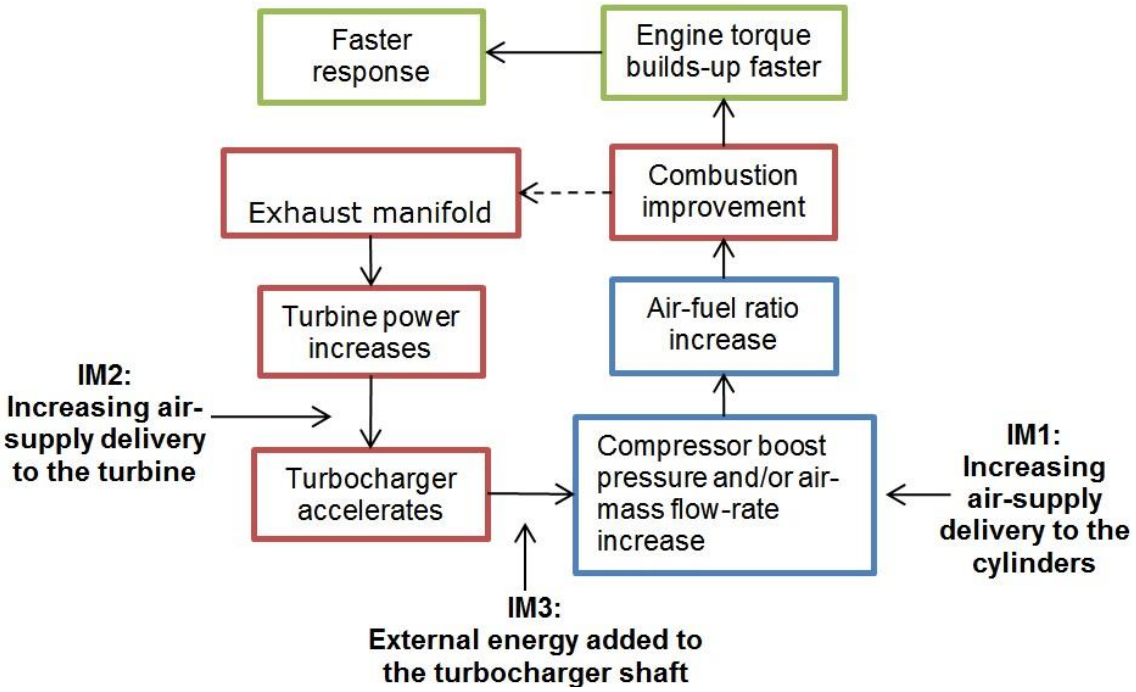

Figure 6-3 Main mechanism of improving turbocharger transient response

Improvement Method 1 (IM1): On the inlet side, directly increasing the air-supply delivery to the cylinders.

Improvement Method 2 (IM2): On the exhaust side, delivering air under pressure directly to the turbine.

Improvement Method 3 (IM3): For the turbocharger shaft, utilizing an external energy source is recognized as a practical choice.

6.3.2.1 Improvement Method 1

IM1 increases air delivery to the cylinders and can be realized by injecting pressurized air stored in the air tank(s) into the intake manifold or directly into the cylinders. The injected air is instantly available to the engine for combustion. Therefore, the duration of combustion discrepancies is reduced since the direct increase of air-supply will also match the increased fuel quantity to meet the load requirements. As a result, the full combustion process gives both high combustion torque and the normal exhaust enthalpies required to bring the turbocharger up to speed.

Nowadays, increased engine ratings generally result in higher inlet manifold volumes, hence slower response in the intake side [86]. Because the compressed air must both increase the manifold pressure as well as increase air delivery to the cylinders, the position at which air is injected into the intake manifold is an important factor in the response improvement. The nature of the improvement brought about by IM1 is apparent in Figure 6-3. IM 1 is closest of all the proposed changes to the combustion process. As a result, IM1 should have the fastest air-supply increase and consequently the greatest effect on response time.

One example of the implement of this method is the Pneumatic Boost System (PBS) which is reported by Marx et al. in [85]. The PBS has been developed by the Knorr-Bremse Company to realize a significant improvement in the response and acceleration behaviour of the engine and the vehicle [85]. Figure 6-4 shows the system diagram for a PBS equipped engine and the structure of the most important components of the system.

In normal operation where rates of change of engine condition are low, the engine's air demand is met by the turbocharger, during which time the PBS is in the rest position with the flap fully opened and injection inactive (Figure 6-4, below left). In more dynamic situations, when the turbocharger is not able to meet the engine's air demand, the flap is closed and air injection takes place (Figure 6-4, below right). The injection of air normally ends when the pressure built up by the compressor in front of the closed flap has reached the level of the pressure created by the PBS downstream of the flap. Both pressures are measured continuously by the pressure sensors. From this point on, the turbocharger is able to supply the engine with sufficient air.

Figure 6-5 shows a torque curve measured on an engine test bench with a spontaneous torque request at idle speed. The engine, an 8 l diesel engine with EGR and two-stage turbocharging, without PBS achieves 90% of its maximum torque in almost 5 s, whereas the same engine with PBS achieves this value in 0.7 s [85].

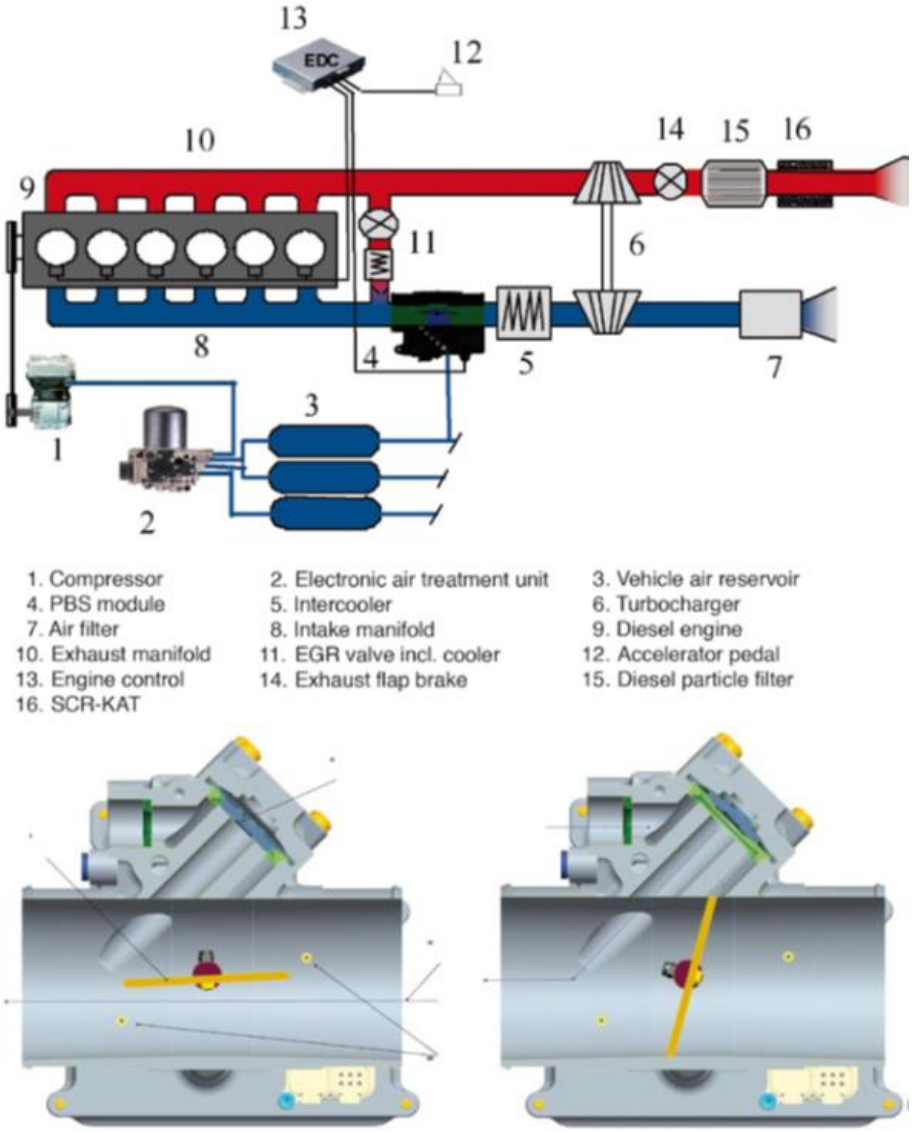

Figure 6-4 System diagram of PBS integration and PBS key component [85]

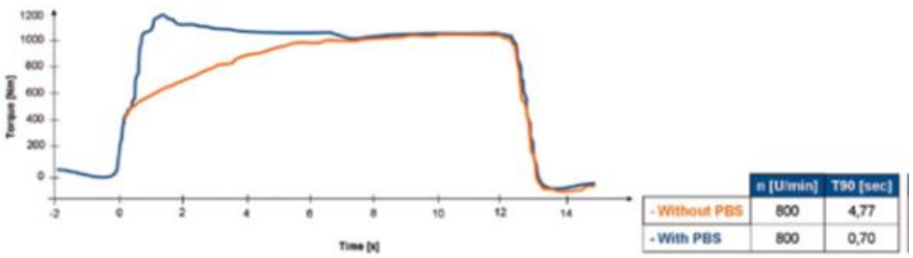

Figure 6-5 Torque curve of an 8-l-diesel engine with EGR and 2-stage turbocharging with/without PBS [85]

6.3.2.2 Improvement Method 2

IM2 which increases the air-supply delivery to the turbine, can also be realized by implementing the pneumatic hybrid technology to inject the compressed air into the exhaust manifold as an additional flow of energy to the turbine. Air injection into the exhaust manifold is less efficient than air injection into the intake manifold, since there is still a lag between the intake and exhaust side. There is also the loss of availability resulting from injection of relatively cool air into the exhaust manifold during the acceleration process. Although the exhaust manifold pressure is increasing following the boost in fuelling, the inertia of the turbocharger as well as the gas dynamics of filling the intake manifold cause a further lag on the intake side. From Figure 6-3, it can be seen that the IM2 is the most remote from combustion with changes having to propagate through turbine, compressor and intake manifold.

An implementation of this method, the BRaking Exhaust Energy Storage (BREES) is demonstrated in [87]. The experiments had been conducted by using a 2.0 l light-duty diesel engine equipped with EGR and Variable Geometry Turbine (VGT) to evaluate the engine transient response during in-gear braking and acceleration.

Figure 6-6 shows the system diagram for the BREES. It can be seen that to implement the reported functions only a compressed gas tank, additional exhaust manifold connection and a single control valve are necessary as shown in Figure 6-6.

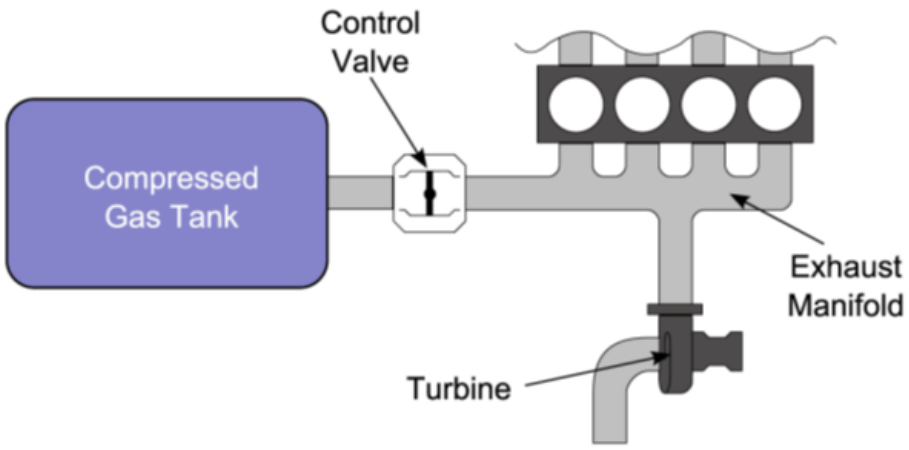

Figure 6-6 System diagram of BREES [87]

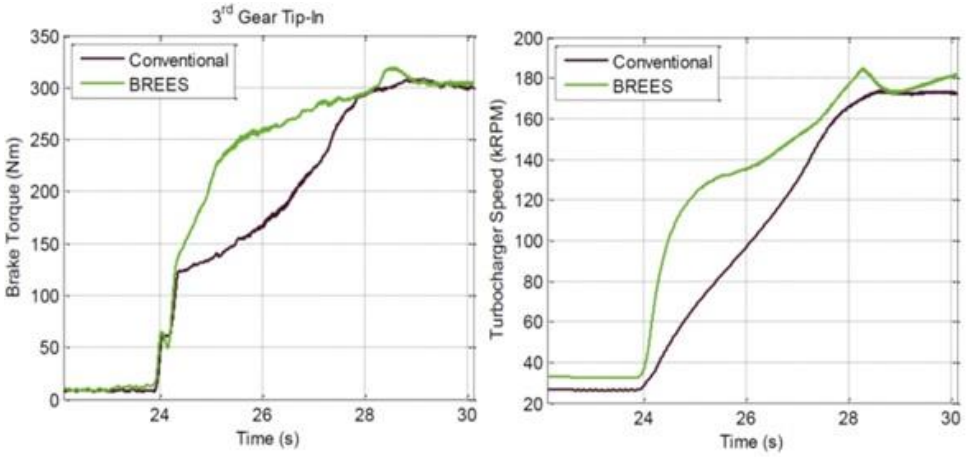

Figure 6-7 The effect of compressed air injection on brake torque and turbocharger speed [87]

Figure 6-7 shows the effect of compressed air injection on brake torque and turbocharger speed. It can be seen, the BREES system has a much sharper brake torque rise when the conventional configuration clearly shows the turbo-lag between 24 to 28 second. Also, the figure confirms the effectiveness of exhaust manifold injection to rapidly accelerate the turbocharger, which was enabled between 24 and 26 second. Additional, the experimental results confirm that the proposed system reduces the time to reach the torque requirement during the 3rd gear tip-in by about 60% [87].

6.3.2.3 Improvement Method 3

With IM3, external energy added to the turbocharger shaft, can be realized by using different kind of energy source such as electrical or hydraulic assistance.

One possible solution is Electric Assist Technology (EAT) using an electric motor mounted on the turbocharger shaft. The motor offers additional torque to the turbocharger when a load or speed increase is required. A schematic diagram of a diesel engine with turbocharger EAT is shown in Figure 6-8.

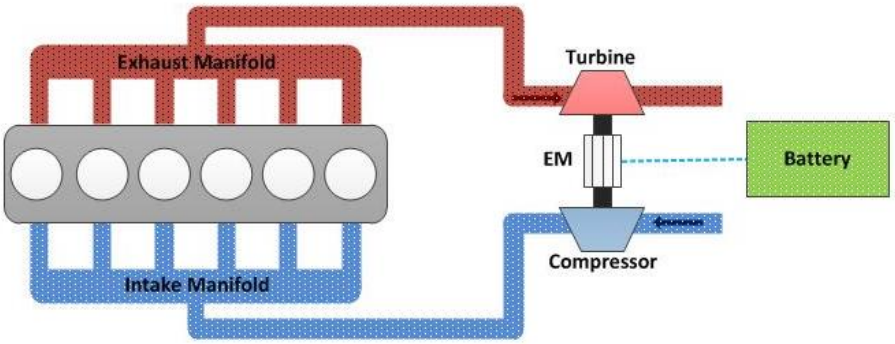

Figure 6-8 Schematic diagram of diesel engine with EAT

An alternative configuration makes use of an electric motor driving a separate compressor which is installed upstream or downstream of its turbocharger counterpart in an arrangement that resembles a combined supercharging scheme [86]. The schematic diagram is shown in Figure 6-9.

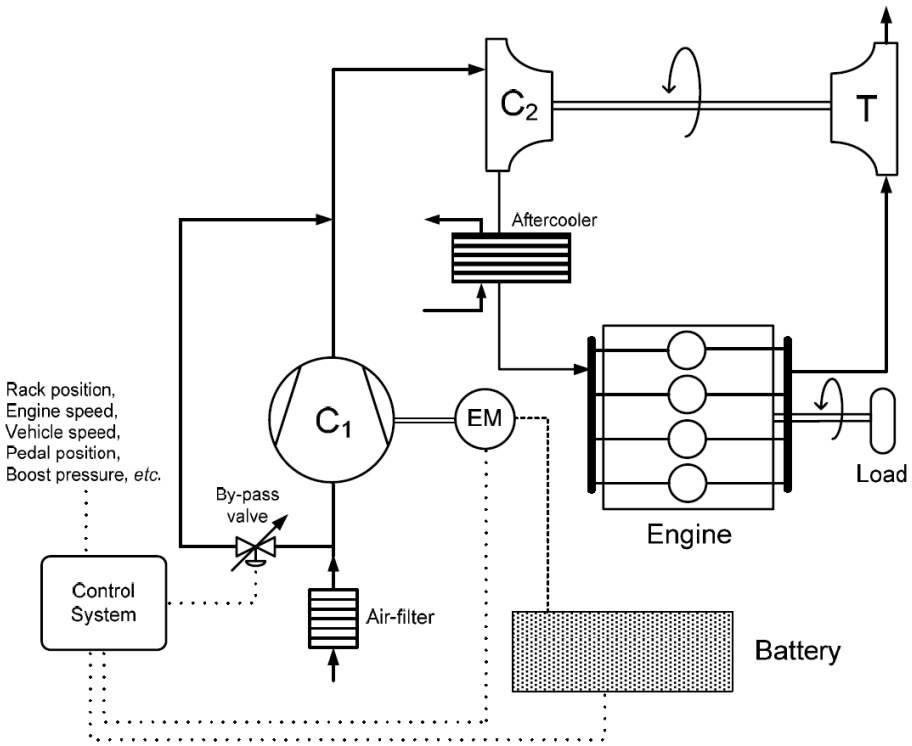

Figure 6-9 Alternative combined supercharging configuration with electrically driven compressor [86]

The Equation (6-1) described the relation between the normal, unassisted turbocharger shaft torque and the turbocharger angular acceleration. For the turbocharger with the electric motor assist, the respective balance is given by Equation (6-2).

$$\eta_{mTC}\tau_T + \tau_{EM} - |\tau_C| = G_{TC+EM}\frac{d\omega_{TC}}{dt} \quad \text{(6-2) [86]}$$

where, t_C – instantaneous value for the compressor indicated torque,

t_T – instantaneous value for the turbine indicated torque,

t_{EM} – electric motor torque,

η_{mTC} – turbocharger mechanical efficiency,

G_{TC+EM} – combined turbocharger and EM mass moment inertia,

ω_{TC} – turbocharger angular velocity.

For a successful integration of the electric motor, the established turbocharger shaft acceleration must fulfil the following relation.

$$\frac{\eta_{mTC}\tau_T+\tau_{EM}-|\tau_C|}{G_{TC+EM}} > \frac{\eta_{mTC}\tau_T-|\tau_C|}{G_{TC}} \quad \text{(6-3) [86]}$$

From Equation (6-3), the electric motor torque can be represented from Equation (6-4).

$$\tau_{EM} > \frac{\Delta G}{G_{TC}}(\eta_{mTC}\tau_T - |\tau_C|) \quad \text{(6-4)}$$

where, t_C – instantaneous value for the compressor torque,

t_T – instantaneous value for the turbine torque,

t_{EM} – electric motor torque,

η_{mTC} – turbocharger mechanical efficiency,

G_{TC} – turbocharger rotating inertia,

ΔG – increment of the rotating inertia.

Equation (6-4) indicated that when electric motor added to the turbocharger, the balance of the motor torque and increment of shaft inertia, when the electric motor installed, should be carefully considered.

There are two benefits to adopting the electric motor assist to the turbocharger. Respectively, firstly the ability of the engine to operate at overall higher boost pressure levels [86]. Secondly the electric motor not only can function also a turbocharger accelerator, but also a generator. At low engine speed, when there is a load or speed increase transient event, electric power is supplied to the turbocharger shaft aiding its fast acceleration. At high engine speed, instead of wasting the energy that exceeds the compressor requirement, the electric motor can convert to the electricity generator to

recover the energy and store in energy storage such as a battery or a supercapacitor. But the EAT has same disadvantages that prevent widespread application at low cost. First is a more complex control system which includes the control strategy of the electric motor. Second is the durability and reliability of the turbocharger remain to be proven.

6.4 Using Pneumatic Hybrid Technology to Improve the Turbocharger Transient Response

6.4.1 Introduction of Reducing Turbo-lag by Using Pneumatic Hybrid Technology

As mentioned before, increasing the air supply to the cylinders or to the turbine both can be considered as effective methods to improve the engine transient response. The pneumatic hybrid boost systems have inherent advantages to implement these methods above to improve the transient response because of the ready availability of an air supply. The air stored in the air tank(s) can be reused to improve turbocharger response time by injecting air into the intake or exhaust manifold. To realize the Boost Function, there are two different engine structures can be considered as candidates.

The first proposed structure, Intake Side Boost (ISB), is a realisation of IM1. In order to increase the air-supply to the cylinders for combustion, the air can be injected into the intake at different points such as the intake manifold or the intake ports. An example of ISB is shown in Figure 6-10, in which the compressed air stored in the air tank is supplied to the cylinders through the intake manifold at the time when acceleration of the turbocharger is required. When the load or speed demand is made, the compressed air is injected into the intake manifold in order to match the increased fuel injection mass. The precise air flow is controlled by the Air Tank Valve (ATV). The Intake Manifold Valve (IMV) will fully close during the injection period to prevent the compressed air being injected back to the compressor. Because the air can be immediately used to support combustion in the cylinders, the resulting high exhaust gas energy causes a faster turbocharger and engine response to reduce turbo-lag. In order to avoid the compressor enter an unstable operation condition, two methods can be implemented. The first is when the pressure of the volume between the IMV and compressor reaches a threshold value, the IMV will open to avoid the stall condition of the compressor. The second method is to set a

bypass or wastegate after the compressor which can keep the compressor output pressure constant.

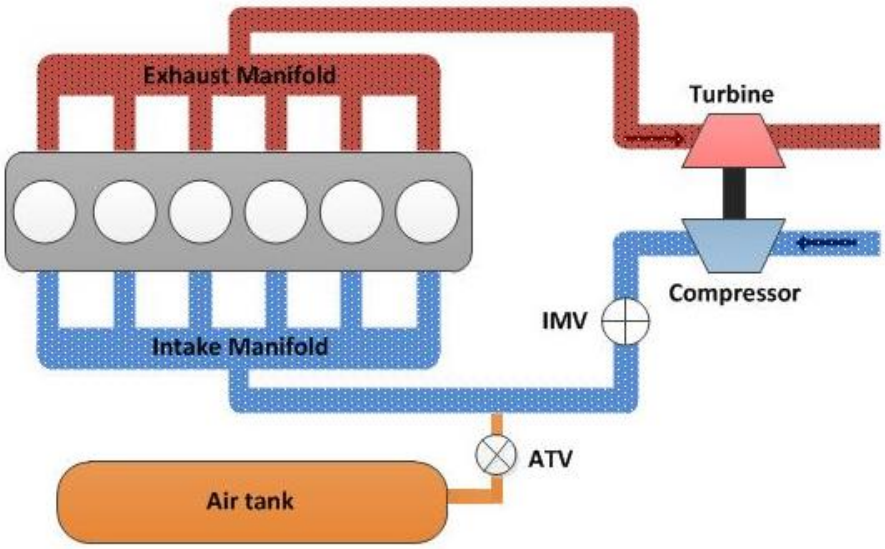

Figure 6-10 The diagram of engine structure can realize the Intake Side Boost

The second proposed structure, Exhaust Side Boost (ESB), realises IM2. An example of ESB called System E is shown in Figure 6-15, in which compressed air in the air tank is supplied to the exhaust system to speed up the turbine directly. As a result, the compressor will accelerate to increase the flow of air into the inlet manifold and build up the intake manifold pressure. The injection of compressed air will cease, when the turbocharger reaches its normal operating point (in relation to engine speed and load).

6.4.2 Intake Side Boost

There are several ways to implement ISB in the pneumatic hybrid engine. Each requires some new devices to be added into the engine. Two different structures will be considered:

(i) System I - Intake Boost System,

(ii) System IP - Intake Port Boost System.

How to control the air mass injecting into the intake manifold or intake port is explained here. From the basic engine model, the intake manifold and intake port pressures at different engine speed and brake torque can be learned. The intake manifold pressure at maximum brake torque is the target pressure for the System I. When the System I is

working, the sensor will detect the intake manifold pressure. Once the pressure reaches the target pressure, the System I will stop injecting the air from air tank. The System IP uses the intake port pressure as the target pressure. The reason for choosing this control algorithm is to keep the control system simple. And it will not change the air mass injected to the engine and the air inlet behaviours of the engine.

6.4.2.1 System I

Figure 6-11 shows the arrangement of equipment with some new devices added to the original pneumatic hybrid engine structure that was first shown in [11]. The original pneumatic hybrid engine devices like the air tank, compression release engine braking device, air tank, air motor, check valve and throttle valve are retained. The new devices are respectively the connection pipes between the air tank and the intake manifold with the ATV1, and the IMV in the intake manifold downstream of the intercooler. The IMV is to prevent the compressed air being injected back to the compressor. Such an increasing pressure has the tendency to move the compressor operating point towards surge.

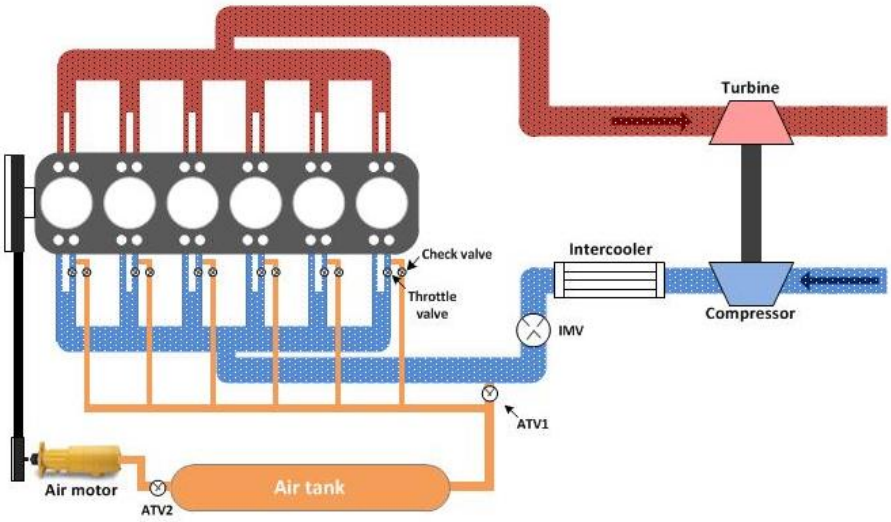

Figure 6-11 System diagram of System I

In normal operation, when the engine does not require high air demand and the compressor can supply enough pressure, both IMV and TVs, fully open to let the engine operate in the normal turbocharged mode.

When the compressor cannot supply enough air to the engine in a highly dynamic situation like acceleration or on steep gradients, System I is activated. The high pressure

air from the air tank injects into the manifold through the ATV1. The IMV closes and TVs fully open. The injection of air ends when the compressor delivery pressure is higher than the pressure of the injected air. At this point, IMV opens and ATV1 closes.

The injection of the air from the air tank only requires a short period of operation, because after few engine cycles, the turbocharger will accelerate to a normal operating speed. As a result, the compressor can supply sufficient air to the engine to realise a satisfactory acceleration. The time to reach maximum torque is significantly reduced. Rakopoulos et al. [86] reported that, for a 0 to 60% load acceptance aided by a 2 s air-injection duration right after the onset of the transient event, the engine response time was approximately halved in a medium-speed, turbocharged diesel engine rated at 1410 bhp at 750 rpm in Figure 6-12. Furthermore, for an air-injection assist on a six-cylinder, turbocharged diesel of 11.32 l displacement volume revealed a reduction in the time period with peak smoke from 3 to 0.5 s as well as improvement in the speed response from 4 to 1.5 s for severe load acceptance transient at 1000 rpm [86].

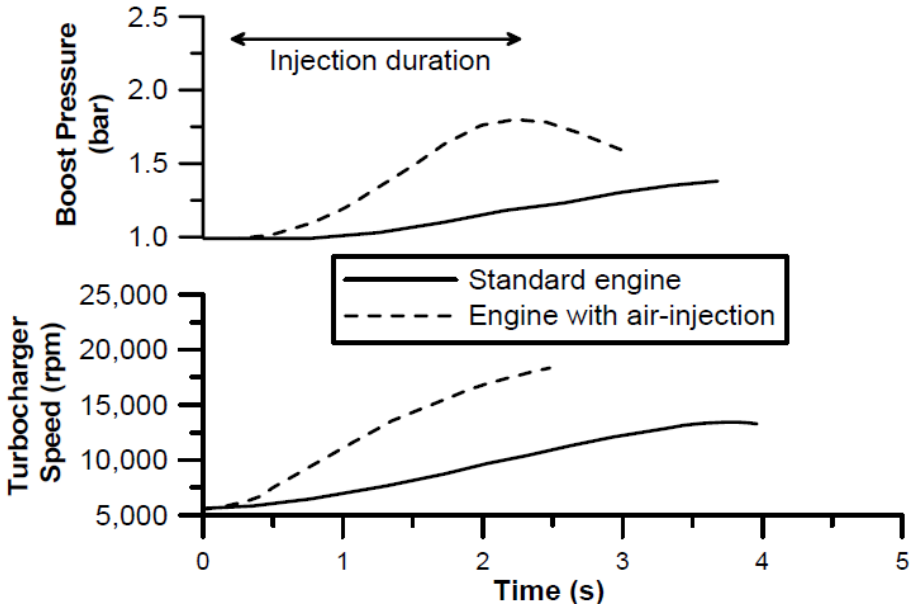

Figure 6-12 Effect of air-injection on transient response after a load step of 60% full-load [86]

An alternative way of presenting the transient response improvement made by the different pneumatic hybrid technologies are depicting in on the turbocharger compressor map compared with the normal engine without any response improvement methods which are illustrated in Figure 6-13. Normally, turbo-lag happens at the early stage of the

event as the compressor delivery pressure build-up slowly [86]. In Figure 6-13, the red line is the operating point of the normal engine without any transient response improvement methods. The blue line in Figure 6-13 is the operating point of the engine with ISB. When the engine works at the early stage during the load or speed increase transient event, the compressed air is injected into the intake manifold to enhance the compressor output pressure immediately. To prevent the compressor entering the surge, the injected air need to be controlled by monitored the intake manifold pressure. Once the compressor operating point is near the surge line, to move the compressor operating point far away the surge line, two methods can be implemented. The first one is, stop the compressed air injection, and the second one is, open the wastegate valve of the turbocharger if there is one at the turbine.

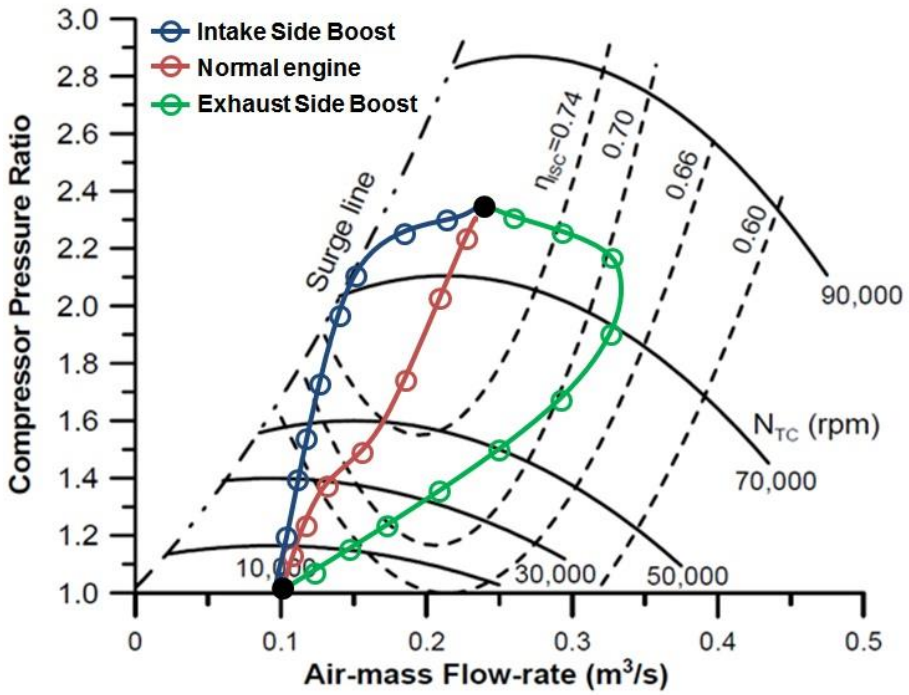

Figure 6-13 Different engine transient responses on the turbocharger compressor map [88]

6.4.2.2 System IP

Compared with System I, System IP injects the compressed air directly into the cylinders by connecting the air tank and the intake port with pipes and six Intake Port Valves (IPVs) as shown in the Figure 6-14. Also, six TVs are installed at each intake port to prevent

compressed air being injected back into the compressor. A high pressure common air rail connects ATV1 and IPVs on each intake port.

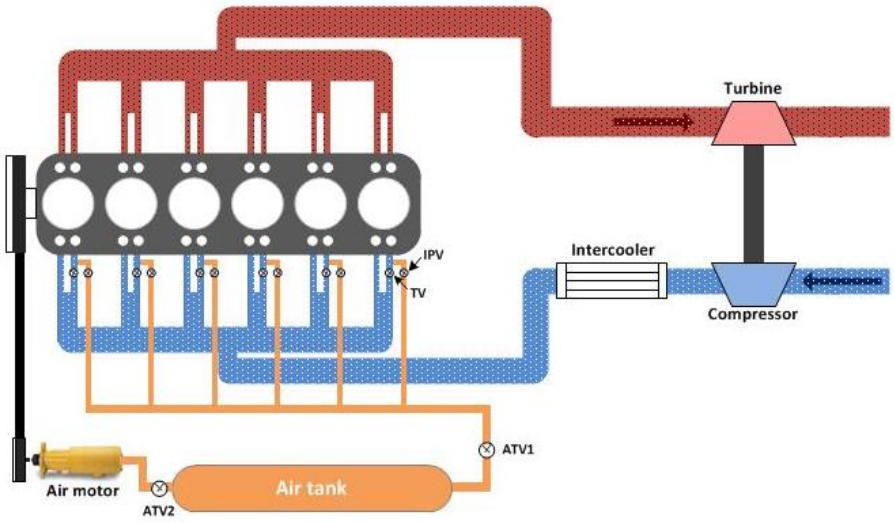

Figure 6-14 System diagram of System IP

In the normal operation, when the engine does not require high air demand and the compressor can supply enough pressure, the TVs fully open while the IPVs and ATV1 fully close.

During an engine transient when the compressor is unable to supply enough air to the engine, System IP is activated. The high pressure air from the air tank is injected into the high pressure air rail through ATV1, and in turn the air is injected into the cylinder by means of the IPVs. The TVs on each intake port fully close during the injection. The injection will end when the pressure that the compressor builds is higher than the pressure of the injected air. The TVs fully open again and the IPVs close.

According to where the compressed air is injected into the intake manifold the dynamics of the air supply change. Pressurising the whole manifold compared with supplying air to the inlet ports will be a slower, but more complex in the mechanical design. Compared with System I, System IP can deliver the compressed air more quickly since it only needs fill a small volume auxiliary chamber between the TV, IPV and intake valve in each intake port. Moreover, System IP allows the compressor to accelerate to its normal operating condition without risking surge or stall. Only one intake port is blocked by the TV during

the compressed air injection. The compressor will continue to deliver the air into the intake manifold at its operation point approach the normal value.

6.4.3 Exhaust Side Boost

Injecting compressed air into the intake manifold has received considerable attention, but the performance improvement offered by this concept is severely constrained by the compressor surge limit [87]. Injecting the compressed air into the exhaust manifold avoids compressor surge and is another method to reduce turbo-lag by using the pneumatic hybrid technology.

6.4.3.1 System E

System E has a similar structure with System I. Figure 6-15 shows system diagram of System E. Unlike System I, the air tank connects the exhaust manifold with the ATV1.

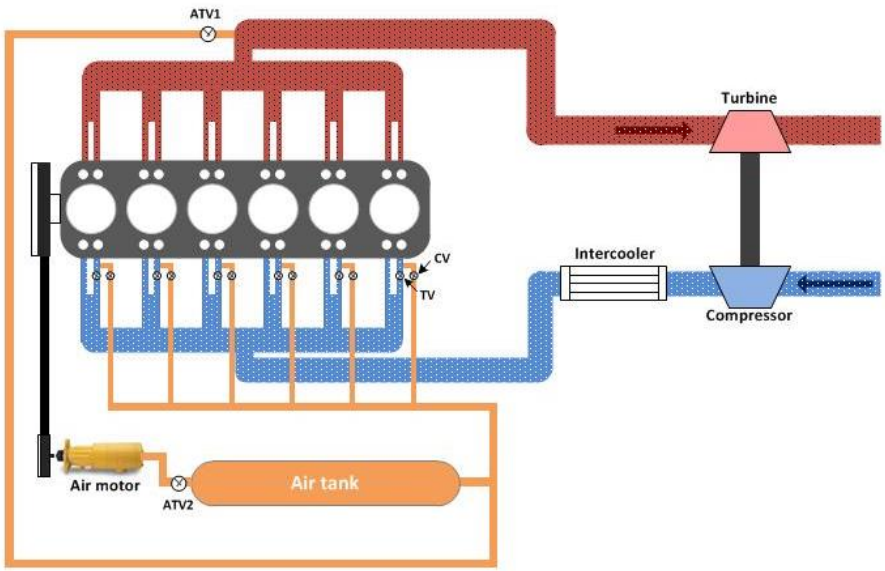

Figure 6-15 System diagram of System E

In normal operation, when the engine does not require high air demand and the compressor can supply enough pressure, System E will not be activated, the TVs are fully open and the CVs fully closed to with the engine operating in normal mode.

When System E is working, the high pressure air from the air tank is injected into the exhaust manifold through ATV1 to accelerate the turbocharger to its target speed. Air

injection ends when the intake manifold pressure reaches its normal working pressure according to engine speed and load.

From this analysis, it can be observed that System E is least effective of the methods under review because of the long process path apparent from the process diagram for boost, Figure 6-3. But it has a substantial advantage that the compressor operating point is reached without risk of surge or stall.

6.5 Engine with Pneumatic Hybrid Boost System Simulation Models and Result

6.5.1 Basic Engine Simulation Model

To simulate the transient response improvement made by three different pneumatic hybrid boost systems, respectively Systems I, IP and E, a 1-D engine simulation code, GT-POWER, is used to simulate the engine performance when a load transient is applied to the engine.

A heavy-duty, six cylinders, turbocharged & intercooler diesel engine based on the YUCHAI YC6A Series engine is modelled in GT-POWER as shown below in Figure 6-16. The Information of the GT-POWER models in this research is introduced in detail in Appendix-II. The YC6A series diesel engine is a new type turbocharged & intercooler diesel engine co-developed by YUCHAI in China, and FEV Company in Germany [89]. The main technical parameters of YC6A series engines are shown in Table 6-1.

Here, the YC6A240-30 is chosen as the base engine for the study. Its GT-POWER engine model which includes a 'DIWiebe' combustion sub model and a 'WoschniGT' heat transfer sub model is shown in Figure 6-16. The 'DIWiebe' model imposes the combustion burn rate for direct-injection, compression-ignition engines using a three-term Wiebe function, and is used to define the injection system, cylinder geometry, valve lift and valve timing [90]. 'WoschniGT' indicates that the in-cylinder heat transfer will be calculated by a formula which closely emulates the classical Woschni correlation without swirl [91]. Both 'DIWiebe' and 'WoschniGT' models are introduced in detail in Appendix-III.

Table 6-1 Main technical parameters of YC6A series engines [89]

Model	YC6A 240-30	YC6A 260-30	YC6A 280-30	YC6A 220-31	YC6A 240-31	YC6A 260-31
Type	Vertical, in-line, water-cooled, 4 strokes, electronic control, direct injection					
Electronic control system	High pressure & common rail			Electronic unit pump		
No. of Cylinders (-)	6					
Bore (mm)	108					
Stroke (mm)	132					
Displacement (l)	7.25					
Intake way	Turbo-charging & inter-cooling					
Rated power at 2300 rpm (kW)	177	191	206	162	177	191
Max. torque at 1400 - 1600 rpm (Nm)	900	1000	1100	850	900	1000
Application	11 - 13.7 m City Bus, 9 - 11 m Coach					

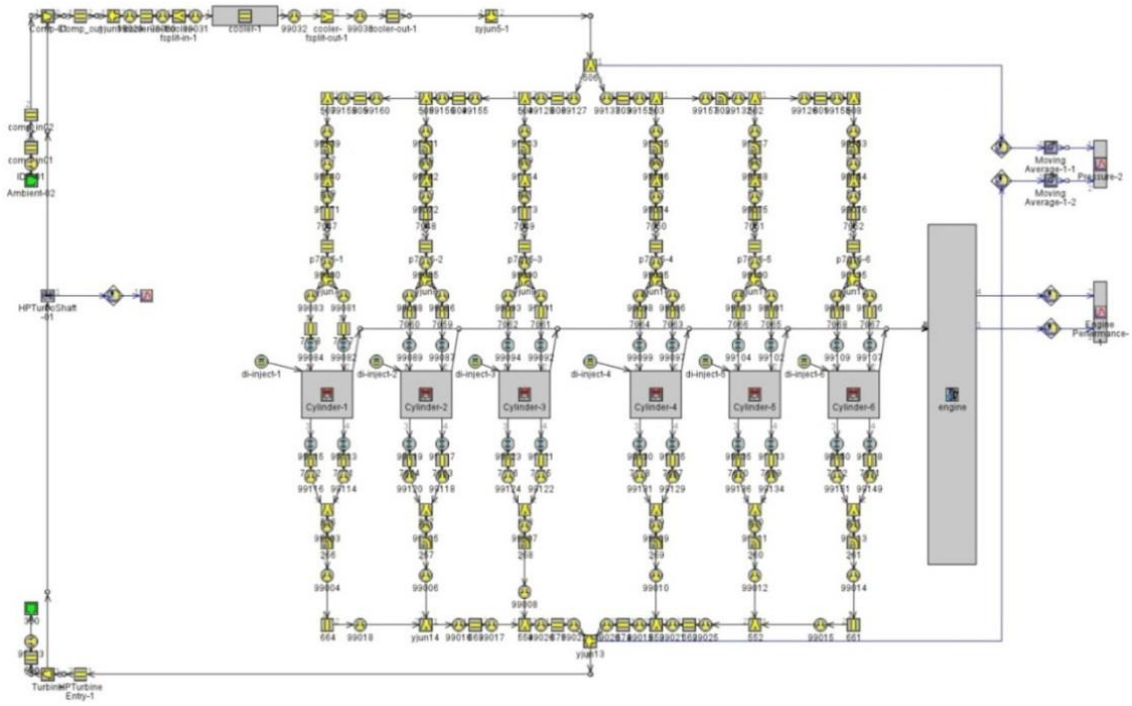

Figure 6-16 GT-POWER model of the basic engine

6.5.2 Simulation of the Engine with System I

Figure 6-17 shows the GT-POWER model of the engine with System I. Compared with the basic engine model, some new modules, ISystem-Control-Unit (highlighted in green), and pneumatic hybrid system (highlighted in red) are added into the model. The pneumatic hybrid system includes one air tank, pipes, one air tank valve and an intake manifold valve. The check valves and throttle valves at each intake port, as shown in the Figure 6-11 are removed here because, the function of these valves is to recover the air when the engine is working in compressor mode during braking (see [11]). In this simulation model, only the ability of System I to improve engine performance aspect is investigated. Other components, not included in the simulation of this function are excluded from the model.

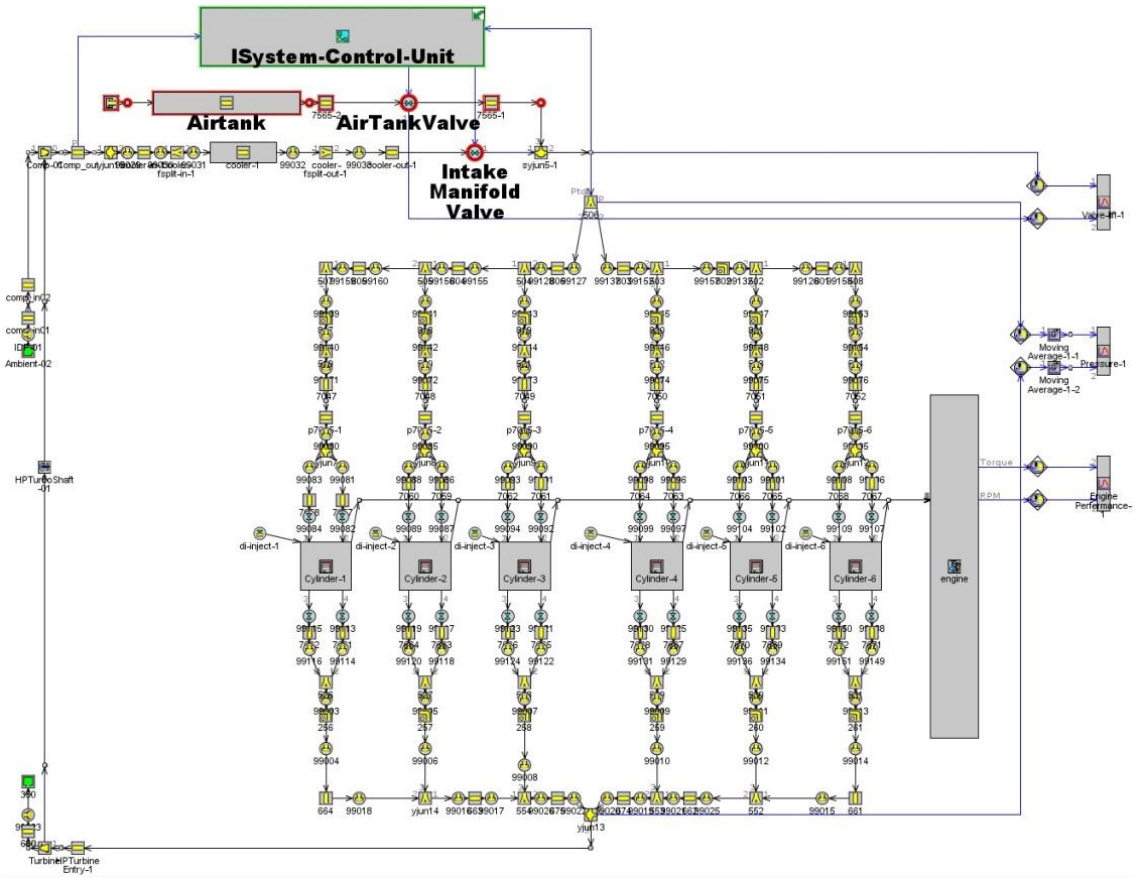

Figure 6-17 GT-POWER model of the engine with System I

The purpose of this simulation model is to investigate first the feasibility and then the performance capability of System I. Also the simulation result will be compared with other kinds of pneumatic hybrid boost system. The dimensions and characteristics of

System I are shown in Table 6-2. The size of the air tank follows the recommendation of the air starter manufacturer manual [68] to store sufficient compressed air for the usage of the air starter. To save space when the pneumatic hybrid system installed on the vehicle in the future, the minimum recommendation air tank volume, 151 l, is chosen here. The dimensions of other parts are based on the previous research conducted by Lee [34].

For simulation purpose, the valves are idealised. Flow losses and valve dynamics are neglected. It could be believed the effects to be of second order and not influential on the initial conclusions. However, a detailed investigation will need to consider valve behaviour in order to evaluate the detailed effect on systems response and the fuel economy gains. Valve operating procedures will also change air flow in manifolds and the engine cylinders, changing the patterns of losses. Again it should be believed such effects are second order, but require investigation in the next phase of our work.

Table 6-2 Dimensions and characteristics of System I

Part Name	Type	Dimensions	
Airtank	Round Pipe	Volume (l)	151
		Initial pressure (bar)	5
7565-1	Round Pipe	Diameter (mm)	25.4
		Length (mm)	30
AirTankValve	Valve that the lift is imposed by an Actuator Part	Diameter (mm)	25.4
7565-2	Round Pipe	Diameter (mm)	25.4
		Length (mm)	1000
IntakeManifoldValve	Valve that the lift is imposed by an Actuator Part	Diameter (mm)	80

Figure 6-18 is the system diagram of the System I Control Unit. The function of the System I Control Unit is to control the two valves based on the pressure from two pressure sensors:

(i) Compressor outlet pressure p_2 (comes through *ToPart_Comp_out*),

(ii) Pressure downstream of the IMV (comes through *ToPart_506*) – which in turn becomes the target pressure for a control loop controlling ATV lift.

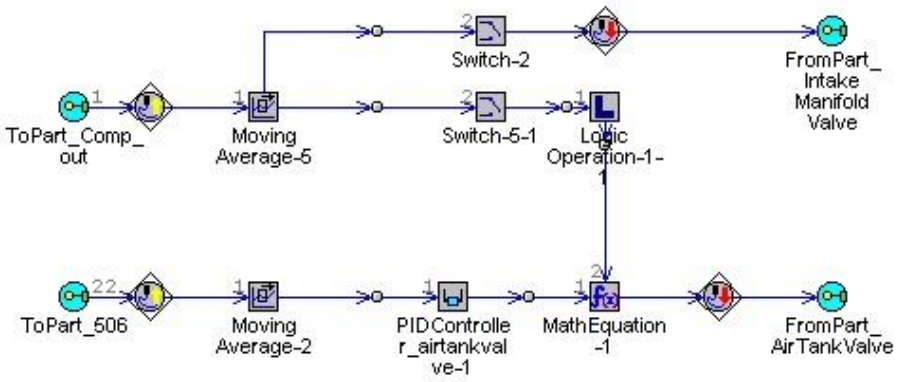

Figure 6-18 System diagram of System I control-unit

Based on the results of comparing the pressures of two positions mentioned before, the ISystem-Control-Unit will control the two valves. The flow chart of System I control strategy is also shown in Figure 6-19.

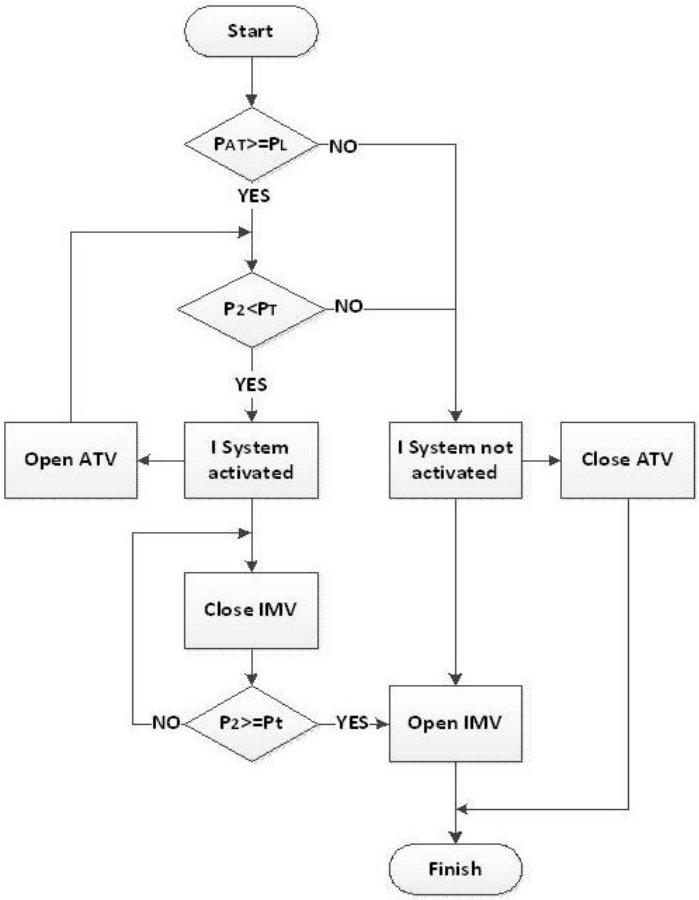

Figure 6-19 Flow chart of the System I control strategy

(i) If the air tank pressure is sufficient to boost the engine, which means the air tank pressure p_{AT} is greater than the limit pressure p_L, and the compressor is unable to supply the target boost pressure p_T ($p_2 < p_T$), System I will be activated. The control unit will open the Air Tank Valve to inject compressed air into the manifold, while the Intake Manifold Valve will be closed. When p_2 is greater than the IMV opening threshold pressure p_t, the IMV will open to prevent the compressed air causing compressor a surge. The system will be turned off and the ATV will be closed until the intake manifold pressure reaches the target boost pressure.

(ii) If the air tank pressure is not sufficient, which means the air tank pressure p_{AT} is less than the limit pressure p_L, to boost the engine the control unit will not activate System I. As a result, the ATV will be closed and the IMV will be opened to supply air to the cylinders.

6.5.3 Simulation of the Engine with System IP

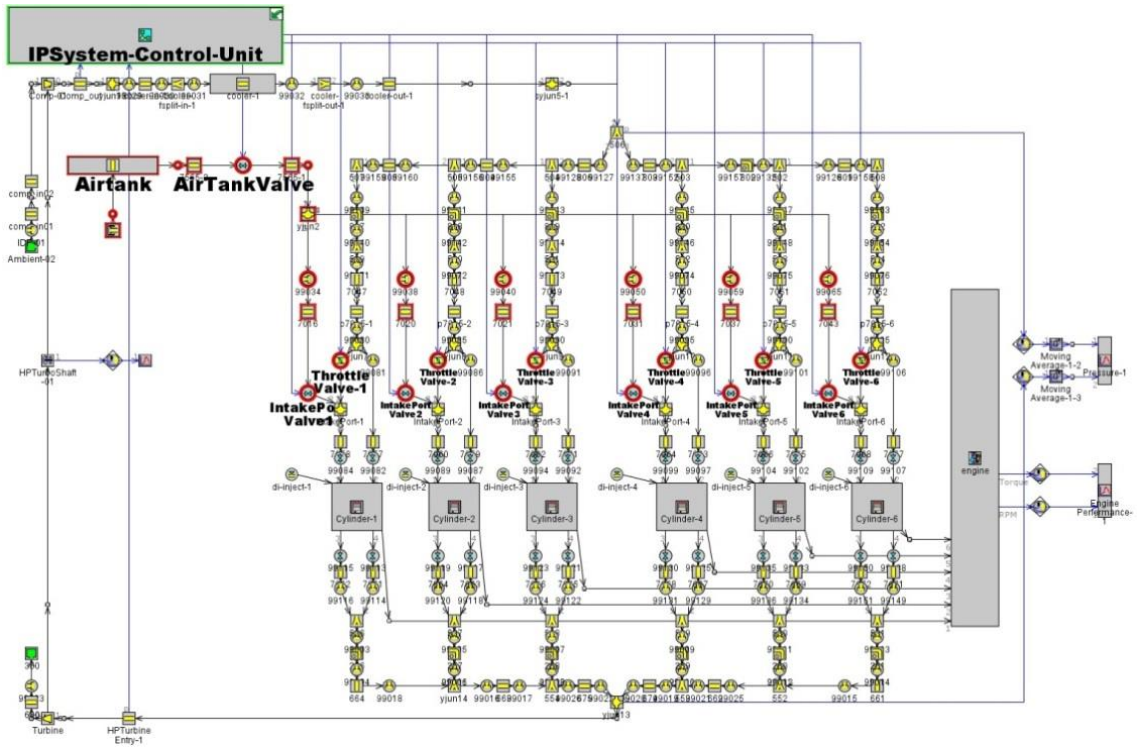

Figure 6-20 GT-POWER model of the engine with System IP

As shown in the Figure 6-20, some new modules, IPSystem-Control-Unit (highlighted in green), and pneumatic hybrid system (highlighted in red) are added to the basic engine

model. The system includes one air tank, pipework, a single ATV, six IPVs and six TVs. The ATV and six IPVs are connected to using a high pressure air rail.

When System IP is activated, the high pressure air from the air tank is injected into the high pressure air rail through the ATV. In turn, the air will be injected into the cylinder by means of the IPVs. The function of the TVs on each intake port is to prevent the compressed air leaking back into the inlet manifold. The injection will end when the pressure that the compressor builds is higher than the pressure of the injected air. The TVs will fully open again and the IPVs will close.

The dimensions and characteristics of System IP are shown in Table 6-3. The air tank is kept at the same volume for consistency. Other design parameters are same as the System I.

Table 6-3 Dimensions and characteristics of System IP

Name	Type	Dimensions	
Air Tank	Round Pipe	Volume (l)	151
		Initial pressure (bar)	5
7565-2	Round Pipe	Diameter (mm)	25.4
		Length (mm)	1000
Air Tank Valve	Valve that the lift is imposed by an Actuator Part	Diameter (mm)	25.4
7565-1	Round Pipe	Diameter (mm)	25.4
		Length (mm)	30
Intake Port Valve 1-6	Valve that the lift is imposed by an Actuator Part	Diameter (mm)	12.7
Yjun2	A spherical-shaped flow split volume connected to one or more flow components	Diameter (mm)	45.7
7016,7020,7021,7031 ,7037,7043	Round Pipe	Diameter (mm)	32.4
		Length (mm)	60
Throttle Valve 1-6	Throttle that the throttle angle is imposed by an Actuator Part	Diameter (mm)	32.4

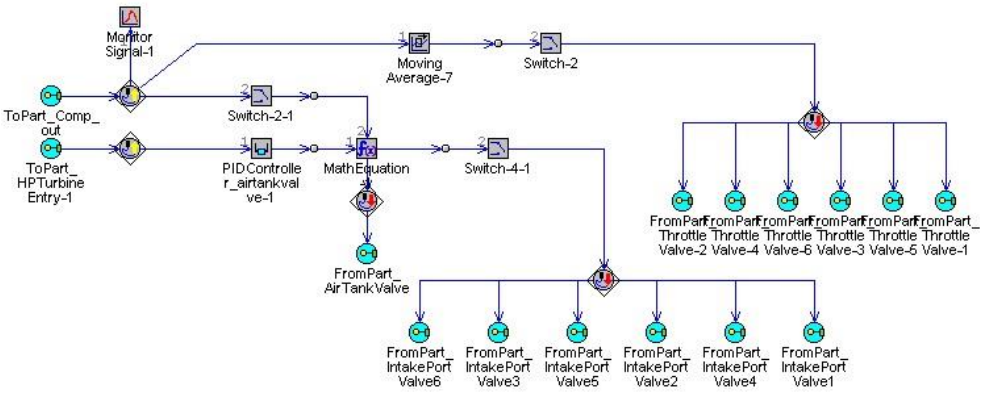

Figure 6-21 System diagram of System IP control-unit

Figure 6-21 is the system diagram of the System IP Control Unit. Compared with System I, the deployment of the pressure sensors is changed:

(i) Compressor outlet pressure p_2 (comes through *ToPart_Comp_out*),

(ii) Exhaust manifold pressure p_3 (comes through *ToPart_HPTurbineEntry-1*).

Measurement of p_3 is required because when System IP is working, the compressed air is injected into the small chamber composed by the IV, TV and intake valve in each intake port, the intake manifold pressure does not behave as in Systems I. Based on the pressure measurements, the valves are controlled to facilitate two operating modes. The flow chart of System IP control strategy is shown in Figure 6-22.

(i) If the air tank pressure p_{AT} is greater than the limit pressure p_L, which means the air tank pressure is sufficient to boost the engine, and at the same time, the compressor is unable to supply the target boost pressure, which means the turbine input pressure p_3 is less than the target exhaust manifold pressure p_E, System IP will be activated. The control unit will open the ATV and the IPVs to inject compressed air into the cylinders, while the TVs in the intake ports will be closed to prevent the compressed air leaking back into the inlet manifold. When the compressor outlet pressure p_2 is greater than the TVs opening threshold pressure p_t, the TVs will fully open. System IP will be turned off when p_3 is greater than p_E, and the ATV and IPVs will be closed.

(ii) If the air tank pressure is not sufficient to boost the engine, which means the air tank pressure p_{AT} is less than the limit pressure p_L, whether the compressor can supply the target boost pressure or not, the control unit will not activate System

IP. As a result, the ATV and IPVs will be closed and all six TVs will be opened to supply the air flow to the cylinders.

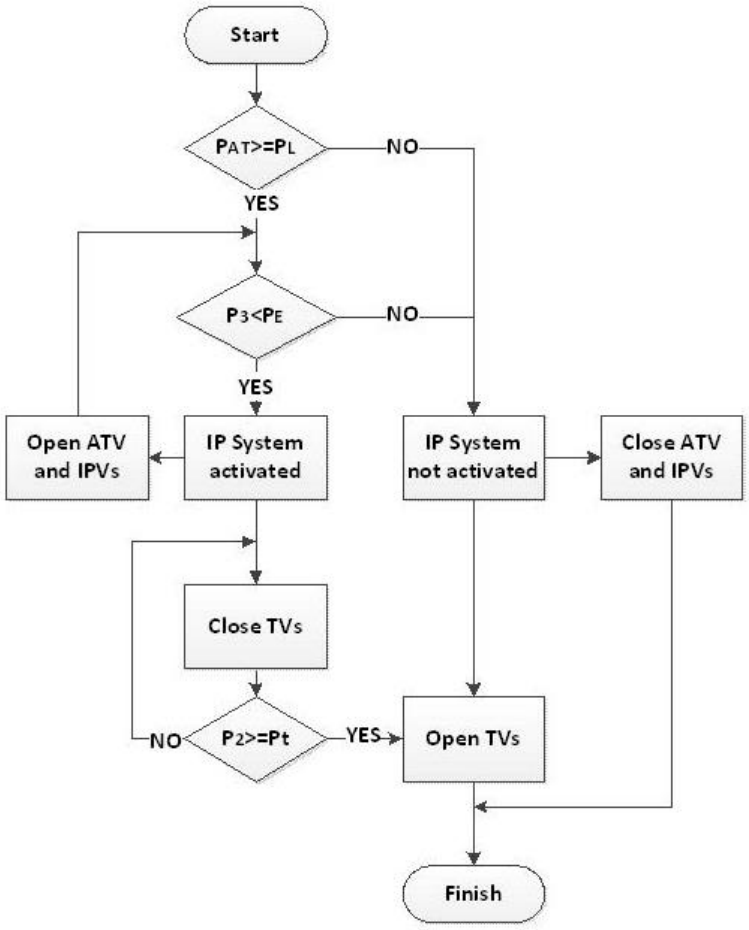

Figure 6-22 Flow chart of the System IP control strategy

6.5.4 Simulation of the Engine with System E

New modules, ESystem-Control-Unit (highlighted in green), and pneumatic hybrid system (highlighted in red) are added into the basic engine model to realise System E as shown in the Figure 6-23. The pneumatic hybrid system includes one air tank, one ATV and pipework connected the air tank with the exhaust manifold.

The dimensions and characteristics of System E are shown in the Table 6-4. The size of the air tank, pipes and ATV are the same as used for the Systems I and IP to maintain consistency.

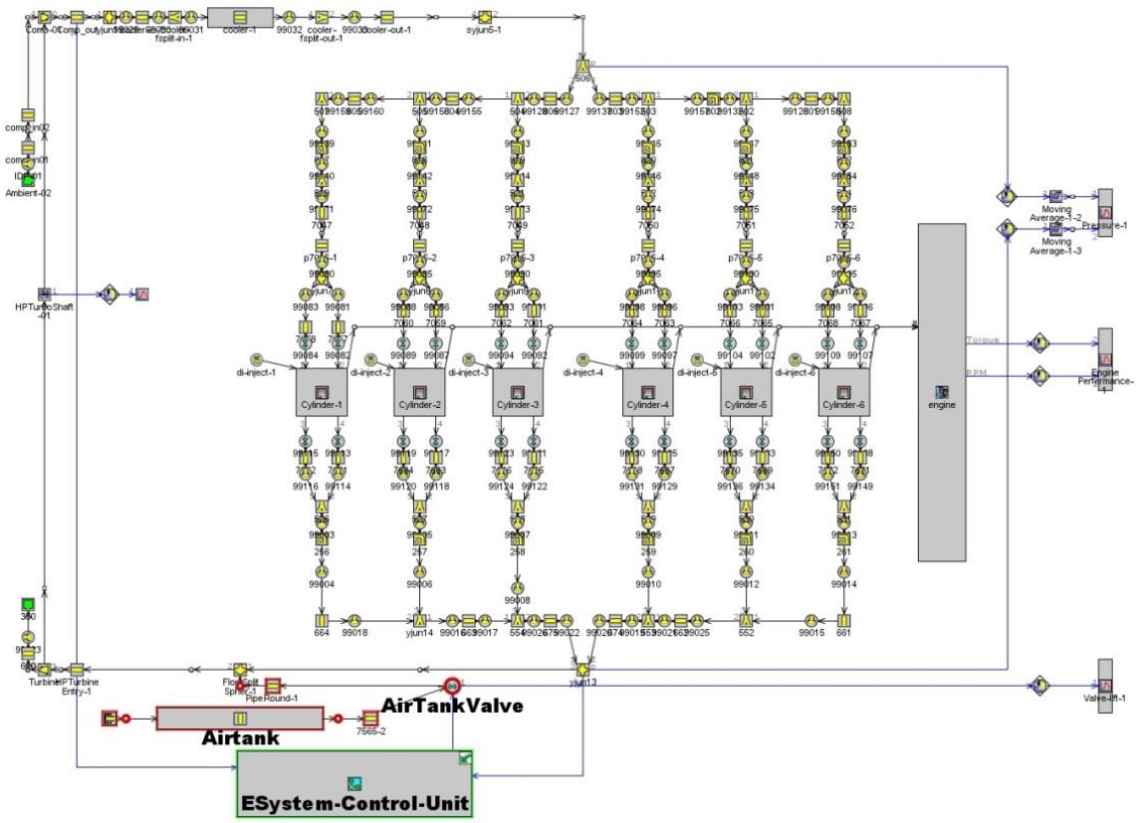

Figure 6-23 GT-POWER model of the engine with System E

Table 6-4 Dimensions and characteristics of System E

Name	Type	Dimensions	
Air Tank	Round Pipe	Volume (l)	151
		Initial pressure (bar)	5
7565-2	Round Pipe	Diameter (mm)	25.4
		Length (mm)	1000
Air Tank Valve	Valve that the lift is imposed by an Actuator Part	Diameter (mm)	25.4
PipeRound-1	Round Pipe	Diameter (mm)	25.4
		Length (mm)	30
FlowSplitSpher-1	A spherical-shaped flow split volume connected to one or more flow components	Diameter (mm)	54

Figure 6-24 is the system diagram of the System E Control Unit. The function of the System E Control Unit is to control the ATV in System E. During a transient System E is activated. The System E Control Unit uses two sensors to detect the pressures in the system:

(i) Compressor outlet pressure p_2 (comes through *ToPart_Comp_out*),

(ii) Exhaust manifold pressure p_3 (comes through *ToPart_yjun13*).

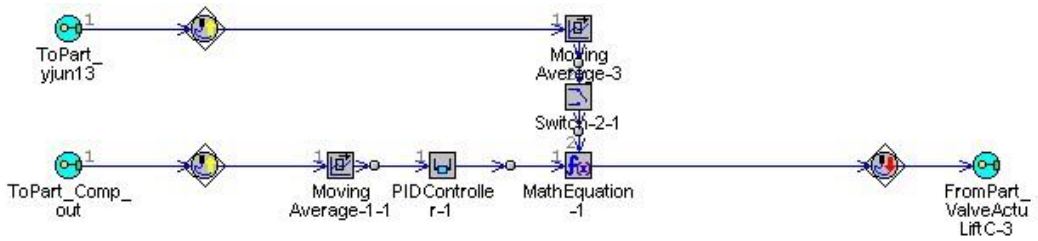

Figure 6-24 System diagram of System E control-unit

Similar to System IP, the exhaust manifold pressure had been chosen as the set point for control of the ATV opening. The ATV opening is controlled to facilitate two operating modes. The flow chart of System E control strategy is also shown in Figure 6-25.

(i) If the air tank pressure p_{AT} is greater than the limit pressure p_L, the air tank pressure is sufficient to boost the engine. If at the same time, the compressor is unable to supply the target boost pressure (turbine input pressure p_3 less than the target exhaust manifold pressure P_E), System E will be activated and the control unit will open the ATV to inject compressed air into the exhaust manifold to speed-up the turbocharger. When the exhaust manifold pressure p_3 is equal or greater than the target exhaust manifold pressure p_E, the ATV will fully close.

(ii) If the air tank pressure is not sufficient to boost the engine, which means the air tank pressure p_{AT} is less than the limit pressure p_L, the control unit will not activate the controller. As a result, the ATV will remain fully closed.

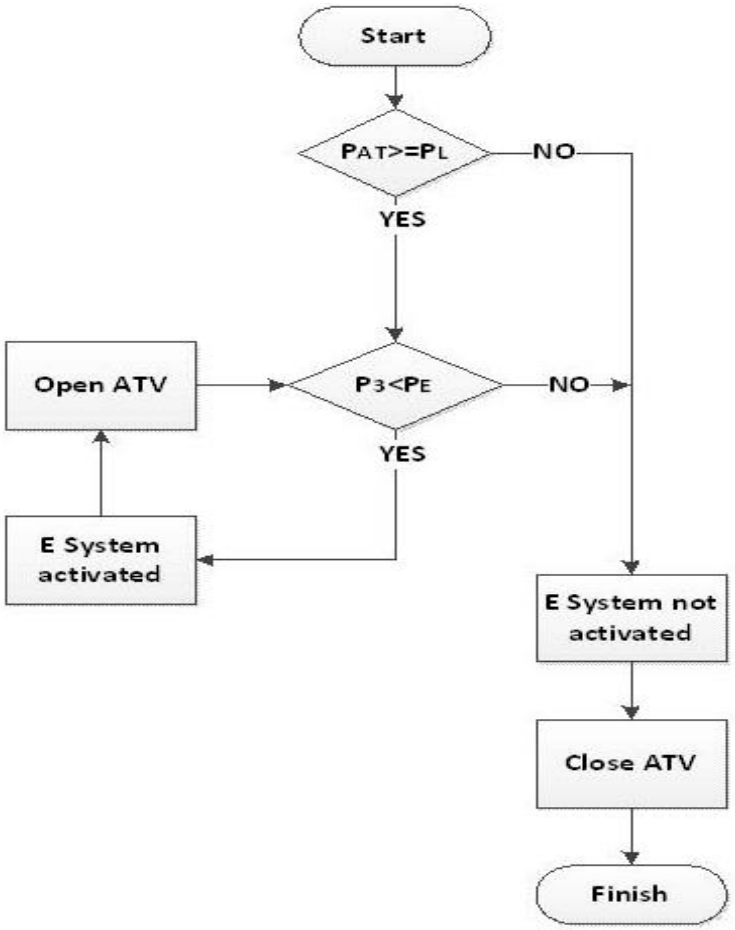

Figure 6-25 Flow chart of the System E control strategy

6.5.5 Engine with Pneumatic Hybrid Boost System Simulation Result

In this section, the maximum achievable performance from the three candidate pneumatic hybrid boost systems are compared for the situation when the engine accelerates from no load to full load at 1600 rpm. The obvious baseline for the result is the performance of the basic engine without any pneumatic hybrid boost system. The evaluation is done from each of three aspects.

(i) Engine performance improvement,
(ii) Air usage during the boost period,
(iii) Turbocharger operation condition.

6.5.5.1 Engine Performance Improvement

Figure 6-26 shows the simulated full load acceleration response of the engine in the terms of engine brake torque. In the basic engine without any pneumatic hybrid boost

system, torque can be seen to rise very slowly to reach the peak torque. The three pneumatic hybrid boost system all have a much sharper brake torque rise. Table 6-5 gives the time taken in each case to reach its peak torque output and their improvement to the basic engine performance expressed as the % reduction in response time.

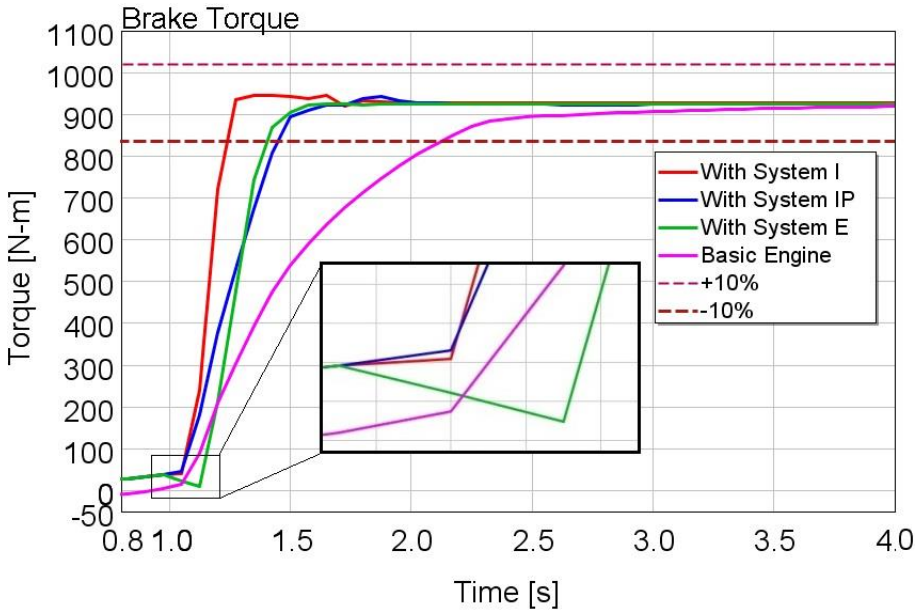

Figure 6-26 Brake torque response for each pneumatic hybrid boost system

Table 6-5 Time to reach peak torque output of the four engine configurations

	Time to 90% peak torque output (s)	Improvement (-)
Basic engine	1.15	-
Engine with System I	0.25	78.3%
Engine with System IP	0.42	63.5%
Engine with System E	0.45	60.9%

From Figure 6-26, it can be seen that Systems I and IP both have the fastest response in the very earliest stages of the acceleration while the engine with System E shows a decrease in brake torque output in this period. Such a decrease is likely to have an effect on drivability and represents a serious shortcoming. The reason is because in the engine with System E the whole manifold requires to be brought to its normal working pressure, slowing the response. Also the cold air in the air tank injected to the exhaust manifold

reduces the available energy in the exhaust gas which decreases the energy to the turbine. As a result, it will decrease the air delivery to the cylinder which causes a drop in the brake torque output. These results also support the hypothesis that the location of air injection is fundamental to the result. It also can be seen in Figure 6-26 (inset) that compared with System I, the engine with System IP has the faster initial brake torque response because the compressed air is more quickly delivered to the cylinders in the first few cycles. Finally System I gives the shortest time to reach maximum brake torque.

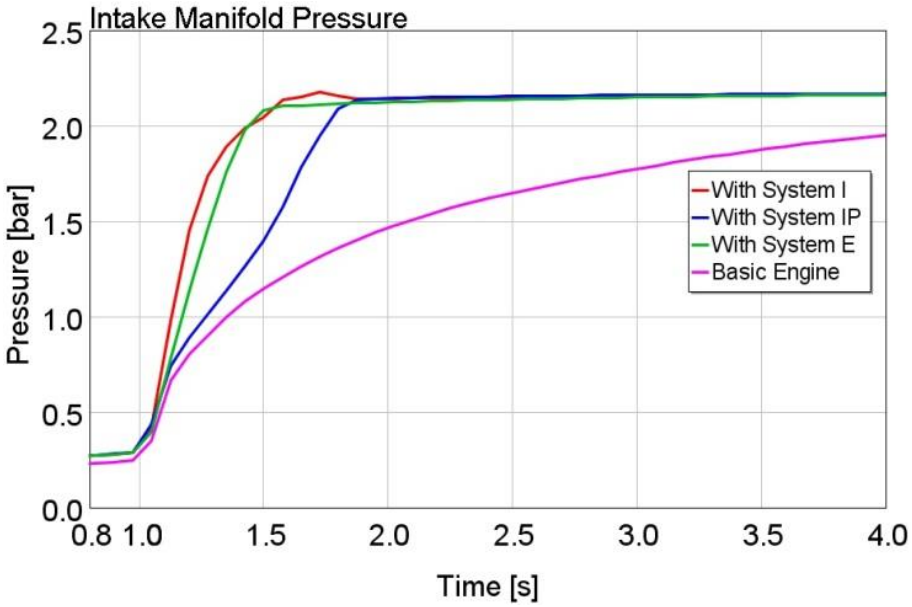

Figure 6-27 Intake manifold pressure for each pneumatic hybrid boost system

Figure 6-27 shows the intake manifold pressure change during the full-load acceleration at an engine speed 1600rpm for each of the four engine configurations. The engine with System I sees a rapid increase in intake manifold pressure. Once the engine with System E has reached normal turbocharger operating conditions, it has the same ability to increase the intake manifold pressure. The reason that System IP is slower to build inlet manifold pressure is because as System IP simply needs less air from storage to achieve the changed state of the turbocharger. It remains that System IP still demonstrates a much faster intake manifold pressure build-up compared with the basic engine.

6.5.5.2 Air Usage during the Boost Period

Figure 6-28 shows the air tank pressure drop for one full-load acceleration. The reason for the engine with System E using the least air is because the System E needs minimum

time to accelerate the compressor to reach the require operation point. As a result, the System E consumes the least air. The difference between the System I and System IP is because at the injection beginning stage, the air flow rate of the System IP is smaller than the System I. The air tank pressure drops of the pneumatic hybrid boost systems are shown in Table 6-6.

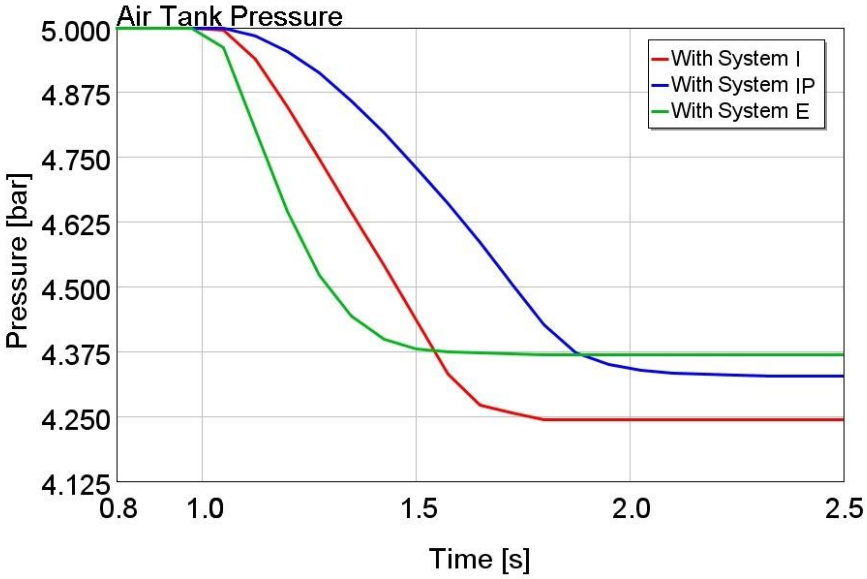

Figure 6-28 Air tank pressure for each pneumatic hybrid boost system

Table 6-6 Air tank pressure drops of the pneumatic hybrid boost systems

	Air tank pressure drop (bar)
Engine with System I	0.756
Engine with System IP	0.667
Engine with System E	0.632

6.5.5.3 Turbocharger Operation Condition

Figure 6-29 shows the turbocharger speed response during the simulation of a full-load acceleration at an engine speed 1600rpm for four engine configurations. The engine with System E shows the fastest acceleration of the turbocharger because of the direct path from the introduced high pressure air to the turbine rotor. The engine with Systems I and IP respectively both need to increase the turbocharger speed through the intermediary of

high efficiency combustion in the cylinders. As a result, it can be seen in the Figure 6-29, from 1 to 1.3 s, the engine with Systems I and IP demonstrate similar turbocharger shaft speed compared with the basic engine, and all slower than the engine with System E.

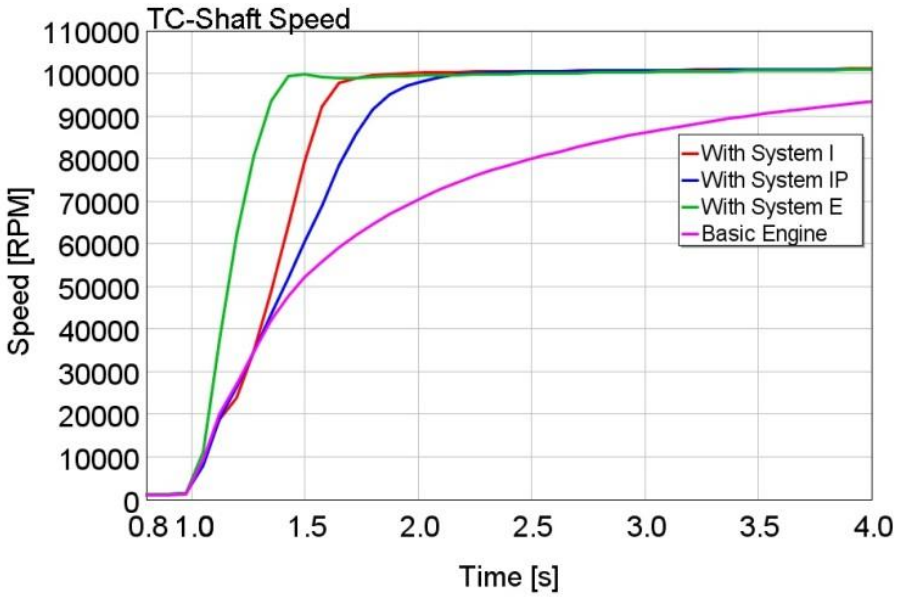

Figure 6-29 TC-Shaft speed for each pneumatic hybrid boost system

Figure 6-30 shows operating points and loci on the compressor map. For each system type, it can be seen that the compressor of the engine with System I has already entered surge. This is because when System I is working, the compressed air is injected into the intake manifold while the IMV is closed. This behaviour substantially increases the risk that the compressor enters surge because the output of the compressor has been blocked by the IMV. To prevent the compressor entering surge, the injected air needs to be controlled by monitoring the compressor delivery pressure. Once the compressor operating point is near surge, the control unit will stop compressed air injection and open the IMV to move the compressor operating point away from the surge line.

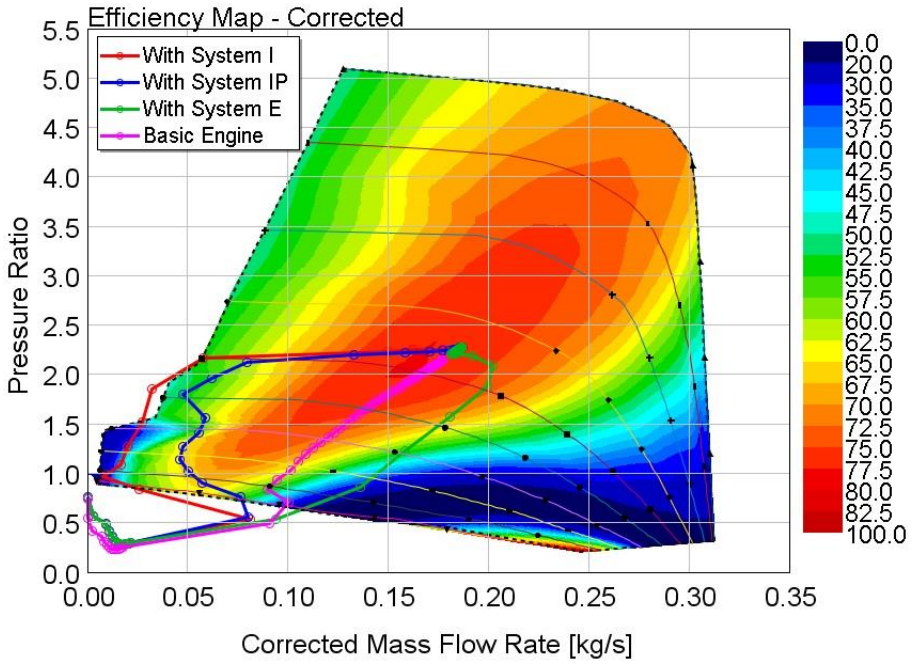

Figure 6-30 Turbocharger operation points on compressor efficiency map for each pneumatic hybrid boost system

Figure 6-30 demonstrates that with System IP there is less chance to cause the compressor to enter surge. This is because, for System IP, only one intake port is blocked by the TV during compressed air injection. The compressor still can deliver the air into the cylinder through another intake port.

From Figure 6-30, System E can be recognized as the safest method to increase the turbocharger response compared with the Systems I and IP. The injection into the exhaust manifold accelerates the turbocharger shaft speed, as a result, the compressor's output pressure increases rapidly and well away from the surge line.

From the analysis before, it can be seen the engine with System I get the fast brake torque response and the most air usage. The System IP has the almost the same brake torque response and air usage. But at the beginning stage, the System IP has the ability that deliver the compressed air into cylinders as soon as possible. As a result, the engine with System I and the engine with System IP have been chosen to the candidate to the vehicle simulation model with pneumatic hybrid boost system. In the next section, the basic vehicle, the vehicle with System I and the vehicle with System IP model are built in GT-POWER and their simulation results will be compared.

6.6 Vehicle with Pneumatic Hybrid Boost System Simulation Result

6.6.1 Vehicle GT-POWER Simulation Models

A 16 ton city bus equipped with the YUCHAI YC6A diesel engine is modelled using the GT-POWER code with parameters given in Table 6-7.

Table 6-7 City bus parameters

Vehicle weight (kg)	16500
Aerodynamic drag coefficient (-)	0.5
Frontal area (m^2)	5.69
Air density (kg/m^3)	1.225
Wheel radius (m)	0.508
Rolling resistance coefficient (-)	0.013
Air tank volume (l)	151
Starting tank pressure (bar)	6
1st gear ratio (-)	6.9
2nd gear ratio (-)	4.13
3rd gear ratio (-)	2.45
4th gear ratio (-)	1.49
5th gear ratio (-)	1
Final drive ratio (-)	5.125

The System I and IP respectively have been integrated into the basic bus model giving two different pneumatic hybrid vehicle configurations. The GT-POWER models of the basic vehicle, the vehicle with System I and the vehicle with System IP are shown in Figure 6-31, Figure 6-32 and Figure 6-33 respectively.

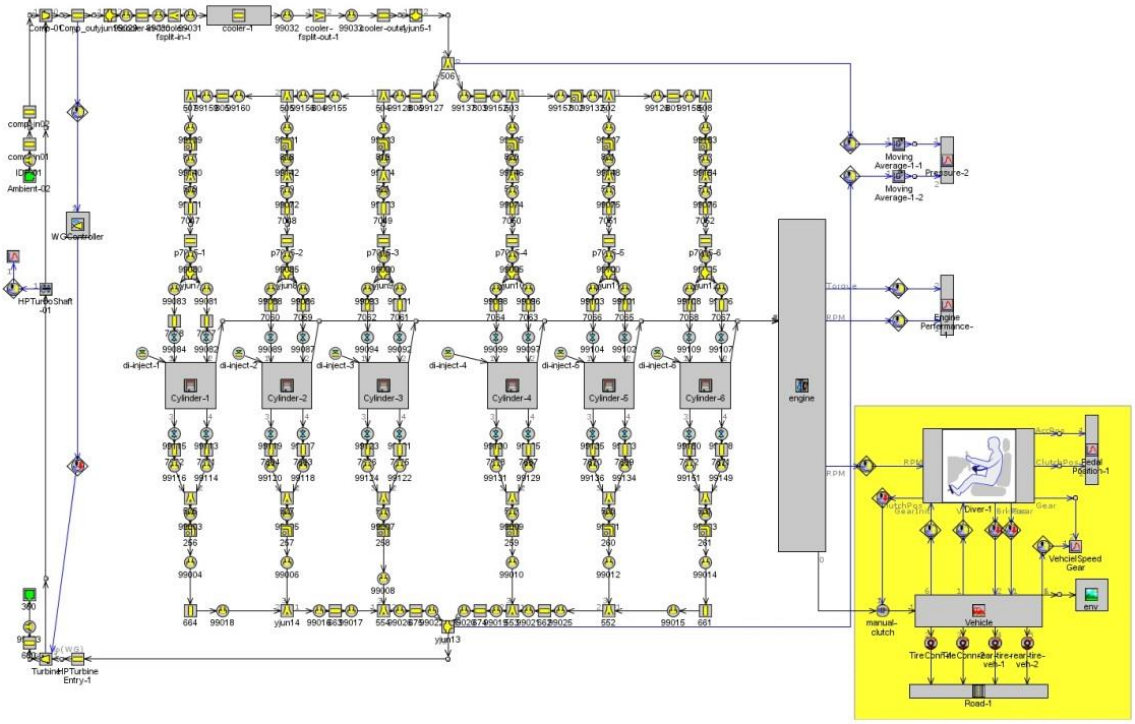

Figure 6-31 The basic vehicle simulation model

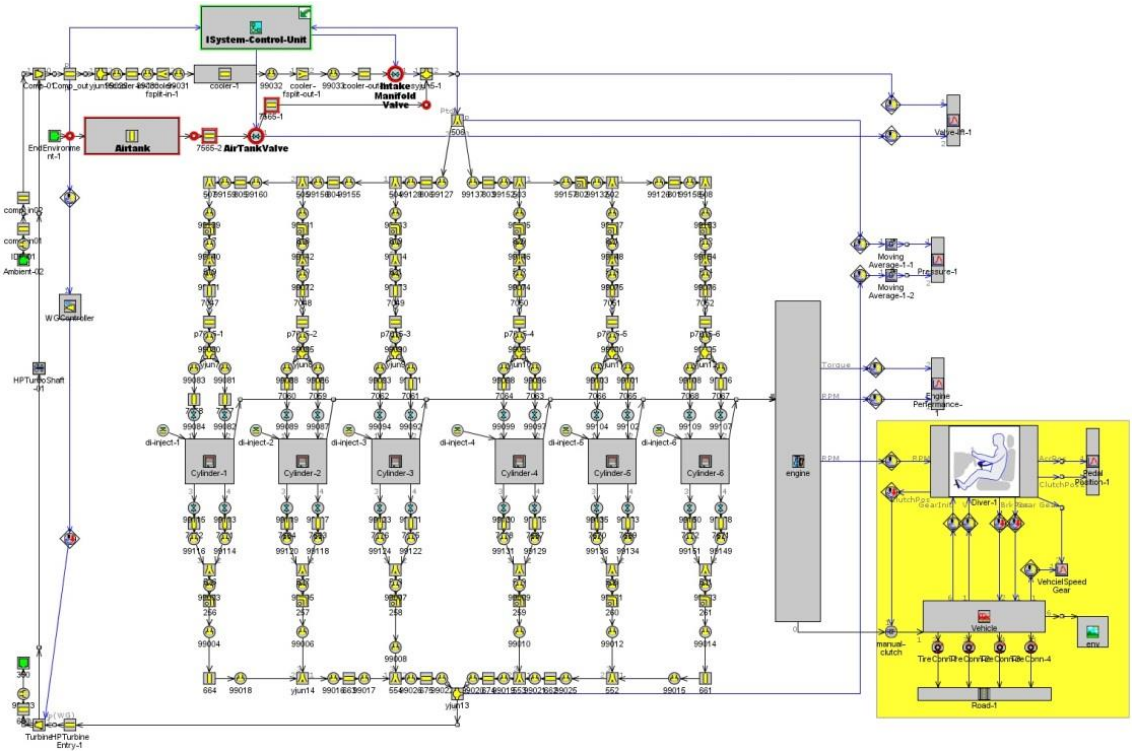

Figure 6-32 The vehicle with System I simulation model

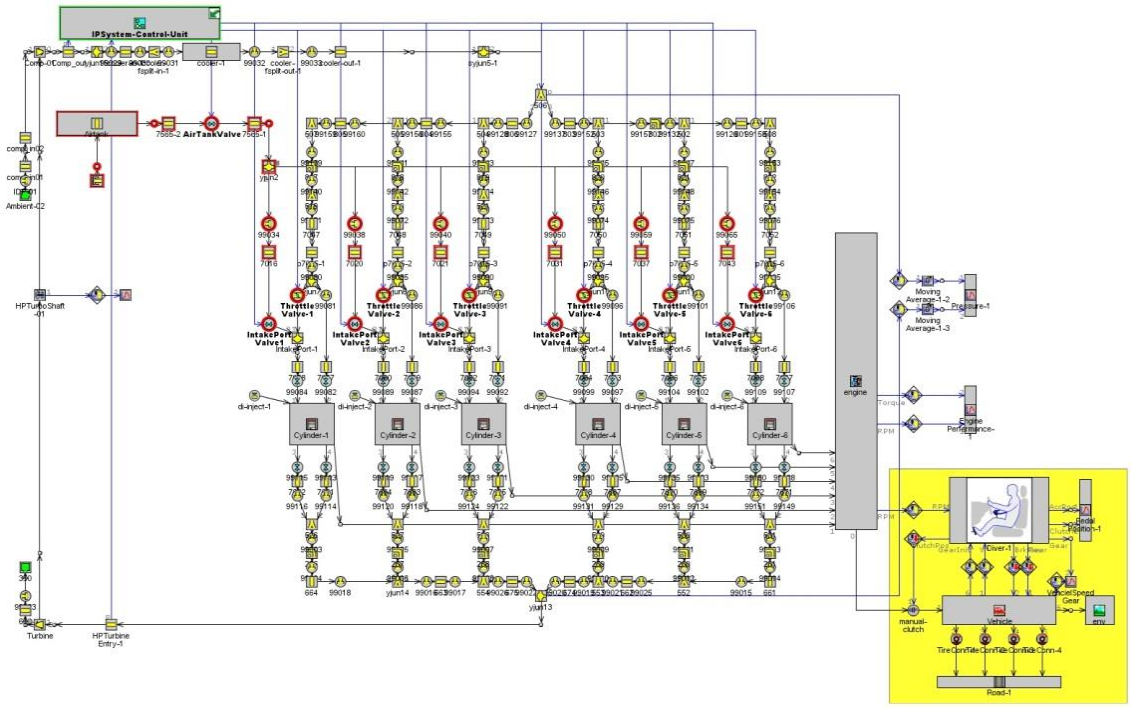

Figure 6-33 The vehicle with System IP simulation model

6.6.2 Vehicle with Pneumatic Hybrid Boost System Simulation Result

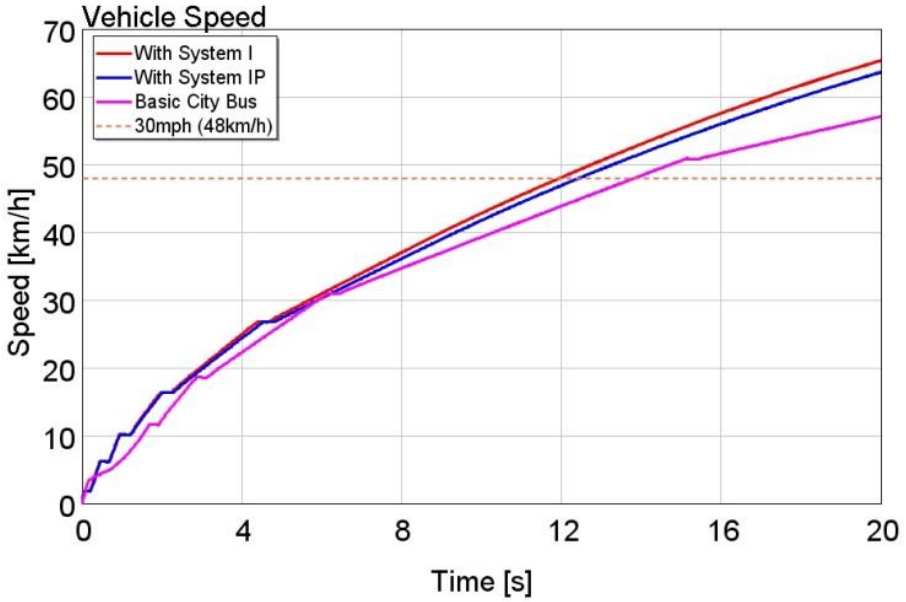

Figure 6-34 Vehicle speed during the acceleration

Figure 6-34 shows the vehicle speed change during the acceleration from 0 to 20 second. Here, due to GT-POWER setting, when the vehicle start with engine Off, it need some preparation time to start the engine and then keep the engine speed at the idle speed.

After that, the vehicle starts to move. As a result, the vehicle is stationary for the first 1 s in Figure 6-34. Then it fully accelerates to the maximum speed. Therefore, a very steep acceleration at the initial of the test reflects in Figure 6-34. It also can be seen, the vehicle with System I has the fastest acceleration performance. After 19 s acceleration, it reaches the speed of 65.3 km/h. The vehicle with System IP has the second fastest acceleration performance and reaches the speed of 63.5 km/h. The basic vehicle has the slowest acceleration performance, which reaches the speed of 57 km/h after 19 s acceleration. Table 6-8 shows the time for three vehicles to reach 48 km/h (30 mph) which is the speed limit for the most urban city roads in the UK. The Systems I and IP reduce the acceleration times by 14.7% and 9.7% respectively.

Table 6-8 Time to reach the speed of 48km/h

	Time to reach 48km/h (s)	Improvement (-)
Basic vehicle	12.9	-
Vehicle with System I	11.0	14.7%
Vehicle with System IP	11.7	9.3%

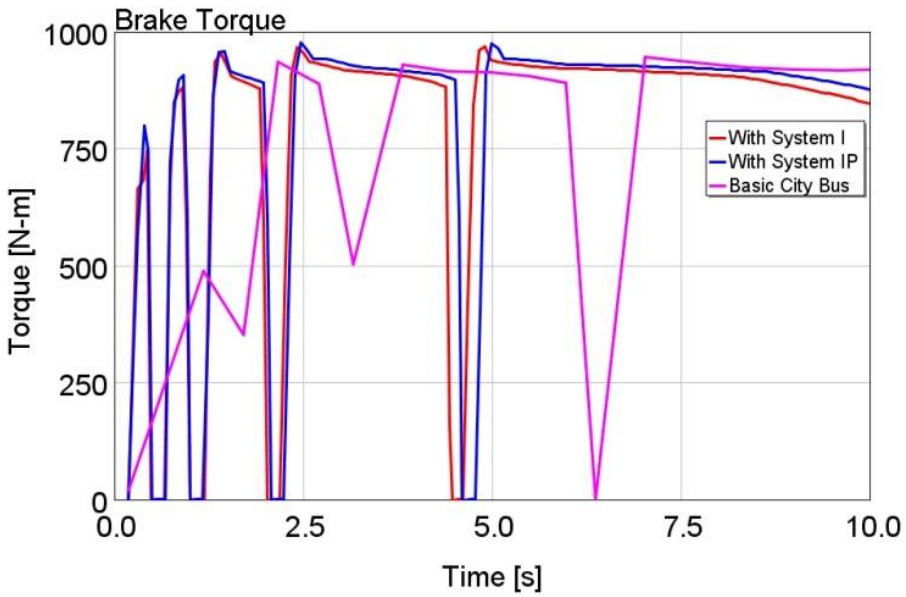

Figure 6-35 Engine brake torque response during the acceleration

Figure 6-35 shows the engine brake torque during acceleration. From the figure, it can be

seen, at the beginning stage that the vehicle with the Systems I and IP respectively both have the greatest capability to build up the brake torque especially in lower gears.

Figure 6-36 shows the air tank pressure drop during the acceleration. From the figure, it can be seen that System I use 1.02 bar air which is 0.32 bar more than the air usage of System IP which is 0.69 bar. The difference in air consumption is due to the efficiency of delivery in System IP. While air is delivered directly to the cylinders, the manifold is pressured by the slowly accelerating compressor in System I. It also can be learned from the figure that, the System I and IP activated when the vehicle start and after every gear change, and the lower gear, the more System I and System IP working time.

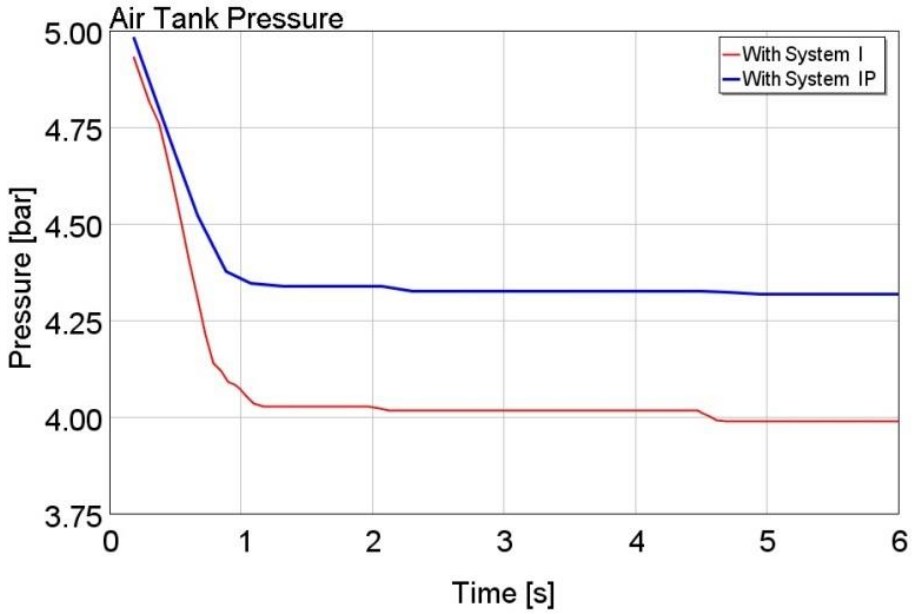

Figure 6-36 Air tank pressure drop during the acceleration

From the simulation result, it can be seen that System IP has advantages over System I at two aspects:

(i) Less use of air to achieve a similar brake torque response,

(ii) Less likely to cause the compressor surge.

6.7 Conclusion

An analysis of the reasons for engine turbo-lag and the methods developed for reducing the turbo-lag and improving transient response have been presented first. Then, three kinds of pneumatic hybrid boost systems for managing a rapid energy transfer into the

powertrain to assist acceleration of the turbocharger, respectively Systems I, IP and E integrated into a six cylinders 7.25 l heavy-duty diesel engine for a city bus application have been proposed and investigated from engine brake torque response by using the 1-D engine simulation. The findings show

(i) The engine with System I has the fastest engine response: 0.25 s to reach its 90% maximum brake torque, compared with 1.25 s for the basic engine. The System I, IP and E all improve torque response time (to maximum torque) by 78.3%, 63.5% and 60.9% respectively. The engine with System E has a significantly lower brake torque output during the first few cycles which reduce the quality of the engine response.

(ii) The simulation result indicates that System I carries the highest risk of compressor surge. To avoid surge, a control strategy can be implemented to ensure the compressor operating point is kelp away from conditions where surge can develop. System IP carries a lower risk of surge because it does not block the output of the compressor. Because System E does not need a valve in the intake system, there is no risk of the surge.

The performance of the vehicle (city bus) has been also considered. A 16 ton city bus equipped with this engine has been modelled using GT-POWER. The Systems I and IP have been integrated respectively into the basic bus model. Both the Systems I and IP can be seen to significantly reduce the vehicle acceleration time through the reduction of turbo-lag. For the speed range from 0 to 48 km/h (30 mph) which is the speed limit for most urban roads in the UK, the vehicle with the Systems I and IP can reduce the acceleration time 13.7% and 9.3% respectively.

System IP offers considerable advantages over System I at both less use of air and less likely to cause the compressor surge. As a result, System IP should be the appropriate candidate for the future research such as to develop a pneumatic hybrid system can achieve three functions: the regenerative braking when decelerating, boosting engine and eliminating the turbo-lag when accelerating, and the stop-start operation.

CHAPTER 7
DESIGN AND OPTIMIZE THE PNEUMATIC HYBRID CITY BUS CONTROL STRATEGY

7.1 Introduction

After comparing the three principal hybrid vehicle control strategies, respectively rule-based, global optimisation and real-time optimisation, an energy control strategy based on the use of thresholds in the degree of energy storage and regeneration (a "logic threshold" methodology) for the pneumatic hybrid city bus has been designed. By employing the control strategy, six operation modes of the pneumatic hybrid city bus can be changed dynamically and the energy distribution of the pneumatic hybrid system can be controlled to realize the three principal functions of the pneumatic hybrid system, respectively Stop-Start Function, Boost Function, and Regenerative Braking Function.

A forward facing pneumatic hybrid city bus simulation model which includes the detailed engine model has been developed in GT-POWER with MATLAB/Simulink co-simulation. The pneumatic hybrid city bus dynamic performance, engine transient response, fuel economy and energy usage can be analysed from this model.

To obtain the maximum overall fuel economy, the amount of air and energy recovered during the braking and minimum loss of availability during acceleration, a number of variables in the control strategy must be optimized. Three global optimisation algorithms, Pattern Search (PS), Genetic Algorithm (GA) and multi-objective Non-dominated Sorting Genetic Algorithm II (NSGA-II), are compared and employed for the optimisation of the control strategy considered at three levels.

(i) Using the PS to optimize the initial air tank pressure for every stop-start event to maximize the pressure increment in the air tanks.
(ii) Conducting the GA optimisation to find out the best gear change strategy during braking to maximize the energy recovery to the air tanks.

(iii) Implementing the multi-objective optimisation to simultaneously minimize a) the fuel consumption and b) the loss of availability in the air flow during a vehicle acceleration (Using the NSGA-II).

7.2 Pneumatic Hybrid City Bus Control Strategy

Unlike HEVs, the pneumatic hybrid city bus cannot be driven by pneumatic energy alone. But pneumatic hybrid technology has the potential to be a low-cost alternative to the electric motor based micro hybrid technology by converting kinetic energy to pneumatic energy during braking, re-using the stored energy to power an air starter to realize a stop-start operation. Normally the micro hybrid system is the integration of starter and alternator in the conventional IC engine vehicle, in which the starter should also function as an electric motor which tends to add both cost and weight to the vehicle [92]. As mentioned in Chapter 6, the pneumatic hybrid system also has another advantage which can improve the engine performance by injecting compressed air into the inlet manifold to build-up engine torque more rapidly compared with the unassisted engine. So the pneumatic hybrid city bus control strategy should ensure three functions:

(i) Stop-Start Function: when the vehicle starts, the air starter is cranking the engine; when the vehicle is stopped, the IC engine is switched off to save the idle fuel consumption if stop conditions are satisfied.
(ii) Boost Function: during the acceleration, the Boost Function is switched ON to eliminate the turbo-lag and improve the engine transient response.
(iii) Regenerative Braking Function: During deceleration, the Regenerative Braking Function is engaged to recover energy.

7.2.1 Overview the Control Strategy of Hybrid Vehicles

The control strategy of a hybrid vehicle is defined as an algorithm which regulates the operation of the vehicle powertrain [93]. It is usually implemented in the hybrid vehicle controller which has a supervisory role in regard to the operation of the vehicle. The main objectives of the hybrid vehicle control strategy are to continuously monitor the driver's demand, vehicle status, current traffic information, and even the information provided by the Global Positioning System (GPS) to determine the proper vehicle operating state for optimal fuel economy, minimum overall energy use, and vehicle performance [69, 93,

94]. Hybrid vehicle control strategies can be divided into three categories: ruled-based, numerical optimisation-based and real-time optimisation [95]. All the main solutions are classified according to Figure 7-1.

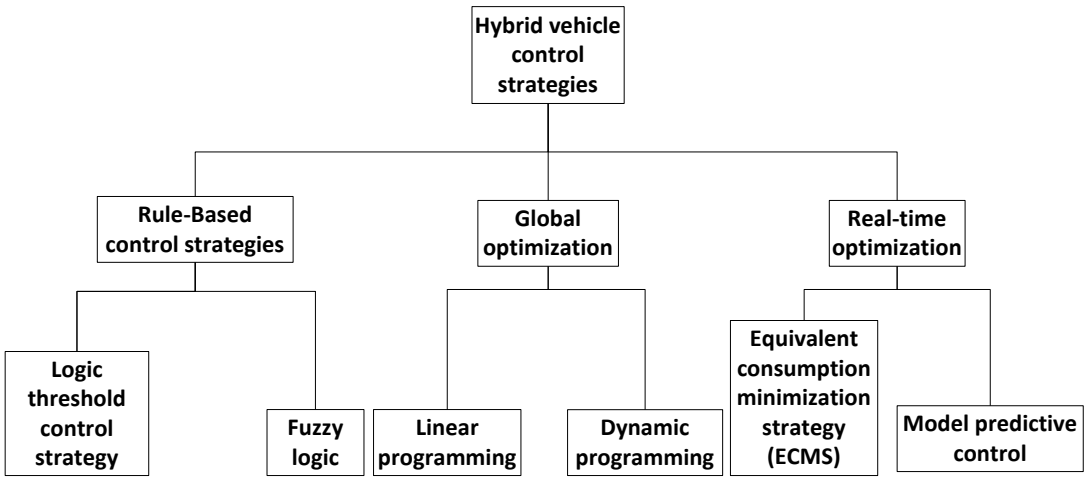

Figure 7-1 Classification of hybrid vehicle control strategies

7.2.1.1 Rule-based Control Strategies

The rule-based control strategies are designed without *a priori* knowledge of the driving cycle. Therefore, they are effective in the real-time supervisory control of the power flow in the hybrid powertrain. The rules can be obtained by using heuristics, intuition, human expertise, and even mathematical models [93]. The objective of rule-based control strategies is often "load-levelling" which tends to shift the actual IC engine operating point as close as possible to the optimal point of the efficiency, fuel consumption, or emissions at a particular engine speed. Although the control approaches can offer an improvement in energy efficiency, it is clear that they do not guarantee an optimal result in all conditions [95]. Two typical rule-based control strategies are introduced here: respectively (i) a logic threshold control strategy and (ii) a fuzzy logic control strategy.

The logic threshold control strategy is widely used because of its speed and simplicity [12]. It based on analysis of power flow in a hybrid powertrain, efficiency/fuel or emission maps of an IC engine, and human experience is utilized to design deterministic rules, generally implemented via lookup tables, to split the requested power between power converters [93]. In other words, the logic threshold control strategy selects the operating mode of the powertrain according to the prevailing and predicted conditions of

the vehicle. The transition between operating modes is decided based on a change in driver demand, or a change in vehicle operating condition.

Looking into the hybrid powertrain as a multi-domain, nonlinear, and time-varying plant, a fuzzy logic control strategy offers a number of advantages including an accessible format and the potential for non-linear behaviour [93]. The fuzzy logic control strategy is an extension of the conventional rule-based control strategy typified by a logic threshold control strategy [93]. The fuzzy logic control strategy uses the decision-making property instead of using deterministic rules. As a result, it can be adopted to realize a real-time though possibly suboptimal power split. The main advantages of the fuzzy logic control strategy are robustness and the potential for adaptive behaviour [93].

7.2.1.2 Global Optimisation

The global optimisation approach can find the global optimum solution by performing the optimisation over a prescribed driving cycle. It is non-causal in nature and requires *a priori* knowledge of the driving cycle information and could be used directly for real-time hybrid vehicle control strategy. However, the result of the global optimisation can be considered as the benchmark for designing rules for online implementation or comparison for evaluating the quality of other control strategies. The most common global optimisation approach, Dynamic Programming (DP), is introduced later.

DP seems to be a reasonable approach for optimal power split in hybrid vehicles, since it is a powerful tool to save general dynamic optimisation problems, easily handling the constraints and nonlinearity of the problem while obtaining a globally optimal solution [93]. DP calculates every possible combination energy output of the IC engine and another power source in the hybrid powertrain such as motor power at each step, ensuring that the global optimum can be reached. When utilizing DP in the hybrid powertrain optimisation, the model of hybrid vehicle can be expressed in the form of Equation (7-1) where X_K is the state vector that includes vehicle speed, State of Charge (SOC) of the energy store, engine speed, motor speed, etc. While u_K is the control vector that covers gear number, generator torque, engine torque, motor torque, etc. The optimisation goal is to find the control u_K at each step to minimize a cost function shown at Equation (7-2). Also, the constraints in Equation (7-3) are necessary for the optimisation process.

$$X_{K+1} = f(X_K, u_K) \quad \text{(7-1) [96]}$$

$$\begin{cases} J_0(X_0) = J_0 \\ J_k(x_k) = \min_{u_k \in U_k}[fuel(x_k, u_k) + J_{k-1}(x_{k-1})] \quad k = 1, \dots, N \end{cases} \quad \text{(7-2) [96]}$$

$$\begin{cases} \omega_{ICE\,min} \le \omega_{ICE} \le \omega_{ICE\,max} \\ T_{ICE\,min}(\omega_{ICE}(k)) \le T_{ICE}(k) \le T_{ICE\,max}(\omega_{ICE}(k)) \\ T_{m\,min}(\omega_m(k), SOC(k)) \le T_m(k) \le T_{m\,max}(\omega_m(k), SOC(k)) \\ SOC_{min} \le SOC(k) \le SOC_{max} \end{cases} \quad \text{(7-3) [96]}$$

Where $\omega_{ICE\,min}$ – minimum speed of the engine,

$\omega_{ICE\,max}$ – maximum speed of the engine,

T_{max} – torque limitation of the engine,

$T_{m\,min}$ and $T_{m\,max}$ – motor torque limitation,

The variable *SOC(k)* is constrained within the permitted minimum value SOC_{min} and the maximum value SOC_{max} of the battery.

When the energy management strategy is designed, the constraints have to be respected [97]. For example, in order to mitigate battery degradation, the SOC should be maintained within a certain range. The torque capacity of the engine and electric motor vary with their rotational speed or environmental temperature, and the speed of the engine and electric motor must be limited to the specific range to ensure safety and reliability [97].

DP will supply a benchmark which can be compared with the rule-based control strategy's result. Although the DP can find the global optimum, it is an off-line algorithm.

7.2.1.3 Real-time Optimisation

In order to develop a cost function to be used in a real-time optimisation process, the rate of fuel consumption must be available as a measurement. Variations of the stored electrical energy should also be taken into account to guarantee electrical self-sustainability [93]. Although the solution to such a problem is not globally optimal, it is particularly suited to real-time implementation and is reported to be close to optimal in practice [98]. The most well-known approach of the real-time optimisation is the Equivalent Consumption Minimization Strategy (ECMS).

The "equivalent fuel consumption" of the ECMS is the electrical energy flow costed according how much it will cost in fuel terms to restore that energy to the store. Application of the ECMS method includes an assessment of the relative value derived from a drive cycle of electricity and fuel. The process includes the notion of the "free" energy that is derived from regenerative braking [95]. In [93], one approach, that of calculating the equivalent fuel consumption using mean efficiencies is used when not all components set points are known is introduced as follows:

$$C_{Eq}\big(k(t),T_e(t)\big)=\begin{cases}T_e<0 & \frac{SFC_{rech}\cdot P_c(\omega_c,T_c)}{c\cdot\overline{\eta}_e\cdot\overline{\eta}_{batt}}\\ T_e\geq 0 & \frac{SFC_{dis}\cdot P_e(\omega_e,T_e)\cdot\overline{\eta}_e\cdot\overline{\eta}_{batt}}{c}\end{cases} \quad \text{(7-4) [93]}$$

where SFC_{rech} – mean specific fuel consumption for the recharge cases,

SFC_{dis} – mean specific fuel consumption for the discharge cases,

$\overline{\eta}_e$ – mean efficiencies of the motor during recharge,

$\overline{\eta}_{batt}$ – mean efficiencies of the battery during recharge,

c – constant.

The Electric Motor (EM) power to produce T_e at ω_e is denoted by P_e. And, the total equivalent fuel consumption $C_{TOT}(k(t),T_e)$ is the sum of the real fuel consumption of the IC engine $C_{ICE}(k(t),T_e)$ and the equivalent fuel consumption of the EM $C_{Eq}(k(t),T_e)$. This allows a unified representation of both the energy used from the battery and the IC engine respectively. As a result, the instantaneous control problem is

$$\min_{T_e(t),k(t)} J = C_{TOT}(k(t),T_e(t))\cdot\Delta \quad \text{(7-5) [93]}$$

Zhao *et al.* [95] used the idea of the ECMS to realize a real-time optimisation of the fuel economy of an HEV. The optimisation problem can be explicitly formulated as minimizing the following cost function in terms of energy:

$$J_f\big(t_f,\mu,SOC\big)=\int_{t_0}^{t_f}\dot{m}_f(\tau,\mu,x)\,d\tau+\varphi(SOC(t_0),SOC(t_f)) \quad \text{(7-6) [95]}$$

where μ – control variables,

x – engine, motor, and battery states,

$SOC(t_0)$ – initial SOC values,

$SOC(t_f)$ – final SOC values,

$\varphi(\cdot)$ – penalty function regarding any SOC deviation from its initial value to the final value.

The penalty function is also called the equivalent fuel consumption. For the sake of optimality, the boundary condition of the terminal state

$$SOC(t_0) = SOC(t_f) \quad (7\text{-}7)\ [95]$$

is to be satisfied.

Although the ECMS is designed for the HEV, it still can be transferred to control the pneumatic hybrid vehicles. As mentioned in Chapter 2, some of the pneumatic hybrid vehicles use the pneumatic energy to drive the vehicle in the AM mode or APA mode. It means it can save the fuel by using the pneumatic instead of. As a result, the "equivalent fuel consumption" of the ECMS in the pneumatic hybrid vehicle is the pneumatic energy flow costed according how much it will cost in fuel terms to restore that energy to the store. Application of the ECMS method includes an assessment of the relative value derived from a drive cycle of air and fuel. Furthermore, in the commercial vehicle like buses and trucks, some auxiliaries are driven by the electricity now. It could be driven by the air in the future. Therefore, in the pneumatic hybrid vehicles, the fuel used to drive the auxiliaries can be saved by using the air. As a result, the air usage can be calculated how much it cost in fuel terms. Here, in this research, the pneumatic hybrid powertrain is to realize three special functions. It does not drive the vehicle alone by realizing the AM mode or APA mode. So there is no fuel saved by using the pneumatic energy. Consequently, there is no energy to be calculated in fuel term. Therefore, the ECMS will not be chosen for controlling the pneumatic hybrid city bus in this research and not be discussed in detail.

7.2.2 Logic Threshold Based Energy Control Strategy for Pneumatic Hybrid City Bus

Compared with other hybrid vehicle control strategies such as DP and ECMS, the logic threshold based energy control strategy fits for the pneumatic hybrid system requirement and because it is fast, simple and practical [12].

The store of pneumatic energy helps achieve three principal functions. The energy control strategy for the pneumatic hybrid city bus enables the vehicle to realize the specific functions mentioned before and summarized below, as well as the normal operation of the vehicle.

(i) Stop-Start Function: the IC engine is off when the vehicle is stop, to save the idle fuel consumption if the condition is satisfied; when the vehicle starts, the air starter is cranking the IC engine.
(ii) Boost Function: during the acceleration, the Boost Function is ON to eliminate the turbo-lag and improve the engine transient response.
(iii) Regenerative Braking Function: During the deceleration, the Regenerative Braking Function is ON to recover the energy.

The schematic diagram of the control strategy for the pneumatic hybrid city bus is shown in Figure 7-2. It can be seen that there are three sub-controllers which are in charge of realizing the three specific functions above from Figure 7-2. The conditions of the pneumatic hybrid city bus at each time step form the basis for a decision to transfer the operating mode or not are also shown in Figure 7-2. In each operating mode, there may be some sub-states which the vehicle can operate between these states. As the vehicle enters a new state, the output signals will be implemented to affect the new control state. The parameters of the logic threshold based energy control strategy for the pneumatic hybrid city bus are shown in Table 7-1. To obtain the maximum overall fuel economy, the amount of air and energy recovered during the braking and minimum loss of availability during acceleration, these variables in the control strategy must be optimized. The goals and cost function of three optimisations are shown in Figure 7-3.

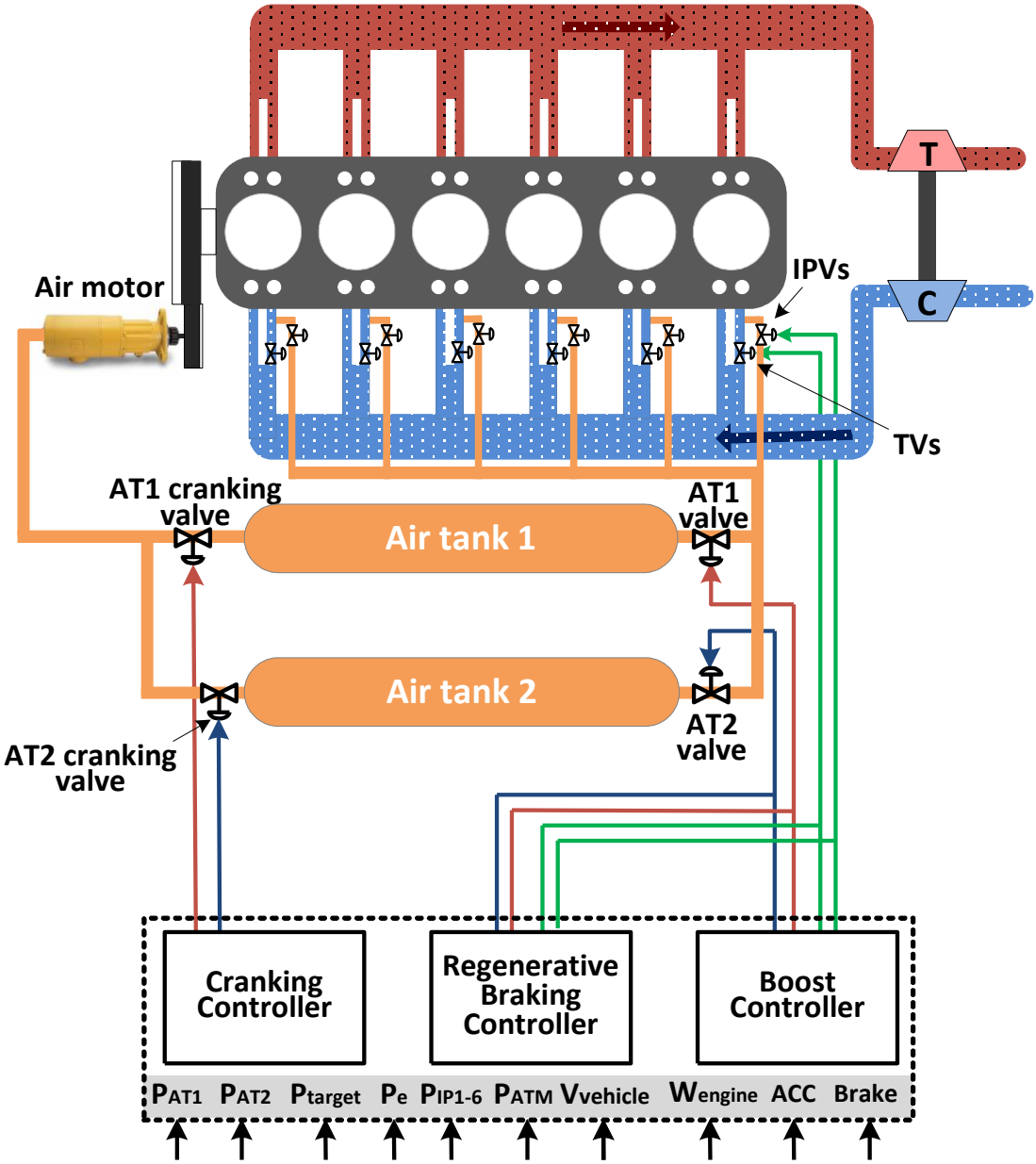

Figure 7-2 Schematic diagram of the control strategy for pneumatic hybrid city bus

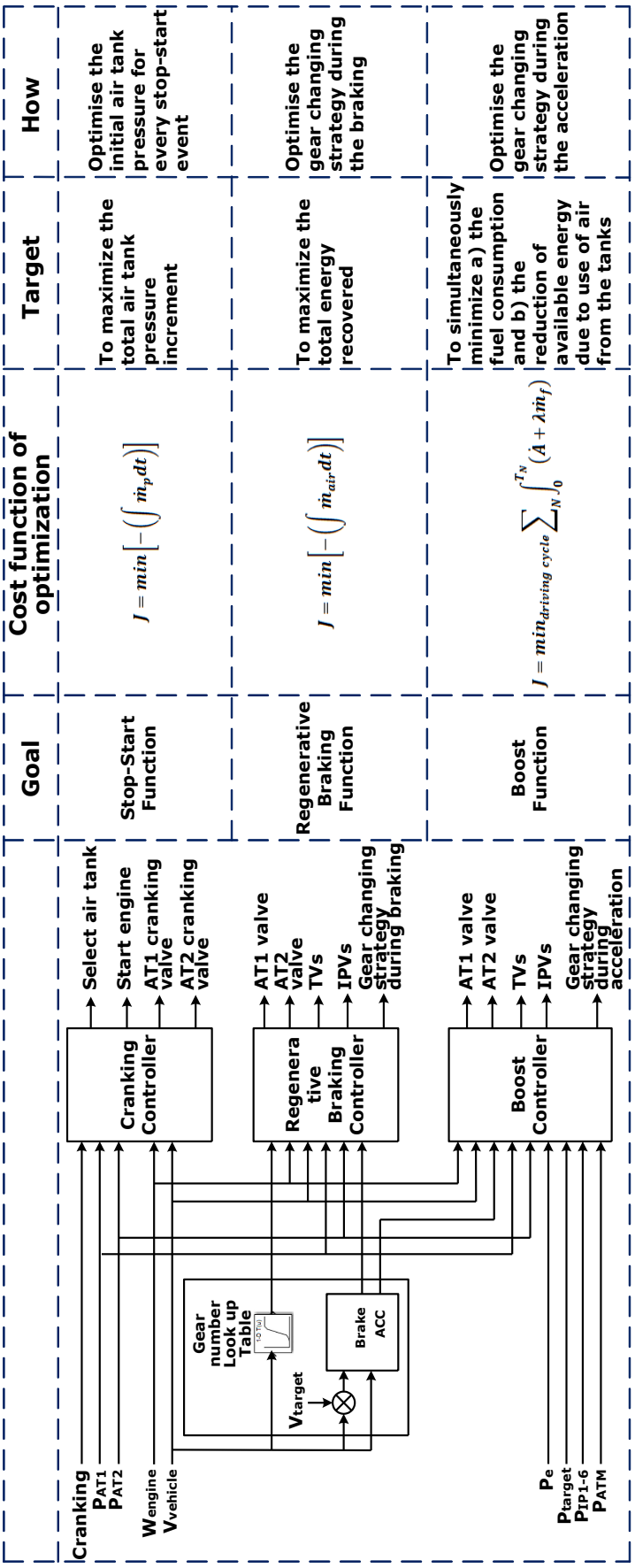

Figure 7-3 Schematic diagram of the control strategy optimisation

Table 7-1 Parameters of the logic threshold control strategy for the pneumatic hybrid city bus

Variables	Unit	Description
P_1	bar	The initial pressure of air tank 1
P_{22}	bar	The initial pressure of air tank 2
gear12	km/h	The gear shift-up point from first to second gear at vehicle speed
gear23	km/h	The gear shift-up point from second to third gear at vehicle speed
gear34	km/h	The gear shift-up point from third to fourth gear at vehicle speed
gear45	km/h	The gear shift-up point from fourth to fifth gear at vehicle speed
gear21	km/h	The gear shift-down point from second to first gear
gear32	km/h	The gear shift-down point from third to second gear
gear43	km/h	The gear shift-down point from fourth to third gear
gear54	km/h	The gear shift-down point from fifth to fourth gear

The principal fuel economy measure comes from the reduction in the idle time of the engine because during idle, the engine produces no useful work although it may still be required to manage the air conditioning and electrical loads. During deceleration or braking, there is no fuel consumption; recovery of the energy by transferring the kinetic energy to the pneumatic energy also enhance the system's energy efficiency through removing the need for an electrical flow of energy from the engine alternator. The Boost Function assists the engine in reaching a high efficiency working condition more quickly than otherwise. These principal functional requirements set the goals for the individual sub-system control objectives.

The operations modes of the pneumatic hybrid city for a typical driving condition are explained in Figure 7-4. The figure shows a typical manoeuvre that starts with the engine off. The engine is started and the vehicle proceeds to accelerate before reaching a steady

speed. The vehicle continues to accelerate before being brought to rest. The engine is switched off for the duration of the stop.

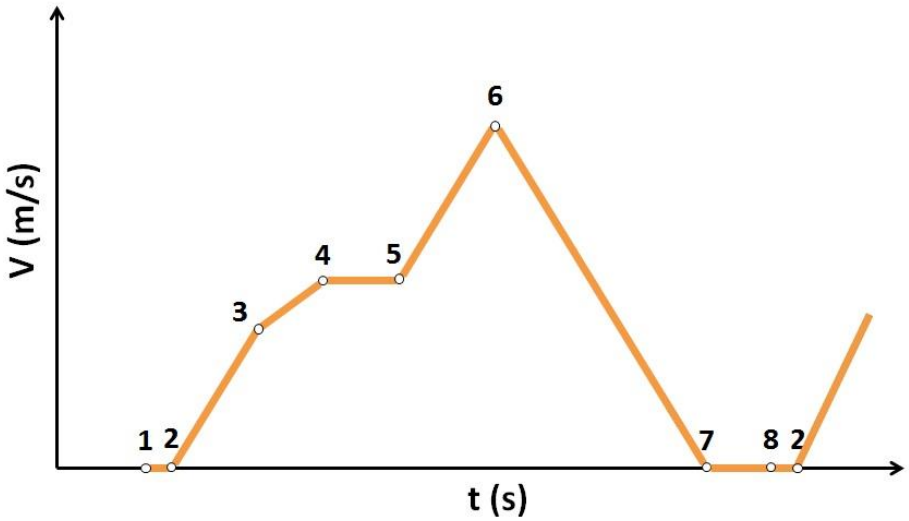

Figure 7-4 Operation modes for the pneumatic hybrid city bus

Stateflow in the MATLAB software platform is used to complete the modelling and simulation to achieve modularization of control system development. Stateflow is an environment for modelling and simulating combinatorial and sequential decision logic based on state machines and flow charts [9]. Because of the functions of the Stateflow such as state machine animation, static and run-time checks for testing design consistency and completeness before implementation, it is easy for model debugging and updating. The principal reason however for using Stateflow is that the function of the pneumatic hybrid city bus naturally consists of a number of states. Based on different state transition conditions, the model will transfer from one state to another. In complex circumstances, secondary models manage a state transition within high level states.

Figure 7-5 shows the state diagram of the control strategy for the pneumatic hybrid city bus and its implementation in Stateflow is shown in Figure 7-6.

The conditions of the pneumatic hybrid system, output signals are summarized in Table 7-2. The status of the system includes: the respective air tank pressures, engine speed, vehicle speed, acceleration, accelerator pedal position, and brake pedal position. When the control strategy controls the vehicle operating in different modes, as a result, in the different model states there are different output signals in each state.

The control modes which govern the vehicle during this process are now described in more detail: (Each mode is referred to the Stages shown in Figure 7-4)

(i) Cranking mode (1-2)

In this mode, based on the input signals and the pressure in the two air tanks, the control strategy assigns one air tank to start the engine by opening the valve of this air tank. The control strategy for this operation mode is in the sub-stateflow state ***Cranking*** shown in the Figure 7-6.

(ii) Fully acceleration mode (2-3, 5-6)

In the full acceleration mode, the driver demands full (100%) acceleration. The mode can be either part of an acceleration event like stage 2-3 or a full acceleration event such as stage 5-6. The control strategy chooses one air tank to realize the boost function by opening the valves. Based on the finding of Chapter 3, the lower air tank pressure can recover more braking energy during the deceleration. As a result, the control strategy chooses the air tank with lower pressure to implement the boost function. In the Stateflow representation of this control strategy, in the state ***Acceleration***, the states ***AT1Boost*** and ***AT2Boost*** compose this operation mode.

(iii) Acceleration mode (3-4)

Acceleration mode is selected when the driver demand is less than 100%. Referring to Figure 7-6 there is a sub-state ***BoostOff*** in the state ***Acceleration***. ***BoostOff*** defines the acceleration mode. The vehicle operation modes can transfer between these two modes depending on the driver demand.

(iv) Cruise mode (4-5)

In this mode, the vehicle has a fixed speed.

(v) Deceleration mode (6-7)

The deceleration mode is the ***Brake*** state in the Figure 7-6. Based on the pneumatic hybrid system condition, the control strategy controls the vehicle to operate between three states:

a) Regeneration to air tank 1 (RegenerativeBrakingOnAT1RecoveryAir = TRUE)

b) Regeneration to air tank 2 (RegenerativeBrakingOnAT2RecoveryAir = TRUE)

c) Regeneration off (RegenerativeBrakingOff = TRUE)

(vi) Stop mode (7-8)

Based on the condition in the pneumatic hybrid system, the control strategy turns the engine on (EngineOn= TRUE) or off (EngineOff = TRUE) during the vehicle stop period.

It can be learned that the three special functions, Stop-Start, Boost and Regenerative Braking Functions, are activated in the different vehicle modes respectively. Normally, the activation time of the special functions is less than the period of each mode. It means when each special functions finish, the system return to the initial state and enter the quasi state. So the valves such as ATV and CV also return to the initial state waiting for the next step control signals. As a result, there is no overlap between the three special functions and therefore no handover process.

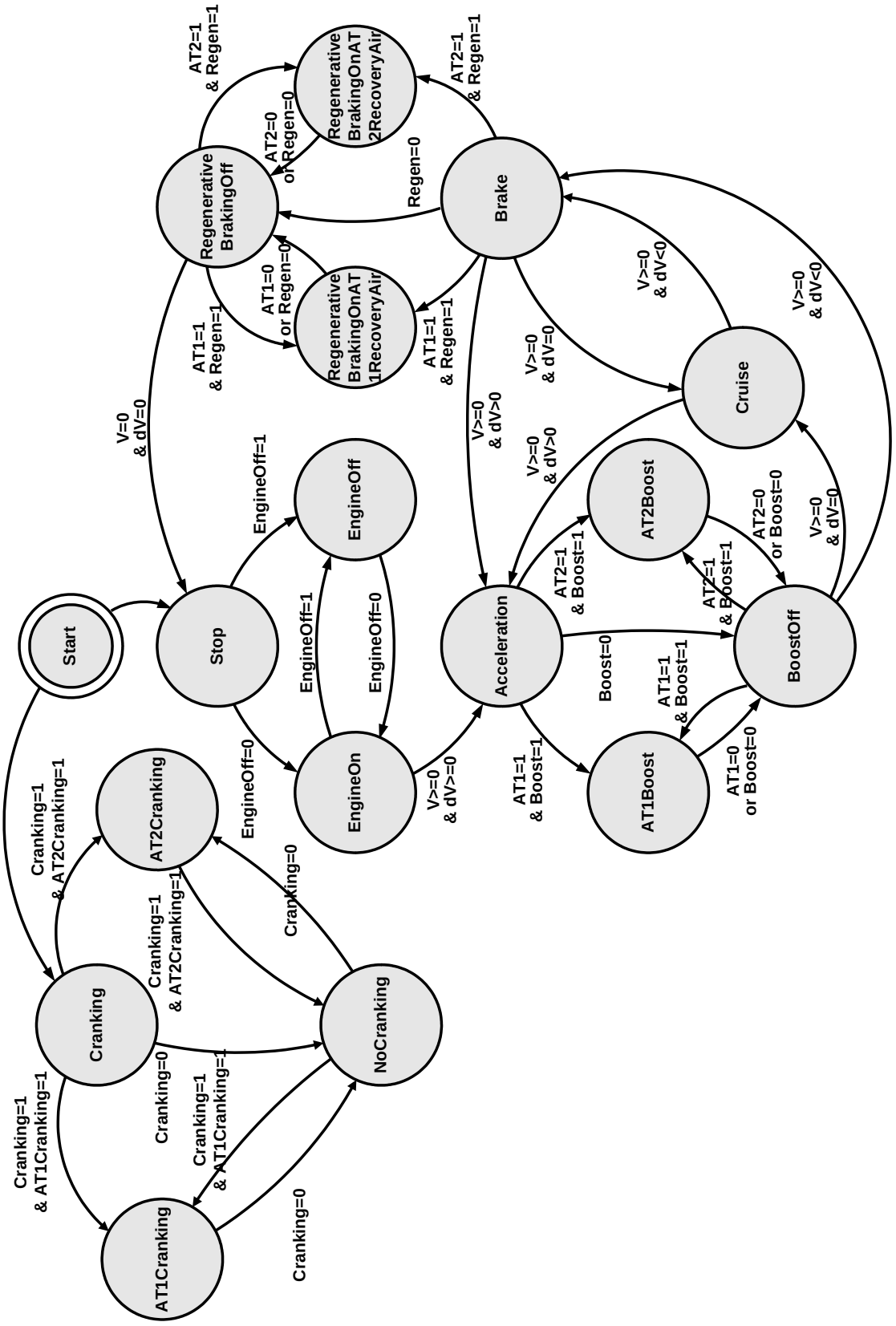

Figure 7-5 State diagram of control strategy for the pneumatic hybrid city bus

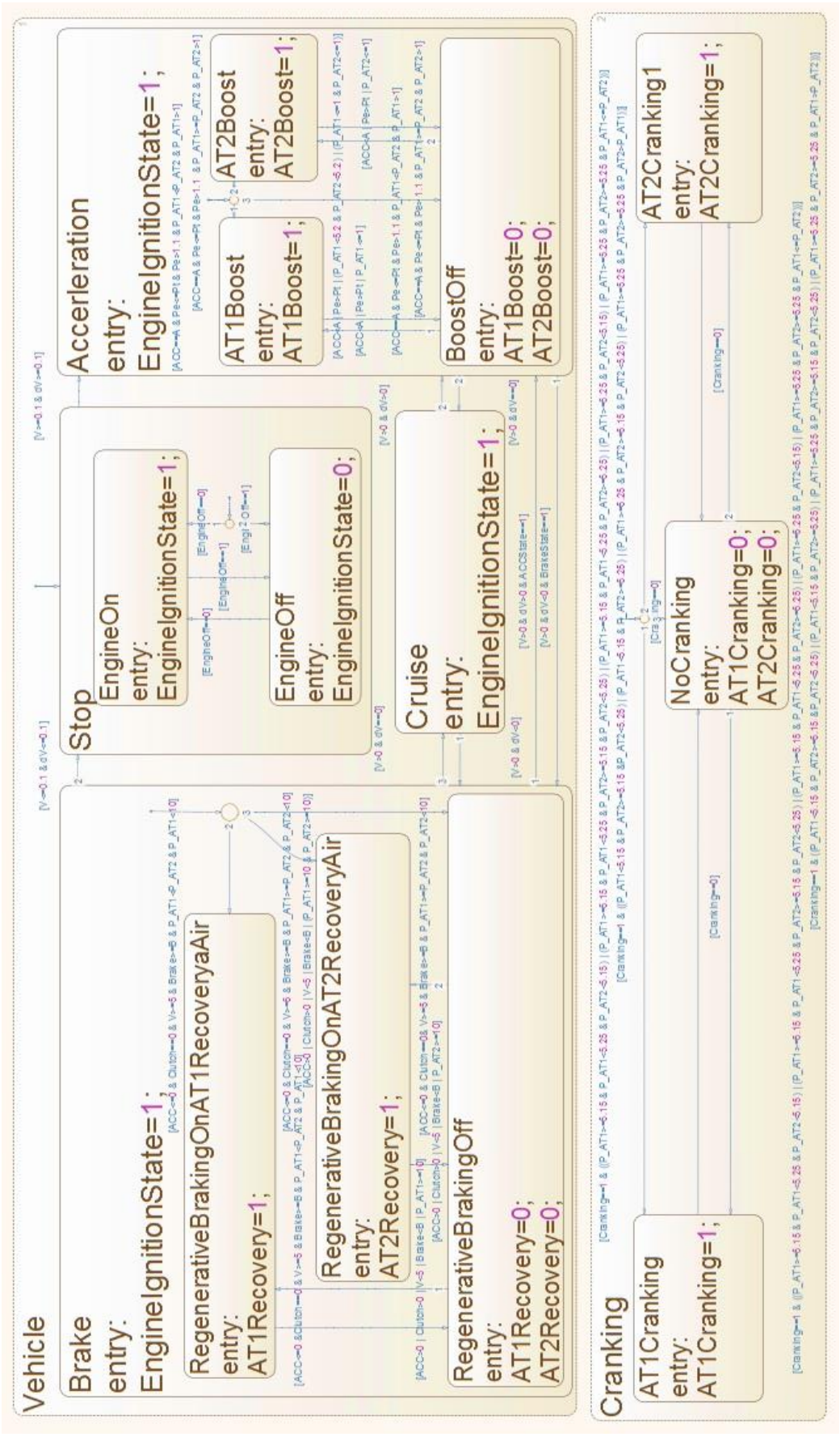

Figure 7-6 Stateflow diagram of control strategy for the pneumatic hybrid city bus

Table 7-2 Conditions and output signals of the control strategy

Mode	State	Conditions								Outputs signals					
		P_{AT1}	P_{AT2}	$P_{AT1} > P_{AT2}$	ω	v	dv	*ACC ped*	*BRA ped*	AT1 CV	AT2 CV	AT1	AT2	IPVs	TVs
Cranking	*AT1 Cranking*	≥ 5.2	< 5.2	Y	= 0	= 0	= 0	= 0	= 0	O	C	C	C	C	O
		≥ 5.2	≥ 5.2	Y	= 0	= 0	= 0	=0	= 0	O	C	C	C	C	O
	AT2 Cranking	< 5.2	≥ 5.2	N	= 0	= 0	= 0	= 0	= 0	C	O	C	C	C	O
		≥ 5.2	≥ 5.2	N	= 0	= 0	= 0	= 0	= 0	C	O	C	C	C	O
	No Cranking	< 5.2	< 5.2	-	= 0	= 0	= 0	= 0	= 0	C	O	C	C	C	O
Fully Acceleration	*AT1Boost*	-	-	Y	≥ 650	> 0	> 0	= 100%	= 0	C	C	O	C	O	C
	AT2Boost	-	-	N	≥ 650	> 0	> 0	= 100%	= 0	C	C	C	O	O	C
Acceleration	*BoostOff*	-	-	-	≥ 650	> 0	> 0	< 100%	= 0	C	C	C	C	C	O
Cruise	*Cruise*	-	-	-	≥ 650	> 0	0	< 100%	= 0	C	C	C	C	C	O
Braking	*RegenerativeBrakingOnAT1RecoveryAir*	≤ 10	≤ 10	N	= 0	> 5	< 0	= 0	> 0	C	C	O	C	O	C
	RegenerativeBrakingOnAT2RecoveryAir	≤ 10	≤ 10	Y	= 0	> 5	< 0	= 0	> 0	C	C	C	O	O	C
	RegenerativeBrakingOff	> 10	> 10	-	= 0	> 5	< 0	= 0	> 0	C	C	C	C	C	O
		-	-	-	= 0	≤ 5	< 0	= 0	> 0	C	C	C	C	C	O
Stop	*EngineOn*	< 5.2	< 5.2	-	≥ 650	= 0	= 0	= 0	= 0	C	C	C	C	C	O
	EngineOff	≥ 5.2	-	-	≥ 650	= 0	= 0	= 0	= 0	C	C	C	C	C	O
		-	≥ 5.2	-	≥ 650	= 0	= 0	= 0	= 0	C	C	C	C	C	O

Where, P_{AT1} – Air tank 1 pressure,
P_{AT2} – Air tank 2 pressure,
ω – Engine speed,
v – Vehicle speed,
dv – Vehicle acceleration,
TVs – Throttle Valves,
IPVs - Intake Port Valves,
CV - Cranking Valve,
ACC ped – Accelerator pedal position,
BRA ped – Brake pedal position,
O – Open,
C - Close.

7.3 Pneumatic Hybrid City Bus Simulation Model

The vehicle simulation model has been built in the GT-POWER and MATLAB/Simulink. Figure 7-7 shows the GT-POWER model, and Figure 7-8 shows the MATLAB/Simulink model. The connections between these two models are the part *PneumaticHybridVehicle_Controller_Simulink*, highlighted in blue in Figure 7-7, and part *GT-SUITE Model1*, highlighted in red in Figure 7-8. The part *PneumaticHybridVehicle_Controller_Simulink* belongs to the 'SimulinkHarness' template in the GT-POWER. Its function is to couple GT-POWER to MATLAB/Simulink and to enable the co-simulation process. This is a common practice in the industry where the engine, powertrain, and vehicle physics are modelled in GT-POWER, and electronic controllers are modelled in Simulink [99]. How to run the GT-POWER and Simulink co-simulation is introduced in Appendix-II in detail.

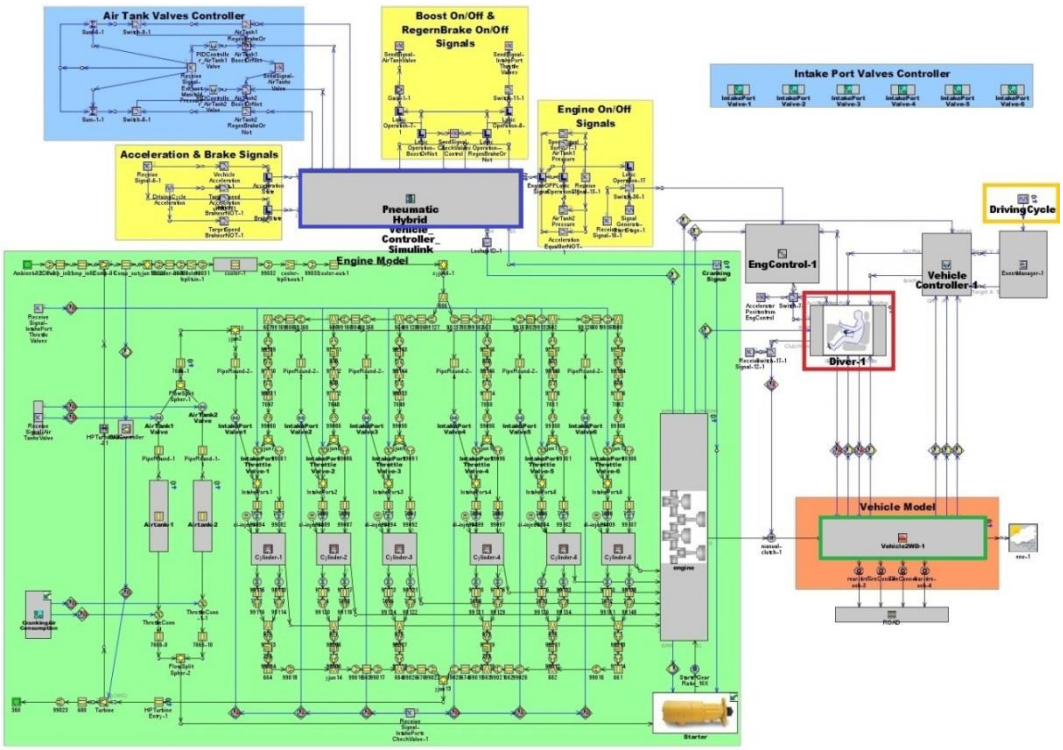

Figure 7-7 The pneumatic hybrid city bus GT-POWER part simulation model

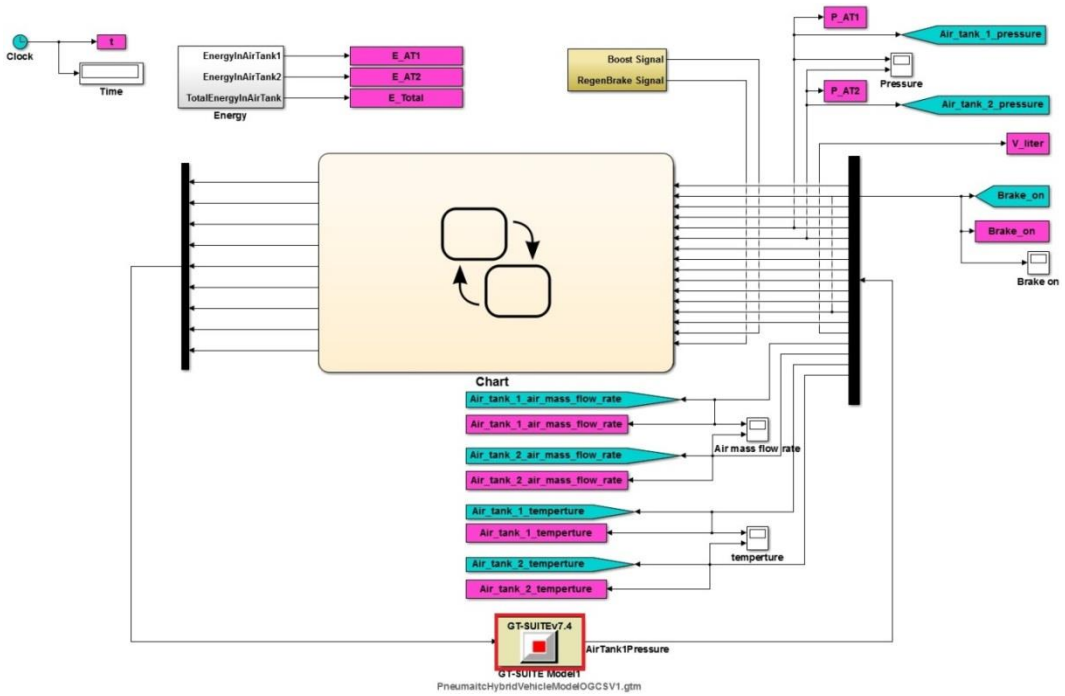

Figure 7-8 The pneumatic hybrid city bus MATLAB/Simulink part simulation model

These two models combined together to form a forward facing simulation model which includes a driver model to simulate the human driver behaviour in regard to acceleration or braking the vehicle to meet the target speed. Compared with the backward facing simulation model, there are several benefits of forward facing simulation model.

(i) The forward facing model gives insight to the drivability of the vehicle which can be learned from Figure 7-9. Therefore, it provides better understanding of the dynamic and physical limits of the powertrain [100].

(ii) The forward facing simulation model can simulate the transient performance of the vehicle especially the internal combustion engine transient response in the powertrain, by contrast, the backward facing simulation model cannot do it because the backward facing model normally determines the performance of the internal combustion engine based on the efficiency models or maps.

The backward facing model is commonly considered as 'quasi-static' models [100]. In addition, the dynamic models can be included naturally in a forward facing model because the forward facing model deals in quantities that are measurable in a real drivetrain and with the correct causality. Such a model can be implemented in an HIL test system [101]. The disadvantage of the forward facing model is it runs with a

relatively smaller time step when compared to the backward facing model, resulting in very much longer simulation time. For example, most time step value for continuous simulation in the GT-POWER is 0.001 s [90].

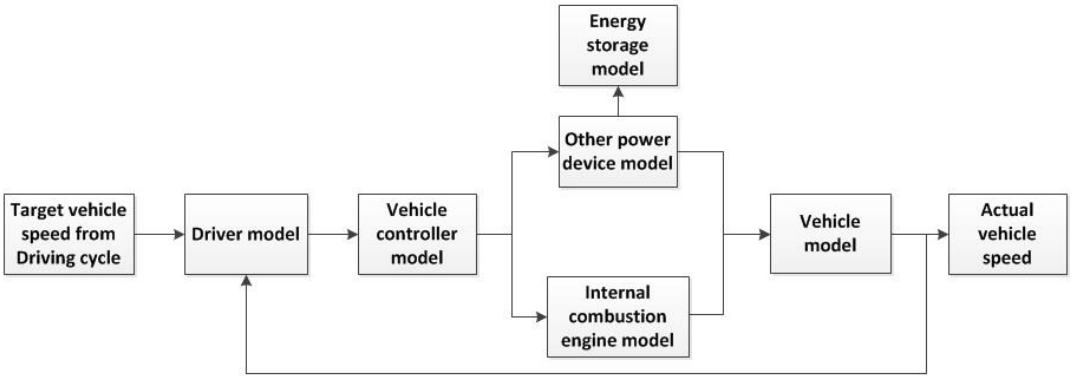

Figure 7-9 Forward facing hybrid vehicle model

In this research, the forward facing model is utilised for the purpose of vehicle control strategy optimisation in order to produce more precise results than would be produced by a backward facing model [102].

7.3.1 Engine and Pneumatic Regenerative System Model

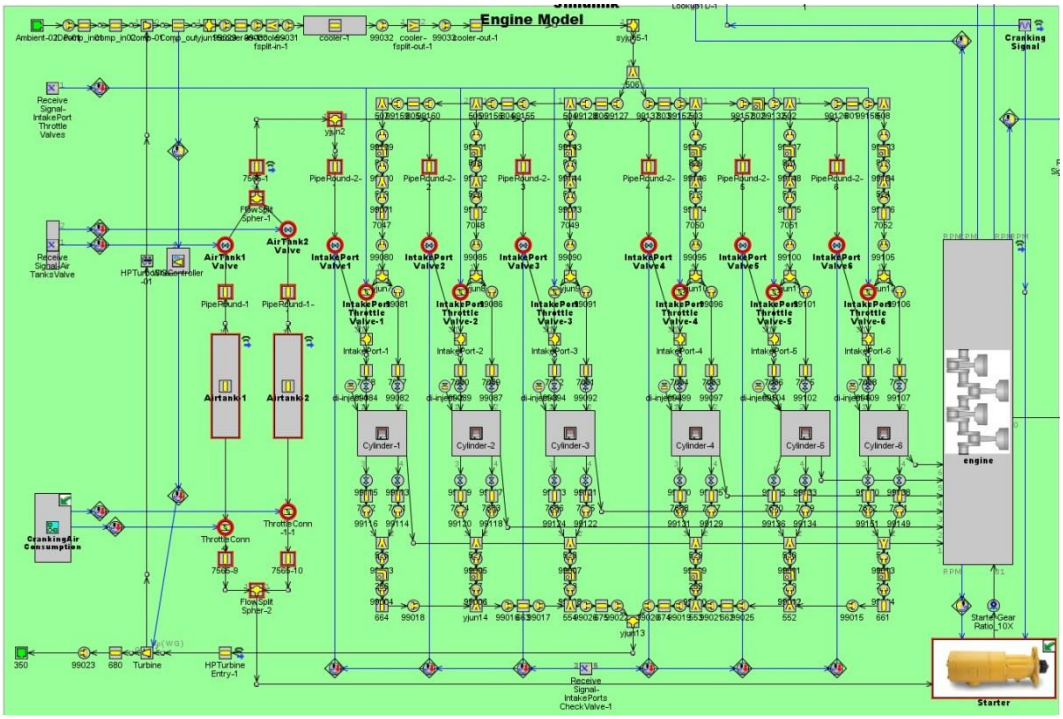

Figure 7-10 Engine and pneumatic regenerative system model in GT-POWER

The engine and pneumatic regenerative system model are shown in Figure 7-10, where the parts of the pneumatic regenerative system are highlighted in red which includes two air tanks, pipes, valves and the simulated air starter. This model using here is developed from the pneumatic hybrid engine concept mentioned in Chapter 1 and two air tanks pneumatic hybrid engine backward facing model in Chapter 4. It is based on the engine with System IP model using in Chapter 6 and with an added air tank. It has the same parameters of the pneumatic regenerative system and the engine main technical parameters are summarized in Table 7-3.

Table 7-3 Main technical parameters of the engine and pneumatic regenerative system

Displacement (l)	7.25
Electronic control system	High pressure & common rail
No. of Cylinders (-)	6
Bore (mm)	108
Stroke (mm)	132
Compression ratio (-)	17.5:1
Intake way	Turbo-charging & inter-cooling
Rated power/speed (kW/rpm)	177/2300
Max. torque/speed (Nm/rpm)	900/1400~1600
Intake valve (-)	2
Diameter (mm)	32.5
Opening point (normal)	61°BTDC
Closing point (normal)	91°ABDC
Exhaust valve (-)	2
Diameter (mm)	29.5
Opening point (normal)	105°BBDC
Closing point (normal)	67°ATDC
Air tank volume (l)	151
No. of Air tank (-)	2

The GT-POWER model also includes a 'DIWiebe' combustion sub model and a 'WoschniGT' heat transfer sub model used also in Chapter 6. These two sub models are introduced in Appendix-III in detailed.

7.3.2 Vehicle Model

In this research, the main objective is to study the relationship between the vehicle performance, the engine fuel consumption and the pneumatic hybrid powertrain energy recovery efficiency. The schematic representation of the forces acting on the city bus is presented in Figure 7-11.

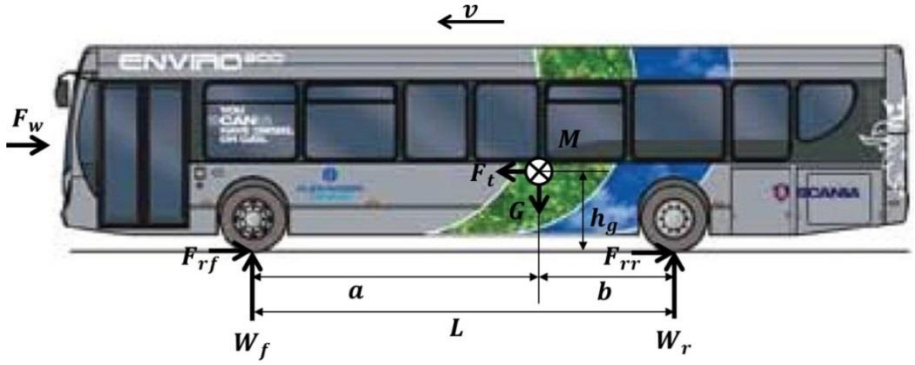

Figure 7-11 Forces acting on the city bus

The elementary equation that describes the longitudinal dynamics of a road vehicle has the follow equation.

$$M\frac{d}{d_t}v = F_t - (F_w + F_r + F_g) \tag{7-8}$$

where F_w – aerodynamic friction,

F_r – rolling friction,

F_g – force caused by gravity when driving on non-horizontal roads,

F_t – traction force,

M – vehicle mass,

v – vehicle speed.

The aerodynamic friction F_w can be expressed through Equation (7-9).

$$F_w = \frac{1}{2}\rho_a A_f c_d v^2 \tag{7-9}$$

where v – vehicle speed,

ρ_a – density of the ambient air,

c_d – aerodynamic drag coefficient,

A_f – frontal area of the vehicle.

The rolling friction F_r is modelled as

$$F_r = F_{rf} + F_{rr} = c_r M g \cos\alpha \tag{7-10}$$

where M – vehicle mass,

g – acceleration due to gravity and

c_r – coefficient of the rolling resistance.

F_{rf} – rolling friction on the front axle,

F_{rr} – rolling friction on the rear axle.

The term *cosa* models the influence of a non-horizontal road. For this research, only the horizontal road is considered, as a result, a is 0.

The uphill driving force F_g is modelled by the relationship

$$F_g = M g \sin\alpha \tag{7-11}$$

The normal load on the front axle W_f can be determined as

$$W_f = \frac{b}{L} M g \cos\alpha - h_g (F_t - F_r (1 - \frac{r_d}{h_g})) \tag{7-12}$$ [6]

Similarly, the normal load acting on the rear axle W_r can be expressed as

$$W_r = \frac{a}{L} M g \cos\alpha + h_g (F_t - F_r (1 - \frac{r_d}{h_g})) \tag{7-13}$$ [6]

where r_d – effective radius of the wheel,

h_g – gravity centre height of the vehicle,

a – distance from gravity centre to front wheel centre,

b – distance from the gravity centre to front wheel centre,

L – wheelbase.

From the Equation (7-14), the traction force F_t for a rear-wheel-drive vehicle can be expressed as

$$F_t = \frac{\mu M g \cos\alpha [L - C_r(h_g - r_d)]/L}{1 - \mu h_g / L} \tag{7-14}$$

where μ – the friction coefficient.

The kinetic energy of the vehicle can be calculated by the following equation

$$E = \frac{1}{2} M \Delta v^2 \tag{7-15}$$

where, Δv – the speed decrement from regenerative braking start to end during the braking.

Equation (7-15) indicates that the maximum kinetic energy can be recovered during the braking. But in the real practice, because of the friction loss, only a percentage of the initial kinetic energy of the car can be recovered.

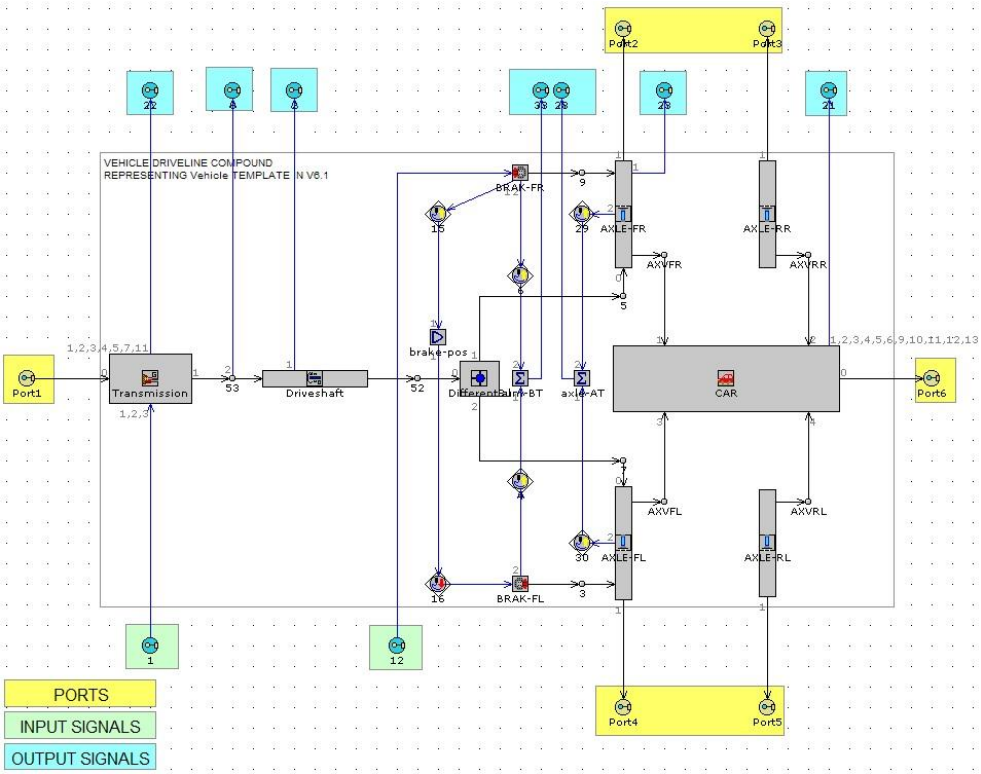

Figure 7-12 Vehicle subsystem model in GT-POWER

The vehicle model is composed of the *Vehicle2WD-1* part and the tyre model which are in the orange background shown in the Figure 7-7. The vehicle model *Vehicle2WD-1* is highlighted in green in the Figure 7-7 which is a Vehicle2WD template in the GT-POWER. It is a compound part which encapsulates a 2-wheel drive vehicle and its drivetrain

together which may be connected to an appropriate engine model through a clutch or torque converter. Its subsystem configuration is shown in the Figure 7-12.

The subsystem includes the transmission model, vehicle model, driveshaft model, and brake model. Their functions are summarized in Table 7-4.

Table 7-4 Summary the function of the parts in the vehicle subsystem

Part name	Function
Transmission	Set the gear number, gear ratio, gear transition time, friction mechanical efficiency and inertia.
Driveshaft	Set the shaft moment of inertia and friction mechanical efficiency.
CAR	Set vehicle mass, fuel density, vehicle drag coefficient, vehicle lift coefficient, vehicle frontal area, centre of pressure, vehicle wheelbase and mass centre position.
Brake	Define the braking torque model map beads on the brake actuator position.

The *Vehicle2WD-1* transmits a vehicle load (including vehicle's inertia load) back to the engine model as a torque. The speed of the engine and the vehicle drivetrain (which are geared together by the transmission) is then calculated by the engine model. This speed is calculated taking the engine's brake torque and subtracting from it the load torque applied by the vehicle (as well as any auxiliary torque applied to the engine model), and then using any remaining "positive" torque to accelerate the powertrain. As a result, the simulation includes the transient response of the engine facilitating the investigation of the control of both the engine and its subsystems.

7.3.3 Driver Model

The driver model, *Driver-1* is highlighted in red in Figure 7-7. Its function is used to represent the driver who controls accelerator position, brake pedal position, transmission gear number, clutch pedal position. It is primarily used for controlling vehicles with manual transmissions as it contains the necessary functions for vehicle launch (*driveaway* event) and gear shifting. The input and output of the driver model are shown in the Figure 7-13.

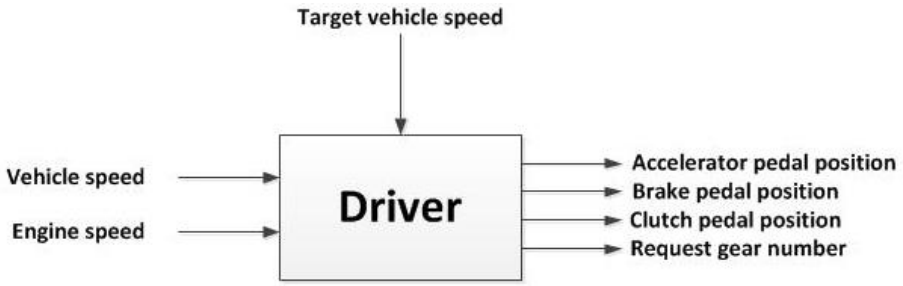

Figure 7-13 Input and output of the driver model

7.3.4 Driving Cycles Model

The Driving Cycles model is highlighted in yellow in Figure 7-7. It is a signal generator template in the GT-POWER. The generated signal may be generated via several options, including constant, equation, or imposed time series. This template can also be used to generate a signal of the current time, angle, or cycle at each time step.

7.3.5 Air Tanks Energy Recovery Model

In order to evaluate the energy recovery efficiency, a twin air tank energy recovery sub model has been implemented in MATLAB/Simulink, *Energy* and is shown in Figure 7-8. Its diagram is shown in Figure 7-14.

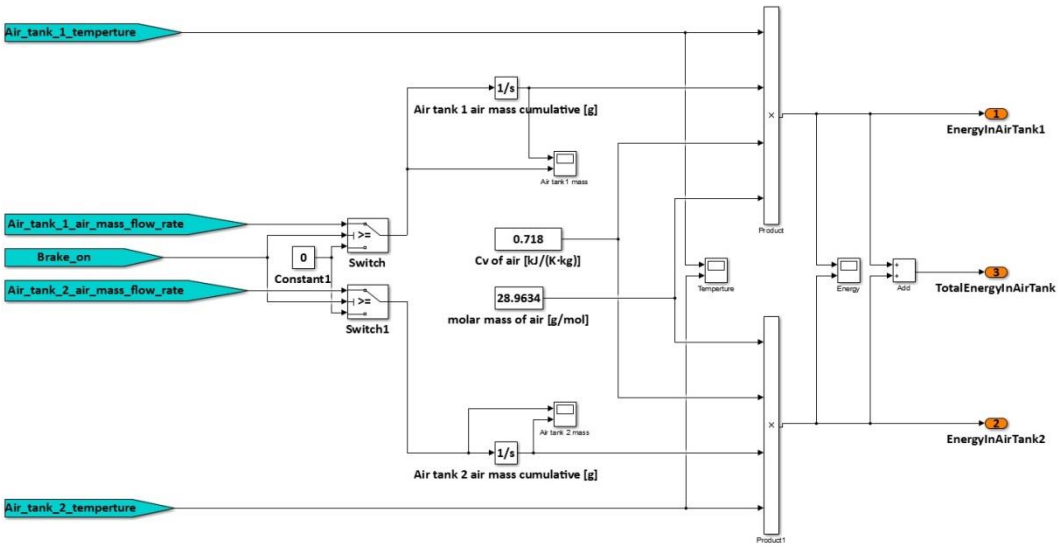

Figure 7-14 Air tanks energy recovery model in MATLAB/Simulink

The air tank has been modelled as a control volume, which exchanges air mass only with the pipes connecting the air tank. The air tanks have a fixed volume V_{AT}. It is assumed

that the air tank is well insulated so that there is no heat transfer between the air tanks and the environment. The mean-value model of the air tank state is calculated using the following Equations, (7-16 and 7-17)

$$pv_{AT} = mRT \tag{7-16}$$

where p – air tank pressure,

m – air mass in the air tank,

R – gas constant,

T – air tank pressure.

$$\Delta E = \Delta m c_v T_0 \tag{7-17}$$

where ΔE – energy increment in the air tank,

Δm – air mass increment in the air tank,

c_v – volumetric heat capacity of the air,

T_0 – start temperature in the air tank.

The Equation (7-17) is based on the first law of the thermodynamics. It cannot point out the maximum amount of energy that can be extracted from an energy system. The useful work potential of an energy system at the specified state is called "availability" (also called "exergy") [103]. It is based on the second law of thermodynamics and is the basis for evaluating the capacity of work production in an open, steady flow system or a closed system. Availability is a measure of the maximum work produced by an energy system and it depends on the states of the energy system. The availability of air stored in the air tank is described by the following Equation (7-18). During the acceleration, the boost function is activated, the air flows out the air tank to be injected into the cylinders. Compare with calculating the energy decrement of the air tank, the calculation of availability can present the amount of useful work has been transferred to realize the boost function. The calculation of availability is introduced in Appendix-IV in detail.

$$\Delta A = mRT_0(\ln\frac{p_0}{p_1} + \frac{p_1}{p_0} - 1) \tag{7-18}$$

where ΔA – total availability change in the air tank,

m – air mass increment in the air tank,

p_1 – initial pressure of the air tank,

p_0 – environment pressure,

T_0 – start temperature in the air tank.

7.3.6 Simulation Result

To evaluate the control strategy presented in Section 7.2, the control strategy is implemented in the forward facing model to calculate the fuel consumption of the pneumatic hybrid city bus for a typical driving cycle, and also verify whether the three functions of the pneumatic hybrid system can be realized. Because this is a forward facing model, the detailed engine model takes quite some time to run. The time taken to simulate a complete driving cycle (such as the Braunschweig or MLTB driving cycles) compounded by the time taken to simulate the stop-start process led to the conclusion that the optimisation process should be focussed on a single manoeuvre that exercised all of the control functions. The start-stop process simulation ratio (simulation time/real time) exceeds a value of 60. It means for 1 s simulation time in the GT-POWER, it needs nearly 60 s real time for the desktop to run. One typical stop-start event (Braunschweig-H) in the Braunschweig driving cycle has been chosen here to be the test cycle and is illustrated in Figure 7-15.

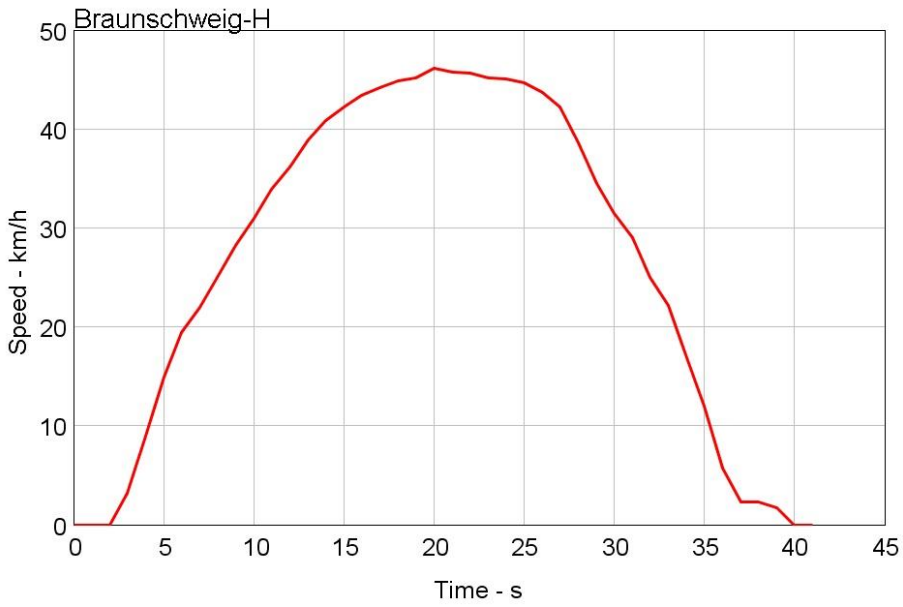

Figure 7-15 Braunschweig-H time–speed diagram

The Braunschweig drive cycle was developed by the Technical University of Braunschweig for an urban bus in Braunschweig city in Germany. It is an urban bus cycle measured in

the Lower Saxony German town of Braunschweig (Brunswick). Figure 7-16 shows the Braunschweig driving cycle time-speed diagram over a period of 1740 s. The total distance is 10.87 km. The Braunschweig driving cycle has 29 separate acceleration-deceleration events and 30 stops. Some acceleration-deceleration events repeated two or three times, so the Braunschweig driving cycle can be classified as 16 stop-start events as shown in Table 7-5. Here, acceleration-deceleration-1 represents the first event, and the acceleration-deceleration-29 represents the final event in the cycle.

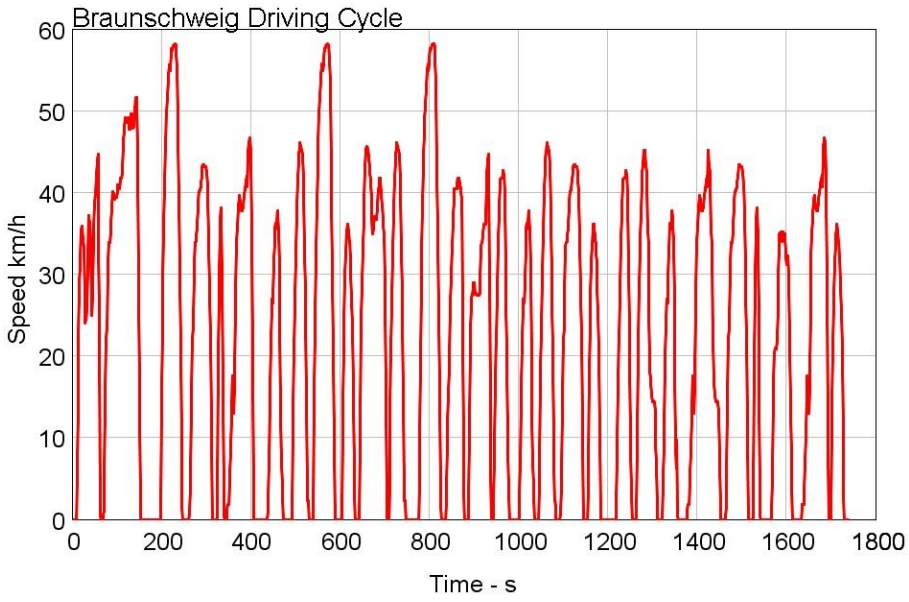

Figure 7-16 Braunschweig driving cycle time–speed diagram

Comparing the characteristics of the 16 stop-start events reveals that some acceleration behaviours are very similar. Therefore, five types of acceleration behaviour have been classified as shown in the Figure 7-17. In a similar way, 8 types of braking have been classified as shown in Figure 7-18.

From the Figure 7-17 and Figure 7-18, it can be seen ACC-I and Brake-I are the typical acceleration and brake behaviours. They lie in the middle range of each type of behaviour being neither too aggressive nor gentle. As a result, they have been chosen to represent the Braunschweig driving cycle in the investigation. From the prior analysis, it can be seen that stop-start event Braunschweig-H has both the ACC-I and Brake-I features, so that Braunschweig-H has been chosen. From the Table 7-5, it can be seen that Braunschweig-H is repeated three times in the Braunschweig driving cycle and is the model feature.

Table 7-5 Stop-start events and acceleration-deceleration events

Stop-start Event	Acceleration-deceleration event
Braunschweig-A	1
Braunschweig-B	2
Braunschweig-C	3, 9, 13
Braunschweig-D	4, 19, 25
Braunschweig-E	5, 26
Braunschweig-F	6, 28
Braunschweig-G	7, 17, 23
Braunschweig-H	**8, 12, 18**
Braunschweig-I	10, 20, 29
Braunschweig-J	11
Braunschweig-K	14
Braunschweig-L	15
Braunschweig-M	16, 21
Braunschweig-N	22
Braunschweig-O	24
Braunschweig-P	27

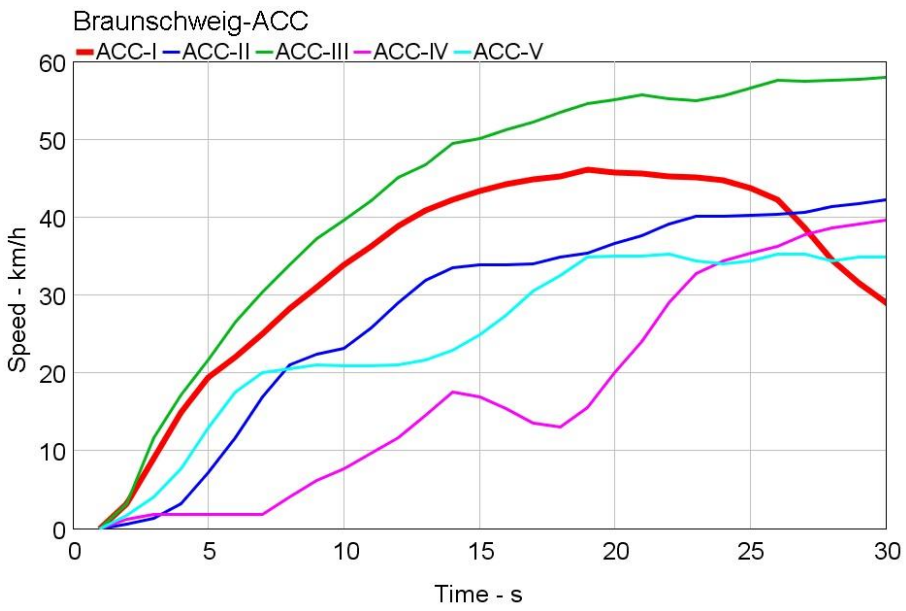

Figure 7-17 Acceleration behaviours of the Braunschweig driving cycle

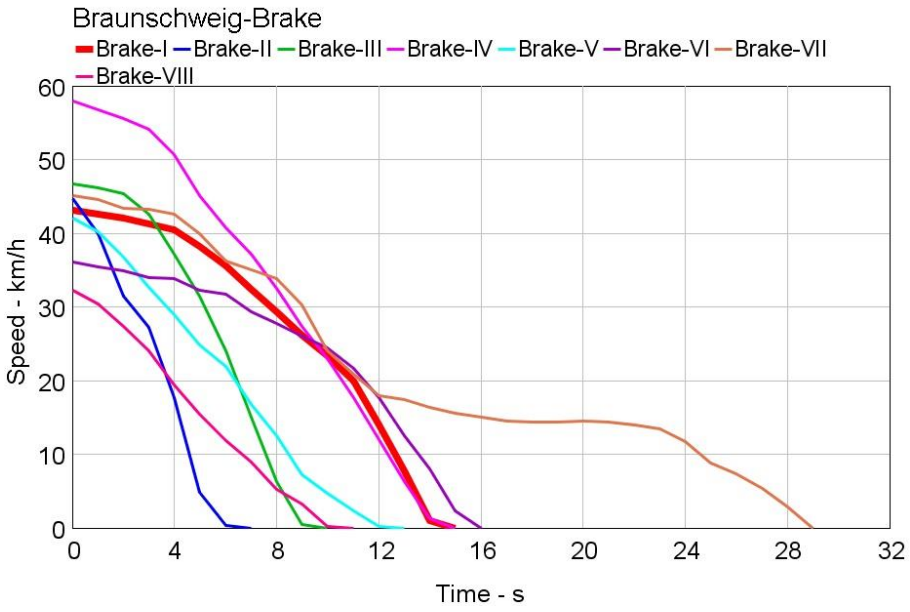

Figure 7-18 Brake behaviours of the Braunschweig driving cycle

Table 7-6 shows the basic parameters of the Braunschweig drive cycle and Braunschweig-H.

Table 7-6 Basic parameters of the Braunschweig driving cycle and Braunschweig-H

	Braunschweig driving cycle	**Braunschweig-H**
Time (s)	1740	41
Distance (km)	10.87	0.31
Acceleration (%)	39.7	46.3
Deceleration (%)	30.8	48.8
Idle (%)	29.5	4.9
Average positive acceleration (m/s^2)	0.424	0.674
Average negative acceleration (m/s^2)	-0.595	-0.61

Figure 7-19 shows the simulation result with the city bus running the Braunschweig-H stop-start event under the logic threshold based energy control strategy compared with the normal city bus. To simulate the start-start operation, the simulation takes 45 s to simulate a full Braunschweig-H cycle and the first 4 s of a repeated Braunschweig-H stop-start event.

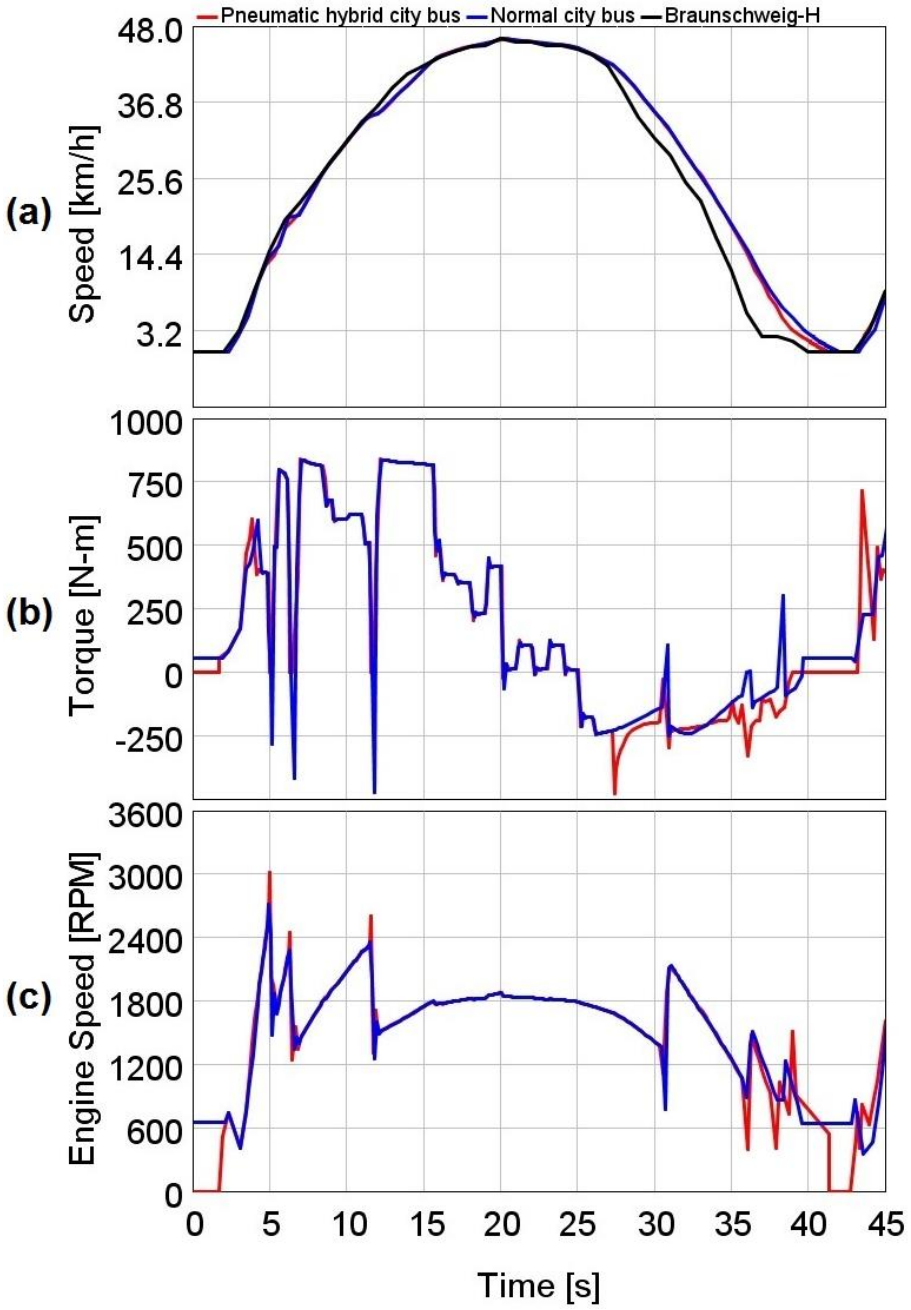

Figure 7-19 Simulation results of the control strategy of the pneumatic hybrid city bus comparing with the normal city bus

From Figure 7-19, it can be seen that the three functions of the pneumatic hybrid system have all been realized. In the Speed diagram (a), both the pneumatic hybrid city bus and the normal city bus can be seen to follow the target driving cycle speed especially in the acceleration event. The Root Mean Square Error (RMSE) of the normal city bus and pneumatic hybrid city bus to the target driving cycle speed are summarized in Table 7-7.

Table 7-7 RMSE of normal city bus and pneumatic hybrid city bus to the target driving cycle speed

	RMSE – Acceleration (3 to 20 s)	RMSE – Deceleration (21 to 42 s)	RMSE – Total (0 to 45 s)
Normal city bus	0.512	2.889	2.941
Pneumatic hybrid city bus	0.338	2.618	2.642

From the Torque diagram (b) and Engine Speed (c) diagram, it can be seen that in the two stop periods, the engine is stopped in order to eliminate the idle fuel consumption. In these two periods, the engine consumes no fuel while in the conventional implementation, the engine load and speed are respectively 56 Nm and 650 rpm, the normal idle condition, which represents a significant fuel consumption. It means the Boost Function has been achieved.

For the Boost Function, it can be seen from the Torque diagram (b) that in the first few seconds of the first start, the hybrid bus develops torque output more quickly compared with the normal city bus.

The Regenerative Braking Function also can be verified from the Torque diagram (c). During the braking period, the engine in the hybrid bus shows a larger brake torque than the normal city bus. This demonstrates that during the braking process the additional work done on the bus comes from the additional braking function of the engine and notably the pumping of air into the respective air tanks.

The Boost Function can be seen in detail in Figure 7-20 and Figure 7-21 respectively. In the first 10 s, the control strategy implements the Boost Function twice. The first happens just after the clutch finishes the engaging operation between 3 to 4 s. The Boost Function increases the air supply to the cylinder to reduce the turbo-lag and improve the engine transient response. The hybrid city bus demonstrates a faster increase in engine brake torque output with a lower fuel consumption. The reason for this is during the boost period, the increased air supply improves the quality of combustion. The engine operation point has been moved to the high efficiency area faster. For the normal engine, more time is needed because the turbocharger cannot build the required pressure in the

intake manifold sufficiently quickly. This also proves that the pneumatic hybrid technology not only can improve fuel consumption by realizing the Stop-Start Function, but also by implementing the Boost Function to improve the engine transient performance and efficiency.

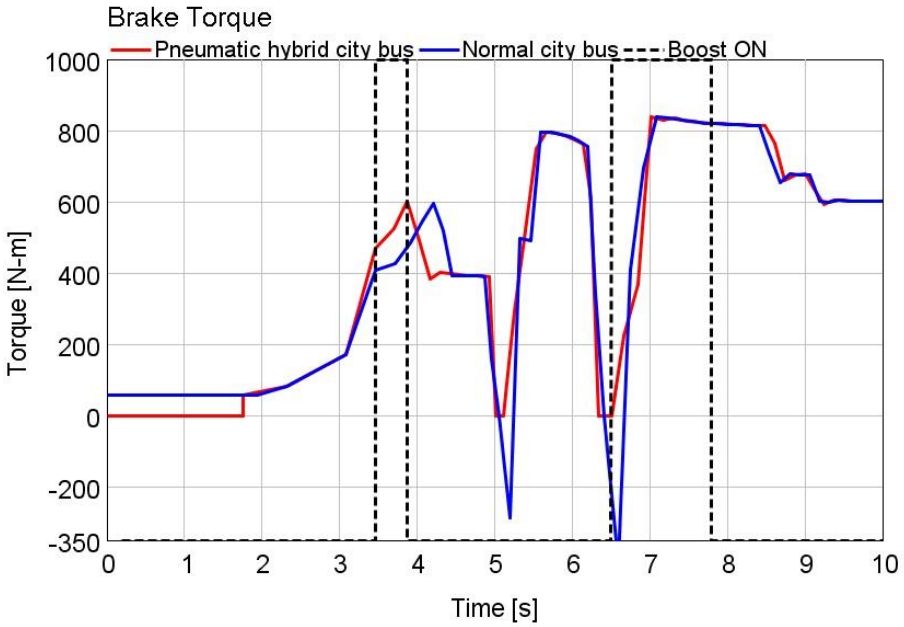

Figure 7-20 Brake torque for the first 10 s

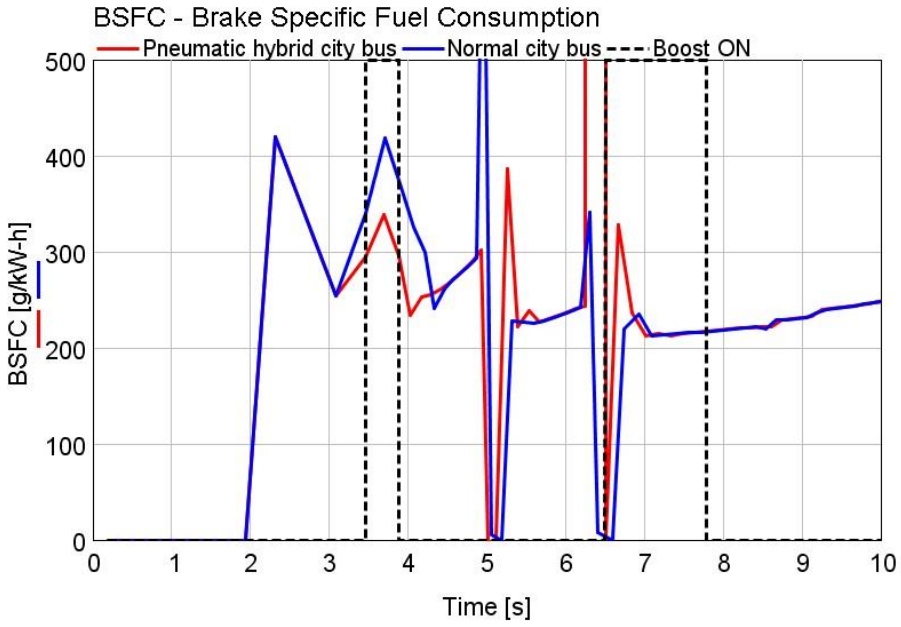

Figure 7-21 Brake specific fuel consumption for the first 10 s

Figure 7-22 shows the average fuel consumption difference between the pneumatic hybrid city bus and the normal city bus during the Braunschweig-H from 0 to 41 s. Due to the Boost Function, the pneumatic hybrid city bus has lower average fuel consumption which is 47.674 l/100km compared with 48.15 l/100km of the normal city bus. The fuel consumption can be further improved 0.8% by implementing the Boost Function as far of the already proved ability to reduce fuel consumption by at least 6% by realizing the stop-start operation (see Chapter 4). Although this improvement of the fuel consumption is small, it has no practical doubt because it is really a critical change. Firstly, from the Figure 7-20 and Figure 7-21 with the previous analysis, it can be learned that from the theoretical analysis and simulation result, the Boost Function improves the quality of combustion. As a result, it should reduce the transient fuel consumption. Second, although this 0.8% result is from the simulation result, it still can be trusted, because the 1-D solver of the simulation code, GT-POWER, is considered accurate and convictive [90]. The result can reflect the difference between the normal vehicles and the pneumatic hybrid vehicles. Finally, this 0.8% improvement in fuel consumption is only in a 42 s driving cycle. And furthermore, the Boost Function is only activated for very short periods during the acceleration. Therefore, if using it in the whole Braunschweig driving cycle, the Boost Function of the pneumatic hybrid city bus can save more fuel.

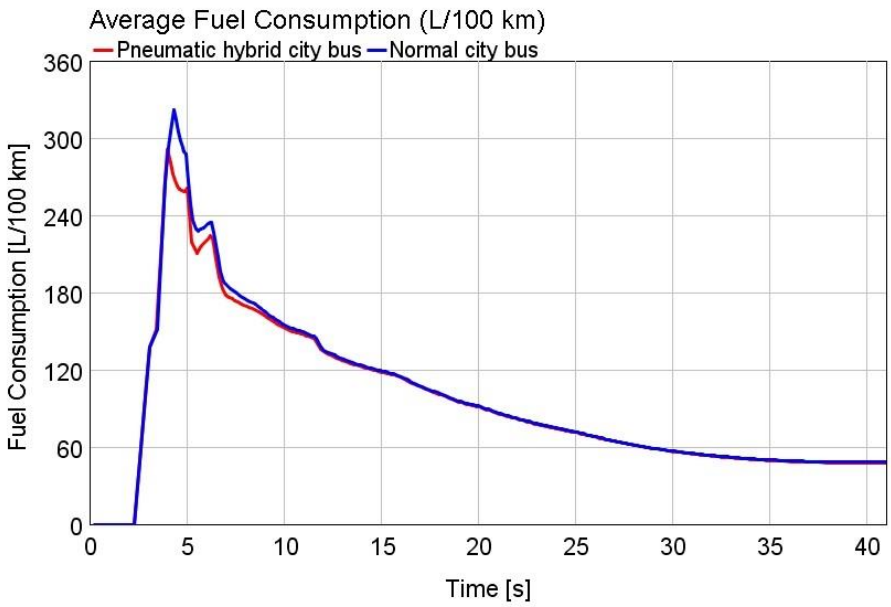

Figure 7-22 Average fuel consumption during the Braunschweig-H

Figure 7-23 and Figure 7-24 show how the Regenerative Braking Function has been achieved by the control strategy. From Figure 7-23, it can be seen that the pneumatic hybrid city bus shows the less energy dissipation during the braking because the kinetic energy of the vehicle has been transferred to the pneumatic energy stored in the air tank. This can be seen in Figure 7-24. During braking, the control strategy controls the air tank 2 to recover the energy. The pressure of air tank 2 increases from 2.92 bar to 5.25 bar.

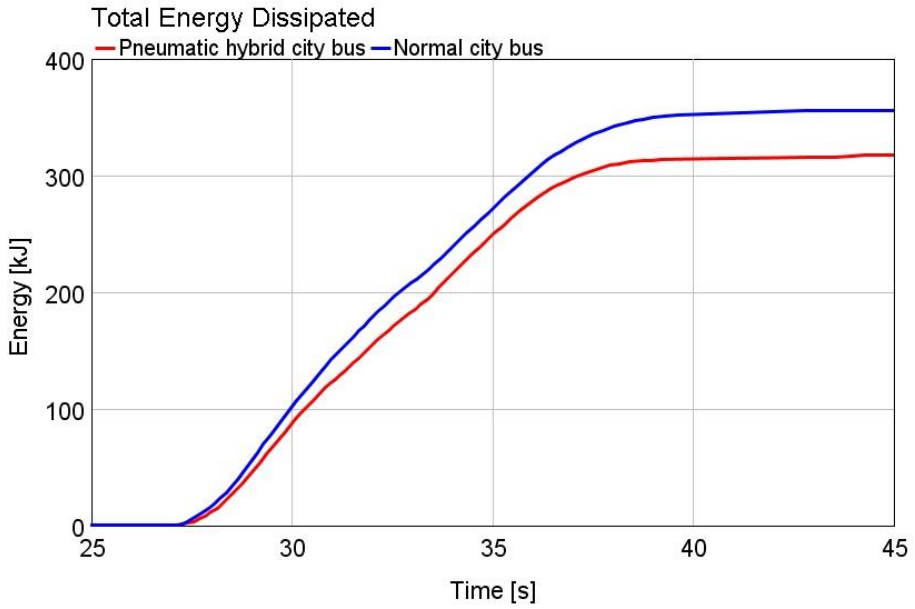

Figure 7-23 Total energy dissipated during the braking

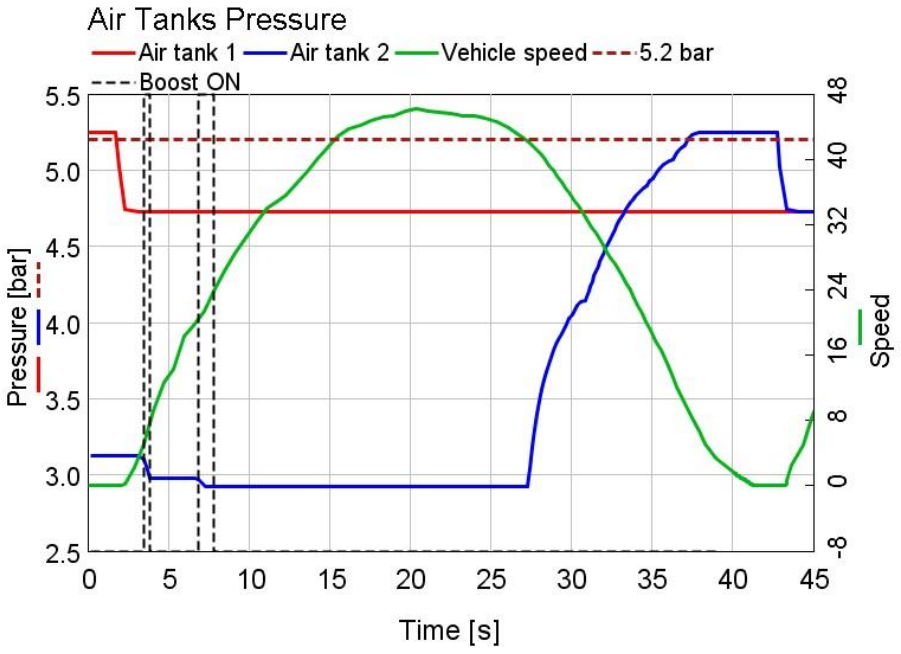

Figure 7-24 Air tanks pressure during the Braunschweig-H

From Figure 7-24, it can be seen that when the vehicle starts, air tank 1 has been chosen to supply the air starter, which results in a pressure drop of 0.48 bar. Later, when boost is required, the control strategy selects the Boost Function, Between 3 s and 10 s, the engine has been boosted twice which consumes 0.15 bar and 0.05 bar respectively. For the second engine start operation, because the air tank 2 has the higher air tank pressure, the control strategy chooses tank 2 to crank the engine. This demonstrates that the control strategy can choose the right air tank to supply the air starter or to realize the Boost Function. This figure is also a demonstration that for a stop-start event, the pneumatic hybrid system can realize the required functions and recover sufficient energy to maintain the air tank pressure.

7.4 Optimisation of the Pneumatic Hybrid City Bus Control Strategy

In general, the optimisation can be defined as minimizing or maximizing an objective function subject to some constraints on the design variables [104]. Overall fuel economy, the amount of air and energy recovery during the braking, and the availability usage during the acceleration are the objectives respectively in this optimisation. The initial air tank pressure for every stop-start event, the gear shift-up points during the acceleration and the gear shift-down points during the deceleration form the control variables for the optimisation process.

The hybrid powertrain system may have a large number of local optimums which mean that the gradient-based optimisation algorithm may not converge to a global solution [82]. Compared with other approaches to optimisation, global optimisation can be used to solve optimisation problems where the objective or constraint functions are continuous, discontinuous, stochastic, may not possess derivatives, or include simulations or black-box functions with undefined values for some parameter settings [83]. As a result, three global optimisation algorithms, Pattern Search, Genetic Algorithm and Multi-objective Non-dominated Sorting Genetic Algorithm II, are compared and employed for the design optimisation of the control strategy of the hybrid city bus in three aspects.

(i) Using the PS to optimise the initial air tank pressure for every stop-start event to maximize the pressure increment of the air tanks.

(ii) Conducting the GA optimisation to find out the best gear changing strategy during the braking to maximize the energy recovery in the air tanks.

(iii) Implementing multi-objective optimisation to simultaneously minimize a) the fuel consumption and b) the availability usage of the air tanks during the acceleration by using the NSGA-II.

The characteristics of the problems and the reasons for each choice are given out in.

Table 7-8 Summary table of the optimisation problems and methods

	Goal	Characteristics of the problem	Optimisation method	Reason
Optimisation I	Maximize the pressure increment of the air tanks	A non-derivative based optimization problem.	PS	To find the global minimum solution, derivative free algorithms, Pattern Search, can be used which don't depend on gradients to find the global minimum solution.
Optimisation II	Maximize the energy recovery in the air tanks	A finite horizon dynamical optimization problem with constraints.	GA	Genetic Algorithms have been proved to be a suitable and an effective strategy to solve complex engineering optimization problems characterized by non-linear, multimodal, non-convex objective functions such as the design optimization of HEV, which is derivative-free method and also good at searching the global optimization.
Optimisation III	Simultaneously minimize a) the fuel consumption and b) the availability usage of the air tanks	An optimisation problem that two objectives are conflicting.	NSGA-II	This optimization problem deals with two conflicting objectives, t therefore, there is no global optimization solution for all of these objective functions. Instead, a family of optimal solutions in the form of a Pareto front can be obtained.

The three optimisations are all simulation-based optimisation in which the optimisation algorithm works together with the computer simulation model in order to identify an optimal solution. There are various simulation codes like GT-POWER, AVL Cruise, AUTONOMIE, etc. for the analysis of hybrid vehicle designs [29, 105, 106]. For this work, GT-POWER with MATLAB/Simulink is selected as the basic simulation tool to study the three optimisation processes.

Another important question about the simulation, that of time duration needs to be explained here. When conducting the GT-POWER and MATLAB/Simulink co-simulation, 1 s simulation time takes 1 min real time on a current technology desktop PC because the detailed engine model is particularly onerous. For the selected driving cycle, Braunschweig-H, running one single simulation takes almost 50 min real time. As a result, the high number of simulations per generation that are required to be calculated, may require a long elapsed time. Distributed computing is one way to solve this problem but cannot be realized because GT-POWER cannot partition this type of simulation into multiple nodes. Therefore, for all three types of optimisation, the optimisation has been configured with particular care so as to limit the total simulation time while allowing the optimisation target to be reached.

7.4.1 Optimize the Initial Air Tank Pressure for Every Stop-Start Event by Using the Pattern Search Optimisation Method

Because the initial air tank pressure for every stop-start event strongly influences the amount of energy recovery during the stop-start event, parameters in the control strategy of the pneumatic hybrid city bus form a clear target for optimisation. The PS algorithm is chosen here to identify optimal initial air tank pressure for every stop-start event in order to maximize the pressure increment of the air tanks.

7.4.1.1 Pattern Search

For the optimisation problems for which the objective function is not differentiable or is not even continuous, the direct search may be used [83]. Direct search can solve the optimisation problems without any information about the gradient of the objective function. Unlike more traditional optimisation methods that use information about the gradient or higher derivatives to search for an optimal point, a direct search algorithm searches a set of points around the current point, looking for one where the value of the objective function is lower [83].

The direct search algorithm chosen here is called the Generalized Pattern Search algorithm. The GPS algorithm computes a sequence of points to approach an optimal point. At each step, the algorithm searches a set of points, called a mesh, around the current point which is computed in the previous step of the algorithm. The mesh is

formed by adding the current point to a scalar multiple of a set of vectors referred to as a pattern. If the pattern search algorithm finds a point in the mesh that improves the objective function at the current point, the new point becomes the current point at the next step of the algorithm [83]. The algorithm will stop when the stopping criteria are met. The definition of PS steps such as polling, expanding and contracting and the particular method used to implement the PS optimisation are introduced in Appendix-V.

7.4.1.2 Problem Statement

The objective of this optimisation is to identify the initial air tanks pressure to increase the total air tank pressure increment for a single start-stop manoeuvre, Braunschweig-H. The cost function is defined as Equation (7-19):

$$J = maxf(X) = min\left[-\left(J_{pressure}(X)\right)\right] = min[-(\int \dot{m}_p dt)] \quad (7\text{-}19)$$

where, $J_{pressure}$ is the instantaneous pressure increment of two air tanks per unit time, X is the variable vector which includes the parameters of the control strategy and is shown in Table 7-9.

Table 7-9 Design variables for PS optimisation

Design variable	Description	Lower bound (bar)	Upper bound (bar)
p_1	The initial pressure of air tank 1	5.2	10
p_2	The initial pressure of air tank 2	2.5	10

In MATLAB, the Global Optimisation Toolbox optimisation functions minimize the objective or fitness function [83]. As the optimisation is to find out the maximum air tank pressure increment, it means the optimisation should minimize *–f(x)* as shown in Equation (7-19). This is because the point at which the minimum of *–f(x)* occurs is the same as the point at which the maximum of *f(x)* occurs [83].

The bounds of the two variables need to be explained here. In order to drive the air motor to crank the engine, the lowest air tank need to above 5.2 bar. As a result, one air

tank's lower bound set to be 5.2 bar. The air tank is designed to have a maximum operation pressure of 10 bar, as a result, the maximum air tank pressure should not be above 10 bar [35]. Therefore, the upper bound for both air tanks is 10 bar. As mentioned in Chapter 6, the air tank pressure needs to be above 2.5 bar to retain sufficient air to realize the Boost Function. So the lower bound on the pressure of the other air tank pressure is 2.5 bar. Start point, the initial point at which the algorithm starts the optimisation, is an important parameter for the optimisation. In Global Optimisation Toolbox, most solvers require to provide a starting point for the optimisation is because that they require a start point to obtain the dimension of the decision variables [83]. The start point of this optimisation is 7.5 and 6 which are both the median of their interval. This means the two air tank initial pressure are set at the 7.5 bar for air tank 1, and 6 bar for air tank 2.

The PS optimisation parameter and options are summarized in Table 7-10.

Table 7-10 Summary table for PS optimisation

Solver	patternserach – Pattern Search
Start point	[7.5 6]
Lower bound	[5.2 2.5]
Upper bound	[10 10]
Poll methods	GPS Positive basis 2N
Complete poll	off
Polling order	Consecutive
Max iterations	30
Function tolerance	0.01

7.4.1.3 Pattern Search Optimisation Result

Table 7-11 shows the PS optimisation result. The total pressure increment of two air tanks during the specific driving cycle, Braunschweig-H, increases from 0.97 bar to 1.42 bar which means the amount of energy recovery has been improved 31.7%. The negative value of the fitness value is because MATLAB can only minimize the objective,

therefore, the cost function has been transferred to minimize the negative maximum total energy recovered as explained before.

Table 7-11 PS optimisation result

	Objective Pressure (bar)	Variables	
		p_1 Initial air tank 1 pressure (bar)	p_2 Initial air tank 2 pressure(bar)
Before optimisation	-0.97	7.5	6
After optimisation	-1.42	5.25	2.5

Figure 7-25 shows the result of pattern search optimisation for the initial air tanks pressure for every stop-start event. It can be seen that after 13 iterations, the objective function value remained unchanged for 4 iterations and the optimisation process stopped. So the global optimum has been found.

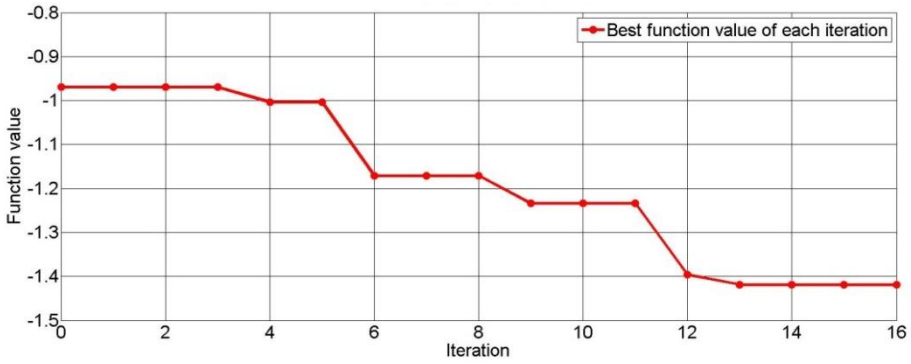

Figure 7-25 Trace of objective function value over iterations of PS optimisation

Therefore, after the optimisation, the two parameters, the initial air tanks pressure p_1 and p_2, in the pneumatic hybrid city bus control strategy should be set at 5.25 bar and 2.5 bar respectively based on the simulation result.

7.4.2 Optimisation of the Gear Changing Strategy during the Braking for Best Energy Recovery Efficiency by Conducting the Genetic Algorithm Optimisation Method

During the braking period, the bus can work in a regenerative braking mode to convert kinetic energy to pneumatic energy by compressing air into air tanks. As discussed in Chapter 3, the engine speed has the relationship with the engine brake performance and the amount of pneumatic energy recovered during braking. Therefore, choosing different gears to obtain different engine speed during the braking can significantly affect the energy recovery efficiency. As a result, the gear shift-down points during the braking are the critical parameters in the control strategy of the pneumatic hybrid city bus and should be optimized.

As mentioned before, the hybrid system control problem can be considered as a difficult optimisation problem which includes the constraints and real-valued objective function, and may have many local optimums which mean that the gradient-based optimisation algorithm may not converge to a global solution [82, 107]. The GA can be applied to solve a variety of optimisation problems that are not well suited for standard optimisation algorithms, such as the problems in which the objective function is discontinuous, non-differentiable, stochastic, or highly nonlinear, and has the advantages of robust character and global character for the non-linear problem of component optimisation [83, 108].

So the Single Objective Genetic Algorithm (SOGA) is chosen here to optimize the gear shift-down points during the braking to maximize the energy recovery of air tanks during one specific driving cycle, Braunschweig-H.

7.4.2.1 Genetic Algorithm

The concept of the GA, was developed by Holland and his colleagues in the 1960s and 1970s [109], is a kind of heuristic searching algorithm based on mechanics of natural selection and natural genetics. GA is inspired by the evolutionist theory explaining the origin of species [110]. In nature, the strong species have a greater opportunity to deliver their genes to future generations via reproduction than the weak and unfit species. After generation by generation, the species which carry the correct combination in their genes become dominant in their population. But, genes may randomly change. If the

changes provide additional advantages in the challenge for survival, new species evolve from the old ones. Unfit species become extinct by natural selection. The terminology of GA is shown in the Table 7-12.

Crossover and mutation are the two most important operators of GA. By iteratively applying the crossover operator, genes of good chromosome are expected to appear more frequently in the population, eventually leading to convergence to an overall good solution [110]. Mutation plays a critical role in GA which reintroduces genetic diversity back into the population and assists the search escape from the local optima. The procedure of a generic GA is given as follow [111]:

Step 1: Set $t = 1$. Randomly generate N solutions to form the first population, P_1. Evaluate the fitness of solutions in P_1.

Step 2: Crossover: Generate an offspring population Q_t as follows:

2.1. Choose two solutions x and y from P_t based on the fitness values.

2.2. Using a crossover operator, generate offspring and add them to Q_t.

Step 3: Mutation: Mutate each solution $x \in Q_t$ with a predefined mutation rate.

Step 4: Fitness assignment: Evaluate and assign a fitness value to each solution $x \in Q_t$ based on its objective function value and infeasibility.

Step 5: Selection: Select N solutions from Q_t based on their fitness and copy them to P_{t+1}.

Step 6: If the stopping criterion is satisfied, terminate the search and return to the current population, else, set $t = t + 1$ go to Step 2.

Table 7-12 The terminology of GA

Name	Definition
Fitness Functions	The fitness function is the function need to be optimized.
Individuals or chromosome	A solution vector which can apply the fitness function.
Populations	A collection of individuals.
Generations	At each iteration, the genetic algorithm performs a series of computations on the current population to produce a new population. Each successive population is called a new generation.
Diversity	Diversity refers to the average distance between individuals in a population.
Parents and Children	To create the next generation, the genetic algorithm selects certain individuals in the current population, called parents, and uses them to create individuals in the next generation, called children.
Genes	The discrete units which constitute chromosome.
Crossover	Two chromosomes are combined together to form new chromosomes.
Mutation	Random changes into characteristics of chromosomes.

In the GA optimisation process implemented here, the fitness function and options of GA is first input by using the Global Optimisation Toolbox in MATLAB and then the Global Optimisation Toolbox completes the genetic steps such as generating the initial population, selection, crossover and mutation to implement the optimisation. The objective function and constraints are calculated using the GT-POWER and MATLAB/Simulink co-simulation model. The flow chart of optimisation simulation is shown in Figure 7-26. The simulation model is embedded into the optimisation procedure. Each set of control parameters is created by the GA and supplied to the simulation. The fitness function value is obtained from running the simulation model with the specific driving cycle, Braunschweig-H.

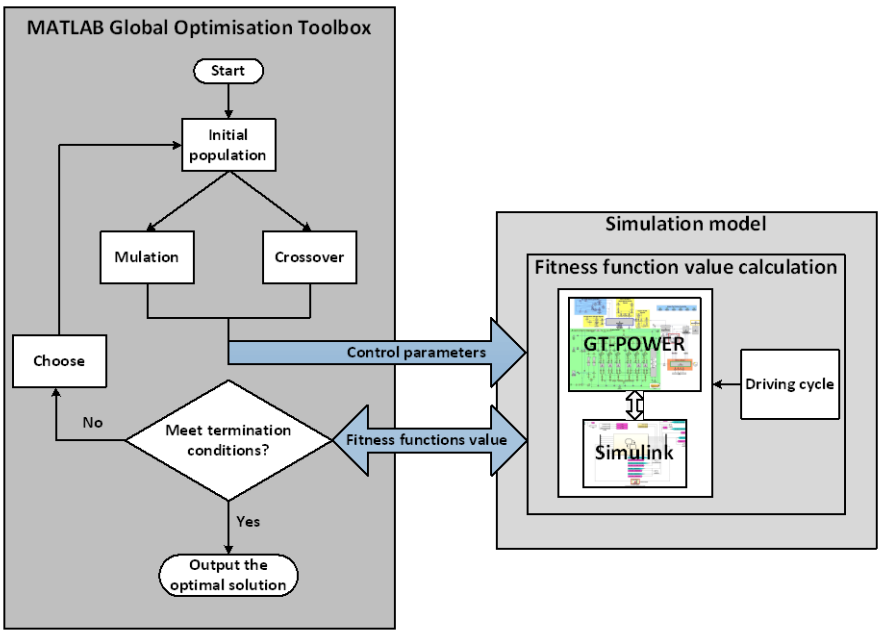

Figure 7-26 Flow chart of optimisation simulation model based on GA

7.4.2.2 Problem Statement

The objective of this optimisation is to select an optimal gear change strategy during the deceleration process in order to increase the total energy recovered over a specific driving cycle. The fitness function of the genetic algorithm for the pneumatic hybrid city bus control strategy optimisation is defined as Equation (7-20):

$$J = maxf(X) = min\left[-\left(J_{energy}(X)\right)\right] = min[-(\int \dot{m_{air}}\, dt)] \qquad (7\text{-}20)$$

where, J_{energy} is the instantaneous the amount of energy recovery of two air tanks per unit time,

X is the variable vector which includes the parameters of the control strategy of pneumatic hybrid city bus shown in Table 7-13.

Similar with the previous optimisation, the cost function has been transferred to minimize $-f(x)$ as shown in Equation (7-20).

Table 7-13 Design variables for genetic algorithm optimisation

Design variable	Description	Lower bound (km/h)	Upper bound (km/h)
gear21	The gear shift-down point from second to first gear	5	15
gear32	The gear shift-down point from third to second gear	15	21
gear43	The gear shift-down point from fourth to third gear	21	36
gear54	The gear shift-down point from fifth to fourth gear	36	58

The start point of this optimisation is 10, 15, 30 and 45 which are the speed (km/h) that gear shift-down points during the deceleration process. This gear change strategy during the braking comes from previous research in Chapter 4 and calculated from the gear ratios to fit the gear change requirement of the Braunschweig driving cycle.

The GA optimisation parameter and options are summarized in Table 7-14.

Table 7-14 Summary table for GA optimisation

Solver	ga – Genetic Algorithm
Number of variable	4
Lower bound	[5 15 21 36]
Upper bound	[15 21 36 58]
Population size	20
Stall generations	15

7.4.2.3 Genetic Algorithm Optimisation Result

Table 7-15 shows the GA optimisation result. Figure 7-27 shows the GA optimisation result after 26 generations with 20 individuals in each generation. The entire optimisation process of the GA algorithm took approximately 520 hours (22 days) to complete. This huge process time is not due to the GA but because of the large time GT-POWER takes to emulate each design point.

Table 7-15 GA optimisation result

	Objective - Energy (J)	Variables			
		gear21 **(km/h)**	***gear32*** **(km/h)**	***gear43*** **(km/h)**	***gear54*** **(km/h)**
Before optimisation	-335.22	10	15	30	45
After optimisation	-473.35	7.5	15.7	34.1	40.7

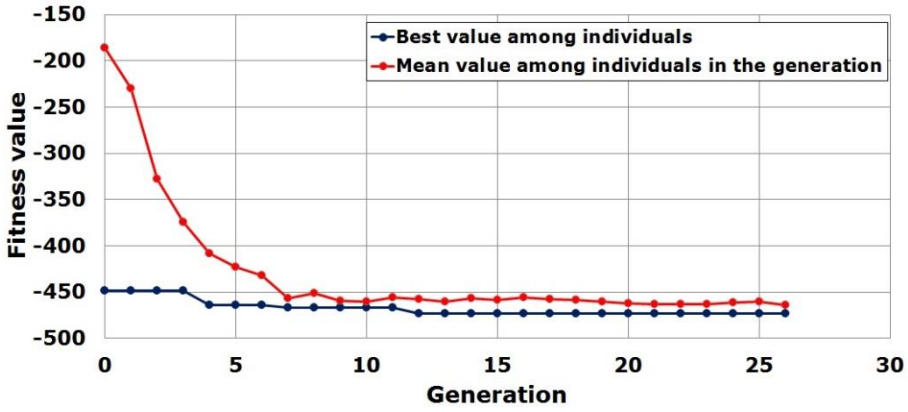

Figure 7-27 Trac of objective minimization over generations

It can be seen in Figure 7-27 that the best individual's fitness in the first few evolutions decreases progressively more slowly until remaining unchanged after 12 generations.

The amount of energy recovery during the braking of the specific driving cycle, Braunschweig-H, before and after GA optimisation are shown in Table 7-15, which shows that the amount of energy recovery has been improved 41.2% by changing the gear shift-down point during the braking.

As a result, based on the optimisation result, the gear changing strategy during the braking will be as shown in Table 7-16.

Table 7-16 The gear changing strategy during the braking after optimisation

	gear21 **From second to first gear (km/h)**	***gear32*** **From third to second gear (km/h)**	***gear43*** **From fourth to third gear (km/h)**	***gear54*** **From fifth to fourth gear (km/h)**
After optimisation	7.5	15.7	34.1	40.7

7.4.3 Optimisation of the Gear Changing Strategy during Vehicle Acceleration

The condition for activating the Boost Function is when the vehicle is in the full acceleration mode while the driver demands 100% accelerator pedal position signal. Normally, this happens after every gear change. Because of the Boost Function's capability to improve the engine transient response and reduce the fuel consumption, the gear up-shift point can be changed. But with more Boost Function operations, there is a greater loss of available energy from the air tanks. As a result, the gear change strategy during acceleration will affect the fuel consumption and availability in the air tanks simultaneously.

The question as how to balance the two conflicting objectives, the fuel consumption and the available energy in the air tanks, by optimizing the gear changing strategy during the acceleration forms the research topic. The Non-dominated Sorting Genetic Algorithm II developed by Deb et al. is used here [112]. As a result, a Pareto front for the gear changing strategy during the acceleration is obtained. The relationship between fuel consumption and the availability usage, the optimal Pareto points and the gear changing strategy during the acceleration of the pneumatic hybrid city bus are analysed and discussed in the following sections.

7.4.3.1 Multi-objective Genetic Algorithm Optimisation

The aim of multi-objective optimisation problems is to find the best candidate solutions among multiple objective functions that are usually conflicting [19]. Multi-objective formulations are realistic models for many complex engineering optimisation problems [110]. In many engineering problems, the objectives, such as minimising cost, maximising performance and reliability, tend to conflict with each other. Meeting a single objective can lead to unacceptable results with respect to the other objectives. To prevent this, the objectives should be simultaneous optimized. A reasonable approach to a multi-objective requirement is to investigate a set of solutions, each of which satisfies the objectives at an acceptable level without being dominated by any other solution [110].

There are two general approaches to multi-objective optimisation. The first is to combine the individual objective functions into a single composite function or move all but one objective to the constraint set [110]. In both cases of the first approach, an optimisation method cannot return a set of solutions which can be examined for trade-offs, which only can return a single solution. The second one is to determine an entire Pareto optimal solution set or a representative subset [110]. A Pareto optimal set is a set of solutions that are non-dominated with respect to each other. When moving from one Pareto solution to another, there is always a certain amount of sacrifice in one objective(s) to achieve a certain amount of gain in the other(s) [110]. The Pareto optimal solution set are often preferred to single solutions because they can be practical when considering real-life problems since the final solution of decision-maker is always a trade-off [110].

Evolutionary algorithms are the good candidate for multi-objective optimisation problems due to their abilities, to search simultaneously for multiple Pareto optimal solutions and perform the better global search of the search space [29]. GA, as the best-known branch among existing evolutionary algorithms, is easy to use and implement because it uses only a simple scalar performance measure that does not require or use derivate information [30]. GA is well fitted for the requirements to solve a multi-objective optimisation problem because it is a population-based approach. Due to evolutionary algorithms' inherent parallelism, they are able to capture a number of solutions concurrently in a single run [113]. These mean a) if problem has single optimum, population members can be expected to converge to optimum, and b) if it has multiple optimal solutions, capture multiple optimal solutions in its final population [114]. There are several advantages for GA to solve the multi-objective problems.

(i) The ability of GA to simultaneously search different regions of a solution space makes it possible to find a diverse set of solutions for different problems with non-convex, discontinuous, and multi-modal solutions spaces [110].
(ii) The crossover operator of GA may exploit structures of good solutions with respect to different objectives to create new non-dominated solutions in unexplored parts of the Pareto front [110].
(iii) Most multi-objective GA do not require the user to prioritize, scale, or weigh objectives [110].

As a result, GA has been the most popular heuristic approach to multi-objective design and optimisation problems [110]. Since the first multi-objective GA, called vector evaluated GA, was proposed by Schaffer [115], several multi-objective evolutionary algorithms have been developed such as Multi-objective Genetic Algorithm (MOGA), Nondominated Sorting Genetic Algorithm (NSGA), Strength Pareto Evolutionary Algorithm (SPEA), and Fast NSGA-II [116-119]. A comprehensive experimental methodology to quantitatively compare multi-objective optimizers has been presented by Zitzler [120]. The widespread opinions that a) multi-objective evolutionary algorithms can have clear advantages over traditional multi-criteria optimisation methods, and ii) NSGA-II and SPEA clearly outperformed other MOEA implementations on the test problems, had been substantiated experimentally [120]. The NSGA-II is chosen for this multi-objective optimisation problem because the NSGA-II, in most problems, is able to find a much better spread of solutions and better convergence near the true Pareto-optimal front compared to other multi-objective evolutionary algorithms [119]. The use of NGSA-II makes it possible to obtain the entire Pareto front of optimal the gear changing strategy during the acceleration in a single optimisation run [121]. This is beneficial not only from the computational standpoint, but also from the perspective of picturing and understanding the trade-offs between the two objectives [121].

Similar to the implementation of the SOGA optimisation in the last section, the Global Optimisation Toolbox in MATLAB is used for multi-objective optimisation in this research. The fitness functions and options of the optimisation problem are notified to the Global Optimisation Toolbox. Then the Global Optimisation functions complete the genetic steps: generating the initial population, selection, crossover and mutation to implement the optimisation. The objective functions and constraints are calculated based on the GT-POWER and MATLAB/Simulink model. The simulation model as a module is embedded into the entire optimisation procedure for implementation, and it is completed in the time domain. For each individual in each generation, the control parameters input to the simulation model is created by NSGA-II, and the fitness functions value are obtained by running the simulation model with the specific driving cycle, Braunschweig-H.

7.4.3.2 Problem Statement

The mathematics description of multi-objective optimisation problem can be defined as follows:

$$\begin{cases} \min_{X\in\Omega} F(X) = [f_1(X), f_2(X_2), \dots, f_m(X)] \\ s.t.\ \ g_j(X) \geq 0 \qquad\qquad j = 1,2,\dots,n \end{cases} \quad \text{(7-21) [122]}$$

where, $X=(x_1, x_2,\dots,x_N)$ – a variable vector in a real and N-dimensional space,

Ω – feasible solution space,

$f_m(X)$ – objective functions for optimisation,

$g_j(X)$ – constraint functions which have already been defined in the GT-POWER simulation model.

In this section, two bus operation optimisation objectives are considered over a driving cycle:

(i) Fuel consumption,

(ii) Loss of available energy in the air tanks.

As a result, the fitness function of the multi-objective genetic algorithm for the pneumatic hybrid city bus control strategy optimisation is defined as Equation (7-22):

$$J = min_{driving\ cycle} \sum_N \int_0^{T_N} \left(\dot{A} + \lambda \dot{m}_f\right) \quad \text{(7-22)}$$

The design variables for multi-objective optimisation are shown in Table 7-17.

Table 7-17 Design variables for multi-objective optimisation

Design variable	Description	Lower bound (km/h)	Upper bound (km/h)
gear12	The gear shift-up point from first to second gear at vehicle speed	7.54	15
gear23	The gear shift-up point from second to third gear at vehicle speed	15.7	21
gear34	The gear shift-up point from third to fourth gear at vehicle speed	34.1	36
gear45	The gear shift-up point from fourth to fifth gear at vehicle speed	40.7	58

This optimisation approach deals with two conflicting objectives; while minimizing the total fuel consumption requires more boost operations to increase the internal combustion engine efficiency, the more boost operations tend to decrease the available energy in the air tanks. Therefore, a single optimal point does not exist; instead, a family of optimal solutions in the form of a Pareto front can be obtained, as presented next.

The GA does not require a start point for the optimisation and it will create one using the Creation function [83]. As a result, in this optimisation, the start point is not specified.

The GA optimisation parameter and options are summarized in Table 7-18.

Table 7-18 Summary table for NSGA-II optimisation

Solver	gamultiobj – Multiobjective optimization using Genetic Algorithm
Number of variable	4
Lower bound	[7.54 15.7 34.1 40.7]
Upper bound	[15 21 36 58]
Population size	12 or 50
Pareto front population fraction	0.5
Generation	20 or 5

7.4.3.3 Multi-objective Optimisation Result

Two different options multi-objective optimisations has been carried out to represent how the options will affect the optimisation result. These two optimisations both use the NSGA-II and their differences of options are shown in Table 7-19. Generations specify the maximum number of iterations the GA performs. Population size specifies how many individuals are in each generation. From Table 7-19, it can be seen that the total calculation times of two optimisations are almost same which are 240 and 250 iterative respectively. The reason for choosing these two options is because of the duration of the simulation time. The entire optimisation process for the NSGA-II algorithm to calculate 250 times took approximately 120 hours (5 days) to complete. This huge process time is not due to the algorithm itself but because of the large time GT-POWER takes to emulate each design point which has been already explained before. As a result, increasing the

number of individual or generations in the optimisation algorithm would increase the total optimisation time beyond the scope of this research. But from the different choose of generations and population size, their effect to the optimisation result can be learned.

Table 7-19 The options of two multi-objective optimisations

	Generations	Population Size
Multi-objective optimisation 1 (MOO 1)	20	12
Multi-objective optimisation 2 (MOO 2)	5	50

Table 7-20 and Table 7-21 show two multi-objective optimisation results using NSGA-II. It can be seen that the multi-objective optimisation does not present an exact or unique solution, but a set of solutions in the balance between the objectives. It also can be learned that more populations in each generation can get more solutions even the optimisation run fewer generations. This is because with a large population size, the genetic algorithm searches the solution space more thoroughly, thereby reducing the chance that the algorithm returns a local minimum that is not a global minimum [83].

Table 7-20 Multi-objective optimisation 1 result

Solutions	Objectives		Variables			
	Objective 1 – Availability (J)	**Objective 2 - Fuel consumption (g)**	***gear12* (km/h)**	***gear23* (km/h)**	***gear34* (km/h)**	***gear45* (km/h)**
1	**0.429**	**95.95**	**9.4**	**17.4**	**34.5**	**43.1**
2	0.152	97.39	12.1	20.2	34.7	43.3
3	0.002	102.65	14.6	21	35.5	47.9

Table 7-21 Multi-objective optimisation 2 result

Solutions	Objectives		Variables			
	Objective 1 - Availability (J)	Objective 2 - Fuel consumption (g)	*gear12* (km/h)	*gear23* (km/h)	*gear34* (km/h)	*gear45* (km/h)
1	0.002	102.65	14.6	21.0	35.5	47.9
2	0.066	98.46	11.0	18.4	34.6	45.8
3	0.248	96.45	8.4	17.4	34.5	43.1
4	0.126	97.15	12.6	20.3	34.5	43.3
5	0.281	96.44	9.6	17.4	34.6	43.5
6	0.048	98.65	13.3	18.6	34.8	45.0
7	0.090	97.52	13.0	19.3	34.7	43.4
8	0.008	100.91	14.6	18.7	35.0	46.6
9	0.304	96.25	9.5	19.3	34.5	43.1
10	0.210	96.77	9.2	17.9	34.6	43.4
11	0.154	97.00	11.9	19.2	34.5	43.3
12	0.234	96.66	9.3	18.3	34.5	43.2
13	0.012	99.19	13.9	20.0	34.9	45.6
14	0.002	102.65	14.6	21.0	35.5	47.4
15	0.229	96.69	11.1	18.3	34.5	43.1
16	0.038	98.95	14.0	19.7	35.2	44.4
17	0.089	97.53	13.3	19.3	34.7	43.4
18	**0.355**	**95.84**	**8.7**	**17.6**	**34.5**	**43.1**

Figure 7-28 shows two Pareto front after optimisation. The MOO 1 result is marked with the red square, and the red dash line shows an estimated Pareto front if both numbers of individuals and generations are increased. The MOO 2 result is marked with the blue triangle, and the blue dash line shows also an estimated Pareto front if both numbers of individuals and generations are increased.

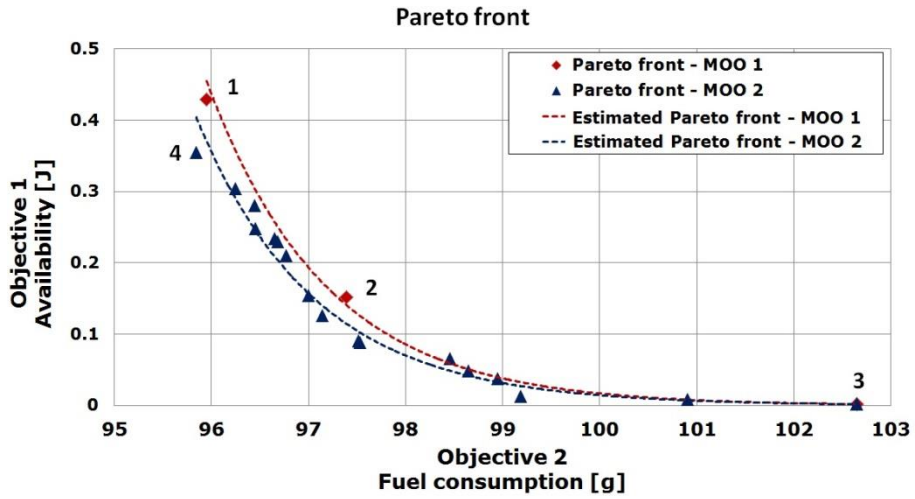

Figure 7-28 Optimal Pareto front for the multi-objective optimisation using NSGA-II

From Figure 7-28, it can be seen that both in two Pareto fronts, a better fuel consumption can be achieved with a high availability usage in the air tanks. For example, for the multi-objective optimisation 1 result, the fuel consumption in the Pareto front ranges between 95.95 to 102.65 g for a specific driving cycle, Braunschweig-H, while the availability usage in the two air tanks varies from 0.02 to 0.429 J. The solution 2 which is point 2 in Figure 7-28 represents a good compromise of fuel consumption and availability usage in the air tanks. Lower fuel consumption would have to be paid for with a relative bigger increase of availability usage in the air tanks supporting boost function operations. One example is Solution 1 which is point 1 in Figure 7-28. It has the lowest fuel consumption 95.95 g but the highest availability loss in the two air tanks which is 0.429 J during one acceleration event. Compared with solution 1 and solution 3, it can be learned that the fuel consumption can be improved 6.5%.

But from Figure 7-28, it also can be seen that the multi-objective optimisation 2 can get a better solution which is Solution 18 in Table 7-21 and point 4 in Figure 7-28. This solution has lower fuel consumption than solution 1 which is 95.84 g, and also has lower availability loss than solution 1 in the two air tanks which is 0.355 J during one acceleration event. This means compared with multi-objective optimisation 1, multi-objective optimisation 2 can supply a better solution which uses less air in two tanks but also has lower fuel consumption.

The result proves:

(i) More populations in each generation can get more solutions even the optimisation run fewer generations.

(ii) The fuel consumption during the acceleration can be improved by optimizing the parameters of the pneumatic hybrid control strategy through the gear changing strategy.

(iii) The fuel consumption and the availability usage during the acceleration are two conflicting objectives which need to be balanced.

As a result, the multi-objective optimisation result supplies a series gear changing strategies during the acceleration which can be chosen to meet the different requirements at two aspects, fuel consumption, and energy usage. Here, to minimize the fuel consumption, the gear changing strategy during the acceleration based on the optimisation has been chosen as shown in Table 7-22.

Table 7-22 The gear changing strategy during the acceleration after optimisation

	gear12 **From first to second gear (km/h)**	***gear23*** **From second to third gear (km/h)**	***gear34*** **From third to fourth gear (km/h)**	***gear45*** **From fourth to fifth gear (km/h)**
After optimisation	8.7	17.6	34.5	43.1

7.4.4 Optimisation Result Validation

To validate the effectiveness of the three optimisations conducted before, the new parameters of the pneumatic hybrid city bus control strategy based on the optimisation results are implemented into the backward facing simulation model of the pneumatic hybrid city bus using in the Chapter 4. The parameters based on the optimisation result are summarized in Table 7-23.

Table 7-23 Parameters in the pneumatic hybrid city bus control strategy after optimisation

Initial air tanks pressure		**Air tank 1 (bar)**	**Air tank 2 (bar)**
		5.25	2.5
Gear change strategy		**Speed range (km/h)**	
		During the acceleration	**During the braking**
	First gear	0 - 8.7	0 - 7.5
	Second gear	8.7 - 17.6	7.5 - 15.7
	Third gear	17.6 - 34.5	15.7 - 34.1
	Fourth gear	34.5 - 43.1	34.1 - 40.7
	Fifth gear	>43.1	>40.7

The fuel consumption of the model running the whole Braunschweig driving cycle with the control parameters before and after optimisations is shown in Table 7-24, which shows that the fuel economy had been further improved 6.03%.

Table 7-24 Fuel consumption before and after optimisations

Driving cycle	**Fuel consumption before optimisations**	**Fuel consumption after optimisations**	**Improvement**
Braunschweig driving cycle	39.93 l/100km 3171.8 g	37.52 l/100km 2980.5 g	6.03%

The improvement of fuel economy indicated that the optimisations implemented before can be used to identify the best control parameters for the pneumatic hybrid city bus control strategy to improve energy efficiency.

7.5 Conclusion

An energy control strategy based on the "logic threshold" methodology for the pneumatic hybrid city bus has been designed. The control strategy can manage the pneumatic

hybrid city bus to realize three special functions: Stop-Start, Boost, and Regenerative Braking as well as the normal operations.

To analyse the pneumatic hybrid city bus dynamic performance, engine transient response, fuel economy and energy usage, a forward facing pneumatic hybrid city bus simulation model which includes the detailed engine model has been developed in GT-POWER and MATLAB/Simulink co-simulation.

Three global optimisation algorithms, PS, GA and Multi-objective NSGA-II, are compared and employed for the different optimisation processes required for the vehicle control strategy. Optimisation criteria were selected from fuel consumption, air mass recovered and the deployment of available energy during regeneration. As a result of identifying optimal conditions – when compared with the original nominal design:

(i) The total pressure increment of two air tanks during the specific driving cycle, Braunschweig-H, has been increased from 0.97 bar to 1.42 bar which means the amount of energy recovery has been improved 31.7% by implementing the pattern search optimisation to optimize the initial air tanks pressure for every stop-start event.
(ii) The amount of energy recovery during the braking in Braunschweig-H, has been improved 41.2% by modifying the gear shift-down point.
(iii) The fuel consumption and the availability usage in the air tanks during the acceleration are two conflicting objectives which need to be balanced: the fuel consumption can improve 6.5% by choosing the best result.

To verify the effectiveness of the optimisation result, an example simulation is carried out by implementing the optimisation in a backward facing vehicle model. The simulation result demonstrated that the fuel economy can be further improved by 6%. This result shows that

(i) Compared with the fuel economy improvement 6.5% in the forward facing model, the backward facing model confirms that 6% fuel consumption can be reduced. The difference is because that in forward facing model, the fuel consumption is calculated by the Braunschweig-H rather than the whole Braunschweig driving cycle.

(ii) The method that choosing one typical stop-start event, Braunschweig-H, to represent the whole Braunschweig driving cycle as the test cycle for the optimisation has been proved feasible. Although the improvements in fuel consumption between the Braunschweig-H and Braunschweig driving cycle are respectively 6.5% and 6% which means 8.3% difference, it still demonstrates that the supposition that using the Braunschweig-H as an alternative to Braunschweig driving cycle.

CHAPTER 8

CONCLUSION AND FUTURE PROSPECTS

To respond to the fact that there is as yet no in-depth study on how to implement the pneumatic hybrid technology on the city bus, the aim of the reported research has been to develop an understanding of the pneumatic hybrid powertrain system and its control strategy. One important aspect is the demonstration of the ability of such systems to improve upon the conventional Powertrain technology. Section 8.1 summarizes the notable conclusions of the study, while Section 8.2 includes an introduction and discussion concerning the improvements, suggestions and recommendations for future work on the pneumatic hybrid technology.

8.1 Conclusion

The works that have been done and the results achieved are listed with the corresponding research aims and objectives listed in Chapter 1.

(i) To fully understand the principle of the operation of the pneumatic hybrid engine and the quantification of the sensitivity of the work done to design parameters during the Compressor Mode.

This objective has been achieved in Chapter 3. The principle of operation has been presented. The potential of the pneumatic hybrid system both to generate a supply of compressed air and to manage the contribution of the engine to vehicle braking had been confirmed. The pneumatic hybrid engine CM is considered from a theoretical perspective based on an air cycle analysis and validated. An understanding of the sensitivity of work done (braking torque created during the CM) to design parameters is given. The results demonstrate

a) The lower air tank pressure can create more brake torque at the same engine speed,

b) The longer CREB intake valve second opening duration decreases the brake torque performance,

c) It always has the maximum engine brake torque output when the CREB intake valve second closing time is right at TDC which means IVSC is 0°CA.

(ii) To evaluate the fuel economy improvement ability of pneumatic hybrid technology for the city bus through different bus driving cycles.

This objective has been fulfilled in Chapter 4. An evaluation of the fuel economy improvement ability of pneumatic hybrid technology for the city bus application by realizing the Stop-Start Function through different bus driving cycles has been presented. Also, an investigation is made into how multiple air tanks give an additional degree of freedom for management of recovered air. A backward-facing simulation model of the city bus with the pneumatic hybrid powertrain has been applied to investigate the improvement of fuel economy by using one and two air tanks in different driving cycles in Simulink with Stateflow. The analysis shows

a) The pneumatic hybrid technology can reduce fuel consumption by at least 6% through stop-start operation, and can eliminate 90% of the idling time,

b) In the case of the modelled bus cycles, significant fuel savings of 7.1% can be achieved during MLTB driving cycles because of the large braking energy and frequent stop–start operations required during the type of bus operation exemplified by this cycle,

c) The two air tanks pneumatic hybrid system has the higher fuel saving potential which is because it can offer the possibility of at least one air tank's pressure being higher than the lower limit and other lower pressure air tank results in higher energy capture during the CM.

(iii) To analyse engine braking characteristics during the vehicle's deceleration and braking process during different bus driving cycles and hence identify appropriate braking system structure and its control strategies for maximum energy recovery.

This objective has been achieved in Chapter 5. It firstly presents an analysis of vehicle braking behaviour through different bus driving cycles and compares two configurations of the hybrid braking system, the parallel hybrid brake system and the fully controllable hybrid brake system. The comparison shows the fully controllable hybrid braking system has a distinct advantage and is chosen to realize the Regenerative Braking Function. A braking simulation model has been built in to support an investigation of an optimum air tank pressure and configuration for energy recovery. Based on the optimisation result, a new control strategy is implemented along with a baseline simulation model to explore the benefits of the new control strategy. The findings include

a) It indicates that in the urban area the bus's braking power can reach to 80% of the total traction power, and the braking of the city bus is very gentle with most of the deceleration rate below 0.2 g, compared with the passenger car,

b) The fully controllable hybrid braking system is fit for the requirement of the pneumatic hybrid regenerative system which can either work at high efficiency to recover as much braking energy as possible and supply the corresponding braking force,

c) The optimisation result shows that the 5.2 bar air tank pressure is the best pressure for braking energy recovery,

d) The model with the newly optimized initial air tanks pressure can enhance 2.7% the total air mass recovered during the braking compared with the previous control strategy which means the air tanks pressure is the function of the energy recovery rate.

(iv) To study the benefits of extra boost on reducing turbo-lag, improved engine performance, and reduce fuel consumption.

This objective has been achieved in Chapter 6. An analysis of the reasons for engine turbo-lag and the methods developed for reducing the turbo-lag and improving transient response have been presented first. Then, a number of architectures for managing a rapid energy transfer into the powertrain to assist

acceleration of the turbocharger have been proposed and investigated from two aspects, engine brake torque response and vehicle acceleration, by using the 1-D engine simulation. The findings show

a) The System I, IP and E all improve torque response time (to maximum torque) by 90.8%, 78.3% and 80.8% respectively, when the engine accelerates from no load to full load at 1600 rpm, and both the Systems I and IP can be seen to significantly reduce the vehicle acceleration time, from 0 to 48 km/h, 13% and 8.6% respectively through reduction of turbo-lag,

b) System I carries the highest risk of compressor surge. System IP carries a lower risk of surge because it does not block the output of the compressor. System E has no risk of surge because it does not need a valve in the intake system,

c) System IP offers considerable advantages over System I at both less use of air and less likely to cause the compressor surge.

(v) To formulate a pneumatic hybrid city bus control strategy and the vehicle driving cycle simulation programme and identify the relationship between respectively the operating parameters, fuel consumption and energy usage according to optimisation criteria.

This objective has been achieved in Chapter 7. An energy control strategy based on the use of thresholds in the degree of energy storage and regeneration (a "logic threshold" methodology) for the pneumatic hybrid city bus has been designed. A forward facing pneumatic hybrid city bus simulation model which includes the detailed engine model has been developed in GT-POWER with MATLAB/Simulink co-simulation. To obtain the maximum overall fuel economy, the amount of air and energy recovered during the braking and minimum loss of availability during acceleration, a number of variables in the control strategy must be optimized. Three global optimisation algorithms, Pattern Search, Genetic Algorithm and multi-objective Non-dominated Sorting Genetic Algorithm II are compared and employed for the optimisation of the control strategy considered at three levels respectively. The results show

a) The proposed energy control strategy for the pneumatic hybrid city bus enables the vehicle to realize the specific functions: Stop-Start, Boost and Regenerative braking, as well as the normal operation of the vehicle,

b) The total pressure increment of two air tanks during the specific driving cycle, Braunschweig-H, has been increased from 0.97 bar to 1.42 bar which means the amount of energy recovery has been improved 31.7% by implementing the PS optimisation to optimize the initial air tanks pressure for every stop-start event,

c) The amount of energy recovery during the braking in Braunschweig-H, has been improved 41.2% by modifying the gear shift-down point,

d) The fuel consumption and the availability usage in the air tanks during the acceleration are two conflicting objectives which need to be balanced: the fuel consumption can improve 6.5% by choosing the best multi-objective optimisation result,

e) By optimizing the variables in the control strategy, the fuel economy of a pneumatic hybrid city bus can be further improved by 6%,

f) The method that choosing one typical stop-start event, Braunschweig-H, to represent the whole Braunschweig driving cycle as the test cycle for the optimisation has been proved feasible.

It can be concluded that the effectiveness of the pneumatic hybrid technology has been successfully proved by this study. The pneumatic hybrid technology can improve the city bus fuel economy by at least 6% for a typical bus driving cycle, reducing the engine brake torque response time and improving acceleration. The pneumatic hybrid technology offers an alternative to the electric hybrid. It offers significant advantages, such as good fuel economy, and vehicle drivability improvement. Unlike the electric hybrid, pneumatic hybrid technology can be implemented without adding a new propulsion system to the vehicle, it has demonstrable advantages in manufacturing cost, lower mass, and suitability for commercially viable large volume production.

8.2 Recommendations for Future Works

Due to limited time and words, this PhD thesis can only discuss those explained above. However around this technology, there have been still numbers of issues worthy to be explored further, for instance:

(i) In order to validate the modelling work in Chapter 3 and Chapter 6, the engine experimental tests should be carried out on a single cylinder engine to verify the Chapter 3 model and results, and a six-cylinder engine to validate the Chapter 6 model and findings.

(ii) Further optimisation of operating parameters such as auxiliary chamber size, air tank(s) volume and valve timing would be desirable by means of more extensive systematic studies to fully evaluate the pneumatic hybrid system potential in fuel savings and vehicle performance improvement.

(iii) The pneumatic hybrid city bus control strategy can be further developed by importing the telemetry data, such as using an electronic horizon generated via the GPS data. Then the route profiles and traffic conditions can be calculated, thus allowing the control strategy to be optimized to enhance the energy efficiency.

(iv) How to start the engine by injecting compressed air into the individual cylinders to propel the pistons during the cranking to replace the air starter using in this research to further reduce the cost of the pneumatic hybrid system.

(v) The compressed air used in combination with EGR technology in a diesel engine to improve the dynamic trade-off between NO_x and smoke emissions.

(vi) Investigations could also look at the possibility of implementing the pneumatic hybrid system as an exhaust energy recovery device, thus further improving the energy efficiency by recovering the useful energy in the exhaust gas.

(vii) Finally, for simulation purpose the valves are idealised in this research. Flow losses and valve dynamics are neglected. However, a detailed investigation will need to consider valve behaviour in order to evaluate the detailed effect on systems response and the fuel economy gains. Also valve operating procedures which change air flow in manifolds and the engine cylinders, changing the patterns of losses requires further investigation in the future work.

REFERENCE

[1] I. E. Agency, "CO2 Emissions from Fuel Combustion 2014 - Highlights," Retrieved from https://www.iea.org/publications/freepublications/publication/CO2EmissionsFromFuelCombustionHighlights2014.pdf, Last accessed: March 24, 2015, 2014.

[2] U. Tietge and P. Mock, "CO2 emissions from new passenger cars in the EU: Car manufacturers' performance in 2013," Retrieved from http://www.theicct.org/sites/default/files/publications/ICCTbriefing_EU-CO2_201406.pdf, Last accessed: March 24, 2015, 2014.

[3] T. V. Johnson, "Vehicular Emissions in Review," SAE Int. J. Engines, vol. 5, pp. 216-234, 2012.

[4] C. Lee, "Computational and experimental study of air hybrid engine concepts," PhD Thesis, Brunel University London, 2011.

[5] E. D. Tate, M. O. Harpster, and P. J. Savagian, "The Electrification of the Automobile: From Conventional Hybrid, to Plug-in Hybrids, to Extended-Range Electric Vehicles," SAE Int. J. Passeng. Cars - Electron. Electr. Syst., vol. 1, pp. 156-166, 2008.

[6] M. Ehsani, Y. Gao, and A. Emadi, Modern Electric, Hybrid Electric, and Fuel Cell Vehicles: Fundamentals, Theory, and Design, Second Edition. Boca Raton: CRC Press, 2009.

[7] T. Christen and M. W. Carlen, "Theory of Ragone plots," Journal of power sources, vol. 91, pp. 210-216, 2000.

[8] S. Miller, "AQMD Hydraulic Hybrid Vehicle Forum and Technical Roundtable," International Truck and Engine, ovember, vol. 15, 2007.

[9] X. Zeng, "Improving the energy density of hydraulic hybridvehicle (HHVs) and evaluating plug-in HHVs," 2009.

[10] S. Ranganathan, "HYBRID BUSES COSTS AND BENEFITS," Retrieved from http://www.eesi.org/files/eesi_hybrid_bus_032007.pdf, Last accessed: December 26, 2015.

[11] R. Bao and R. Stobart, "Using Pneumatic Hybrid Technology to Reduce Fuel Consumption and Eliminate Turbo-Lag," SAE Technical Paper 2013-01-1452, 2013.

[12] T. Liu, J. Zheng, S. Wang, and F. Gu, "Logic Threshold Based Energy Control Strategy for Parallel Hydraulic Hybrid Vehicles," Research Journal of Applied Sciences, Engineering and Technology, vol. 6, pp. 2339-2344, 2013.

[13] R. Prohaska, A. Duran, A. Ragatz, and K. Kelly, "Statistical Characterization of Medium-Duty Electric Vehicle Drive Cycles," 2015.

[14] P. Higelin, A. Charlet, and Y. Chamaillard, "Thermodynamic Simulation of a Hybrid Pneumatic-Combustion Engine Concept," Int.J. Applied Thermodynamics, vol. 5, p. 11, 2002.

[15] M. M. Schechter, "New Cycles for Automobile Engines," SAE Techincal Paper 1999-01-0623, 1999.

[16] L. Guzzella and A. Sciarretta, Vehicle propulsion systems : introduction to modeling and optimization. Berlin: Berlin : Springer, 2007.

[17] C. Tai, T. Tsao, M. B. Levin, G. Barta, and M. M. Schechter, "Using Camless Valvetrain for Air Hybrid Optimization," SAE Techincal Paper 2003-01-0038, 2003.

[18] J. W. G. Turner, M. D. Bassett, R. J. Pearson, G. Pitcher, and K. J. Douglas, "New Operating Strategies Afforded by Fully Variable Valve Trains," SAE Techincal Paper 2004-01-1386, 2004.

[19] P. Higelin, I. Vasile, A. Charlet, and Y. Chamaillard, "Parametric optimization of a new hybrid pneumatic-combustion engine concept," International Journal of Engine Research, vol. 5, pp. 205-217, April 1, 2004 2004.

[20] J. Turner, R. Pearson, and S. Kenchington, "Concepts for improved fuel economy from gasoline engines," International Journal of Engine Research, vol. 6, pp. 137-157, 2005.

[21] M. Andersson, B. Johansson, and A. Hultqvist, "An Air Hybrid for High Power Absorption and Discharge," SAE Techincal Paper 2005-01-2137, 2005.

[22] K. D. Huang, S.-C. Tzeng, and W.-C. Chang, "Energy-saving hybrid vehicle using a pneumatic-power system," Applied Energy, vol. 81, pp. 1-18, 2005.

[23] J. F. F. H. Britto, E. A. Perondi, and J. A. E. Mazzaferro, "Design of a Pneumatic Regenerative Braking System," SAE Techincal Paper 2005-01-3969, 2005.

[24] H. Kang, C. Tai, E. Smith, X. Wang, T.-C. Tsao, J. Stewart, et al., "Demonstration of Air-Power-Assist (APA) Engine Technology for Clean Combustion and Direct Energy Recovery in Heavy Duty Application," SAE Techincal Paper 2008-01-1197, 2008.

[25] L. Guzzella, U. Wenger, and R. Martin, "IC-Engine Downsizing and Pressure-Wave Supercharging for Fuel Economy," 2000.

[26] S. Hounsham, "Optimisation and control of thermal recovery for a hybrid vehicle," PhD Thesis, Loughborough University, 2008.

[27] "Simulink Overview," Retrieved from http://uk.mathworks.com/products/simulink/, Last accessed: March 27, 2015.

[28] "GT-SUITE Applications," Retrieved from https://www.gtisoft.com/applications/applications.php, Last accessed: March 27, 2015.

[29] "GT-SUITE Overview," Retrieved from https://www.gtisoft.com/products/GT-SUITE_Overview.php, Last accessed: March 04, 2015.

[30] "GT-POWER Engine Simulation Software," Retrieved from https://www.gtisoft.com/upload/Power.pdf, Last accessed: March 27, 2015.

[31] H. Zhao, C. Psanis, T. Ma, J. Turner, and R. Pearson, "Theoretical and experimental studies of air- hybrid engine operation with fully variable valve actuation," Int. J. Engine Research, vol. 12, pp. 527-548, 2011.

[32] H. Zhao, C. Psanis, and T. Ma, "Analysis of an air hybrid engine concept with an energy recovery valve " Int. J. Vehicle Design, vol. 55, pp. 49-75, 2011.

[33] H. Zhao, C. Psanis, and T. Ma, "Analysis of a production-oriented air hybrid engine concept and its performance," Int. J. Powetrains, vol. 1, pp. 43-71, 2011.

[34] C. Lee, H. Zhao, and T. Ma, "Analysis of a novel mild air hybrid engine technology, RegenEBD, for buses and commercial vehicles," International Journal of Engine Research, vol. 13, pp. 274-286, 2012.

[35] C. Lee, H. Zhao, and T. Ma, "Pneumatic Regenerative Engine Braking Technology for Buses and Commercial Vehicles," SAE Int. J. Engines, vol. 4, pp. 2687-2698, 2011.

[36] C. Lee, H. Zhao, and T. Ma, "The Performance Characteristics of an Production Oriented Air Hybrid Powertrain," SAE Int. J. Engines, vol. 3, pp. 609-619, 2010.

[37] C. Lee, H. Zhao, and T. Ma, "Analysis of a Cost Effective Air Hybrid Concept," SAE Techincal Paper 2009-01-1111, 2009.

[38] L. Guzzella and C. H. Onder, Introduction to modeling and control of internal combustion engine systems. Berlin: Springer, 2010.

[39] C. Dönitz, C. Voser, I. Vasile, C. Onder, and L. Guzzella, "Validation of the Fuel Saving Potential of Downsized and Supercharged Hybrid Pneumatic Engines Using Vehicle Emulation Experiments," Journal of Engineering for Gas Turbines and Power, vol. 133, pp. 1-13, 2011.

[40] C. Dönitz, I. Vasile, C. Onder, and L. Guzzella, "Realizing a Concept for High Efficiency and Excellent Driveability: The Downsized and Supercharged Hybrid Pneumatic Engine," SAE Techincal Paper 2009-01-1326, 2009.

[41] C. Dönitz, I. Vasile, C. Onder, and L. Guzzella, "Modelling and optimizing two- and four-stroke hybrid pneumatic engines," Proceedings of the Institution of Mechanical Engineers, Part D: Journal of Automobile Engineering, vol. 223, pp. 255-280, 2009.

[42] C. Dönitz, I. Vasile, C. Onder, and L. Guzzella, "Dynamic programming for hybrid pneumatic vehicles," in American Control Conference, 2009. ACC '09., St. Louis, MO, USA, 2009, pp. 3956-3963.

[43] S. Trajkovic, P. Tunestal, and B. Johansson, "Vehicle Driving Cycle Simulation of a Pneumatic Hybrid Bus Based on Experimental Engine Measurements," SAE Techincal Paper 2010-01-0825, 2010.

[44] S. Trajkovic, P. Tunestål, and B. Johansson, "Simulation of a Pneumatic Hybrid Powertrain with VVT in GT-Power and Comparison with Experimental Data," SAE Techincal Paper 2009-01-1323, 2009.

[45] S. Trajkovic, P. Tunestål, and B. Johansson, "Investigation of Different Valve Geometries and Vavle Timing Strategies and their Effect on Regenerative Efficiency for a Pneumatic Hybrid with Variable Valve Actuation," SAE Int. J. Fuels Lubr., vol. 1, pp. 1206-1223, 2008.

[46] S. Trajkovic, P. Tunestål, B. Johansson, U. Carlson, and A. Höglund, "Introductory Study of Variable Valve Actuation for Pneumatic Hybridization," SAE Techincal Paper 2007-01-0288, 2007.

[47] P. Brejaud, P. Higelin, A. Charlet, G. Colin, and Y. Chamaillard, "One Dimensional Modeling and Experimental Validation of Single Cylinder Pneumatic Combustion Hybrid Engine," SAE Int. J. Engines, vol. 4, pp. 2326-2337, 2011.

[48] P. Brejaud, P. Higelin, A. Charlet, G. Colin, and Y. Chamaillard, "Convective Heat Transfer in a Pneumatic Hybrid Engine," Oil Gas Sci. Technol. – Rev. IFP Energies nouvelles, vol. 66, pp. 1035-1051, 2011.

[49] P. Brejaud, A. Charlet, Y. Chamaillard, A. Ivanco, and P. Higelin, "Pneumatic-Combustion Hybrid Engine: A Study of the Effect of the Valvetrain Sophistication on Pneumatic Modes," Oil Gas Sci. Technol. – Rev. IFP, vol. 65, pp. 27-37, 2010.

[50] P. Higelin and A. Charlet, "Thermodynamic Cycles for a New Hybrid Pneumatic–Combustion Engine Concept," SAE Techincal Paper 2001-01-033, 2001.

[51] A. Ivanco, G. Colin, Y. Chamaillard, A. Charlet, and P. Higelin, "Energy Management Strategies for a Pneumatic-Hybrid Engine Based on Sliding Window Pattern Recognition," Oil Gas Sci. Technol. – Rev. IFP, vol. 65, pp. 179-190, 2010.

[52] A. Ivanco, A. Charlet, Y. Chamaillard, and P. Higelin, "Energy Management Strategies for Hybrid-Pneumatic Engine Studied on an Markov Chain Type Generated Driving Cycle," SAE Techincal Paper 2009-01-0145, 2009.

[53] "Compressed-air vehicle," Retrieved from http://en.wikipedia.org/wiki/Compressed-air_vehicle#cite_note-1, Last accessed: March 30, 2015.

[54] "Compressed-Air Vehicles," Retrieved from http://www.douglas-self.com/MUSEUM/TRANSPORT/comprair/comprair.htm, Last accessed: April 02, 2015.

[55] "Pneumatic Options Research Library," Retrieved from http://www.aircaraccess.com/history.htm, Last accessed: April 02, 2015.

[56] "Compressed Air Trams," Retrieved from http://www.tramwayinfo.com/Tramframe.htm?http://www.tramwayinfo.com/tramways/Articles/Compair.htm, Last accessed: April 02, 2015.

[57] "Mekarski system," Retrieved from http://en.wikipedia.org/wiki/Mekarski_system, Last accessed: April 02, 2015.

[58] "History and Directory of Electric Cars from 1834 - 1987," Retrieved from http://www.didik.com/ev_hist.htm, Last accessed: April 02, 2015.

[59] "Motor Development International," Retrieved from http://en.wikipedia.org/wiki/Motor_Development_International, Last accessed: May 02, 2015.

[60] "AIRPod," Retrieved from http://en.wikipedia.org/wiki/AIRPod#cite_note-2, Last accessed: May 05, 2015.

[61] "Hybrid Air - An innovative petrol full-hybrid solution," Retrieved from http://www.psa-peugeot-citroen.com/sites/default/files/content_files/press-kit_hybrid-air_en.pdf, Last accessed: May 10, 2015.

[62] "How It Works: The Hybrid Air Car," Retrieved from http://www.popularmechanics.com/cars/hybrid-electric/a9252/how-it-works-the-hybrid-air-car-15724045/, Last accessed: May 10, 2015.

[63] M. M. Schechter, "Regenerative Compression Braking - A Low Cost Alternative to Electric Hybrids," SAE Techincal Paper 2000-01-1025, 2000.

[64] M. M. Schechter, "Operating a vehicle with braking energy recovery," United States Patent 7231998, 2007.

[65] X. Wang, C. Tai, P. N. Blumberg, H. Kang, and T.-C. Tsao, "Modeling of Compressed Air Hybrid Operation for a Heavy Duty Diesel Engine," Journal of Engineering for Gas Turbines and Power, vol. 131, pp. 052802-052802, 2009.

[66] P. Stouffs, M. Tazerout, and P. Wauters, "Thermodynamic analysis of reciprocating compressors," International Journal of Thermal Sciences, vol. 40, pp. 52-66, 2001.

[67] B. Robert, Automotive handbook. Plochingen: Bosch, 2011.

[68] "Air starters SS175/SS350 Series," Retrieved from http://www.ingersollrandproducts.com/airstarters/pdfs/f-237KB.pdf, Last accessed: March 27, 2015.

[69] L. Guzzella and A. Sciarretta, Vehicle propulsion systems: introduction to modeling and optimization. Berlin: Berlin: Springer, 2007.

[70] M. A. Wijewardane, "Exhaust system energy management of internal combustion engines," PhD Thesis, Loughborough University, 2012.

[71] L. Guzzella and A. Amstutz, "The QSS Toolbox Manual," 2005.

[72] "Stateflow - Model and simulate decision logic using state machines and flow charts," Retrieved from http://uk.mathworks.com/products/stateflow/, Last accessed: March 27, 2015.

[73] T. J. Barlow, S. Latham, I. S. McCrae, and P. G. boulter, "A reference book of driving cycles for use in the measurement of road vehicle emissions," Retrieved from https://www.gov.uk/government/uploads/system/uploads/attachment_data/file/4247/ppr-354.pdf, Last accessed: March 27, 2015.

[74] "Testing & Accreditation (LCEB Certification)," Retrieved from http://www.lowcvp.org.uk/initiatives/lceb/lceb-testing.htm, Last accessed: March 27, 2015.

[75] Ingersoll Rand, "Air starters," http://www.ingersollrandproducts.com/airstarters/pdfs/f-237KB.pdf, Accessed September 2012.

[76] R. Bao and R. Stobart, "Study on Optimization of Regenerative Braking Control Strategy in Heavy-Duty Diesel Engine City Bus using Pneumatic Hybrid Technology," SAE Technical Paper 2014-01-1807, 2014.

[77] J. Zhang, D. Kong, L. Chen, and X. Chen, "Optimization of control strategy for regenerative braking of an electrified bus equipped with an anti-lock braking system," Proceedings of the Institution of Mechanical Engineers, Part D: Journal of Automobile Engineering, 2011.

[78] Y. Gao, L. Chen, and M. Ehsani, "Investigation of the Effectiveness of Regenerative Braking for EV and HEV," SAE Techincal Paper 1999-01-2910, 1999.

[79] J. Y. Wong, Theory of ground vehicles: John Wiley & Sons, 2001.

[80] Y. Gao and M. Ehsani, "Electronic Braking System of EV And HEV---Integration of Regenerative Braking, Automatic Braking Force Control and ABS," SAE Technical Paper 2001-01-2478, 2001.

[81] G. Yimin, C. Liang, and M. Ehsani, "Design and Control Principles of Hybrid Braking System for EV, HEV and FCV," in Vehicle Power and Propulsion Conference, 2007. VPPC 2007. IEEE, 2007, pp. 384-391.

[82] S. Hui, "Multi-objective optimization for hydraulic hybrid vehicle based on adaptive simulated annealing genetic algorithm," Eng. Appl. Artif. Intell., vol. 23, pp. 27-33, 2010.

[83] "Global Optimization Toolbox User's Guide R2014b," Retrieved from http://uk.mathworks.com/help/pdf_doc/gads/gads_tb.pdf, Last accessed: March 04, 2015.

[84] G. Nicosia and G. Stracquadanio, "Generalized Pattern Search Algorithm for Peptide Structure Prediction," Biophysical Journal, vol. 95, pp. 4988-4999, 2008.

[85] M. Marx, H. Németh, and E. Gerum, "Improving the Torque Behaviour of Turbocharged Diesel Engines by Injecting Compressed Air," MTZ worldwide Edition, vol. 70, pp. 30-35, 2009.

[86] C. D. Rakopoulos and E. G. Giakoumis, Diesel Engine Transient Operation: Principles of Operation and Simulation Analysis: Springer London, 2009.

[87] D. Cieslar, N. Collings, P. Dickinson, K. Glover, and A. Darlington, "A Novel System for Reducing Turbo-Lag by Injection of Compressed Gas into the Exhaust Manifold," SAE Techincal Paper 2013-01-1310, 2013.

[88] R. Bao and R. Stobart, "Evaluating the Performance Improvement of Different Pneumatic Hybrid Boost Systems and Their Ability to Reduce Turbo-Lag," SAE Technical Papers 2015-01-1159, 2015.

[89] "Brief Introduction to YC6A Series Engine," Retrieved from http://www.yuchai.com/English/product/1208012224483371.htm, Last accessed: October 08, 2014.

[90] "Engine Performance Application Manual VERSION 7.4," Retrieved from online documents, Last accessed: March 08, 2015.

[91] J. B. Heywood, Internal combustion engine fundamentals. New York: McGraw-Hill, 1988.

[92] C. C. Chan, "The State of the Art of Electric, Hybrid, and Fuel Cell Vehicles," Proceedings of the IEEE, vol. 95, pp. 704-718, 2007.

[93] F. R. Salmasi, "Control Strategies for Hybrid Electric Vehicles: Evolution, Classification, Comparison, and Future Trends," Vehicular Technology, IEEE Transactions on, vol. 56, pp. 2393-2404, 2007.

[94] A. M. Phillips, M. Jankovic, and K. E. Bailey, "Vehicle system controller design for a hybrid electric vehicle," in Control Applications, 2000. Proceedings of the 2000 IEEE International Conference on, 2000, pp. 297-302.

[95] D. Zhao, R. Stobart, G. Dong, and E. Winward, "Real-Time Energy Management for Diesel Heavy Duty Hybrid Electric Vehicles," Control Systems Technology, IEEE Transactions on, vol. PP, pp. 1-1, 2014.

[96] W. Rui and S. M. Lukic, "Dynamic programming technique in hybrid electric vehicle optimization," in Electric Vehicle Conference (IEVC), 2012 IEEE International, 2012, pp. 1-8.

[97] Z. Yuan, L. Teng, S. Fengchun, and H. Peng, "Comparative Study of Dynamic Programming and Pontryagin's Minimum Principle on Energy Management for a Parallel Hybrid Electric Vehicle," Energies, vol. 6, p. 2305, 2013.

[98] C. Musardo, G. Rizzoni, and B. Staccia, "A-ECMS: An Adaptive Algorithm for Hybrid Electric Vehicle Energy Management," in Decision and Control, 2005 and 2005 European Control Conference. CDC-ECC '05. 44th IEEE Conference on, 2005, pp. 1816-1823.

[99] "Controls Coupling Manual VERSION 7.4," Retrieved from online documents, Last accessed: March 08, 2015.

[100] G. Mohan, F. Assadian, and S. Longo, "Comparative analysis of forward-facing models vs backwardfacing models in powertrain component sizing," in Hybrid and Electric Vehicles Conference 2013 (HEVC 2013), IET, 2013, pp. 1-6.

[101] T. Katrašnik, "Hybridization of powertrain and downsizing of IC engine – A way to reduce fuel consumption and pollutant emissions – Part 1," Energy Conversion and Management, vol. 48, pp. 1411-1423, 2007.

[102] A. Sciarretta, M. Back, and L. Guzzella, "Optimal control of parallel hybrid electric vehicles," Control Systems Technology, IEEE Transactions on, vol. 12, pp. 352-363, 2004.

[103] Y. A. Çengel, M. A. Boles, and M. Kanoglu, Thermodynamics : an engineering approach. London: McGraw-Hill, 2011.

[104] A. D. Belegundu and T. R. Chandrupatla, Optimization concepts and applications in engineering. Upper Saddle River, N.J.: Prentice Hall, 1999.

[105] "AUTONOMIE Overview," Retrieved from http://www.autonomie.net/overview/index.html, Last accessed: March 02, 2015.

[106] "AVL CRUISE," Retrieved from https://www.avl.com/cruise, Last accessed: March 02, 2015.

[107] H. Bufu, W. Zhancheng, and X. Yangsheng, "Multi-Objective Genetic Algorithm for Hybrid Electric Vehicle Parameter Optimization," 2006 IEEE/RSJ International Conference on Intelligent Robots and Systems, pp. 5177-5182, 2006.

[108] M. Montazeri-Gh, A. Poursamad, and B. Ghalichi, "Application of genetic algorithm for optimization of control strategy in parallel hybrid electric vehicles," Journal of the Franklin Institute, vol. 343, pp. 420-435, 2006.

[109] J. H. Holland, Adaptation in natural and artificial systems an introductory analysis with applications to biology, control, and artificial intelligence. Cambridge, Mass., London: MIT Press, 1992.

[110] A. Konak, D. W. Coit, and A. E. Smith, "Multi-objective optimization using genetic algorithms: A tutorial," Reliability Engineering & System Safety, vol. 91, pp. 992-1007, 2006.

[111] D. E. Goldberg, Genetic algorithms in search, optimization, and machine learning. Reading, Mass. Wokingham: Addison-Wesley, 1989.

[112] K. Deb and D. Kalyanmoy, Multi-Objective Optimization Using Evolutionary Algorithms: John Wiley & Sons, Inc., 2001.

[113] L. T. Eckart Zitzler, "An Evolutionary Algorithm for Multiobjective Optimization: The Strength Pareto Approach," 1998.

[114] "Population Based Methods," Retrieved from http://www.tik.ee.ethz.ch/education/lectures/DSE/population_based.pdf, Last accessed: June 04, 2015.

[115] J. D. Schaffer, "Multiple Objective Optimization with Vector Evaluated Genetic Algorithms," presented at the Proceedings of the 1st International Conference on Genetic Algorithms, 1985.

[116] C. M. Fonseca and P. J. Fleming, "Multiobjective genetic algorithms," in Genetic Algorithms for Control Systems Engineering, IEE Colloquium on, 1993, pp. 6/1-6/5.

[117] N. Srinivas and K. Deb, "Muiltiobjective Optimization Using Nondominated Sorting in Genetic Algorithms," Evolutionary Computation, vol. 2, pp. 221-248, 1994/09/01 1994.

[118] E. Zitzler and L. Thiele, "Multiobjective evolutionary algorithms: a comparative case study and the strength Pareto approach," Evolutionary Computation, IEEE Transactions on, vol. 3, pp. 257-271, 1999.

[119] K. Deb, A. Pratap, S. Agarwal, and T. Meyarivan, "A fast and elitist multiobjective genetic algorithm: NSGA-II," Evolutionary Computation, IEEE Transactions on, vol. 6, pp. 182-197, 2002.

[120] E. Zitzler, "Evolutionary Algorithms for Multiobjective Optimization: Methods and Applications," PhD Thesis, ETH Zurich, 1999.

[121] S. Bashash, S. J. Moura, J. C. Forman, and H. K. Fathy, "Plug-in hybrid electric vehicle charge pattern optimization for energy cost and battery longevity," Journal of Power Sources, vol. 196, pp. 541-549, Jan 1 2011.

[122] L. Fang and S. Qin, "Concurrent Optimization for Parameters of Powertrain and Control System of Hybrid Electric Vehicle Based on Multi-Objective Genetic Algorithms," in SICE-ICASE, 2006. International Joint Conference, 2006, pp. 2424-2429.

APPENDICES

Appendix-I

Theoretical model in Chapter 3 - MATLAB program

```
%   Sequence of commands required to calculate the work flows in a
pneumatic hybrid cycle. Cycle is proposed through states 1 to 8, and
corresponding state variables, notably temperature and pressure are denoted
p1... and T1..., and so on.

syms p1 p2 p3 p4 p5 p6 p7 p8 p9 p10 p11 p12 p13
syms T1 T2 T3 T4 T5 T6 T7 T8 T9 T10 T11 T12 T13

%   Actual volumes are used
syms V1 V2 V3 V4 V5 V6 V7 V8 V9 V10 V11 V12 V13

%   Work quantities are assigned according to the phase of the cycle
syms W12 W23 W34 W45 W56 W67 W78 W89 W910 W1011 W1112 W1213 Wtotal Power
Torque

%   Manifold and auxiliary chamber conditions
syms mass_m mass_cyl mass_t Tm pm Vm
%   Masses in the cylinder vary, start with m1 in the cylinder and m in the
tank

%   Gas physical properties
syms n  % Polytropic index for air

%   Define function to calculate work done on piston
%   Pre-allocate storage for pV plots

nrows = 1;
ncols = 605;
p_history = zeros(nrows, ncols);
V_history = zeros(nrows, ncols);%

%   Set physical variables

R = 287;                % J/kgk, Value of R for dry air
pa = 1.0 * 10^5;        % bar,   Intake system pressure
pe = 1.0 * 10^5;        % bar,   Exhaust system pressure

Ta = 298;               % K,     Intake system temperature
Te = 298;               % K,     Exhaust system temperature
Tt = Ta;                % K,     Air tank temperature
Tm = Ta;                % K,     Auxiliary chamber temperature

clearanceV = 0.000069; % m3,    Cylinder clearance volume
Vm = 0.0001984;         % m3,    Auxiliary chamber volume
Vt = 0.151;             % m3,    Air tank volume
sweptV = 0.001143;      % m3,    Cylinder swept volume
```

```
n = 1.3;
Cd = 0.78;              %        Check valve Discharge
                        %        Coefficient
Ar = 0.0001267;         % m2,    Check valve Effective area of flow
restriction
r = 1.4;                %        Specific heat ratio of air
Pair = 1.29;            % kg/m3  Density of the air
count = 1;
pt = 5 * 10^5;          % pa,    Air tank pressure
D = 100;                % CA,    Duration of the intake valve
                        %        second opening in crank angle
IVSC = 30;              % ATDC,  Intake Valve Second Close in crank angle
                        %        After Top Dead Centre
N = 1500;               % rpm,   Engine speed

%   Calculate mass as pV/RT

mass_t = (pt*Vt)/(R*Tt);    % kg, Needs to be set to mass of air in the tank

mass_m = (pa*Vm)/(R*Tm);    % kg, Needs to be set to the mass of air in the
                            %     auxiliary chamber

p1 = pa;
T1 = Ta;                    % Cylinder temperature at point 1

V1 = sweptV+clearanceV;     % Cylinder volume at BDC
V2 = (D-IVSC)*V1/180+(180+IVSC-D)*clearanceV/180;
% Use the crank angle and valve timing to present the V2 volume

mass_cyl = (p1*V1)/(R*Ta);

% Calculate W12
% Air in the cylinder is now being compressed

[W12, p2, T2]= work_done(p1, T1, V1, V2, n );

for V = V1:(V2-V1)/100:V2
    p = p1 * (V1/V)^n;
    p_history(count) = p;
    V_history(count) = V;
    count = count + 1;
end

% Calculate W23
% Valve opens connecting the cylinder to the manifold.
% During this phase of the cycle there is no piston motion and no work done.

W23 = 0;

% Calculate new states assuming equilibrium conditions

T3 = (mass_m*Tm+mass_cyl*T2)/(mass_m + mass_cyl);
p3 = (mass_m*Tm + mass_cyl*T2)*R/(V2+Vm);
V3 = V2 + Vm;

p_history(count)=p3;
V_history(count)=V3;
count = count + 1;

% Calculate W34
```

```
% p4 is the tank pressure - that is the pressure at which the check valve
opens assuming no hysteresis

p4 = pt;
V4 = ((p3/p4)^(1/n)) * V3;
m4 = mass_m + mass_cyl;

[W34, p4, T4]= work_done(p3, T3, V3, V4, n );

for V = V3:(V4-V3)/100:V4
    p = p3 * (V3/V)^n;
    p_history(count)=p;
    V_history(count)=V;
    count = count + 1;
end

% Calculate W45

delta_V = (V4-clearanceV-Vm)/50;

t = 0.6 * (V4-clearanceV-Vm)/(sweptV*N);

V45 = V4 - delta_V;

[W45,p5,T5] = work_done(p4,T4,V4,V5,n1);

for V = V5:(V5-V4)/50:V4
    p = p4 * (V4/V)^n1;
    p_history(count)=p;
    V_history(count)=V;
    count = count + 1;
end

fc45 = Cd * Ar * ((2*Pair)^(1/2)) * ((p5-pt)^(1/2));
delta_m_5 = fc45 * t;
m5 = m4 - delta_m_4;
p5= (m5 * T5) * R / V5;
p_history(count)=p5;
V_history(count)=V5;
count = count + 1;

% Calculate W56
% For the next stage of the cycle, let p6 = p4: this allows the calculation
of V6 - but still need to calculate V6 first

p6 = pt;
V6 = V5;
T6 = T5;
W56 = 0;

p_history(count)=p6;
V_history(count)=V6;
count = count + 1;

% Calculate W67
% The stage 6-7 is the expansion up until the intake valve closes

V7 = IVSC*V1/180 + (180-IVSC)*clearanceV/180 + Vm;

[W67, p7, T7]= work_done(p6, T6, V6, V7, n3 );
```

```
for V = V6:(V7-V6)/100:V7
    p = p6 * (V6/V)^n3;
    p_history(count)=p;
    V_history(count)=V;
    count = count + 1;
end

% Calculate W78
% Now the intake valve closes - the volume is reduced at constant pressure

V8 = V7 - Vm;
W78 = 0;
p8 = p7;
T8 = T7;

p_history(count)=p8;
V_history(count)=V8;
count = count + 1;

% Calculate W89
% Now intake valve closes and the expansion is completed
% Re-calculate mass assuming the thermodynamic conditions are similar

V9 = V1;

[W89, p9, T9]= work_done(p8, T8, V8, V9, n4 );

for V = V8:(V9-V8)/100:V9
    p = p8 * (V8/V)^n4;
    p_history(count)=p;
    V_history(count)=V;
    count = count + 1;
end

% Calculate W910
% Now the exhaust valves open, the air come into the cylinder from the
exhaust valves, the pressure increase to the exhaust system pressure.

W910 = 0;

T10 = Te;
p10 = pe;
V10 = V1;

p_history(count)=p10;
V_history(count)=V10;
count = count + 1;

% Calculate W1011
% At point 10, the piston is going up to compress the air out of the
cylinder, the pressure keeps constant.

W1011 = p10*(clearanceV-V1);

T11 = Te;
p11 = pe;
V11 = clearanceV;

p_history(count)=p11;
V_history(count)=V11;
count = count + 1;
```

```
% Calculate W1112
% Now the intake valves open, the air come into the cylinder from the
intake valves, the pressure increase to the intake system pressure.

W1112 = 0;

T12 = Ta;
p12 = pa;
V12 = clearanceV;

p_history(count)=p12;
V_history(count)=V12;
count = count + 1;

% Calculate W1213
% At point 10, the piston is going down, and the air come into the cylinder,
the pressure keeps constant.

W1213 = p12*(V1-clearanceV);

T13 = Ta;
p13 = pa;
V13 = V1;

p_history(count)=p13;
V_history(count)=V13;
count = count + 1;

%%%%%%%%%%

Wtotal = W12 + W23 + W34 + W45 + W56 + W67 + W78 + W89 + W910 + W1011 +
W1112 + W1213;

% This is the contribution of torque from one cylinder for two engine
cycles

Power = Wtotal*N/(120*1000); % In one minute, total work is Wtotal*N/2 (W),
as a result, the power is ((Wtotal*N/2)/60)/1000 (kW)

Torque = Power*1000/(2*pi*(N/60));

w = N*2*pi/60; % Angular velocity (rad/s)
Torque_1 = Power*1000/w;

plot(V_history,p_history);
```

work_done model – MATLAB program

```
function [work,pfinal,Tfinal] = work_done( p1, T1, V1, V2, m )
% work_done Calculates the work done during this phase of the cycle, Work
is calculated according to a polytropic compression or expansion with index
m, the final pressure is calculated on the same basis.

work = (p1*(V1^m)/(m-1))*((V1^(1-m))-(V2^(1-m)));
pfinal = p1*((V1/V2)^m);
Tfinal = T1*((V1/V2)^(m-1));

end
```

Appendix-II

Chapter 6 - GT-POWER model of the basic engine

A heavy-duty, six cylinders, turbocharged & intercooler diesel engine based on the YUCHAI YC6A Series engine is used as the basic engine in this research. The pneumatic hybrid systems are added to this engine to realize the different functions discussed in Chapter 6 and 7. The GT-POWEER model of the basic YC6A engine is shown in Figure A-1. The dimensions and characteristics of the basic engine GT-POWER model are shown in Table A-1.

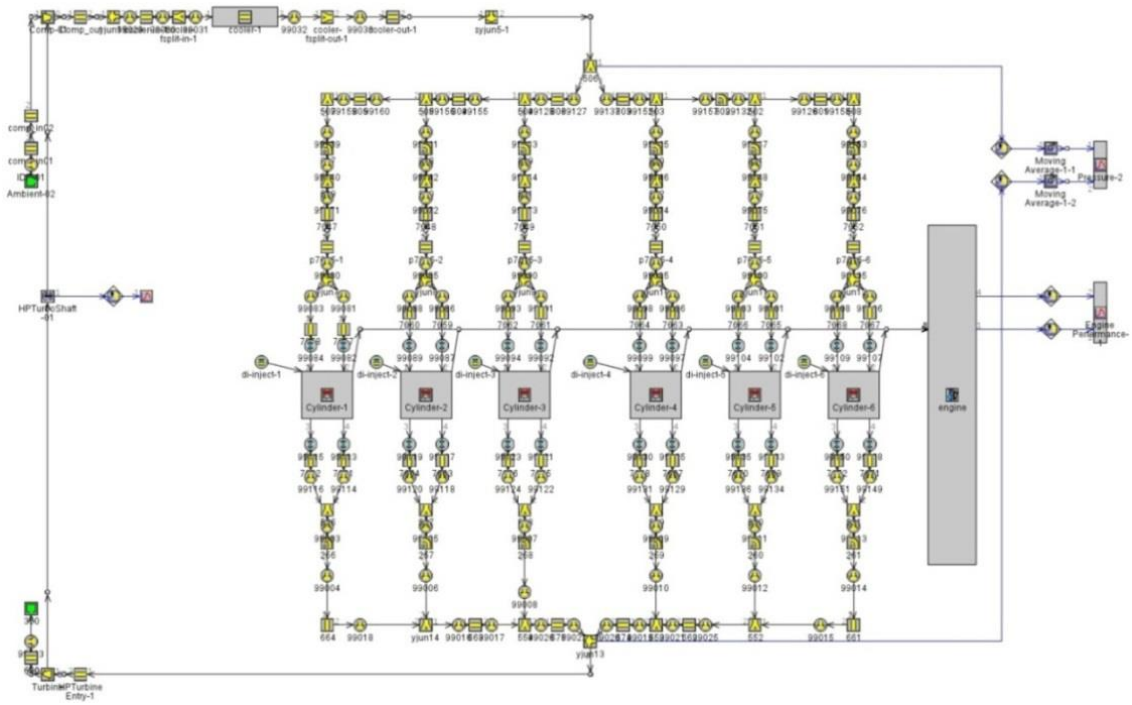

Figure A-1 GT-POWER model of the basic engine

Table A-1 Dimensions and characteristics of the basic engine GT-POWER model

Part Name	Type	Dimensions	
Ambient-02, 350	Environment End	Pressure (bar)	1
		Temperature (k)	298
comp_in01	Round Pipes	Diameter (mm)	101
		Length (mm)	304

comp_in02	Round Pipes	Diameter (mm) Length (mm)	84 250
cooler-in-1	Round Pipes	Diameter (mm) Length (mm)	66.5 55
cooler-1	Round Pipes	Diameter (mm) Length (mm)	5 450
cooler-out-1	Round Pipes	Diameter (mm) Length (mm)	80 550
803, 806	Round Pipes	Diameter (mm) Length (mm)	58.7 34
802, 804	Round Pipes	Diameter (mm) Length (mm)	58.7 66
801, 805	Round Pipes	Diameter (mm) Length (mm)	58.7 132
7047, 7048, 7049, 7050, 7051, 7052	Round Pipes	Diameter (mm) Length (mm)	45.7 57.4
P7015-1, P7015-2, P7015-3, P7015-4, P7015-5, P7015-6	Round Pipes	Diameter (mm) Length (mm)	45.7 10
7058, 7060, 7062, 7064, 7066, 7068, 7057, 7059, 7061, 7063, 7065, 7067	Round Pipes	Diameter (mm) Length (mm)	32.4 210
7662, 7664, 7666, 7668, 7670, 7672, 7661, 7663, 7665, 7667, 7669, 7671	Round Pipes	Diameter (mm) Length (mm)	37.8 168.7
661, 664	Round Pipes	Diameter (mm) Length (mm)	40 71
662, 663	Round Pipes	Diameter (mm) Length (mm)	40 71
674, 675	Round Pipes	Diameter (mm)	40

		Length (mm)	86.5
HPTurbineEntry-1	Round Pipes	Diameter (mm)	50
		Length (mm)	80
680	Round Pipes	Diameter (mm)	110
		Length (mm)	120
yjun15	A spherical-shaped flowsplit volume	Diameter (mm)	66.5
syjun5-1	A spherical-shaped flowsplit volume	Diameter (mm)	80
yjun13	A spherical-shaped flowsplit volume	Diameter (mm)	31
99084, 99089, 99094, 99099, 99104, 99109, 99082, 99087, 99092, 99097, 99102, 99107	A cam-driven valve	Diameter (mm)	32.5
99115, 99119, 99123, 99130, 99135, 99150, 99113, 99117, 99121, 99125, 99133, 99138	A cam-driven valve	Diameter (mm)	29.5
yjun7, yjun8, yjun9, yjun10, yjun11, yjun12	A spherical-shaped flowsplit volume	Diameter (mm)	45.7
cooler-fsplit-in-1, cooler-fsplit-out-1	A flowsplit volume connected to one or more flow components	Volume (mm^3)	900000
		Surface Area (mm^2)	40000
502, 503, 504, 505, 506, 507, 508	A flowsplit volume connected to one or more flow components	Volume (mm^3)	105904
		Surface Area (mm^2)	10825
519, 520, 521, 522, 523, 524	A flowsplit volume connected to one or more flow components	Volume (mm^3)	56826.9
		Surface Area (mm^2)	7148.03
526, 527, 528, 529, 530, 531	A flowsplit volume connected to one or more flow components	Volume (mm^3)	28279.6
		Surface Area (mm^2)	4488.83
552, 553, 554, yjun14	A flowsplit volume connected to one or more flow components	Volume (mm^3)	33510.3
		Surface Area (mm^2)	5026.55
817, 818, 819, 820, 821, 822	Pipes that have a round cross-section and an optional bend	Diameter (mm)	47.7
		Length (mm)	72
		Angle of bend (deg)	45

256, 257, 258, 259, 260, 261	Pipes that have a round cross-section and an optional bend	Diameter (mm)	37.8
		Length (mm)	1403
		Angle of bend (deg)	60

Furthermore, some important parameters are introduced here.

Discretization length

Based on the 'Engine performance tutorials' from GT-POWER, for general performance analysis (Engine cycle simulation a discretization length of approximately 0.4 times the cylinder bore diameter is recommended for the intake system and 0.55 times the bore is recommended for the exhaust system. The difference in the recommendation for intake and exhaust discretization is the result of differences in the speed of sound due to the temperature. The bore diameter in this model is 105 mm, therefore the intake side discretization length is 42 mm, and the exhaust side discretization length is 60 mm.

Cylinder Geometry

Table A-2 Cylinder Geometry

Bore (mm)	105
Stroke (mm)	132
Connecting rod length (mm)	210
Compression ratio (-)	17.5
TDC clearance height	1
Wrist pin to crank offset (mm)	0

Firing order

1-5-3-6-2-4

Intake and exhaust valves lift and timing

The intake valves lift and timing is shown in Figure A-2.

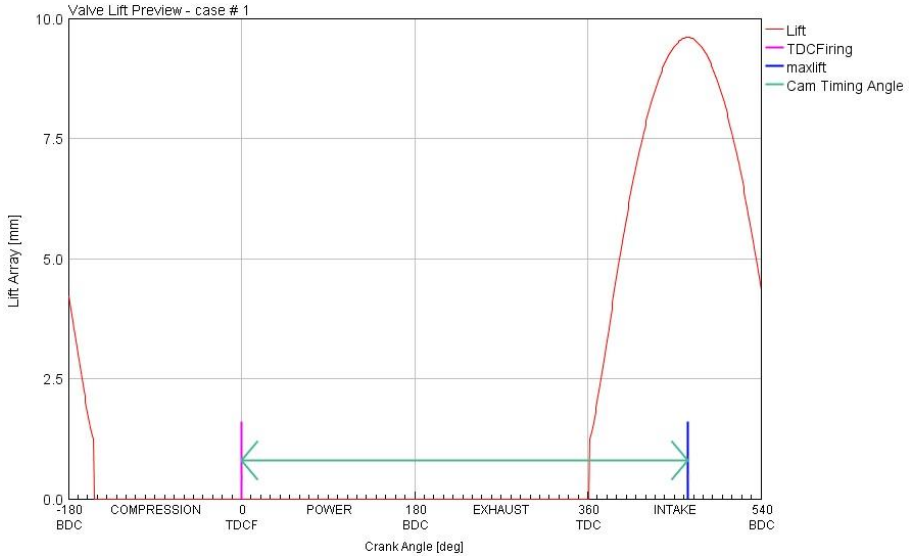

Figure A-2 Intake valves lift and timing

The intake valves lift and timing is shown in Figure A-3.

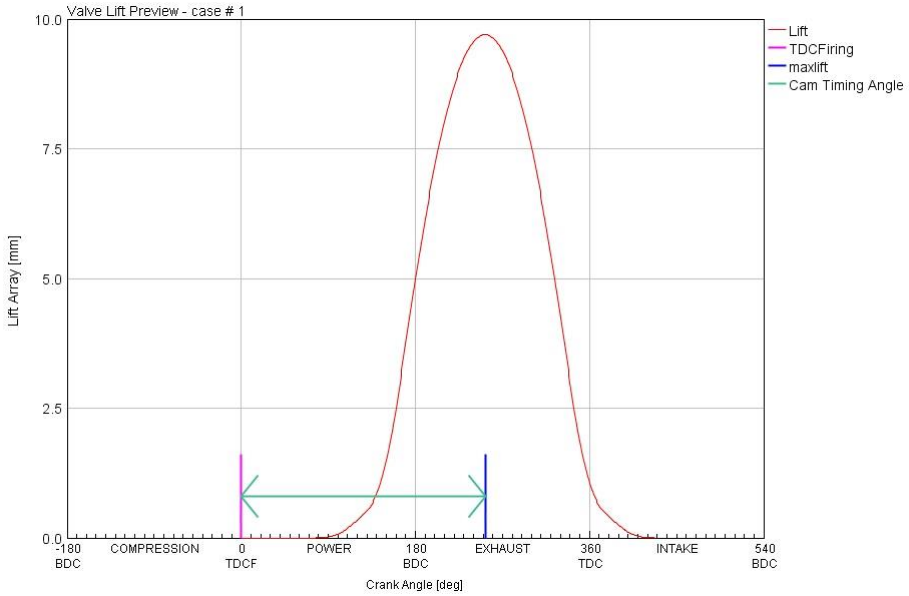

Figure A-3 Exhaust valves lift and timing

Fuel injection system

The 'Injection Profile Connection' is used here as the fuel injector. This injection connection allows for injection of a periodic mass flow rate or pressure profile. It may be used to inject fluid into any cylinder, pipe, or flowsplit, but it is typically used for direct-injection diesel engines. This template may be used with any cylinder combustion model. The parameters of the nozzles are shown in Table A-2.

Table A-3 Cylinder Geometry

Nozzle hold diameter (mm)	0.17
Number of holes per nozzle (-)	6

The introduction of how to run the GT-POWER and Simulink co-simulation

Any GT-POWER signals can be passed to or from Simulink via a 'SimulinkHarness' component. There are two methods in which this can be accomplished:

(i) Running a GT-SUITE model from the Simulink interface.
(ii) Compiling Simulink model(s) into .dll/.so files and importing them into a GT-SUITE model.

The advantage of the first method is that all the functions of MATLAB/Simulink can be implemented. For example, the Global Optimisation Toolbox can be used to search for global solutions to problems that contain multiple maxima or minima by running the problem several times with different variables. For the second method, once the Simulink model is compiled to the .dll/.so files, the parameters in the Simulink model cannot alter any more. But in the first method, there is a restriction that only one 'SimulinkHarness' part may be used in the GT-SUITE model while the second method allows up to an infinite number of 'SimulinkHarness' parts with the same or different imported Simulink models. As the goal of this research is to develop the pneumatic hybrid city bus control strategy, the optimisation will be one part of the develop process, as a result, the first method has been chosen in this research.

Appendix-III

In GT-POWER, the 'DIWiebe' model imposes the combustion burn rate for direct-injection, compression-ignition engines using a three-term Wiebe function which is the superposition of three normal Wiebe curves. These Wiebe curves approximate the "typical" shape of a DI compression ignition, single main injection burn rate. The purpose of using three functions is to make it possible to model the premixed and diffusion portions of the combustion process.

The Wiebe equations are given below.

Constants calculation: Main Fraction (F_M), Wiebe Premix Constant (WC_P), Wiebe Main Constant (WC_M), Wiebe Tail Constant (WC_T).

$$F_M = (1 - F_P - F_T) \quad \text{(A-1) [90]}$$

$$WC_P = \left[\frac{D_P}{2.302^{\,1/(E_P+1)} - 0.015^{\,1/(E_P+1)}}\right]^{-(E_P+1)} \quad \text{(A-2) [90]}$$

$$WC_M = \left[\frac{D_M}{2.302^{\,1/(E_M+1)} - 0.015^{\,1/(E_M+1)}}\right]^{-(E_M+1)} \quad \text{(A-3) [90]}$$

$$WC_T = \left[\frac{D_T}{2.302^{\,1/(E_T+1)} - 0.015^{\,1/(E_T+1)}}\right]^{-(E_T+1)} \quad \text{(A-4) [90]}$$

where D_P – premix duration,

D_M – main duration,

D_T – tail duration,

F_P – premix fraction,

F_T – tail fraction,

E_P – premix exponent,

E_M – main exponent,

E_T – tail exponent.

Burn Rate Calculation: the cumulative burn rate is calculated, normalized to 1.0. The combustion starts at 0.0 (0.0% burned) and progresses to the value specified by the "Fraction of Fuel Burned Attribute", which is typically 1.0 or 100%.

$$Combustion(\theta) = (CE)(F_P)\left[1 - e^{-(WC_P)(\theta - SOI - ID)^{(E_P+1)}}\right] + (CE)(F_M)\left[1 - e^{-(WC_M)(\theta - SOI - ID)^{(E_M+1)}}\right] + (CE)(F_T)\left[1 - e^{-(WC_T)(\theta - SOI - ID)^{(E_T+1)}}\right] \quad \text{(A-5) [90]}$$

where θ – instantaneous Crank Angle,

CE – fraction of Fuel Burned (also known as "Combustion Efficiency"),

SOI – start of Injection, and

ID – ignition Delay.

'WoschniGT' model indicates that the in-cylinder heat transfer will be calculated by a formula which closely emulates the classical Woschni correlation without swirl as detailed described in [91]. This heat transfer model is used to define heat transfer characteristics of the flow component in the engine model.

Appendix-IV

Availability calculation:

Let V, T_0, p_0 be the air tank volume, environment temperature and pressure. Also, let a_1, u_1, p_1, T_1 and m_1 be the availability, internal energy, pressure, temperature and mass of air tank at the initial point, and let a_2, u_2, p_2, T_2 and m_2 be the availability, internal energy, pressure, temperature and mass of air tank at the finish point, respectively (see Figure A-4).

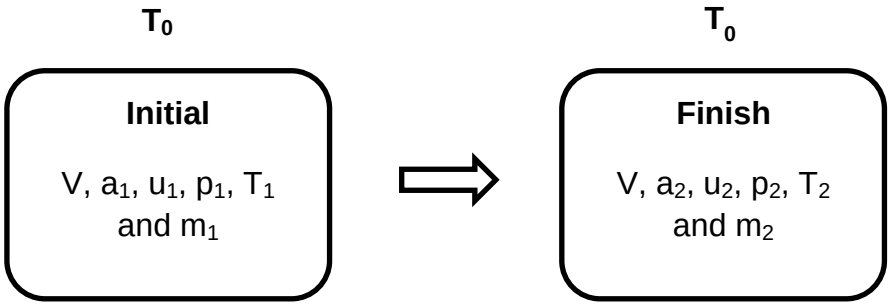

Figure A-4 Availability calculation

First, there are some assumptions should introduce before:

(i) Air is an ideal gas.
(ii) The kinetic and potential energies are negligible.
(iii) The properties of air at the environment remain constant during the entire charging process.

If the air mass in the air tank is m_1, the specific volume v_1 is:

$$v_1 = \frac{V}{m_1} \tag{A-6}$$

Since the temperature remains unchanged and

$$pv_{AT} = mRT \tag{A-7}$$

$$v_1 = \frac{RT_0}{p_1} \tag{A-8}$$

Similar,

$$v_2 = \frac{RT_0}{p_2} \tag{A-9}$$

By definition:

$$a_1 = c_v T_0 - T_0 S_1 \tag{A-10}$$

$$a_2 = c_v T_0 - T_0 S_2 \tag{A-11}$$

And

$$u_1 = u_2 = c_v T_0 \tag{A-12}$$

$$E = m_1 u_1 - m_2 u_2 = m_1 c_v T_0 - m_2 c_v T_0 = \Delta m c_v T_0 \tag{A-13}$$

For availability

$$Tds = du + vdp \tag{A-14}$$

Giving

$$\Delta S = S_2 - S_1 = \left(c_p \ln\frac{T_2}{T_1} - R \ln\frac{p_2}{p_1}\right) = -R \ln\frac{p_2}{p_1} \tag{A-15}$$

So

$$\Delta a = \Delta u - T\Delta S + p_0(v_2 - v_1) = RT_0(\ln\frac{p_0}{p_1} + \frac{p_1}{p_0} - 1) \tag{A-16}$$

Finally, the availability change during the process can be presented

$$\Delta A = mRT_0(\ln\frac{p_0}{p_1} + \frac{p_1}{p_0} - 1) \tag{A-17}$$

Appendix-V

In the Generalized Pattern Search optimisation implemented at Chapter 4 and Chapter 7, the fitness function and options of GPS is first input by using the Global Optimisation Toolbox in MATLAB. Then the Global Optimisation Toolbox completes the pattern search steps such as polling, expanding and contracting to implement the optimisation. All are pattern search algorithms that compute a sequence of points that approach an optimal point. At each step, the algorithm searches a set of points, called a mesh, around the current point—the point computed at the previous step of the algorithm. The mesh is formed by adding the current point to a scalar multiple of a set of vectors called a pattern. If the pattern search algorithm finds a point in the mesh that improves the objective function at the current point, the new point becomes the current point at the next step of the algorithm [83]. The terminology of pattern search is shown as follows [83].

Patterns - A pattern is a set of vectors $\{v_i\}$ that the pattern search algorithm uses to determine which points to search at each iteration. The set $\{v_i\}$ is defined by the number of independent variables in the objective function, N, and the positive basis set.

Meshes - At each step, pattern search searches a set of points, called a mesh, for a point that improves the objective function. Pattern search forms the mesh by (i) Generating a set of vectors $\{d_i\}$ by multiplying each pattern vector v_i by a scalar Δ^m. Δ^m is called the mesh size, and (ii) Adding the $\{d_i\}$ to the current point - the point with the best objective function value found at the previous step.

Polling - At each step, the algorithm polls the points in the current mesh by computing their objective function values.

Expanding and contracting - After polling, the algorithm changes the value of the mesh size Δ^m. The default is to multiply Δ^m by 2 after a successful poll, and by 0.5 after an unsuccessful poll.

Complete Poll - By setting Complete poll to On in Poll options can make the pattern search poll the entire mesh. This is because for problems in which there are several local minima, it is sometimes preferable to make the pattern search poll all the mesh points at

each iteration and choose the one with the best objective function value. This enables the pattern search to explore more points at each iteration and thereby potentially avoid a local minimum that is not the global minimum. By default, if the pattern search finds a mesh point that improves the value of the objective function, it stops the poll and sets that point as the current point for the next iteration. When this occurs, some mesh points might not get polled. Some of these unpolled points might have an objective function value that is even lower than the first one the pattern search finds.